UNIVERSIDADE DE LISBOA
FACULDADE DE CIÊNCIAS

Assessment of the spatio-temporal variability and estimation accuracy of drought indices and evapotranspiration

"Documento Definitivo"

Doutoramento em Ciências Geofísicas e da Geoinformação
Especialidade de Meteorologia

Diogo Miguel dos Santos Martins

Tese orientada por:
Professor Doutor Carlos Alberto Leitão Pires
Professor Doutor Luis Santos Pereira
Professora Doutora Ana Ambrósio Paulo

Documento especialmente elaborado para a obtenção do grau de doutor

2019

UNIVERSIDADE DE LISBOA
FACULDADE DE CIÊNCIAS

Assessment of the spatio-temporal variability and estimation accuracy of drought indices and evapotranspiration

Doutoramento em Ciências Geofísicas e da Geoinformação
Especialidade de Meteorologia

Diogo Miguel dos Santos Martins

Tese orientada por:
Professor Doutor Carlos Alberto Leitão Pires, Professor Doutor Luis Santos Pereira, Professora Doutora Ana Ambrósio Paulo

Júri:

Presidente:

- Doutor João Manuel de Almeida Serra, Professor Catedrático
  Faculdade de Ciências da Universidade de Lisboa.

Vogais:

- Doutora Elsa Estevão Fachadas Nunes Moreira, Professora Auxiliar
  Faculdade de Ciências e Tecnologia da Universidade Nova de Lisboa;
- Doutor João Carlos Andrade dos Santos, Professor Auxiliar com Agregação
  Escola de Ciências e Tecnologia da Universidade de Trás-os-Montes e Alto Douro;
- Doutora Paula Cristina Santana Paredes, Professora Auxiliar
  Instituto Superior de Agronomia da Universidade de Lisboa;
- Doutor Carlos Alberto Leitão Pires, Professor Auxiliar
  Faculdade de Ciências da Universidade de Lisboa (orientador).

Documento especialmente elaborado para a obtenção do grau de doutor

Doutoramento financiado pela Fundação para a Ciência e a Tecnologia (SFRH/BD/92880/2013)

2019

Acknowledgments

First, I would like to thank my advisors, Professor Carlos Pires, Professor Luis Santos Pereira and Professor Ana Paulo. Your support, guidance, shared knowelge and friendship was invaluable during this PhD.

A sincere thank you to Dr. Paula Paredes, for the all friendship and help in this journey and to Professor Teresa do Paço for the patience and freedom given in this past year, which allowed me to finish this Thesis.

I also want to thank all the Professors and collegues I had the pleasure to work within the framework of this Thesis: Doctor Tayeb Raziei, Doctor Elsa Moreira, Mr. Xiaodong Ren, Doctor Abdelaaziz Merabti and Professor Jorge Cadima.

I acknowledge the support provided by the Fundação para a Ciência e Tecnologia under the grant SFRH/BD/92880/2013.

Agradecimentos

Agradeço, também, aos meus excelsos, caros e nunca assaz louvados amigos. A Cavia, a uma amizade que, espero, não tenha fim. À Daniela, Maria e Virgilio, por tornarem as semanas de trabalho mais divertidas e interessantes.

Por último um agradecimento especial aos meus pais, por tudo. Pelo apoio e pelo carinho, sem duvida que sem eles não conseguiria concluir este trabalho. À minha família e, claro, à Zoey.

Abstract

Understanding the spatial and temporal variability of droughts is important to improve drought predictability and ultimately to support drought risk management in agriculture. Several studies were developed, to better understand drought characteristics and variability. For that, the Standardized Drought Index (SPI) was used to identify the main spatial and temporal patterns of drought variability in Portugal, to search for regions with similar drought variability in continental Portugal and significant cycles using a Fourier analysis applied to the SPI, which revelead cycles of 6 and 9.4 years, likely influenced by the North Atlantic Oscillation (NAO) and two stable sub-regions, in the northern and southern regions of Portugal. Moroever, another study using the SPI suggested that for drought monitoring, when using non-stationary time series of precipitation, the reference period used for obtaining the Gamma distribution parameters is important.

Altough the SPI is widely used it only uses precipitation, however, for assessment of agricultural drought conditions indices such as the Palmer Drought Severity Index and its modification for the Mediterranean region, the MedPDSI, may be a better option since they consider the interaction between precipitation and evapotranspiration within a soil water balance. For that reason, in this Thesis the different methodologies to estimate evapotranspiration, on a monthly and daily basis, were tested for different climates conditions.

The results obtained during the course of this Thesis led to the development of the MedPDSI. The MedPDSI improves upon the PDSI mainly by modifying its soil water balance, adapting it to the Mediterranean climate conditions. MedPDSI was computed using reference evapotranspiration based on reanalysis data. Comparing to the PDSI, with the MedPDSI, droughts are generally identified earlier, are longer and more severe, which is an advantage for drought management, since coping management schemes can be implemented earlier to manage drought impacts and thus mitigating its potential negative consequences.

Keywords: drought indices; MedPDSI; Reanalysis products; reference evapotranspiration; soil water balance

Resumo

A água é um bem essencial para a existência de vida, determinante para o desenvolvimento socioeconómico e para a manutenção dos ecossistemas. O rápido crescimento económico e populacional tem provocado uma enorme pressão sobre os recursos hídricos. Muitos países vivem, atualmente, em condições extremas de escassez de água, com graves consequências humanitárias, económicas e ambientais. Embora as ações do homem tenham um peso significativo na disponibilidade e qualidade da água existem fatores naturais, difíceis de controlar, como a ocorrência de secas que agravam consideravelmente o fenómeno da escassez. Estes impactos, são ainda mais severos em regiões áridas e semiáridas com uma elevada variabilidade climática.

As secas são um fenómeno climático extremo que provocam desequilíbrios naturais e temporários na disponibilidade de água, de ocorrência aleatória, severidade incerta sendo encaradas como risco e como desastre. As características das secas (duração, severidade e extensão espacial) determinam a sua importância a nível da região, e é fundamental um melhor conhecimento do fenómeno para que seja possível promover uma melhor gestão dos recursos de forma preventiva, tentando atenuar os impactos negativos das secas.

Nas últimas décadas vários índices de seca têm sido desenvolvidos para a caracterização e compreensão das secas em todo o Mundo. Os mais amplamente estudados para esse efeito têm sido o Standardized Precipitation Index (SPI) e o Palmer Drought Severity Index (PDSI) e ambos são utilizados nesta Tese, bem como uma modificação do PDSI para as condições mediterrânicas, o MedPDSI, que é proposta visando a criação de um índice de seca, adaptado e calibrado às condições climáticas de Portugal e do Mediterrâneo, usando o olival tradicional como cultura de referência.

Compreender a variabilidade espacial e temporal das secas é importante para melhorar a sua previsibilidade e tem como objetivo o apoio à gestão de risco às secas. No âmbito desta Tese, foram desenvolvidos estudos com o objetivo de melhor compreender a variabilidade da seca. No Capítulo 2 estudou-se a estabilidade dos padrões espaciais e temporais de secas em Portugal aplicando a Análise de Componentes Principais ao SPI para várias escalas temporais, calculado para três conjuntos de dados relativos ao período comum de 1950-2003: (1) conjunto de séries de precipitação mensal provenientes de 193 estação meteorológicas e udométricas e (2) Dados de precipitação mensal em grelha,

provenientes das bases de dados GPCC e PT02, com resoluções horizontais de 0.5º e 0.2º, respetivamente. Os resultados sugerem elevada estabilidade dos padrões espaciais de seca, independentes da escala temporal do SPI, da base de dados usada e do período de referência considerado para o cálculo, identificando-se duas sub-regiões no Norte e Sul de Portugal como os principais modos de variabilidade das secas. É identificada no Centro-Este de Portugal uma terceira sub-região, mas apenas quando usando o SPI-24 calculado com a base de dados PT02. No âmbito da análise da variabilidade temporal do SPI em Portugal, analisou-se ainda a ciclicidade das secas recorrendo a uma análise de Fourier aplicada a 74 séries temporais do SPI-12 com 66 anos. Os ciclos significativos mais frequentes foram identificados e analisados para o mês de Dezembro. Os resultados mostraram que as periodicidades variam espacialmente em Portugal, apontando, contudo, para um ciclo de 6 anos comum a todo o país e um ciclo de 9.4 anos muito mais frequente no centro e sul de Portugal. Ambos os ciclos estão provavelmente relacionados com a influência da Oscilação do Atlântico Norte sobre a ocorrência e gravidade das secas em Portugal.

No Capítulo 3 estudou-se também o efeito da variabilidade da precipitação sobre o SPI efetuando a partição de 10 séries longas de precipitação, em sub-períodos e obtendo as séries de SPI para cada sub-período. Calcularam-se, assim, limiares de precipitação correspondentes às categorias de seca moderada, severa e extrema do SPI. As mudanças dos padrões de precipitação refletem-se no valor destes limiares. Em 8 das 10 localidades estudadas os limiares de precipitação do período mais recente, 1976-2007, são inferiores aos limiares equivalentes do período antecedente. Os limiares de precipitação permitem avaliar a magnitude do défice, expresso em altura de precipitação, complementando informação fornecida pelo índice de seca SPI.

O SPI é um índice de seca padronizado que é calculado recorrendo apenas a dados de precipitação. Existem outros índices que consideram não só a influência da precipitação como da evapotranspiração, como por exemplo o Palmer Drought Severity Index (PDSI) que combina precipitação e evapotranspiração num balanço hídrico e, portanto, poderá ser mais adequado para a caracterização da seca na agricultura. Portanto, no Capítulo 3 estudou-se também o impacto da variação temporal a longo prazo das secas, usando o PDSI. Para tal usou-se dados da reanálise do Século XX NOAA-CIRES, previamente validados com dados observados, que abrange o período 1851-2014, com uma resolução espacial de 2.0ºx2.0º. Dados de temperatura máxima e mínima, humidade relativa,

velocidade do vento e radiação foram retirados da reanálise do Século XX para calcular a evapotranspiração de referência pelo método da FAO-56, que, juntamente, com dados de precipitação provenientes de estações meteorológicas foram usados para o cálculo do PDSI. Para avaliar como a variabilidade de longo prazo do clima influencia a identificação de eventos secos pelos índices de seca, cinco períodos de calibração diferentes foram selecionados para estimar os valores potenciais de evapotranspiração, escoamento superficial, recarga de água no solo e perdas do balanço hídrico do PDSI. A mesma análise foi feita em paralelo com o SPI com uma escala temporal a 9 meses, usando os mesmos 5 períodos de calibração para a estimação dos parâmetros da função de distribuição do SPI. Os resultados mostraram índices distintos, dependendo dos períodos de calibração usados. Com os mesmos padrões para todas as localizações estudas, quando os índices de seca foram calibrados com o período mais recente (1974-2014), a quantidade de eventos de seca (severa ou extrema) identificados foi menor, tanto no PDSI e SPI-9, quando comparado com os índices calculados com os outros períodos de calibração. Contudo a deteção de eventos húmidos extremos e severos identificados foi maior quando os índices de seca foram calculados usando este período. Em contraste, se o período de calibração selecionado foi o período 1892-1932, o oposto ocorreu com uma maior quantidade de eventos secos detetados e menor frequência dos húmidos. Estes resultados mostraram a importância que a seleção do período de calibração tem tanto para o PDSI quanto para o SPI-9.

O impacto nos índices de seca como o PDSI da seleção do método usado para o cálculo da evapotranspiração é relevante e não deve ser negligenciado. Tradicionalmente o PDSI usa a evapotranspiração potencial obtida com recurso à equação de Thornthwaite. Contudo, existem outros métodos, de base física, como é caso da equação da evapotranspiração de referência calculada pelo método da FAO-56, que permitem estimações mais corretas da evapotranspiração embora necessitem de dados relativos à temperatura máxima e mínima, radiação solar, velocidade do vento e humidade relativa, que muitas vezes não estão disponíveis. No Capítulo 4 compararam-se três metodologias de cálculo de evapotranspiração, nomeadamente, o método da FAO-56 usando as cinco variáveis enumeradas anteriormente e duas equações baseadas somente em temperatura, usando dados diários e mensais para o período 1981-2012 na região da Mongólia interior permitindo a análise dos diferentes métodos em vários tipos de clima. Os resultados do Capítulo 4 mostraram que os métodos baseados em temperatura para o cálculo da

evapotranspiração são insuficientes para descrever corretamente a sua variabilidade e amplitude em todos os tipos de clima. Seguindo esses resultados, no Capítulo 5, produtos de reanálise foram testados como uma alternativa quando dados *in situ* não estão disponíveis, levando à conclusão de que dados climáticos da reanálise com correção de de viés são uma boa alternativa às observações para estimativas da evapotranspiração de referência mensal e diária.

Seguindo os resultados dos Capítulos anteriores, o PDSI foi modificado para responder melhor às condições do clima em Portugal (Capítulo 6). Esta modificação, o MedPDSI, melhora o PDSI principalmente modificando o seu balanço hídrico, adaptando-o às condições climáticas do Mediterrâneo. A evapotranspiração de referência foi calculada recorrendo a um conjunto de dados de reanálise e de dados observados, de modo a corrigir o viés nas variáveis de superfície, cuja performance foi aferida no Capítulo 5 e seguindo a metodologia de correção de viés testada, também, no Capítulo 5. Os resultados mostraram que o balanço hídrico do MedPDSI apresentou diferenças relevantes quando comparado ao do PDSI. A evapotranspiração real (ET_{act}) do MedPDSI, apresentou uma variabilidade mais realista, principalmente na transição dos meses secos para os húmidos quando comparado com a ET_{act} do PDSI. Mais ainda, as secas identificadas com o MedPDSI começam, geralmente, mais cedo, são mais longas e mais severas, o que é uma vantagem para a gestão da seca, já que os sistemas de gestão do risco de seca poderão ser implementados mais cedo para melhor gerir os seus impactos, mitigando as potenciais consequências negativas de eventos secos.

Palavras-chave: índices de seca; MedPDSI; produtos de reanálise; evapotranspiração de referência; balanço hídrico do solo.

Contents

α_1	shape parameter ()
$\widehat{PRE}$	expected precipitation to maintain normal climate conditions (mm)
$\widehat{\alpha_1}$	shape parameter estimator ()
$\widehat{\beta_1}$	scale parameter estimator ()
$\widehat{ET_o}$	estimated values of reference evapotranspiration (mm)
$\widehat{\rho_j}$	estimated multiple regression coefficients ()
$\tilde{\phi}$	estimators of ϕ ()
s_O^2	variance of O ()
X_i	severity of the event relative to the current month ()
X_{i-1}	severity of the event relative to the previous month ()
γ_1	asymmetry ()
I_j	periodogram function of the j-th periodic component ()
$\widetilde{K}$	first approximation of the climatic characteristic ()
$\bar{O}$	(in the same units as the variables used in the linear regression)
$\bar{P}$	mean value of the dependent variable vector (in the same units as the
$\hat{P}$	predicted values of P (in the same units as the variables used in the
R^2	coefficient of determination computed with the ordinary least squares
g_{AB}	congruence coefficient ()
g_j	statistical test that tests for he significance of the j-th periodic
y_t	general model for a cyclic fluctuation ()
ε_t	white noise process ()
θ_j	amplitude of the j-th periodic component (Hz)
μ	expected value (in the same units as the variables)
a	intercept of a linear regression (in the same units as the variables used
AI	aridity index ()
AMJ	April - May- June
ANN	artificial neural networks
AO	arctic oscillation
ARIMA	auto regressive integrated moving averages
ASW	available soil water (mm)
a_T	dew point temperature correction based on aridity (℃)
b	slope of a linear regression ()
b_0	coefficient of regression of the regression forced to the origin ()
b_{jA}	loading from the rotated loading vector A from one solution ()
b_{jB}	loading from the rotated loading vector B from one solution ()
c	extreme dry (c= -4) and wet events (c=4) ()
c(t)	difference between the mean values of the P and O (mm)
cdf	cumulative distribution function
CDI	combined drought indicator
COTR	centro operativo e tecnológico de regadio
Cov_{OP}	covariance between the values O and P ()
CP	calibration period
CRU	Climate Research Unit
D	moisture departure mm $month^{-1}$)
DFJ	December–January–February

DP	deep percolation (mm)
DTS	deterministic trend scheme
e_a	actual vapor pressure (kPa)
ECMWF	European center for medium range weather forecasts
EDO	European drought observatory
EF	modeling efficiency ()
ENSO	El Niño–southern oscillation
e_s	saturation vapor pressure (kPa)
ET	Evapotranspiration (mm)
ET_{act}	actual evapotranspiration (mm)
ET_c	crop evapotranspiration (mm)
ET_o	grass reference evapotranspiration(mm)
ET_r	ASCE alfalfa reference evapotranspiration (mm)
FAO	food and agriculture organization
FAO-PM	food and agriculture Organization Pennam-Monteith reference evapotranspiration equation
fin	at the end of the month ()
FTO	regression forced to the origin (mm)
GCM	global circulation models
GG	Granger and Gray
GPCC	Global Precipitation Climatology Centre
GWP	Global Water Partnership
HS	Hargreaves-Samani evapotranspiration equation
ini	in the beginning of the month ()
IPMA	instituto português do mar e da atmosfera
JAS	July – August - September
JFM	Jannuary- February – March
JJA	June-July-August
K	climatic characteristic ()
K´	climatic coefficient ponderation factor ()
K_c	crop coefficient ()
K_{cb}	basal crop coefficient ()
K_{cor}	adjustment coefficient of K_e according to soil characteristics ()
K_e	soil evaporation coefficient ()
KPSS test	Kwiatkowski–Phillips–Schmidt–Shin test
k_{Rs}	empirical radiation adjustment coefficient
L	soil water loss (mm)
LAS SAF	Land Surface Analysis - Satellite Applications Facility
L_s	water loss in the surface layer (mm)
L_u	water loss in the underlying layer (mm)
m	n/2 if n is even or m = (n – 1)/2
MAM	March-April-May
MedPDSI	modification of the PDSI for the Mediterranean climate ()
MK	Mann-Kendall test
MM5	Fifth-Generation Penn State/NCAR Mesoscale Model
MMK	modified Mann-Kendall test
MPDSI	modified PDSI ()
MSE	mean square error (in the same units as the variables used in the linear
n	number of observations of a vector ()

NAO	north Atlantic oscillation
NCEP/NCAR	national center for environmental prediction/national center for atmospheric research
NCEP2	NCEP–DOE AMIP-II Reanalysis
NDVI	normalized difference vegetation index ()
NRMSE	Normalized root mean square error ()
N_s	maximum possible duration of sunshine or daylight hours (h)
n_s	actual duration of sunshine (h)
O	vector with the independent variables (in the same units as the
OBS	observations
OLS	ordinary least squares ()
OND	October – November - December
OYT	optimal yield threshold (mm)
p	duration factor associated to X_{i-1} ()
P	vector with the dependent variables (in the same units as the variables
p’	soil water depletion fraction for no stress
p_0	false alarm probability ()
PBIAS	percent bias (%)
PC	principal componente
PCA	principal component analysis
pdf	probability distribution function
PDSI	Palmer drought severity index ()
$PDSI_{2nd}$	second percentile of the PDSI series
$PDSI_{98th}$	98^{th} percentile of the PDSI series
PET	potential evapotranspiration (mm)
PHDI	Palmer hydrological drought index ()
p_j	wavelength of the j-th periodic component ()
PL	potential loss (mm)
PL_s	potential loss in the surface layer (mm)
PL_u	potential loss in the underlying layer (mm)
PM-ET_o	reference evapotranspiration computed using the FAO-PM equation (mm)
PMT	FAO-PM equation using temperature data only
PP	Phillips and Perron test
PR	potential recharge (mm)
PRE	Precipitation (mm)
PRO	potential runoff (mm)
PT02	high-resolution gridded precipitation data set for mainland Portugal
q	duration factor associated to Z_{index} ()
R	soil water recharge (mm)
R_a	radiation on the top of the atmosphere (MJ m^{-2} day^{-1})
RCM	regional circulation models
RDI	reconnaissance drought index ()
REAN	reanalysis
REOF	rotated loadings from the principal component analysis
RH	relative humidity (%)
R_{max}	soil moisture at saturation (mm)
RMSE	root mean square error (in the same units as the variables used in the
R_n	net radiation at the surface (MJ m^{-2} day^{-1})

RO	Runoff (mm)
RPC	rotated principal components
RR	regional reanalysis
R_s	short wave incoming radiation (MJ m^{-2} day^{-1})
Sc-PDSI	self calibrating PDSI ()
SD	sunshine duration (h)
SEDI	standardized evapotranspiration deficit index ()
SMA	soil moisture anomaly
SNIRH	sistema nacional de informação de recursos hídricos
SnsPI	nonstationary SPI ()
SON	September-October-November
SPDI	standardized Palmer drought index ()
SPEI	standardized precipitation evapotranspiration index ()
SPI	Standardized Precipitation Index ()
SPIt	time-dependent SPI ()
S_s	available soil water at the end of the previous month in the superficial
STL	seasonal and trend decomposition using loess
S_u	available soil water at the end of the previous month in the underlying
SWB	soil water balance
SWC	water holding capacity (mm)
T	mean temperature (ºC)
t	time (month)
T	mean air temperature (℃)
TAW	total available water (mm m^{-1})
TAW	total available soil water (mm)
TCI	temperature condition index ()
Tdew	dew point temperature (℃)
T_j	ratio between the average moisture demand and the average moisture
T_{max}	maximum temperature (℃)
T_{min}	minimum temperature (℃)
u_{10}	wind speed at 10 m height (m s^{-1})
u_2	wind speed at 2 m height (m s^{-1})
UNEP	United Nations environment programme
UR	un-rotated loadings
USDM	United States drought monitor
VCI	vegetation condition index ()
VHI	vegetation health index ()
VPD	vapor pressure deficit (kPa)
VR	varimax rotated loadings
WMO	world meteorological organization
WPDSI	weighed PDSI ( )
WRF	weather research and forecasting model
WS	wind speed (m s^{-1})
Z	maximum value of the periodogram ()
z_0	threshold for detecting if a peak is significant ()
Z_{index}	moisture anomaly index ()
Z_r	root depth (m)
α	evapotranspiration climatic coefficient ()
β	recharge climatic coefficient ()

β_1	scale parameter ()
Γ	gamma function ()
γ	runoff climatic coefficient ()
γ_c	psychometric constant (kPa $°C^{-1}$)
Δ	slope of vapor pressure curve kPa $°C^{-1}$
δ	soil moisture depletion coefficient ()
λ	latent heat of vaporization (MJ kg^{-1})
ρ_j	multiple regression coefficients ()
σ^2	variance ()
ϕ	estimable parameters of the used in the cyclic fluctuation equation ()
ω	frequency (Hz)
Φ	cumulative distribution function of a standard normal distribution ()

List of Figures

List of Tables

Chapter 1

Introduction

Water is a finite resource essential for all socio-economic development and for maintenance of ecosystems (Pereira et al. 2009). Human growth and development is responsible for the increase pressure on water resources. Moreover, the increased variability of climate, which is becoming less predictable, due to climate change, with higher temperatures and a larger variability in precipitation and temperature ranges, extreme events such as floods, heat waves, droughts, will become more frequent and intense. Thus, a better water management is a key for the adaptation of society and ecosystems to climate change (UNEP 2006; Pereira 2017).

Irrigated agriculture is still the largest user of freshwater, accounting for 46% of the Europe's total water withdrawal (European Environment Agency 2018). The effects of climate change, combined with the increasing demand for food supply, makes irrigated agriculture quite vulnerable to the future climate conditions. Thus, this reality, combined with the large uptake of water by irrigated agriculture exacerbates the need to make irrigated agriculture more efficient, regarding water use, which can be achieved by adopting improved irrigation methods and less consumptive crops. This would allow for an increase in irrigation efficiency and the use of other sources of water for irrigation, like wastewater or other forms of low quality waters that cannot be used for other purposes must be considered (Pereira et al 2009). Increasing water demand is due to a variety of factors: expansion of irrigation in agriculture, worlds population increase, changes in consumption patterns and living habits (Vörösmarty et al. 2000). All these factors combined with an increased uncertainty in climate, is leading towards an intensification of water scarcity, i.e., when the available water in a determined moment is not enough to meet local and global demands of water, endangering the sustainable development of human society.

Water scarcity occurs when there is a geographic and temporal negative balance between fresh water requirements and fresh water availability (Mekonnen and Hoekstra 2016).

Furthermore, water scarcity is not only due to physical shortage of quality freshwater but also due to the failure of regular supply of freshwater or because of inadequate infrastructure conditions. While reviewing the diversity of water scarcity definitions and indicators, Rijsberman (2006) defined water scarcity as lack of accessibility to safe and affordable water to satisfy the needs of a person. When this affects more people on a larger scale, that area is considered water scarce. Using the definition by Hoekstra et al. (2012) and Mekonnen and Hoekstra (2016) of blue water (fresh surface water and groundwater) scarcity, these authors found consistent yearly blue water scarcity worldwide, most noticeable in forest areas such as the Amazon or Congo basins. Furthermore, water scarcity was observed in southern and Western Europe, and was more frequent and intense in the summer months (July, August and September) but also ocurred throughout the rest of year, being less severe and spatially spread in the months from January to March. Hoekstra et al. (2012) and Mekonnen and Hoekstra (2016) concluded that 71% of the global population suffer from moderate to severe water scarcity every year.

Pereira et al. (2009) considered four different xeric regimes that may cause water scarcity, which may be natural or anthropogenic or may be permanent or temporary. Those regimes are:

(1) Aridity is a permanent and natural phenomenon of a region characterized by extremely low annual average rainfall and aggravated by high spatial and temporal variability in its occurrence, which has significant implications for the maintenance of ecosystems and limits any human activity. Aridity is usually studied as the ratio between precipitation and potential evapotranspiration, computed using the Thornthwaite equation (Thornthwaite 1948);
(2) Droughts, are also natural phenomenons, althought temporary, and are extreme events characterized by persistently below-average rainfall, often with uncertain duration and severity, and their occurrence is very difficult to predict. Droughts consequences results in a temporary decrease in the availability of water for their various uses. It is the uncertainty associated with the droughts that make this phenomenon extraordinarily complicated to manage;
(3) Desertification is permanent and man-induced, and develops over several generations, in which the imbalance in water availability is due to the impoverishment of the land (for example through soil erosion and salinization),

unsustainable use, on groundwater exploration, increasing frequency of rapid floods, degradation of riparian systems and the sustainability of ecosystems in general. Desertification effects are more noticeable in arid, semi-arid and sub-humid climates and are aggravated by the occurrence of droughts.

(4) Water shortage is not only related to the amount of water available to satisfy demand, but also due to the quality of water, which, sometimes, does not have enough quality to be used, for example, for domestic consumption or industrial applications. Water shortages are of anthropogenic, albeit temporary, origin and consist of overexploitation and quality degradation of surface or underground water resources, incorrect land use, and changes in ecosystem support capacity.

1.1 Droughts

Droughts are stochastic, natural phenomenons that stem from persistent conditions of low precipitation amounts, below average, for a specific period in a region. (Wilhite 2000; Zargar et al. 2011). From a physical standpoint, drought is a reduction, of the water balance terms, for a given location and period that affects soil water content, deep percolation and surface runoff (Pires 2015). Moreover, droughts are common to all types of climate and can occur in high or low rainfall areas and are spatially and context dependent (Quiring 2009). Droughts occurrence, especially in vulnerable regions, such as poor and arid countries can result in significant humanitarian problems. Being a climate event of slow-onset, drought effects accumulate over time, making the determination of the start and end of a dry spell very difficult to assess and thus hindering policy making regarding drought risk management (Wilhite and Glantz 1985). It is also difficult to assess drought severity and its impacts, because it depends not only on the duration of drought but of its intensity and the spatial extent of a dry spell, but also depend upon the local water demand, the local water management policies and the resilience of the ecosystems or human activities to droughts.

Drought impacts are felt on a multiplicity of areas (agriculture, environment, meteorology, hydrology, geology). Reported impacts of droughts are always associated with losses in agriculture and livestock farming being the most affected sector, but drought are also related with forest fires, freshwater supply and ecosystems, water quality and droughts impact significantly the energy, industry and tourism sectors (Stahl et al. 2016). The extreme drought of 2005-2006 that affected most of Iberian Peninsula had

significant impacts on cereal yield on the European Union, with an estimated reduction of 10% of cereal yields (UNEP 2006). Because drought affect most of human activities and ecosystems it does not have a consensual definition, since it depends on the point of view of the stakeholder and affected sector (Pereira et al. 2009; Mishra and Singh 2010). The World Meteorological Organization (WMO) defines drought as a normal and recurring event of the climate (Monacelli et al. 2005). It differs from aridity, in which very low precipitations are characteristic of the climate of the region. Drought should be relative to the average conditions of the balance between precipitation and evapotranspiration in a given area. Dracup et al. (1980) and Tate and Gustard (2000) provided a review of the many drought definitions. Moving from a conceptual definition to an operational one, Wilhite and Glantz (1985) distinguishes four types of drought: meteorological, agricultural, hydrologic, and socio-economic. This distinction of drought types is associated with a temporal evolution of the impacts, which is due primarily by the deficiencies in precipitation, called meteorological drought. Then the agricultural drought is felt, through the loss of moisture in the soil and then hydrological drought is noticed by the reduction of river flows and water storage in aquifers. When the reduction of available freshwater water starts to affect human activities and consumption it is considered that a socio-economic drought is occurring. Pereira et al (2009) defined drought as a natural temporary imbalance of water availability, consisting of a persistent lower-than-average precipitation, of uncertain frequency, duration and severity, of unpredictable or difficult to predict occurrence, resulting in diminished water resources availability and carrying capacity of the ecosystems. This definition provided a cohesive and multidisciplinary view of drought origins, its characteristics and potential impacts and is used throughout this Thesis.

The effects of drought will be felt first in agriculture, since there is less available water in the soil, only later the hydrological drought is felt, because the decrease in percolation and runoff continues over time, which results in a reduction of the recharge of aquifers and in surface water flows. All these constraints will have an impact on socio-economic activities, starting with agriculture, industry and reducing water availability for domestic consumption. These categories may be described in detail:

(1) Meteorological drought is characterized based upon the duration of the dry period and the degree of dryness (taking into account normal conditions). This type of

drought has to be addressed to the scale of the region since there is a high spatial variability of the precipitation that results from the atmospheric conditions.

(2) Agricultural drought is fundamentally caused by precipitation deficits, which affect the development of agricultural or forestry crops. This type of drought will depend upon the type of crop considered, that is, on the biological characteristics of the crop, and on the growth stage of the crop when drought settles. This category is ambiguous since the scarcity of water for agriculture is not only the result of deficit amounts of precipitation, but also due to a lack of adequate water and drought risk management in the region. This can occur either, because of an unsustainable increase of the agricultural area or because of the adoption of crops which are more water demanding, or simply by the lag between the precipitation regimes and the stages of growth of the crop.

(3) The hydrological drought is associated to the effects caused by the periods of lack of precipitation in the reduction of river flows, groundwater reservoirs, and storage in lakes, for example. This type of drought has to be considered at the level of the river basin. Changes to land use, such as dam construction, deforestation, and any type of soil degradation have significant consequences at the river basin level that may accentuate drought problems.

(4) Socioeconomic droughts arise when the lack of water begins to affect the general population and there is not enough water supply to fulfill all the demands. This type of drought relates more to an economic issue of supply and demand rather than with unfavorable climatic conditions. Climate change combined with increase in water consumption and lack of adequate management policies are exacerbating socioeconomic droughts.

1.1.1 Drought indicators and indices

Drought indices are numerical representations of drought (WMO and GWP 2016), and measure the various characteristics of drought, namely: duration, magnitude, intensity and spatial extent (Mishra and Singh 2010). The duration of a drought is expressed in years, months or weeks and is given by the period in which a series is below a pre-determined threshold. The magnitude of a drought is given by the sum of the drought index values for all the months within a dry event. The intensity is calculated from the ratio between magnitude and duration, and spatial extent is the area affected by a drought spell. Another usual term used to characterize droughts is severity, which is normally

associated with the degree of precipitation or moisture deficit, i.e., the numerical value of the drought index in a given moment in time.

Drought indices are tools used for measuring different events and conditions, since they can reflect climate dryness anomalies, when using precipitation based indices, or may be useful to quantify impacts on agricultural and hydrological systems by analyzing anomalies of soil moisture or of reservoir levels (Zargar et al. 2011). These indices are based upon inputs, which are climatic or hydrometeorological variables, and may be called drought indicators. These indicators can be precipitation, temperature, evapotranspiration, soil moisture, streamflow, groundwater or reservoir levels and even snowpack, or can be based upon combinations of these variables. The selection of what drought indicators to use depend upon the drought index and the types of drought the index aims at measuring (Zargar et al. 2011; WMO and GWP 2016).

Drought indices often result from a combination of these indicators or climatological variables. The essential variable used to compute meteorological drought indices is precipitation. Nevertheless evapotranspiration has been recognized as an equally important variable, measuring evaporative demand and was incorporated recently in drought indices, combining the contribution of precipitation and evapotranspiration: Such indices include the RDI (Reconnaissance Drought Index) (Tsakiris et al. 2007) or the Standardized Precipitation Evapotranspiration Index (SPEI) (Vicente-Serrano et al. 2010).

The impacts of temperature on droughts were given larger importance in recent years (Hobbins et al. 2017). However, the Palmer Drought Severity Index (PDSI) (Palmer 1965) was the first index to incorporate the effects of climate demand, by combining monthly precipitation and potential evapotranspiration, computed using the Thornthwaite equation (Thornthwaite 1948) in a water balance to obtain a moisture anomaly index, that after standardized could be used as a measurement of drought severity.

Although evapotranspiration (ET) is now considered an important climatic variable for drought monitoring, especially when temperature is increasing due to climate change, it is still a challenge to accurately incorporate this variable in drought indices. Evapotranspiration cannot be easily measured, like precipitation, and the best ET estimation is achieved using the FAO-PM equation (Allen et al. 1998), to compute the

reference evapotranspiration (PM-ET_o). PM-ET_o is the rate of evapotranspiration from a hypothetical crop with an assumed fixed height (12 cm), surface resistance (70 s m^{-1}) and albedo (0.23), closely resembling the evapotranspiration from an extensive surface of a disease-free green grass cover of uniform height, actively growing, completely shading the ground, and with adequate water and nutrient supply. Moreover, this equation provides appropriate estimates of the atmospheric evaporating capability and it can be applied to support irrigation management in agriculture, or to support drought management (e.g. Dai 2011). However, the computation of the PM-ET_o equation requires data relative to several climate variables: solar radiation (R_s) or sunshine duration, air relative humidity (RH), maximum and minimum temperature (T_{max} and T_{min}) and wind speed at 2 m height (u_2), most of which are often not available. This increased the research for alternative equations, capable of describing ET with lesser amount of variables and other data sources. Reanalysis products, remotely sensed data and forecast products, that have been improving in time, may provide such data with reasonable accuracy and with good spatial and temporal resolution, and thus may be useful for drought monitoring (Hobbins et al. 2017).

The use of temperature based equations to estimate ET_o for drought indices is common. Such equations are usually, the Hargreaves-Samani (HS) (Hargreaves and Samani 1985) or the Thornthwaite equation (Thornthwaite 1948). For example, the PDSI, SPEI and RDI were all introduced with potential evapotranspiration (PET) computed using the Thornthwaite equation. Nevertheless, since then, these indices have been tested with different ET_o estimates, including the PM-ET_o (e.g.: Dai, 2011; Vangelis et al., 2013; Vicente-Serrano et al., 2015). The RDI was not significantly influenced by different ET_o estimations (Vangelis et al. 2013; Vicente-Serrano et al. 2015), whereas the SPEI showed a larger sensitivity to ET_o computation methods (Vicente-Serrano et al. 2015). However, studies analyzing the influence of the ET_o equation on the PDSI showed contradictory examples: while Sheffield et al. (2012) observed decreasing trends PDSI over large areas of the world, when the PDSI was computed using PM-ET_o, which did not occur when the PDSI was computed with PET. Both Dai (2011) and van der Schrier et al. (2011) did not find significant changes on the PDSI computed with both evapotranspiration equations. The results by Sheffield et al. (2012) are in agreement with other studies, which observed decreasing trends in reference evapotranspiration even though mean temperature is increasing (Espadafor et al. 2011; Vicente-Serrano et al. 2014). This review showed that

additional studies were required to further understand the differences between temperature based methods to compute ET and ET estimated with the full sets of climatological variables, such as the PM-ET_o. Moreover, alternative sources of data to estimate PM-ET_o should also be tested so they can be used in drought indices to help accurate drought characterization and drought monitoring. Thus, given the importance of evapotranspiration, an important part of this Thesis, focused on analyzing the accuracy of different ET_o estimators, for different climates, in Chapter 4 and tested different data sources, such as reanalysis products, to estimate reference evapotranspiration in Chapter 5. The conclusions from these Chapters were then useful for Chapters 3 and 6 in which the drought indices, using evapotranspiration as input, were computed with PM-ET_o from reanalysis data sets.

The ubiquity of drought in all types of climate and affecting almost all sectors of society and environment systems as led to the creation of many drought indices, with over 150 indices developed (Niemeyer 2008; Zargar et al. 2011; WMO and GWP 2016). Drought indices may be grouped according to the type of impacts they relate (Zargar et al. 2011). However, Niemeyer (2008) suggested two new categories: remotely-sensed drought indices that use data retrived from remote sensing and composite or combined drought indices that result from the combination of many drought indices and indicators to monitor drought and its impacts. Accordingly, WMO and GWP (2016) followed a similar taxonomy to group drought indices using the following classification: (a) meteorology, (b) soil moisture, (c) hydrology, (d) remote sensing and (e) composite or modelled.

The most relevant drought indices for this Thesis were listed on Table 1-1. Thus, this Table included drought indices such as the Standardized Precipitation Index (McKee et al. 1995), the Palmer Drought Severity Index (PDSI) (Palmer 1965) and all its variations and drought indices, that despite not being used in the following chapters, are often studied and compared against the SPI and the PDSI, such as the abovementioned RDI and SPEI. Futhermore, in Table 1-1 some examples of drought indices based on remote sensing data and composite drought indices, were also included due to its relavance for drought monitoring. Similar reviews of drought indices are available in WMO and GWP (2016), Zargar et al. (2011). Table 1-1 differs from those studies regading the input requirements for the SPEI, RDI and PDSI and its variants, because it was considered that those indices require both precipitation and evapotranspiration data instead of precipitation and temperature data. As discussed above, those indices may be computed

using ET estimated based on temperature data only, however, is it preferable to use more realistic equations that consider the contribution of other variables such as radiation, wind speed or humidity rather than only temperature. The SPI characteristics and computational procedures were explained in detail in Chapters 2 and 3 and the PDSI and its variants including the MedPDSI were reviewed and described in Chapter 6.

Table 1-1 List with selected drought indices as examples of the diversity of indices and indicators available for drought monitoring. PRE is precipitation; ET is evapotranspiration; SWC is water holding capacity; T is temperature; WS is Wind speed;

Drought Index	**Input data**	**Distinctive characteristics**
Comprehensive drought indices		
Standardized Precipitation Index (SPI) (McKee et al. 1995)	PRE	Standardized, multiscalar index. Quantifies deviations from normal precipitation conditions. SPI is computed by adjusting a probability distribution function to the precipitation cumulated over a given number of months denoted as time scale. Gamma and Pearson III distributions are most used.
Reconnaissance Drought Index (RDI) (Tsakiris et al. 2007)	PRE, ET	Similar procedure to the SPI computation but considers the ratio PRE/ET to estimate departure from normal climate conditions.
Standardized Precipitation Evapotranspiration Index (SPEI) (Vicente-Serrano et al., 2010)	PRE, ET	Same as the SPI but the relation between the climate variables is given by PRE-ET.
Palmer Drought Severity Index (PDSI) (Palmer 1965)	PRE, ET, SWC	Combines PRE and ET in a simple water balance. It was created to characterize and evaluate meteorological droughts by measuring the deviations between the observed and the expected precipitation, which are first transformed into an anomaly moisture index and then into a drought index, which is classified in terms of severity. Over the years many limitations regarding the PDSI computation have

		been revealed (Alley 1985; Heddinghaus and Sabol 1991; Wells et al. 2004).
Self-calibrating PDSI (Sc-PDSI) (Wells et al. 2004)	PRE, ET, SWC	Based upon the PDSI. Changes all the empirical values of the original computation of the PDSI by values calculated dynamically based upon the characteristics present at each location. Allows for consistent results for different climates.
Z_{index} (Palmer 1965)	PRE, ET, SWC	An intermediary output of the PDSI. The Z_{index} was considered a better indicator of short-term agriculture drought because it is sensible to variations in soil-moisture (Karl 1986).
Weighed PDSI (WPDSI) (Heddinghaus and Sabol 1991)	PRE, ET, SWC	The WPDSI removes the backtracking procedure proposed by Palmer in the PDSI to make it more adequate for real-time monitoring of drought.
PHDI (Palmer 1965) Palmer hydrological drought index	PRE, ET, SWC	Modification of the PDSI to account for longer-term dryness that will affect water storage, streamflow and groundwater.
standardized Palmer drought index (SPDI) (Ma et al. 2014)	PRE, ET, SWC	Multiscalar, standardized index based upon the moisture departure index obtained from the PDSI water balance.
MedPDSI (Pereira et al. 2007) and Chapter 6)	PRE, ET, SWC	Modifies the original PDSI soil water balance to one applied to an olive orchard, by estimating separately soil evaporation and transpiration of the olive crop adopting the dual crop coefficient approach and uses PM-ET_o as the evapotranspiration input.
Modified PDSI (MPDSI) (Mo and Chelliah 2006)	Regional reanaysis data sets	Changed the PDSI original water balance to include reanalysis based data which are more accurate than those estimated by the original water balance. Such data included: potential evapotranspiration, evaporation, runoff, total soil moisture, and soil moisture change.
Standardized Evapotranspiration Deficit	T, WS	SEDI is a standardized multiscalar drought index, similar to SPEI but the P-ET component was

Index (SEDI). (Kim and Rhee 2016)		replaced by an ET deficit. ET deficit is difference between Potential evapotranspiration (PET) and actual evapotranspiration (ET_{act}). Both PET and ET_{act} were obtained using empirical function based on the modified Granger and Gray (GG) method (Anayah and Kaluarachchi 2014).
Remote sensing drought indices		
Vegetation Condition Index (VCI) (Kogan 1990)	Remotely Sensed	Remotely-sense based. The VCI is estimated using the Normalized Difference Vegetation Index (NDVI) and measures the vegetation water stress and is computed as the difference between current NDVI and the minimum NDVI of a long NDVI time series. The NDVI describes the difference between visible and near-infrared reflectance of vegetation and is used as an indicator of the greenness of the vegetation. (Zargar et al. 2011).
Temperature Condition Index (TCI) (Kogan 1990)	Remotely Sensed	Remotely-sense based. TCI estimates stress on vegetation caused by temperatures and excessive wetness, and is a modification of the VCI in which the NDVI is replaced by Land Surface Temperature (Zargar et al. 2011)
Vegetation Health Index (VHI) (Kogan 1990)	Remotely Sensed	Remotely-sense based. Is a weighed combination of TCI and VCI used for drought monitoring. Traditionally TCI and VCI components have equal weight in the definition of VHI (Zargar et al., 2011; Bento et al., 2018)
Composite drought indices		
United States Drought Monitor (USDM) (Svoboda et al. 2002)	Composite drought index	The USDM results from the combination of multiple indices and indicators such as the PDSI, SPI and vegetation and hydrologic data. It is considered ideal for monitoring agricultural droughts over all climate regimes, and is used to monitor drought in the United States of America.

European Drought Observatory (EDO) (Sepulcre-Canto et al. 2012)	Composite drought index	EDO is the European Commission's Joint Research Centre tool for assessing, monitoring and forecasting droughts in Europe. For that, it combines several drought indices and indicators including the SPI, a Soil Moisture Anomaly (SMA) index and the Combined Drought Indicator (CDI), which integrates data relative on anomalies of precipitation, soil moisture and satellite-measured vegetation condition, into a single index.

1.1.2 Drought indices as measure for agricultural water management and drought predictability

Vicente-Serrano et al. (2012) compared four versions of the Sc-PDSI (PDSI, WPDSI, PHDI and Z_{index}) the SPEI and SPI, the last two computed for several time scales, against streamflow data, soil moisture data, tree growth data and wheat yield and found that the SPI performed better than other indices in explaining the variability of all those variables. However, with SPEI, better correlations were achieved for the summer months (May – September) when compared against streamflow, and between May to October when compared against soil moisture. Similar results were obtained by Wang et al. (2015) in which the SPI, SPEI, Z_{index}, PDSI and Sc-PDSI were compared against soil moisture measures at different depths for various Chinese locations. Results showed that SPI and SPEI (using the optimum time-scale for the best correlation) had higher correlations with soil moisture for all soil depths than the PDSI counterparts did. Moreover, Z_{index} had better correlations with soil-moisture measure between 0-5 cm than the PDSI and the PDSI performed better when compared against the soil moisture measured at in the layer 40-50 cm depth. These results also agree with the results by Dai et al. (2004) in which the PDSI values were more consistently correlated with soil moisture than the Z_{index}, in many locations in China in the first 1 m of soil. However, Quiring and Papakryiakou (2003) found that the Z_{index} was better suited to measure agricultural drought in the Canadian prairies than the PDSI or the SPI. These good results of the SPI and SPEI when compared to the PDSI may be explained by the fact that they are multiscalar indices and the authors

computed the time-scales from 1 to 48 months and kept the strongest correlations between those two indices and the analyzed variables.

Vasiliades and Loukas (2009) found very good correlations between standardized hydrological variables (soil moisture and runoff) and the PDSI in its different variations (Z_{index}, PDSI, WPDSI and PHDI) in Greece. Soil moisture was better correlated with the Z_{index} with correlations values ranging from 0.85 to 0.89, which agrees with the study by (Karl 1986) in which the the Z_{index} was considered a better indicator of short-term agriculture drought because it is more sensible to variations in soil-moisture. Moreover, the WPDSI was found to better represent river discharges with correlations ranging from 0.78 to 0.82.

Another approach studied to assess the adequacy of drought indices to be used for drought management in agriculture is to relate drought indices with crop yields. These studies showed that the PDSI and its self-calibrating version were more apt to predict wheat yields in Greece (Mavromatis 2007) and Olive yields in Turkey (Tunalıoğlu and Durdu 2012), when compared to the SPI. Moreover, significant correlations were found between relative forms of the Z_{index} and main growing period of 8 crops and respective yield departures in the Czech Republic (Hlavinka et al. 2009). These authors also defined regional, crop-specific thresholds, using the Z_{index}, under which a soil moisture deficit has significant impacts on crops, that could be useful for drought monitoring and agricultural management (Hlavinka et al. 2009).

Although drought indices are useful to monitor and characterize drought, this assessment is mostly performed to evaluate past conditions, or at best, to characterize the current state of moisture anomalies. Thus, drought predictions schemes should be tested in order for drought indices to be used in early alerts systems tools.

The seasonal predictability of weather variables, from 1 to 6 months ahead, may be the most useful temporal scales for drought risk management and are associated with a temporal persistence of large-scale atmospheric circulation patterns (Pires 2015). One of the most important is the North Atlantic Oscillation (NAO) and it is responsible for controlling wet and dry rainfall regimes over Western Europe and positive phases of the NAO are associated with below-average precipitation or drought over southern and central Europe, the Mediterranean regions and the north of Africa, and conversely, above-average precipitation in Northern Europe (Moreira et al. 2016). Other relevant large

circulation patterns for Portugal and southern Europe include the East-Atlantic (EA) pattern, the Scandinavian (SCAND) pattern, and the East-Atlantic Western Russia (EAWR) pattern (Moreira et al. 2018). The seasonal predictability of droughts depends essentially on the predictive capacity of the evolution of these patterns (Pires 2015).

Drought prediction techniques may be grouped into three categories: statistical methods, physical based techniques or combinations of these two methods, which are usually called hybrid techniques (Pires 2015). The statistical methods consider the properties of drought indices time series or the indicators used to compute the drought indices. These are usually applied to the SPI and techniques range from time series modelling such as Markov Chains and the more complex ARIMA (Auto Regressive Integrated Moving Averages) models, but also, methodologies using artificial neural networks or log-linear models (e.g.: Paulo et al. 2005; Mishra and Desai 2005; Moreira et al. 2016). Another possible approach for drought forecasting is using physical models such as the one produced the by European Center for Medium Range Weather Forecasts (ECMWF) that provide probabilistic ensemble-based forecasts up to six months of several weather variables that can used to compute drought indices. Dutra et al (2014) used these ensemble forecasts to predict SPI values up to 6 months in the future. However, the skill score of predictions for the mid-latitude is not high and the computational requirements of using these models are still too demanding, which hinders a more frequent use of these methodologies. Hybrid methods combine these two approaches, statistics and physical-based techniques (e.g.: Moreira et al. 2016; Ribeiro and Pires 2016).

Drought forecasting using other drought indices besides the SPI are not common, however, Kim and Valdés (2003) tested artificial neural networks to forecast regional drought using the PDSI and Liu and Hwang (2015) studied local nonparametric autoregressive model with designed stochastic residual-resampling approach to produce ensemble drought forecasts using the PDSI.

1.2 Thesis objectives and structure

Improving knowledge regarding drought is of upmost important for better drought risk management, especially for agriculture systems, which is the economic sector most vulnerable to this extreme, natural, event. Thus, this Thesis focused on understanding the spatial and temporal variability of droughts and how these patterns vary with different drought indices, how those indices were parameterized and how the selection of the input

variables impact the detection of drought occurrence and its characteristics, such as duration and severity. Moreover, aiming at creating tools more adequate to help characterize drought impacts in agriculture, the importance of selecting accurate evapotranspiration estimates was assessed and alternative sources for this climatic variable were tested. Lastly, and considering previous results regarding drought variability and relevance of accurate evapotranspiration estimation, a modification of the PDSI was assessed, the MedPDSI, with the objective of better representing the Mediterranean climate and more specifically to better express the variability of soil moisture, with the final objective of being a useful tool for drought risk management in agriculture.

This Thesis is focused on three main topics, which were divided into five Chapters. Chapters 2 and 3 approach the subject of the spatial and temporal patterns of the SPI, and the analysis of the influence of long-term variability of precipitation on the SPI and of precipitation and evapotranspiration on the PDSI. Chapter 4 and 5 study evapotranspiration by, firstly, analyze the differences of ET estimated with temperature methods compared against PM-ET_o, which considers the contribution of other climate variables and, then, in Chapter 5, daily and monthly reanalysis products were tested as alternatives to estimate PM-ET_o when it cannot be computed due to lack of observed data sets. In Chapter 6, considering the results from the previous studies (Chapters 2 to 5), a version of the PDSI, the MedPDSI, adapted to local climate conditions was tested, in which the soil water balance was updated and modified and PM-ET_o from reanalysis was used in the computation of the MedPDSI. Moreover, in Chapter 1 a brief introduction was provided, containing the concepts of water scarcity, drought, and how drought indices may be used to monitor drought in agriculture. The last Chapter, 7, summarizes the overall conclusions of the PhD program and discuss future topics of research. Chapters 2 to 6 are adapted reproductions of studies that were published (or are in preparation for submission) in peer reviewed papers, and, in which, my contribution to each study was significant and which content is relevant for this Thesis. Table 1-2 discriminates my contribution to the development of each study.

The specific objectives of Chapters 2 to 6 are as follow:

1. Chapter 2: Identify and understand the main spatial patterns of drought in Portugal using different precipitation databases to compute the SPI at various time-scales.

2. Chapter 2: Detect significant linear trends of the SPI in Portugal and analyze the cyclic behavior of droughts throughout Portugal to determine the most common drought cycles in the region.
3. Chapter 3: Understand the impact of climate variability on drought indices such as the SPI and PDSI by analysing the influence of precipitation changes on the SPI dynamics and assess the impact of using different calibrations periods for the PDSI and SPI.
4. Chapter 4: Test different temperature based methods to compute ET, namely the HS equation and the FAO-PM equation using temperature data only, the PMT (Allen et al. 1998) in different climate conditions.
5. Chapter 4: Assess the spatial and temporal variability of these ET estimates and the respective climatic variables, in order to understand the contribution of the latter for the observed trends on the different methodologies for ET estimation.
6. Chapter 5: Assess the performance of different reanalysis products in estimating monthly PM-ET_o for the Iberian Peninsula and daily PM-ET_o for Continental Portugal, so they can be used for drought monitoring or water management in agriculture applications.
7. Chapter 6: Test the modifications to the PDSI, from which resulted the MedPDSI and analyze how these changes affect the overall behavior of the drought index for various locations in mainland Portugal comparatively to PDSI. Intermediary outputs of the MedPDSI and PDSI were also compared and the impacts of the self-calibrating procedures implemented were also assessed, by analyzing the frequency of extreme events, the severity of extreme wet and dry events.

Table 1-2 Personal contribution to the peer-reviewed papers adapted in Chapters 2 to 6.

Contributed to:	Raziei et al. (2015)	Moreira et al. (2015)	Paulo et al. (2016)	Martins et al. (2017)	Ren et al. (2016a)	Ren et al. (2016b)	Martins et al. (2017)	Paredes et al. (2018)	Pereira et al. (in prep.)
Study Conception				X		X	X		
Study design and implementation	X			X		X	X		X
Data collection	X			X			X	X	X
Data analysis	X		X	X	X	X	X	X	X
Results analysis	X	X	X	X	X	X	X	X	X
Original draft preparation	X	X		X	X	X	X		X
Artwork preparation	X	X	X	X	X	X	X	X	X

Chapter 2

SPI modes of drought spatial and temporal variability in Portugal: comparing observations and gridded data sets and assessment of drought cycles using Fourier analysis.

TAYEB RAZIEI, DIOGO S MARTINS, ISABELLA BORDI, JOÃO F SANTOS, MARIA M PORTELA, LUIS S PEREIRA, ALFONSO SUTERA (2015) SPI MODES OF DROUGHT SPATIAL AND TEMPORAL VARIABILITY IN PORTUGAL: COMPARING OBSERVATIONS, PT02 AND GPCC GRIDDED DATA SETS. 2015. WATER RESOURCES MANAGEMENT 29: 487-504

AND

ELSA MOREIRA, DIOGO S MARTINS, LUIS S PEREIRA (2015) ASSESSING DROUGHT CYCLES IN SPI TIME SERIES USING A FOURIER ANALYSIS. NATURAL HAZARDS AND EARTH SYSTEM SCIENCES 15:571-585

SPI modes of drought spatial and temporal variability in Portugal: comparing observations and gridded data sets and assessment of drought cycles using Fourier analysis.

Abstract. Regional drought modes in Portugal are identified applying the Principal Component Analysis (PCA) and Varimax rotation to the Standardized Precipitation Index (SPI) computed on various time scales using three precipitation data sets covering the period 1950–2003: (i) The observation data set composed of 193 rain-gauges distributed almost uniformly over the country, (ii) the PT02 high-resolution gridded data set provided by the Portuguese Meteorological Institute, and (iii) the GPCC data set with 0.5° spatial resolution. The main regions identified using PCA were then combined with cluster analysis applied to 74 time series with a 66 years length of SPI computed for a time-scale of 12 months to create homogenous groups of time series with similar temporal variability patterns in order to search for significant cycles of drought occurrence in Portugal using a Fourier analysis, applied to the SPI time series considering one SPI value per year relative to every month for each cluster identified. Results suggest that the three data sets agree in identifying the principal drought modes, i.e. two sub-regions in northern and southern Portugal with independent climate variability. The two sub-regions appear stable when the SPI time scale varied from 3- to 24-month, and the associated rotated principal component scores (RPCs) do not show any statistically significant linear trend. The degree of similarity between the rotated loadings or REOFs of different SPI time scales for the three used data sets was examined through the congruence coefficients, whose results show a good agreement between the three data sets in capturing the main Portuguese sub-regions. A third spatial mode in central-eastern Portugal was identified for SPI-24 in PT02, with the associated RPC characterized by a statistically significant downward trend. The stability of the identified sub-regions as a function of studied time period was also evaluated applying the same methodologies to a set of three different time windows and it was found that the southern sub-region is very stable but the northern and central-eastern sub-regions are very sensitive to the selected time window. The Fourier analysis revealed that the most frequent significant cycles in the three clusters that were identified showed that, drought periodicities vary among the clusters, pointing to a 6-year cycle across the country and a 9.4-year cycle in central and southern Portugal. Both of these cycles may have some correlation with the cycles of occurrence of weather regimes

mostly affecting Portugal. Relative to other months it was observed that cycles varied according to the common occurrence of precipitation: for the rainy months – November, December and January – cycles are similar to those for December; for the dry months – May to September – where the lack of precipitation masks the occurrence of drought, the dominant cycles are of short duration and cannot be related to the NAO or other large circulation indices to explain drought variability; for the transition months – February, March, April and October – 6-year and 3-year cycles were identified, the latter being more strongly apparent in central and southern Portugal. NAO influence is again identified relative to the 6-year cycles. The short cycles are apparently associated with positive SPI, thus with wetness, not drought.

Keywords: SPI, Principal component analysis, regional drought patterns, Trend analysis, Fourier Analysis, cluster analysis, North Atlantic Oscillation; regional drought patterns.

2.1 Introduction

Drought originates from a deficiency of precipitation (less than normal) over an extended period of time. It may occur in all climatic zones and are triggered by large-scale features of the atmospheric circulation, such as high-pressure systems, winds carrying continental rather than oceanic air masses, or high temperatures. However, drought characteristics vary significantly from one region to another due to local effects and its impact on local water resources availability compared to needs (Pereira et al. 2009). Thus, the identification of homogeneous regions within a country with distinct drought behaviors is of particular interest for drought risk assessment and for a more efficient water resources management at regional level.

Being drought a creeping phenomenon, it slowly sneaks up and impacts many sectors of the economy, the environment, and operates on many different time scales (Rossi 2000; Wilhite et al. 2007). Droughts can be grouped into various categories as meteorological, agricultural, hydrological, water supply and groundwater drought, which refer to both the time when a precipitation deficit is observed and the lag time for perception of effects of the precipitation deficit, by different sectors (Pereira et al. 2009). For example, soil moisture responds to precipitation deficits occurring on a relatively short time scale, whereas streamflow, reservoir storage and groundwater respond to precipitation deficits arising over many months. Among several available indices the Standardized Precipitation Index (SPI) (Mckee et al. 1993) is suited to monitor those kinds of drought (Heim 2002; Keyantash et al. 2002) since it is a standardized and multi-scale index and

allows objectively comparing dry/wet conditions of regions with different hydrological regimes.

Using the SPI and/or other indices, many authors have analyzed spatial modes and time variability of drought in different areas (e.g., Bordi and Sutera 2002; Bonaccorso et al. 2003; Vicente-Serrano 2006; Santos et al. 2010; Raziei et al. 2013). However, spatial modes of drought over a region might change as a function of the time scale considered, i.e. the type of drought analyzed. Vicente-Serrano (2006) showed that using rain-gauge data over the Iberian Peninsula the spatial modes of droughts are conditioned to the SPI time scale, pointing out the increasing spatial complexity of drought modes as the time scale of the index is increased. Raziei et al. (2011) identified four sub-regions for Iran applying the Principal Component Analysis (PCA) and Varimax rotation to the SPI on 12-month time scale computed using observations, gridded (Global Precipitation Climatology Centre, GPCC) and reanalysis (National Center for Environmental Prediction/National Center for Atmospheric Research, NCEP/NCAR) data sets. The stability of drought spatial modes as a function of SPI time scale and spatial resolution was also investigated for Iran applying PCA to SPI index computed for different time scales using the GPCC precipitation data set with 2.5-, 1- and 0.5-degree resolution (Raziei et al. 2013). Results showed that drought modes are quite stable when a coarse spatial resolution is used whereas at finer resolutions drought modes appear more sensitive to the index time scale becoming less spatially homogeneous as the time scale is increased.

Time variability of drought has been investigated for Portugal at regional level by Paulo et al. (2005) and Moreira et al. (2006) based on the stochastic properties of the SPI drought index time series using Markov chains and log-linear models. Drought linear trends in mainland Portugal were investigated by Paulo et al. (2012) using the Mann-Kendall trend test (Mann 1945; Kendall 1975). The spatial and temporal patterns of drought in mainland Portugal have been also investigated by Santos et al. (2010) and Martins et al. (2012) through the application of spatial classification methods to the SPI field on given time scales, identifying 3 and 2 sub-regions, respectively. However, the stability of the identified sub-regions with respect to different SPI time scales and precipitation data set was not taken into account.

Another important aspect of time variability of drought is its cyclicity and is often studied using time series of precipitation, streamflow and drought indices. To assess the cyclicity

of drought occurrence, various methods can be used and applied to those time series. Such approaches include the Fourier analysis (Rodrigo et al. 2000; Yadava and Ramesh 2007) also called spectral analysis (Mitra et al. 1991; Bordi et al. 2004a, b; Telesca et al. 2013) and the wavelet transform analysis (Labat 2006; Prokoph et al. 2012; Li et al. 2013). Research generally aims at finding a better explanation of time and space variability of the processes and relating the detected cycles with the periodicity of sea surface temperature, the solar cycles or teleconnection patterns.

Studies with annual or monsoon precipitation data series often identified cycles of around 11 years which were related with solar activity cycles (Mitra et al. 1991; Mazzarella and Palumbo 1992; Yadava and Ramesh 2007; Chattopadhyay and Chattopadhyay 2011). Studies on solar cycles are reported by Tsiropoula (2003) and Hathaway (2010). The cycle of solar activity is characterized by the rise and fall in the number and surface area of sunspots ranging between 9 and 13 years and averaging 11 years (Hathaway, 2010). Streamflow periodicity could also be related to solar cycles (Prokoph et al. 2012). A streamflow periodicity study has shown interannual 4- to 5-y, 14-y and multidecadal 25- and 50-y oscillations for Europe (Labat, 2006). The influence of North Atlantic Oscillation (NAO) and the Arctic Oscillation (AO) was considered in the study by (Lucero and Rodríguez 2002) showing that the European rainfall variability exhibits a 20- to 22-year NAO related bidecadal component of NAO. Gámiz-Fortis et al. (2011) studied streamflow variability in the Ebro basin and found that respective oscillation have different periodicity among the sub-regions considered. Rodríguez-Puebla et al. (2000) used 50 years series of 3-month cumulated precipitation in the Iberian Peninsula and applied Principal Components Analysis (PCA). They detected that NAO was the major source of interannual variability in winter precipitation and observed that the time series of precipitation and the NAO had a common peak at about 8 years while showing a significant coherence. An analysis of rainfall variability on decadal and centennial scales relative to southern Spain found an alternation of wet and dry periods, with various decades of duration (Rodrigo et al. 2000). This study also reported various periodicities in data series that allowed authors to identify NAO among the most possible causal mechanisms in the region. The precipitation variability study by Lucero and Rodriguez (2002) has shown both decadal and bidecadal oscillations averaging respectively 12 years and 20 to 22 years. A main conclusion of the study is that “the first principal component of the transformed bidecadal component of annual rainfall anomalies attains its positive

(negative) peak about 3 years before the bidecadal component of NAO reaches its negative (positive) peak" (Lucero and Rodriguez, 2002). Various studies later demonstrated the influence of NAO on precipitation and droughts (Trigo et al. 2004; Pires et al. 2007; Bierkens and van Beek 2009; Sousa et al. 2011).

Bordi et al. (2004a) using PCA applied to SPI-24 for the Elba basin and Sicily found significant peaks for periodicities of 9.6 year for Sicily and 12.0–9.6 year for Elbe basin. However, significant relations with NAO or the El Niño–Southern Oscillation (ENSO) were not found. In addition, other relevant peaks were close to the 11-year solar cycle. Telesca et al. (2013) used the SPI with various time scales of 1 up to 48 months, and applied a spectral analysis to each of local time series in the Ebro basin, Spain. For the SPI-12, 24 the 3.1-year, 4.1-year, the 5.3-year, the 8.8-year and the 17.6-year cycles are common to most locations. The 3-5 years band was considered as related to NAO Telesca et al. (2012).

Bordi et al. (2004b) characterized droughts with SPI-24 and studied their variability with PCA in Eastern China. The application of a spectral analysis to a principal component led to detect peaks characterizing the interdecadal, decadal, and interannual variability. A broad band peak was found for the interannual time scale of 4.0–3.7 years suggesting a link with ENSO. The other peaks lie near 6.9–8 up to 16 years and near 24 years. The precipitation study by Liang et al. (2011) applied to the North Western China identified significant periods of 2.3 and 3.3 years on a regional scale, which authors related with ENSO. Liu et al. (2013b) using Palmer Drought Severity Index (PDSI) (Palmer 1965) also detected cycles of 3-5, 5-7 and 8-10 years throughout the Qinghai Province, Northwest China. Results by Li et al. (2013) using the PDSI, also detected cycles of 3–5, 5–7 and 8–10 years throughout the Qinghai Province. Li et al. (2013) used clustering to define drought sub-regions in Southwest China with SPI and observed distinctive temporal evolution patterns of droughts in each subregion. The cycles varied from 2–3 years to 5–7 years.

The various studies reported above show that cyclicity is found for precipitation, streamflow and droughts, different methodological approaches lead to coherent results, cycles relate well with those of NAO, AO and ENSO as well as with solar cycles, and that detected cyclicity varies among sub-regions when PCA and cluster analysis identify those inside the region under study.

Results of a former study with loglinear models applied to droughts in southern Portugal have shown the existence of a long-term periodicity that could reflect the natural variability of the climate (Moreira et al. 2006). This long-term periodicity was expressed by the alternation between long periods with high and low frequency of severe and extreme droughts. A recent study using ANOVA-like inference coupled with log-linear models applied to 10 long series across Portugal also suggested a cyclic behavior of droughts with periodicity ranging from 26 to 30 years, mostly for the sites in central and southern Portugal (Moreira et al. 2012). These studies suggested using the Fourier analysis to detect the various cycles that contribute to the variability of droughts. Moreover, since cyclicity varies from one region to another (Bordi et al. 2004a, b, 2006; Raziei et al. 2009; Santos et al. 2010; Telesca et al. 2013), the use of PCA and cluster analysis has been considered for identifying possible regions within the country. Recently, Martins et al. (2012) used PCA applied to the SPI with 12 months time scale (SPI-12) to draw the spatial patterns of precipitation and drought in Portugal. This approach could then be combined with the Fourier analysis and verify if the cycles would change with the considered region. The Fourier analysis, also called spectral analysis, uses the Fourier decomposition of time series and the periodogram device (Pollock 1999; Bloomfield 2000) with the aim of find cycles within a given series. As referred before, various applications in hydrology and climatology studies are reported.

Considering the review presented before, this Chapter aims at understanding the stability of the spatial patterns of drought and, for that purpose, various SPI time scales (3-, 6-, 12- and 24-month) and three precipitation data sets: observations, the high-resolution gridded precipitation data set for mainland Portugal (PT02) (Belo-Pereira et al. 2011) and GPCC data set at 0.5-degree resolution were considered. Furthermore, to characterize the temporal variability of droughts in the region and considering the spatial patterns detected in this study, and in the literature, linear trends were investigated followed by Fourier analysis. This spectral analysis was applied to the SPI-12 time series to assess the cyclic behavior of droughts throughout Portugal, to detect the most representative cycles in each region and to identify the possibly related driving forces that determine the periods characterizing the detected cycles.

2.2 Data and Methods

2.2.1 Precipitation data sets

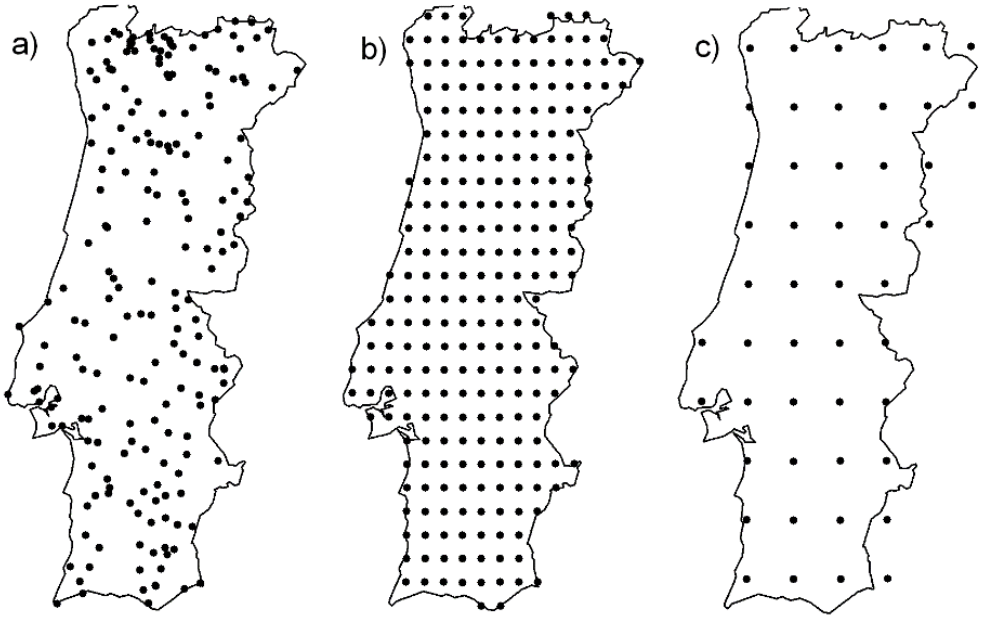

Figure 2-1 Spatial distribution of stations/grid points over Portugal for: a) observations, b) PT02, and c) GPCC data sets.

To study the spatial and temporal variability of drought over Portugal, observations, PT02 and GPCC gridded precipitation data sets for the common period 1950–2003 were used. The selected period was set to coincide with the time period of the Portuguese PT02 high-resolution daily precipitation data set developed by Belo-Pereira et al. (2011).

The observations data set consists of 193 stations uniformly distributed over mainland Portugal (Figure 2-1a). Most of the stations were provided by the Portuguese Water Institute, whereas 27 of the used stations belong to the Meteorological Service of Portugal. The PT02 data set has 250 grid points distributed over mainland Portugal (Figure 2-1b) with 0.2-degree resolution and covers the period 1950–2003. To develop PT02 data set a dense network of rain gauges distributed over Portugal (more than 400 stations) was used. The ordinary kriging method with the exponential variogram was used to interpolate the data set into the 0.2°×0.2° mesh grid. The performance of the gridded output was compared with observations at selected stations through the country using cross-validation method coupled with some statistic tools (Belo-Pereira et al. 2011). The PT02 was also compared with the outputs of some available gridded and reanalysis data sets and it was found that the PT02 well spatially represent the geographical variation of

precipitation field over main land Portugal (Belo-Pereira et al. 2011). For the present study, monthly accumulations of PT02 daily precipitation data were used for the SPI computation at each grid point.

The GPCC Full Data Product Version 5, updated in December 2010, is a gauge-based gridded monthly precipitation data set for the global land surface, available in 2.5º, 1º, and 0.5º degree resolutions. The data set covers the period 1901–2009 and is based on both non real-time and real-time stations (Schneider et al. 2010). GPCC monthly precipitation analysis products are based on anomalies from climatological normals at the stations, or from GPCC high-resolution gridded climatology where no station normal is available. The GPCC precipitation climatology (reference period 1951–2000) consists of normals collected by WMO, delivered by the countries to GPCC, or calculated from time series of monthly data (with at least 10 complete years of data) available in the GPCC data base. Raziei et al. (2011) assessed the spatial and temporal variability of drought over Iran using the GPCC data set and found satisfactory agreement with observations. For the present study, the 0.5-degree spatial resolution (i.e., the finest resolution provided by GPCC) is used. This data set has 49 grid points over mainland Portugal (Figure 2-1c).

The Fourier analysis was conducted using monthly precipitation time series from 1941 to 2006 (66 years) relative to 74 sites across Portugal (Figure 2-2). Data from weather stations were obtained from the meteorological services (IPMA) and those of rainfall stations refer to the environmental services (SNIRH). Data quality was assessed using the Kendall autocorrelation test, the Mann– Kendall trend test and the homogeneity tests of Mann Whitney for the mean and the variance (Helsel and Hirsch 1992). To estimate missing values of monthly precipitation, maintenance of variance extension techniques were applied (Hirsch 1982; Vogel and Stedinger 1985). These data sets, previously used in other studies (e.g.: Martins et al. 2012; Paulo et al. 2012) were completed with techniques described by Rosa et al. (2010). Series retained did not have more than 250 gaps and all series covered the referred period of 66 years.

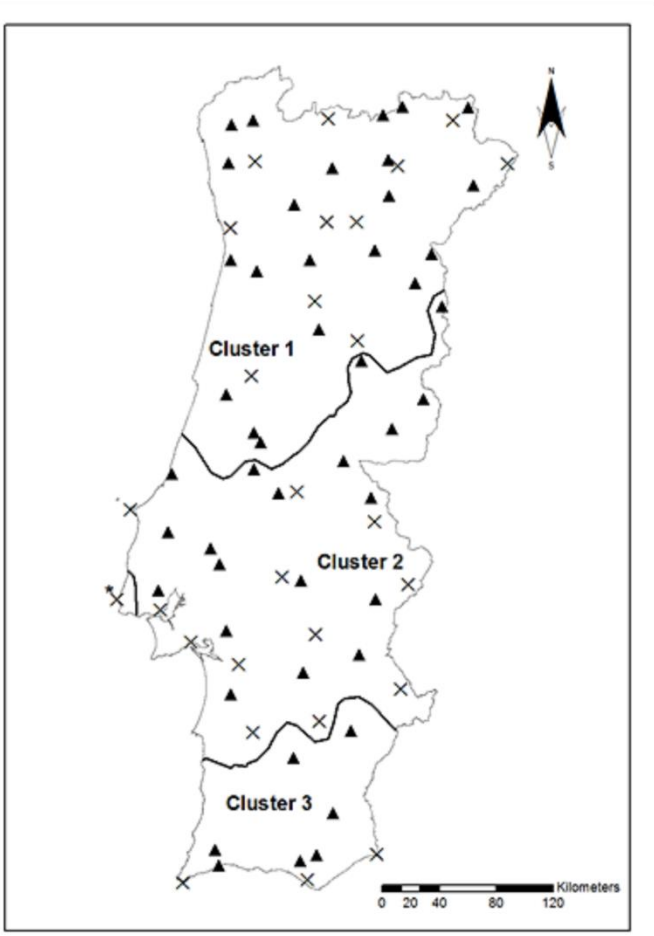

Figure 2-2 Spatial distribution of the meteorological stations (x) and rainfall stations (▲) used in the study and delimitation of drought clusters; (*Station included in cluster 3)

2.2.2 Standardized Precipitation Index

Drought conditions were assessed through the SPI computed on 3-, 6-, 12- and 24-month time scales following the original definition by McKee et al. (1993), thus representing various kinds of drought. The SPI computation for a given location and month of the year is based on the long-term precipitation records accumulated over the selected time scale. The empirical probability distribution of the accumulated precipitation is fitted to a theoretical distribution. Originally McKee et al. (1993) used the two-parameter Gamma distribution for fitting the observed precipitation distribution, which as became the most usual for computing SPI, although, for some regions other distributions (e.g. Pearson III) may be more suitable (Guttman 1999). In the present study, the original definition of the SPI is applied. The cumulative theoretical distribution is then transformed through an equal-probability transformation into a normal distribution. Thus, the SPI represents a Z-score, or the number of standard deviations above or below that a precipitation event is

from the mean. Positive SPI values indicate greater than median precipitation, and negative values indicate less than median precipitation.

Table 2-1 SPI drought class classification (McKee et al. (1993))

Code	Drought classes	SPI values	Time in category (%)
1	Non-drought	$SPI \geq 0$	
2	Near normal	$-1 < SPI < 0$	34.1
3	Moderate	$-1.5 < SPI \leq -1$	9.2
4	Severe	$-2 < SPI \leq -1.5$	4.4
5	Extreme	$SPI \leq -2$	2.3

For the Portuguese conditions, where a dry summer period of near 6 months occurs, droughts impacting the hydrologic regime are better assessed when using the 12-month time scale (Paulo and Pereira 2006; Santos et al. 2010). Hence, former studies on drought variability and drought class transitions were performed with the SPI 12-month (Moreira et al. 2006, 2012; Martins et al. 2012). Therefore, the Fourier analysis was applied to the time series of SPI with a 12-month time scale (SPI-12), computed from the 74 monthly precipitation time series. The respective monthly drought classes were then computed based on Table 2-1.

2.2.3 Principal Component Analysis, congruence coefficient and linear trend analysis

For each time scale considered, the S-mode PCA (Rencher 1998) and Varimax rotation were applied to the SPI field to search for aggregations of climate sub-regions that experienced similar drought (wetness) conditions during the study period. The PCA consists in computing the covariance matrix of the SPI data with the corresponding eigenvalues and eigenvectors (Rencher 1998). The projection of the SPI fields onto the orthonormal eigenfunctions provides the principal components or PC score time series, whereas the spatial patterns of eigenvectors (loadings) are proportional to the correlation field between the original data (SPI time series at single station/grid points) and the corresponding principal component time series. More localized patterns are obtained by applying the Varimax rotation to selected loadings (rotated loadings or REOFs in the text). Since such orthogonal rotation preserves the orthogonality in time, i.e. the rotated principal components are not correlated (Rencher 1998; Mestas-Nuñez 2000), the method allows finding sub-regions within the country that have rather independent drought behaviors. Following the rule by North et al. (1982), the sampling errors at 95%

confidence level of the eigenvalues associated with the principal components have been estimated, allowing to establish how many loadings to retain for rotation.

To assess the degree of similarity between rotated loadings of the SPI on different time scales for a given data set and/or inter-comparisons of the loadings configurations relative to the three used data sets, the vectors of the loadings matrices are compared using the congruence coefficient (Harman 1976):

$$g_{AB} = \frac{\sum_{j=1}^{n}(b_{jA}\, b_{jB})}{\sqrt{\left(\sum_{j=1}^{n} b_{jA}^2\right)\left(\sum_{j=1}^{n} b_{jB}^2\right)}} \qquad (2.1)$$

where b_{jA} is a loading from the rotated loading vector A from one solution, b_{jB} is a loading from the rotated loading vector B from another solution, and n is the number of variables in each eigenvector, which for the S-mode PCA corresponds to spatial configuration of the points. The coefficient ranges in value from +1 for perfect agreement (or –1 for perfect inverse agreement) to 0 for no agreement. The congruence coefficient is preferred to the correlation coefficient (or pattern correlation) for measuring pattern similarity because it preserves the mean (whereas the correlation coefficient measures deviations from the mean), which is an important feature of a PC loading vector (Richman 1986). Following Richman (1986) and the references therein, the guidelines listed below were adopted as an indicator of the degree of likeness between patterns: excellent ≥ 0.98, 0.98 > good ≥ 0.92, 0.92 > borderline ≥ 0.82, 0.82 > poor ≥ 0.68, very poor < 0.68. To do so, all loadings vectors relative to SPI time scales obtained for observations and GPCC data sets were re-gridded to the same mesh grid as for PT02 (i.e., 0.2-degree spatial resolution) to achieve similar spatial dimensions which is prerequisite for computation of the congruence coefficient.

Finally, the time variability of the selected RPC scores were examined for possible trends of drought aggravation or attenuation in the identified sub-regions using linear regression and the Mann-Kendall trend test (Mann 1945; Kendall 1975) and the magnitude of the trends were estimated using the Sen Slope estimator (Sen 1968).

2.2.4 Fourier analysis of time series

Regular or near regular cycles are often encountered in nature. The Fourier analysis methodology can be referred to as a method aimed to uncover hidden periodicities and, in particular, to extract regular cyclical components from the time series when the

quantity of data is not excessively large. The Fourier analysis is a method based upon the Fourier decomposition of a series, which is a matter of explaining the series entirely as a composition of sinusoidal functions. This originates in the idea that, over a finite interval, any analytic function can be approximated, to whatever degree of accuracy is desired, by taking a weighted sum of sine and cosine functions (Pollock 1999).

Let m = n/2 if n is even or m = (n – 1)/2 if n is odd, with n the number of observations in a time series. The general model for a cyclic fluctuation would include the frequencies, $\omega_j = (2\pi j)/n$, j=0,…,m which are equally spaced in the interval $[0,\pi]$ and takes the form

$$y_t = \sum_{j=0}^{m}\{\phi_{j,1}\sin(\omega_j t) + \phi_{j,2}\cos(\omega_j t)\} + \varepsilon_t \qquad (2.2)$$

where t represents time, $\phi_{j,1}$ and $\phi_{j,2}$, j=0,...,m are estimable parameters and ε_t, t=1,...,n are independent and identically distributed random variables with null mean value and variance σ^2, representing the residual element which is called the white noise process (Pollock 1999).

The factor $\theta_j = \sqrt{\phi_{j,1}^2 + \phi_{j,2}^2}$, j=0,…, m, (2.3) is the amplitude of the j-th periodic component and indicates the importance of that component within the sum. The parameters $\phi_{j,1}$ and $\phi_{j,2}$, j=0,...,m are estimated using the least squares method and the expressions for their estimators are given by (Pollock 1999)

$$\tilde{\phi}_{0,2} = \frac{\sum_{t=1}^{n} y_t}{n}; \tilde{\phi}_{j,1} = \frac{2\sum_{t=1}^{n}\sin(\omega_j t)y_t}{n}; \tilde{\phi}_{j,2} = \frac{2\sum_{t=1}^{n}\cos(\omega_j t)y_t}{n}, j = 1, \dots, m \quad (2.4)$$

Then an estimator for θ_j, $\tilde{\theta}_j$, can be obtained and a statistic to test the significance of the j-th periodic component is given by (Fisher 1929; Nowroozi 1967)

$$g_j = \frac{\tilde{\theta}_j^2}{\sum_{i=1}^{m}\tilde{\theta}_i^2}, j = 1, \dots, m \qquad (2.5)$$

The total sample variance is given by $\sum_{j=1}^{m}\frac{\tilde{\theta}_j^2}{2}$ and the proportion of that variance which is attributable to the periodical component at frequency ω_j is $\frac{\tilde{\theta}_j^2}{2}$.

In order to provide a graphical representation of the sample variance decomposition, the elements of the total variance must be scaled by a factor of n. The graph of the function $I_j = \frac{n\,\tilde{\theta}_j^2}{2}$ is known as the classical periodogram (Pollock 1999). The graphic representation of I_j for j=1,...,m (Figure 2-3), allows to detect the existence of relevant

periodic components of the time series, as well as the importance of each one. The wavelength, i.e., the period in time units of the j^{-th} periodic component, is given by $p_j = n/j$.

In the current study, the number of observations is n = 66 in all locations, thus m = 33. For each of the studied time series, the I_j for j=1,...,m was calculated and graphically represented in order to visualize the highest peaks, which correspond to the leading periodic components of the time series. The observation of several high peaks indicates the existence of several periodic components with different periods. However, in general, few of those peaks represent a strong periodical signal that cannot be assigned to statistical fluctuations in a merely white noise process.

The assessment of the statistical significance of a peak involves testing the null hypothesis, H_0, that the observed time series are purely white noise against the alternative, H_1, stating that a periodic signal is present there. The statistical distribution of the periodogram is well known for the even-sampling case, which corresponds to equally spaced observations (Scargle 1982). The most important result is that if the observations in the time series are pure Gaussian noise the I_j, j=1,…,m are independent and exponentially distributed. In this situation, it is reliable to use the false alarm probability to assess the statistical significance of the highest peaks in the periodogram, which states that if $Z = \max I_j$, j=1,…,m is a maximum value of the periodogram, then the probability for Z being over the set of the m periodogram values is given by

$$\Pr(Z > z) = 1 - [1 - \exp(-Z)]^m \qquad (2.6)$$

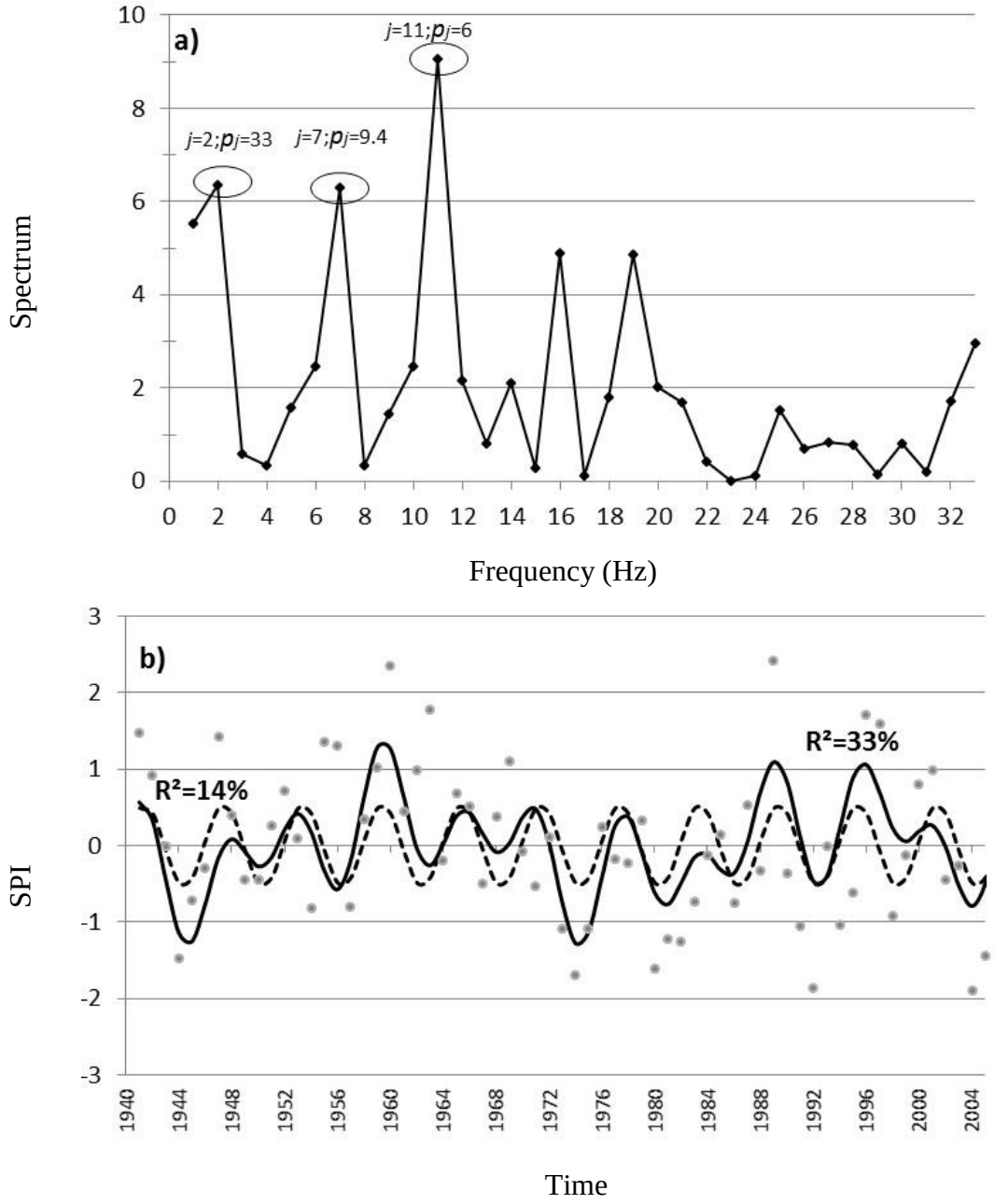

Figure 2-3 Reguengos: (top) graph of I_j , j = 1,...,33; (down) SPI December values (grey dots) vs. fitted sinusoidal wave of 6-year period (dashed line) vs. fitted model resulting from summing up the waves with period 6, 9.4 and 33 years (black line).

So, a threshold z_0 can be used for detecting if a peak is significant, which is defined as

$$z_0 = -\ln\left[1 - (1 - p_0)^{1/m}\right] \quad (2.7)$$

where p_0 is the false alarm probability, a fixed small value usually selected between 0.01 and 0.1 (Scargle, 1982). For instance, in "Reguengos" time series the highest peak is attained for j = 11 (I_{11} = 9.05), which corresponds to a periodic component with 6 years period (Figure 2-3). Choosing a false alarm probability of 0.1, with the number of periodical components m = 33, the value z_0 obtained is 5.75, which allows concluding

that the peak is significant. In this time series, two other peaks are significant, those for j = 2 and j = 7 corresponding to sinusoidal waves with 33 and 9.4 years period (Figure 2-3). If one considers a false alarm probability of 0.01 instead of 0.1, then only the peak for j = 11 with 6 years period can be considered significant.

The fitted sinusoidal function of 6 years period is presented in Figure 2-3 simultaneously with the "Reguengos" time series and obviously has the best goodness of fit to the time series among all other periodic components, R^2=0.14 (grey line). For a better goodness of fit between the sinusoidal wave and the time series, the cycles corresponding to the significant peaks in the periodogram can be summed up, thus j = 2, 7, 11, to build a general model for a non-regular cyclic fluctuation. In Figure 2-3, the wave resulting of summing up the significant cycles with period 6, 9.4 and 33 years (black line) was also represented. Some improvement of the goodness of fit is then obtained, with R^2 = 0.33.

2.3 Results and Discussion

2.3.1 Principal Component Analysis

For each SPI time scale, the number of principal components retained for Varimax rotation was selected based on the scree plot and the North's rule of thumb criterion (Figure 2-4). Based on Figure 2-4, the first leading components relative to the eigenvalues whose 95% confidence intervals do not overlap were retained for Varimax rotation. The first four components were retained for SPI-3, SPI-12 and SPI-24 when using observations data set. The same number of components were retained for SPI-12 and SPI- 24 associated with PT02 data set. For the SPI-6 relative to the observations data set the first three components are selected for rotation, whereas only the first two components are retained for SPI-3 and SPI-6 of PT02 data set. Differently, results for the GPCC data set suggested retaining only the first two leading components for all SPI time scales.

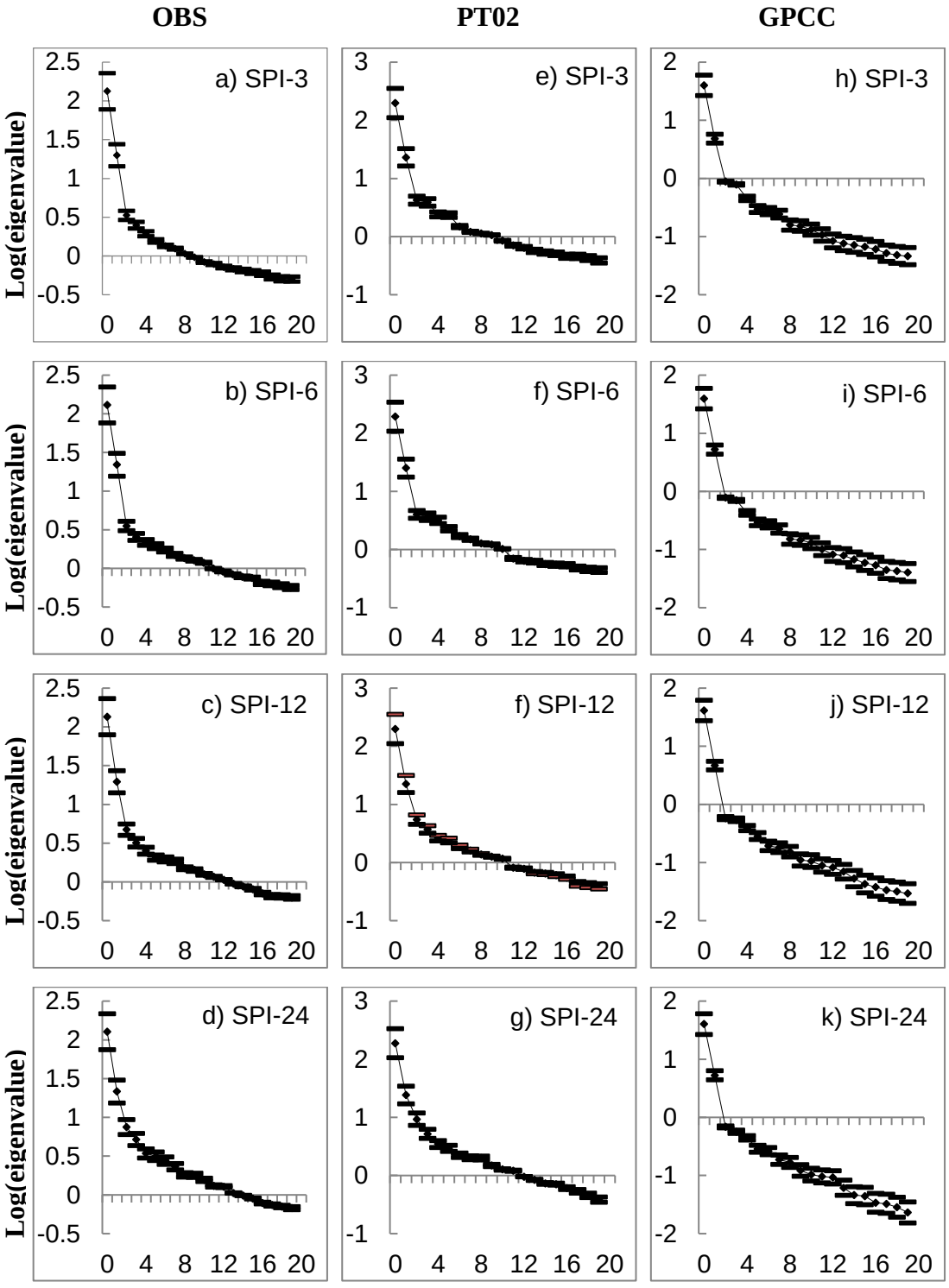

Figure 2-4 First twenty eigenvalues, using the logmartic scale, with the corresponding errorbars at 95% confidence level resulting from the PCA applied to the SPI computed on different time scales (rows) using observations (193 stations) and PT02 and GPCC data sets (columns). Adapted from Raziei et al (2015).

Table 2-2 presents the explained variances of un-rotated and Varimax rotated components relative to the considered SPI time scales and data sets. The Table showed that the first

un-rotated component relative to observation data set explains from 66% to 69.9% of the total variance depending on the time scale, with the minimum and maximum variances observed for SPI-24 and SPI-12, respectively. The second un-rotated component explains about 10% of the total variance, while the third component explains very small variances from SPI-3 to SPI-6 (1.7%–1.8%) and it accounts for 2.4% and 3.9% for SPI-12 and SPI-24, respectively. Similarly, the fourth component accounts for a very small percentage of variance. For the case of PT02 (Table 2-2) the first un-rotated component explains 77.8%–78.3% of the total variance for SPI-3 to SPI-12, but it decreases to 74.5% for SPI-24 due to an increase in the explained variances of the second and third components. Similar results were observed relative to the variances of the first GPCC un-rotated components, ranging between 80.9% and 83.9% (Table 2-2). It can be noted that the variance explained by the first un-rotated component is higher in GPCC than in PT02, and lower than both in the observation data set; this can be attributed to the effect of the coarse spatial resolution of GPCC compared to those for PT02 and observations. This feature is in agreement with the results found by Raziei et al. (2013) who compared the spatial modes of drought variability in Iran using GPCC data sets having different spatial resolutions.

Table 2-2 Percentage of the total variance explained by the un-rotated (UR) and Varimax rotated (VR) loadings of the SPI on different time scales computed using observations and gridded PT02 and GPCC data sets. Units are %

Observations		SPI-3		SPI-6		SPI-12		SPI-24	
	PC	UR	VR	UR	VR	UR	VR	UR	VR
	1	68.9	36.9	67.4	38.1	69.9	39.1	66.0	37.7
	2	10.3	36.5	11.4	35.9	10.1	38.8	11.2	36.3
	3	1.7	4.4	1.8	6.6	2.4	4.1	3.9	6.4
	4	1.3	4.2			1.7	2.0	2.7	3.3
	Total	82.1	82.1	80.6	80.6	84.1	84.1	83.7	83.7
PT02		SPI-3		SPI-6		SPI-12		SPI-24	
	PC	UR	VR	UR	VR	UR	VR	UR	VR
	1	77.8	44.3	76.5	45.0	78.3	41.5	74.5	38.4
	2	9.1	42.5	10.0	41.15	8.9	41.1	9.6	34.6
	3					2.1	5.1	3.7	14
	4					1.5	3.1	2.1	3
	Total	86.8	86.8	86.5	86.5	90.7	90.7	90.0	90.0
GPCC		SPI-3		SPI-6		SPI-12		SPI-24	
	PC	UR	VR	UR	VR	UR	VR	UR	VR
	1	81.1	46.6	80.9	48.6	83.9	49.5	82.1	47.9
	2	9.9	44.3	10.7	43.0	9.5	43.9	10.8	45.5
	Total	90.9	90.9	91.6	91.6	93.4	93.4	93.0	93.0

2.3.2 Drought spatial variability

The rotated loadings (REOFs) for the different SPI time scales and data sets are shown in Figure 2-5. For the SPI on 3-month time scale, the three data sets identified two sub-regions of drought variability in southern and northern Portugal that are characterized by high positive rotated loading values greater than 0.6 (Figure 2-5). A similar drought spatial pattern is obtained for SPI-6 and SPI-12 (Figure 2-5b and Figure 2-5c). When the longer time scale is considered (24-month), a hint of a third sub-region in central-eastern Portugal appears for the PT02 data set with rotated loading values between 0.6 and 0.8 (Figure 2-5d). This feature is also visible at 12-month time scale for PT02 data set (Figure 2-5c, yellow area in the third rotated loading). The identified northern sub-region is a mountainous area and is heavily influenced by the Atlantic air masses that favor in this area the highest precipitation amount of the continental Portugal, whereas the southern sub-region has a much smoother and flatter relief and is characterized by a sub-humid climate. The relatively high elevation of the third sub-region and its distance from the Atlantic Ocean mitigate the direct influence of the maritime air masses, resulting in a different precipitation regime in that area. However, despite that, the identified spatial mode of the third sub-region explains a relatively small percentage of the total variance (14%) and the loadings are not high enough, to consider it of particular relevance for the spatialization of hydrological droughts. These spatial patterns of the loadings appear consistent with the results obtained by Santos et al. (2010) and Martins et al. (2012) pointing to the northern and southern Portugal as distinct areas of drought variability. However, because different critical values of the loadings were used in those studies (0.7 and 0.8, respectively), those authors achieved smaller sub-regions than in the present study.

Thus, results suggested that the northern and southern sub-regions are the leading drought modes for Portugal, that are well captured by the three data sets with high loading values at all selected time scales. Differently, the central-eastern sub-region is less stable with respect to time scales and the data set considered. The absence of the third sub-region in the rotated loadings of GPCC data set could be related to the fact that limited Portuguese stations were included in the GPCC gridding procedure, whereas a much denser network of stations were used in developing the PT02 data set. In addition, the number of stations considered for gridding PT02 data set is larger than the number of stations of the observation data set in the central eastern region. Moreover, the GPCC rotated loadings

show to be spatially more homogeneous when compared with those of observations and PT02 data sets (Figure 2-5). This is in agreement with the results found for Iran by Raziei et al. (2013), indicating that drought modes obtained with the finer spatial resolution have more spatial inhomogeneity. These results also indicate a slight increasing complexity of drought spatial variability for longer SPI time scales as was argued for Spain (Vicente-Serrano 2006) and Iran (Raziei et al. 2013).

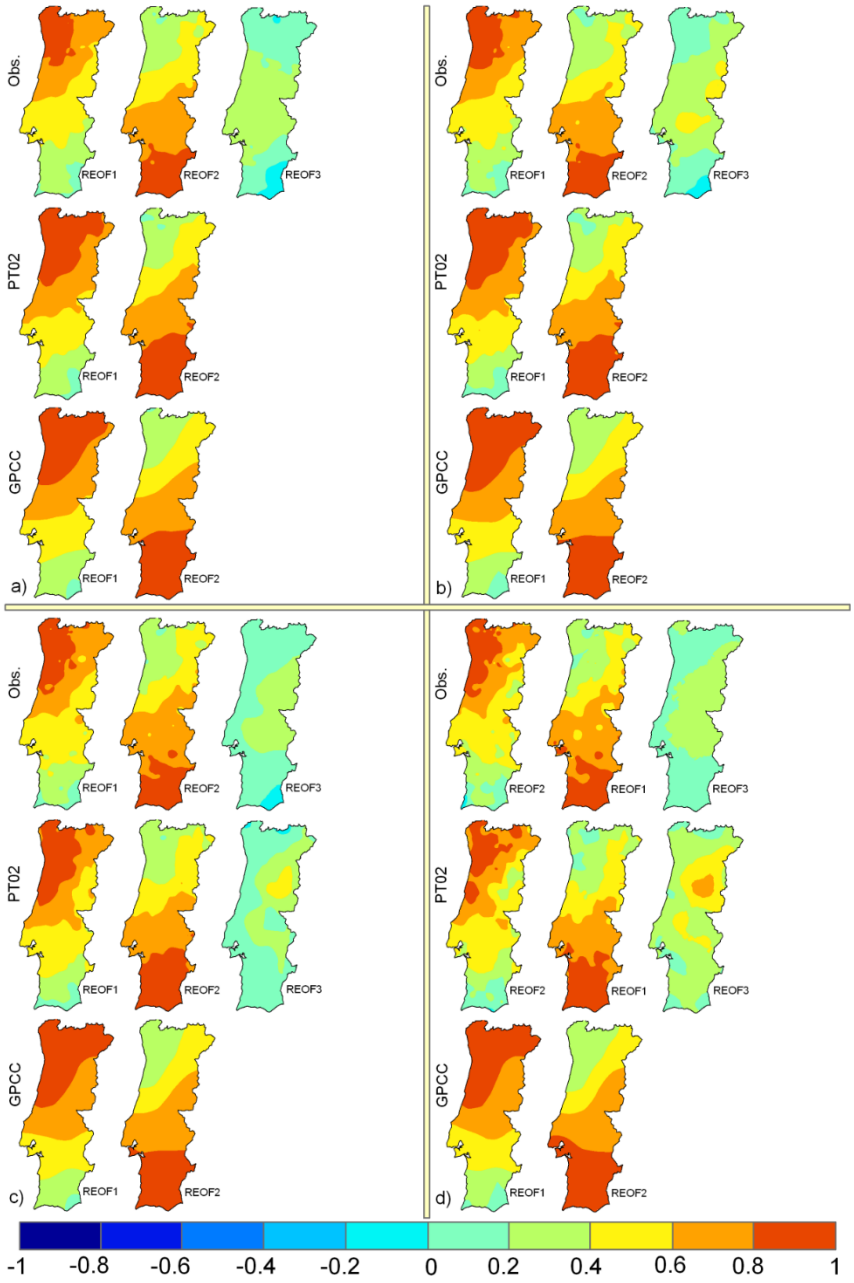

Figure 2-5 Varimax rotated loadings (REOFs) relative to the SPI on a) 3-, b) 6-, c) 12- and d) 24-month time scale, computed using observations (193 stations), and PT02 and GPCC precipitation data sets.

The degree of similarity between rotated PC solutions for different data sets and SPI time scales were quantitatively assessed by comparing their respective loading matrices through the congruence coefficients (Harman 1976; White et al. 1991). Table 2-3 shows the congruence coefficients relating the rotated loadings of different SPI time scales associated with different data sets. It should be noted that only the REOF-1 and REOF-2 of each SPI time scale were considered for assessing the degree of agreement between the data sets in capturing the main country sub-regions (northern and southern sub-regions). The congruence coefficient was not computed for REOF-3 of PT02 since it has no counterpart in other data sets and/or time scales. Results in Table 2-3 suggested that the congruence coefficients between the REOFs associated with the same sub-regions shown in Figure 2-4 are greater than the critical value of 0.98, which indicates an excellent spatial congruence for all the SPI time scales. These results also indicate a perfect agreement between the three data sets in capturing the main Portuguese sub-regions at all considered SPI time scales.

The congruence coefficients between the REOFs of different SPI time scales relative to a given data set were also computed and analyzed. Almost all congruence coefficients were above 0.99 for all sub-regions and the considered data sets, thus indicating a very strong agreement between loading patterns of different SPI time scales identified for each data set. Though the congruence coefficients slightly decrease when comparing the REOFs of shorter SPI time scales with those of longer time scales, they were still high (> 0.99), which indicates an excellent agreement between the REOFs of different SPI time scales for the same sub-region. This fact also reflects a strong spatial consistency between the loading patterns of different SPI time scales captured by a given data set. Thus, results suggested that the spatial patterns of rotated loadings identified by each data set are stable throughout all the considered SPI time scales, i.e., when the SPI time scale changes the identified sub-regions remain about identical. This is evident when visually comparing the identified sub-regions captured by the three used data sets and for all the SPI time scales (Figure 2-5).

Table 2-3 Inter-comparison of the three used data sets by relating their rotated loadings associated with different SPI time scales through congruence coefficients.

SPI-3	Northern Sub-region				Southern Sub-region			
		Obs. REOF-1	PT02 REOF-1	GPCC REOF-1		Obs. REOF-2	PT02 REOF-2	GPCC REOF-2
	Obs. REOF-1	1.000	0.996	0.996	Obs. REOF-2	1.000	0.998	0.998
	PT02 REOF-1		1.000	0.999	PT02 REOF-2		1.000	0.999
	GPCC REOF-1			1.000	GPCC REOF-2			1.000
SPI-6	Northern Sub-region				Southern Sub-region			
		Obs. REOF-1	PT02 REOF-1	GPCC REOF-1		Obs. REOF-2	PT02 REOF-2	Obs. REOF-2
	Obs. REOF-1	1	0.995	0.994	Obs. REOF-2	1.000	0.997	0.998
	PT02 REOF-1		1	0.999	PT02 REOF-2		1.000	0.999
	GPCC REOF-1			1	GPCC REOF-2			1.000
SPI-12	Northern Sub-region				Southern Sub-region			
		Obs. REOF-1	PT02 REOF-1	GPCC REOF-1		Obs. REOF-2	PT02 REOF-2	GPCC REOF-2
	Obs. REOF-1	1.000	0.995	0.994	Obs. REOF-2	1.000	0.997	0.997
	PT02 REOF-1		1.000	0.997	PT02 REOF-2		1.000	0.998
	GPCC REOF-1			1.000	GPCC REOF-2			1.000
SPI-24		Northern Sub-region				Southern Sub-region		
		Obs. REOF-1	PT02 REOF-1	GPCC REOF-1		Obs. REOF-1	PT02 REOF-1	GPCC REOF-2
	Obs. REOF-2	1.000	0.988	0.989	Obs. REOF-1	1.000	0.993	0.995
	PT02 REOF-2		1.000	0.988	PT02 REOF-1		1.000	0.996
	GPCC REOF-1			1.000	GPCC REOF-2			1.000

2.3.3 Stability of drought modes

Previous results suggest that the northern and southern sub-regions identified in the present study are stable with respect to the different data sets as well as to the different types of drought defined by the SPI, from shorter to longer time-scales. However, the identification of the third sub-region, when the PCA was applied to SPI-12 and SPI-24 of PT02 data set, seems to depend on the spatial resolution of the used data set and/or upon the considered time period. The effects of stations density could also be quite relevant as it is somewhat evident when comparing the numbers of grids/stations of the three data sets in the central-eastern Portugal, which is identified as the third mode in the PCA results of SPI-24 of PT02: the PT02 has 52 grid points in this area whereas the observation data set has 29 irregularly distributed stations and GPCC only has 4 grid points in the

same area. Therefore, the third mode captured by PT02 could possibly relate to the higher numbers of grid points of PT02 in that area when compared with those of GPCC and observations data sets.

Table 2-4 Percentage of the total variance explained by the un-rotated (UR) and Varimax rotated (VR) loadings of the SPI-3, SPI-12 and SPI-24 computed using 144 observations data set for three different time sections. Units are in %.

		1910-1949		1950-2003		1910-2003	
	PC	UR	VR	UR	VR	UR	VR
SPI-3	1	59.1	31.9	68.4	36.0	64.2	33.1
	2	8.2	25.4	10.6	35.4	9.5	31.7
	3	2.7	12.7	1.9	9.4	2.2	10.8
	4					1.3	1.5
	Total	70.0	70.0	80.9	80.9	77.1	77.1
SPI-12	1		30.2	69.1	40.9	63.1	32.4
	2	8.1	28.5	10.2	36.5	8.8	21.1
	3	5.8	14.6	2.6	4.5	3.9	20.9
	4					2.3	3.7
	Total	73.4	73.4	82.0	82.0	78.1	78.1
SPI-24	1	55.2	29.9	64.8	39.2	57.2	27.3
	2	9.8	27.3	11.4	33.6	8.9	18.2
	3	7.8	15.6	4.2	7.1	6.2	16.3
	4			3.0	3.5	3.7	14.3
	Total	72.8	72.8	83.3	83.3	76.1	76.1

The selected time window for drought analysis might possibly affect the regional drought patterns through changes in the number of identified sub-regions or their areal coverage. To assess this, a longer observation data set consisting in 144 stations and covering the period 1910–2003 (Santos et al. 2010) was considered for further analysis. This set of stations is sparser than the main observation data set used in this study (193 stations, Figure 2-1a). Therefore, the PCA was applied to the matrix of 144 stations corresponding to the longer (1910–2003) and two shorter (1910–1949; 1950–2003) time windows in order to examine if the identified sub-regions remained stable when the time window changed. Table 2-4 shows the percentages of the total variances explained by the un-rotated and Varimax rotated loadings of SPI-3, SPI-12 and SPI-24 computed using 144 observations for these three time windows. Results showed that the numbers of significant components retained for rotation are three for almost all SPI time scales when shorter time windows are considered, but they increased to four components for the longer time window. The total explained variance is noticeably higher for the 1950-2003 than for the

1910-1949 time window for all SPI time scales. However, the explained variance of the third component is much pronounced for the 1910-1949 time window. Differently, when the longer time window is considered, the first four components were retained for rotation for all SPI time scales, accounting for 77.1%, 78.1% and 76.1% of total variance for SPI-3, SPI-12 and SPI-24, respectively. The explained variance of the third rotated component considerably increased, being comparable to the second rotated component of SPI-12 and SPI-24 when the longer time scale is considered. This may indicate a higher importance of the third mode in the longer time window.

The observed differences shown in Table 2-4 suggested that the eigenvector solution might depend to the sampling data both in space (space resolution) and time (time window). This is supported by Figure 2-5 illustrating the spatial patterns of the rotated loadings of SPI-3, SPI-12 and SPI-24 associated with the three different time windows. The spatial patterns of the rotated loadings corresponding to 1910-1949 (Figure 2-6) are almost identical to those obtained by Santos et al. (2010) who applied PCA to the SPI-12 matrix relative to a longer time window (1910-2004) using the same data set. The spatial configurations of the REOFs associated with the 1910-1949 period are far different from those of 1950-2003 time window (Figure 2-5) when using a denser network of observations. Differently, the REOFs associated with 1951-2003 time window are almost identical to those shown in Figure 2-5 although the number and density of stations used are different. However, comparing the loading patterns shown in Figure 2-6 it appears that the PCA solution for the longer time window mostly reflects the spatial configurations of rotated loadings associated with the 1910-1949 time window. This is particularly clear in the loading patterns of SPI-12 and SPI-24. Results depicted in Figure 2-6 suggest that the northern sub-region is more localized and restricted to a small area in far north-western Portugal, which corresponds to the region in the country with the larger amount of annual precipitation, while by its westward expansion the third sub-region covers the entire north-central Portugal when the 1910-1949 and 1910-2003 time windows are considered. This suggests that the northern sub-region, that is clearly identified by the three used data sets at all considered SPI time scales (Figure 2-5), is also sensitive to the time period used (Figure 2-6). The instability of the third sub-region is evident in Figure 2-6 as its areal extent changes noticeably with respect to the SPI time scale and data time period. Differently, it was found that the southern sub-region is the

most stable sub-region that clearly emerged in the PCA results relative to all considered data sets and time windows here analyzed.

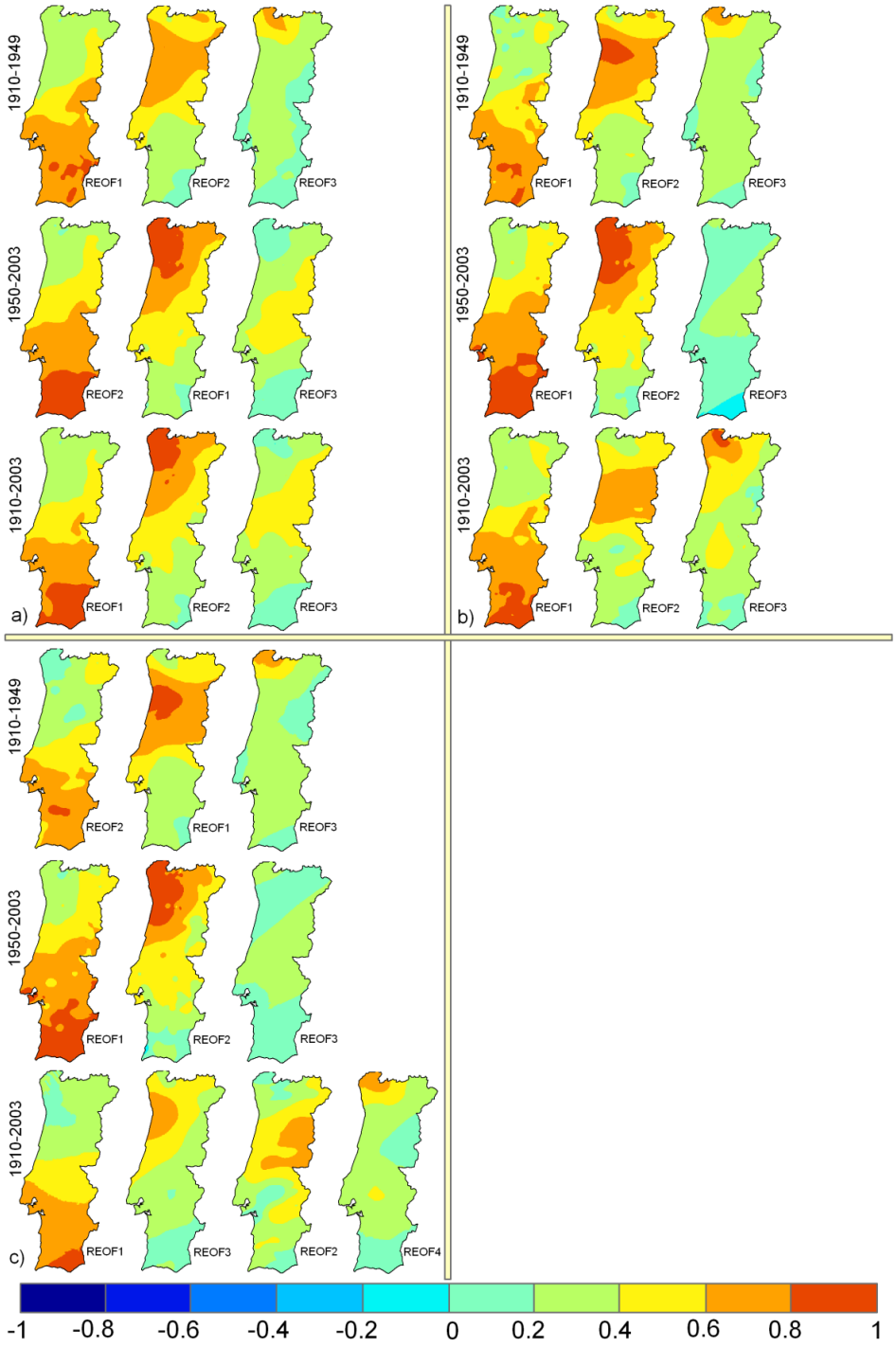

Figure 2-6 Varimax rotated loadings (REOFs) relative to the SPI on a) 3-, b) 12-, and c) 24-month time scale, computed using observations from 144 stations for 1910–1949, 1950–2003 and 1910–2003 time windows.

2.3.4 Linear trends of drought

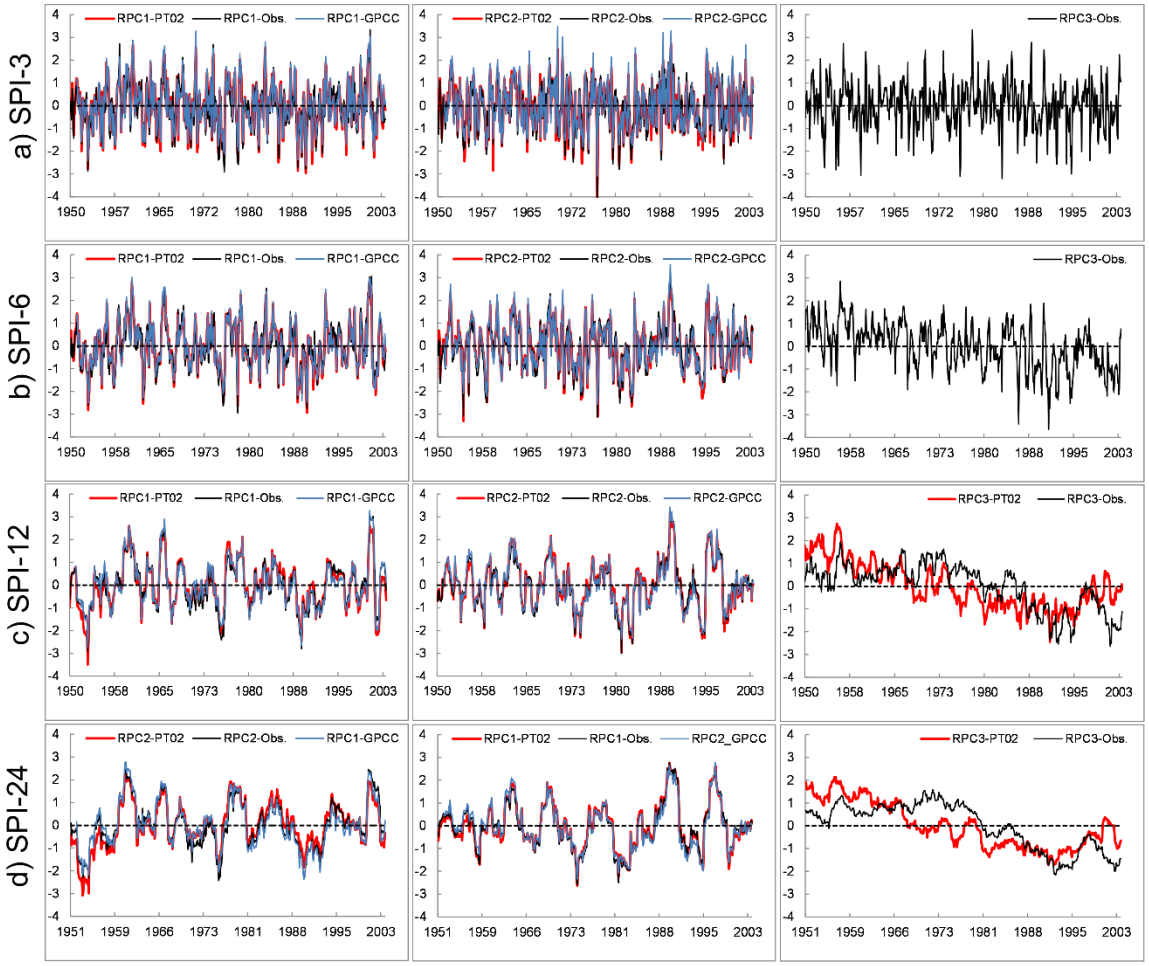

Figure 2-7 Rotated principal component score time series (RPCs) associated with the REOFs illustrated in Figure 2-5. Rows from top to bottom refer to the SPI-3, SPI-6, SPI-12 and SPI-24, respectively. Horizontal dotted line is the zero-line.

The time series of the rotated PC scores relative to observations (193 stations), PT02 and GPCC data sets are displayed and compared in Figure 2-7. The correlation coefficients between the RPC time series for the three data sets are listed in Table 2-5, where those associated with the same sub-region are denoted in bold. According to Figure 2-7 and Table 2-5 it appears that the RPC scores of the different data sets associated with the same sub-region are strongly correlated for all SPI time scales.

The RPC1 and RPC2 time series are characterized by multi-year variability and there are no statistically significant long-term linear trends for the time window here considered. The RPC3 that is associated with the third mode captured by PT02 at longer time scales (12- and 24- month) showed a downward linear trend towards negative values accounting for 0.58% and 0.69% of the variance of the time series for SPI-12 and SPI-24, respectively. Due to very strong co-variability between the RPCs of the three used data

sets (Figure 2-7 and Table 2-5) only the PT02 RPC scores were considered herein for trend analysis computing the Mann-Kendall trend test and the Sen slope estimator for the annual average of the RPC scores relative to SPI-12 and SPI-24 of PT02 (Table 2-6). Table 2-6 shows no statistically significant trends in the annual average of RPC1 and RPC2 for both time scales.

Table 2-5 Correlation coefficients between the RPCs for observations (OBS) and PT02 and GPCC gridded data sets. Correlation coefficients between RPCs associated with the same sub-regions are in bold

		OBS					PT02			
SPI-3	RPC	RPC1	RPC2	RPC3	RPC4		RPC1	RPC2		
PT02	RPC1	**0.96**	0.00	0.18	0.19					
	RPC2	-0.05	**0.97**	0.15	0.12					
GPCC	RPC1	**0.95**	0.01	0.14	0.19		**0.98**	0.01		
	RPC2	-0.04	**0.96**	0.13	0.12		0.01	**0.97**		
SPI-6	RPC	RPC1	RPC2	RPC3	RPC4	RPC5	RPC1	RPC2		
PT02	RPC1	**0.97**	0.00	0.21						
	RPC2	-0.04	**0.98**	0.20						
GPCC	RPC1	**0.97**	0.01	0.19			**0.99**	0.01		
	RPC2	-0.03	**0.97**	0.17			0.00	**0.99**		
SPI-12	RPC	RPC1	RPC2	RPC3	RPC4	RPC5	RPC1	RPC2	RPC3	RPC4
PT02	RPC1	**0.96**	0.01	0.10	0.14					
	RPC2	-0.03	**0.99**	0.06	0.05					
	RPC3	0.11	0.04	**0.58**	-0.59					
	RPC4	0.17	0.09	-0.38	0.15					
GPCC	RPC1	**0.98**	0.03	0.13	0.09		**0.97**	0.00	0.17	0.17
	RPC2	-0.02	**0.99**	0.08	-0.01		-0.02	**0.99**	0.11	0.07
SPI-24	RPC	RPC1	RPC2	RPC3	RPC4	RPC5	RPC1	RPC2	RPC3	RPC4
PT02	RPC1	**0.99**	-0.05	0.02	0.10					
	RPC2	0.01	**0.94**	-0.01	0.26					
	RPC3	0.08	0.25	**0.65**	-0.62					
	RPC4	0.06	0.19	-0.41	-0.13					
GPCC	RPC1	0.02	**0.97**	0.18	0.04		-0.03	**0.93**	0.36	0.11
	RPC2	**0.98**	-0.03	0.12	-0.02		**0.98**	-0.03	0.17	0.05

The average of PC scores corresponding to different individual months and seasons were also examined using the test statistics to reveal if the trend is more evident in any given month and season; however, no differences were found. Considering that the RPC1 and RPC2 are representative time series for the two main Portuguese sub-regions, northern and southern areas, it can be concluded that the results of the present study are in concordance with the previous studies on trend analysis for main land Portugal using either precipitation (Santos and Portela 2007; de Lima et al. 2010) or drought indices time

series (Paulo et al. 2012; Moreira et al. 2012) that detected no trend for the majority of Portuguese stations. The results are particularly in agreement with the findings of Moreira et al. (2012) who found no evidence for aggravation or attenuation of drought severity and frequency for most of the stations situated in either northern or southern sub-regions identified in the present study. Differently, the RPC3 associated with PT02 shows a statistically significant downward trend for both SPI-12 and SPI-24 time scales with -0.054 and -0.061 units per year, respectively. Regarding the observed significant downward trend for the RPC3 of PT02 it is worth noticing that such a negative trend towards dryer periods has been already reported by Paulo et al. (2012) and Santos and Portela (2007), both analyzing monthly precipitation for 1941-2006 and 1910-2004 time periods, respectively, and by Moreira et al. (2012) that highlighted a possible drought aggravation for some stations in the central sub-region.

Table 2-6 Results of the Sen Slope estimates and the Mann-Kendall trend test (in parenthesis) applied to the annual average of RPC scores relative to SPI-12 and SPI-24 of PT02. The statistically significant values at 0.05 significant level are in bold

	SPI-12			SPI-24		
Data set	RPC-1	RPC-2	RPC-3	RPC-1	RPC-2	RPC-3
PT02	0.002	-0.003	**-0.054**	-0.001	0.013	**-0.061**
	(0.16)	(-0.33)	**(-6.30)**	(-0.13)	(1.38)	**(-6.51)**

2.3.5 Drought regionalization with PCA and cluster analysis

Previous sections pointed to the existence of two stable regions considering different SPI time-scales and time windows. Following these results and previous studies (Santos et al. 2010; Martins et al. 2012), a K-means clustering was applied to the PCA results from the SPI-12 computed for the 74 weather and rainfall stations depicted in Figure 2-2. From the PCA two principal components were retained, based on the North's rule of thumb (North et al., 1982), which were submitted to the Varimax rotation. The first component, with the highest loading in the North explains 46% of the total variance and the second one 37.3%, representing the South. Both components explain 83.3% of the total variance (Martins et al., 2012), close to the results showed in Table 2-4 for the SPI computed for the period 1950-2003.

The loadings obtained from the PCA, which represent the correlation between the original data and the principal components series, were then submitted to a Cluster Analysis. This

classification method is used to detect the variables that are more similar with each other and categorize them together in different clusters (Sharma, 1996). From various types of methods, the K-means clustering was used herein since this method is suitable for climate data and eases comparing the results with previous studies that used the same method (Santos et al., 2010).

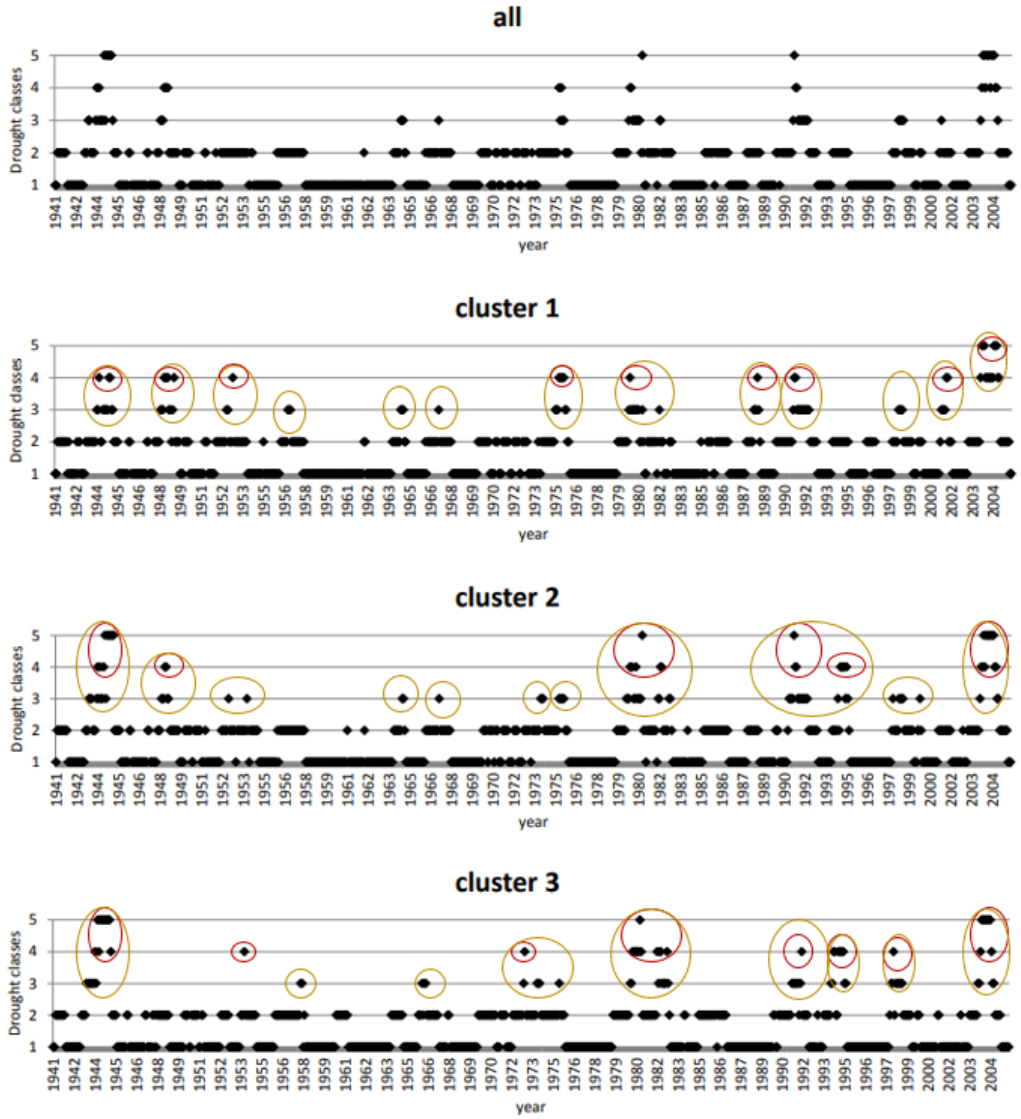

Figure 2-8 The most frequent drought class by month in Portugal (all), cluster 1, cluster 2 and cluster 3 (1 – non drought, 2 – near normal, 3 – moderate, 4 – severe, 5 – extreme) using the SPI with the 12 month time scale. Consequtive dry events with drought class => 3 are highlighted in orange and Consequtive dry events with drought class => 4 are highlighted in red.

The K-means clustering of the loadings of these two principal components shows three significantly different regions within Portugal regarding drought variability, thus separating the north from the central and the south (Figure 2-2). The identified clusters are consistent with the results found by Santos et al. (2010), although using different time

series with different lengths. The specific characteristics of the station of Cabo da Roca (represented with * in Figure 2-2) makes it closer to the drought variability of cluster three relative to the second cluster; for that reason the analysis was performed including that station in the southern cluster.

The most frequent drought class, i.e., the statistical mode in each month for each of the 3 clusters were computed to provide a global overview on the temporal evolution of the drought classes, using SPI-12, in each of the corresponding regions (Figure 2-8). For this application, a drought event is considered a sequence of years with drought class 3 or higher where the interval between droughts do not exceed 2 years. Thus, considering this, when observing Figure 2-8, it can be noticed that during the entire 66 years time period there are 13 groups of droughts events in cluster 1; if considering just the classes 4 and 5, this number decreases to 9. For cluster 2, the number of droughts events of classes 3-5 is 11 and decreases to 6 when considering only the class 4 and 5. For cluster 3 the number of events of the classes 3 or higher is 10 and those, if considering just classes 4 and 5, become 8. These results did not show a clear tendency, as one moves from north to south, regarding the severity and frequency of droughts, but if paying attention only to the extreme droughts it could be observed that there are more events in the central and southern, 4 and 3 against just 1 in the northern region. From the observation of the three clusters in Figure 2-8, one may observe that the minimum time interval between groups of severe and extreme drought occurrences is about 4 years and the maximum time without severe droughts is approximately 27 years. This large period of 27 years without severe and extreme droughts, which is observed in the first half of the studied period, could indicate a trend towards drought aggravation. However, as seen in the previous section (2.3.5) and supported by other studies, there was no evidence of a trend for aggravation in the southern region of Portugal. Differently, for most sites, results pointed to the occurrence of large cycles such that a long period with more frequent and severe droughts is followed by another long period where droughts are less frequent and severe.

2.3.6 Assessment of drought cyclicity with Fourier analysis

The periodograms of each time series were computed and the significance of the cycles were analysed using the false alarm probability considering the 0.05 significance level, i.e., only the peaks above 95% of confidence level were considered significant. The results referring to the periods of the cycles corresponding to the significant peaks recorded in the periodograms of all time series are compiled in Table 2-7, and grouped

by clusters. The counts per period and per cluster are resumed in this Table as well as the corresponding frequency relative to the number of series included in each of the three clusters expressed as percentage.

Table 2-7 The counts per cycle and per cluster and its frequency (%) relative to the number of series included in each cluster (just the significant cycles of the periodograms).

		Period in years												
	Nr of series	33.0	22.0	16.5	9.4	6.6	6.0	5.5	4.7	4.4	3.3	3.1	2.8	2.6	2.0
Total counts per cluster															
Cluster1	32	3	2	1	2	0	27	0	13	3	0	0	0	1	0
Cluster2	30	5	0	0	15	0	27	0	0	0	0	0	0	0	5
Cluster3	12	2	0	0	12	6	11	0	0	0	2	0	0	0	3
		10	2	1	29	6	65	0	13	3	2	0	0	1	8
Frequency (%)															
Cluster1		9.4	6.3	3.1	6.3	0.0	84.4	0.0	40.6	9.4	0.0	0.	0.	3.	0.0
Cluster2		16.7	0.0	0.0	50.0	0.0	90.0	0.0	0.0	0.	0.0	0.	0.	0.	16.
Cluster3		16.7	0.0	0.0	100.0	50.0	91.7	0.0	0.0	0.	16.	0.	0.	0.	25.

Considering the country total, the most frequent cycles ordered by frequency are those with periods of 6-year (65) and 9.4-year (29) (Table 2-7 total counts). When analyzing the counts by cluster, because clusters have different number of series, the frequency in percent for each cluster was computed (Table 2-7). In cluster 1, the most frequent cycles ordered by frequency are 6-year (84.4%) and 4.7-year (43.8%). In cluster 2, they are 6-year (90%) and 9.4-year (50%) and in cluster 3 they are: 6 (100%) and 9.4 (100%). The interdecadal cycles with periods of 33-year are present in all regions but with 22, 16.5 and 13.2-year are only present in the northern region (cluster 1).

Just three of the significant cycles found in the SPI-12 time series have frequencies sufficiently high in the entire country or in each of the three clusters. First, the cycle with a period of 6-years with very high frequency (84-92%) in the three clusters. Second, the cycle with period 9.4-years with very high frequency (100%) in the cluster 3 and median frequency (50%) in the cluster 2. Third, the cycle with periods 4.7-year which is moderately frequent (41%) in the cluster 1. These results showed that the cyclicity of droughts varies among regions. Summarizing, the cycle of 6-year period has very strong presence in the whole country whereas the cycle with 9.4-year period as a stronger presence in the southern rather than in the central/southern region of Portugal. The cycle of 4.7 year period is non-existent in central and southern regions and it only appears in

the northern cluster. However, the large cycles with more than 20 years period have low frequency in all clusters. The reasons for that, may lie on the technique associated with the length of time series. For instance, the large cycles of 33 years are frequent mainly in cluster 2 and 3, but most of them were not found significant in the periodogram.

Looking at the results from a point of view of inference, since the number of time series included in cluster 1 and 2 is large, (32 and 30 stations), each one can be considered as a random sample respectively of northern and central regions. Thus, using the counts from Table 2-7, an estimative for the probability of the return period of droughts to be 6 years in cluster 1, is 27/32=84.4% and in cluster 2, that probability will be 27/30=90% (counts from Table 2-7). However in cluster 3, the probability of 100% for both the return period of droughts to be 6 years and 9.4 years is likely overestimated because the number of time series in the sample is only 12 and their spatial distribution is not the best. Thus the sample may not be representative of the population, even accounting that cluster 3 is smaller. However, as regards to the country total, a reliable estimative for the probability of the return period of droughts to be 6 years is 66/74=89.2%.

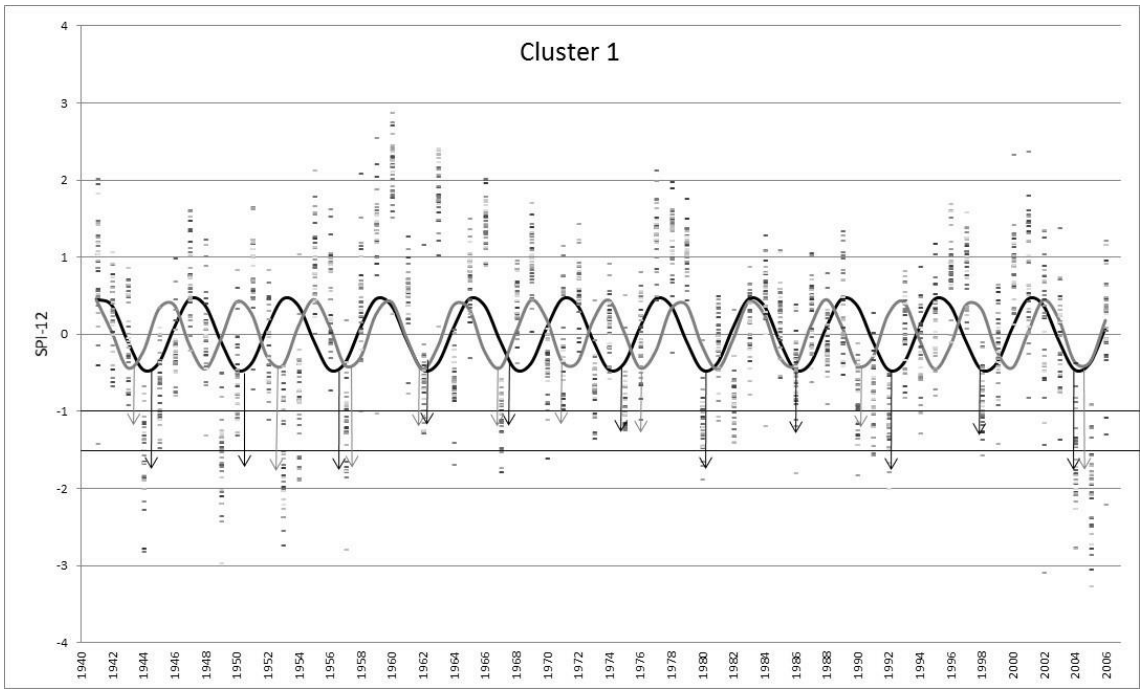

Figure 2-9 SPI-12 December values for northern Portugal (cluster 1) and the waves of period 4.7 years (grey line) and 6 years (black line). The dots represent the SPI-12 time series from all locations in cluster 1.

In Figures 2-9, 2-10 and 2-11, the time series relative to each of the 3 clusters are shown with superposing the most frequent waves: one of 4.7 years period in cluster 1, another of 6 years period in clusters 1, 2 and 3, and a wave of 9.4 years period in cluster 2 and 3.

A correspondence between the minima of the waves and the SPI upper borders for moderate drought (-1) and for severe or extreme drought (-1.5) is established through arrows placed in these pictures. In Figure 2-9 , relative to cluster 1, one can observe that the wave of 6 years period has 11 minima and nearly all of them coincide with events of moderate (-1.5<SPI<-1) or severe and extreme droughts (SPI < -1.5). Just one drought event, in 1957, was missed by the wave. Therefore, a good visual agreement exists between the minima of the sinusoidal wave of 6-year period and the events of moderate or more severe droughts that occurred during the study period. Relative to the wave of 4.7-year period in cluster 1, from a total of 14 minima about 11 coincide with events of moderate, severe or extreme drought. The degree of agreement for this wave is less good than for the one with 6-year period.

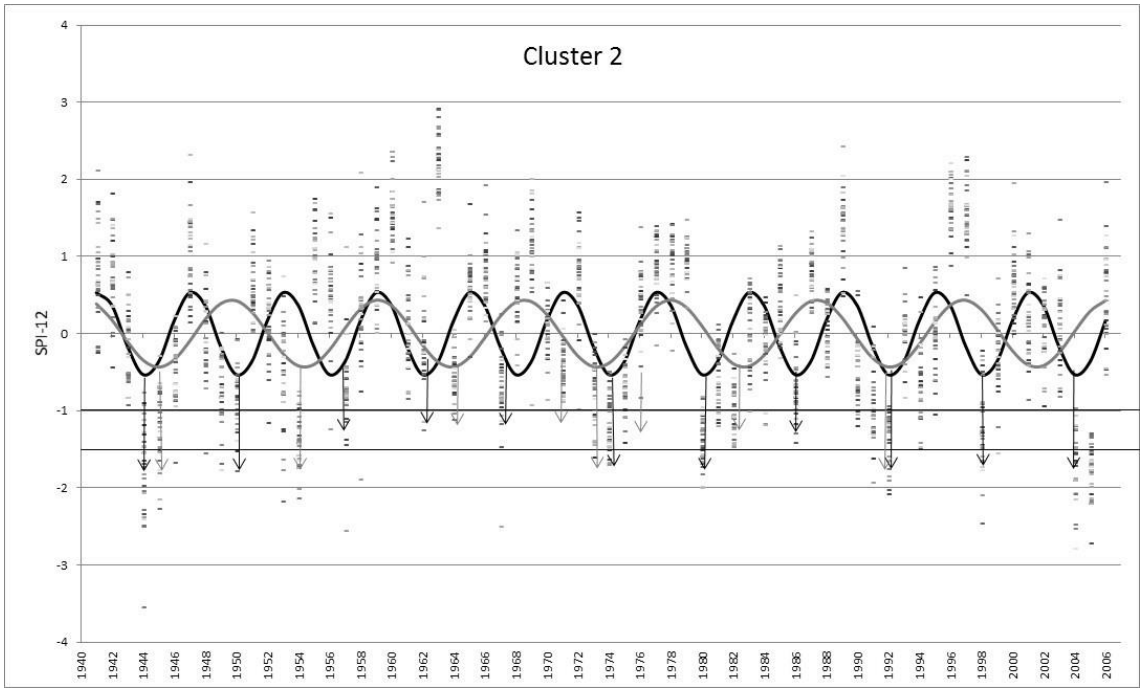

Figure 2-10 SPI-12 December values for central/southern Portugal (cluster 2) and the waves of period 4.7 years (grey line) and 6 years (black line). The dots represent the SPI-12 time series from all locations in cluster 2.

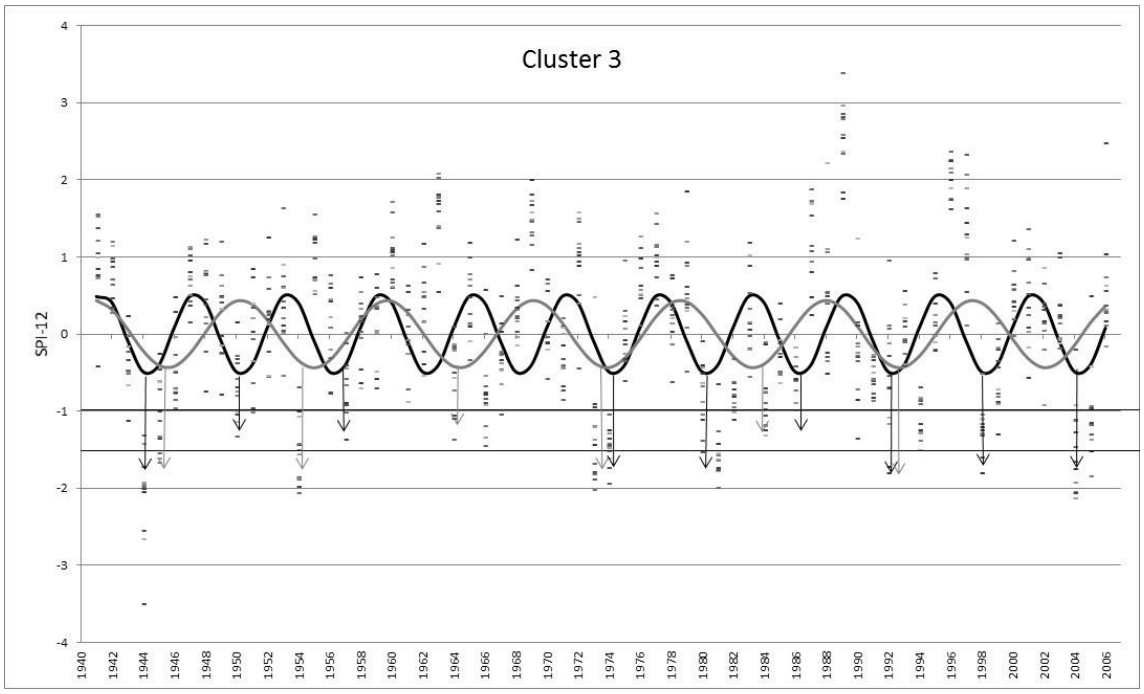

Figure 2-11 SPI-12 December values for southern Portugal (cluster 3) + waves of period 6 (black line) and 9.4 years (grey line). The dots represent the SPI-12 time series from all locations in cluster 3.

For cluster 2 (Figure 2-10) a good agreement between the minima of the 6-year period wave and the events of moderate severe or extreme droughts was observed, also missing the same drought event of 1957 that was missed by the wave in cluster 1. As for the wave of 9.4-years period, from a total of seven minima, six coincide with events of moderate, severe or extreme droughts. For cluster 3 (Figure 2-11), the visual agreement between the wave of 6-years period and the drought events is not as good as for the previous clusters, with three of the minima not coinciding with drought events and with two events of moderate drought and one of severe and severe drought are missed by the wave. As for the 9.4 year wave, one out of the seven minima does not correspond with a drought event. Furthermore, two moderate and one severe and extreme drought events were missed by the wave. However, this less good agreement for cluster 3 may be due to the low number of time series represented there. In general, a visual relation can be established between theses waves and the events of drought occurred in each cluster during the study period. The correspondence between the sinusoidal waves and the drought cyclicity is not perfect but this was expected since cycles in nature are only near-regular, thus not providing for a complete agreement with regular waves.

The Fourier analysis was also applied to the SPI-12 time series relative to the rainy, transition and dry months (January to November). These results are illustrated in

Figure 2-12. The analysis was performed considering three distinct groups: (1) a rainy season including November, December and January; (2) a dry season including the months between May and September; and (3) the transition months of February, March, April and October. The most frequent significant cycles found for December values, namely the 6, 9.4 and 4.7-year, were also observed in the remaining months. The 6-year cycle was present in the applications to all months but was less frequent in the dry season. The 9.4-year cycle was less frequent, and could only be found in cluster 3 for the rainy season. Other short-period cycles with 3.1, 2.6 and 2-year showed up with high frequency for the dry season and the transition months. A closer look to Figure 2-12, the following cycles are in evidence:

- the 2-year cycle was frequent in the south, cluster 3, in the dry season;
- the 2.6-year cycle was found in the dry season and in the transition months in cluster 1 and in the transition months in cluster 2;
- the 3.1-year cycle had high frequency in clusters 2 and 3 in the transition months and the dry season;
- the 4.7-year cycle was present in the three clusters for October and November. Cluster 1 also showed the 4.7 year cycle in December and January;
- the 6-year cycle had high frequency in general in all clusters and months but not in the dry season months in cluster 1;
- the 9.4-year cycle had high frequency in cluster 3 for the months of the rainy season and, for the cluster 2, just for December

The time series relative to every month, January through December, showed a behavior that differs for each month, which relates to the conditions regulating the general circulation of the atmosphere that also vary throughout the year. The short period cycles of 2–3.1 years were in general statistically significant in the months from March to September, thus out of the rainy months. Medium-period cycles are mainly statistically significant in the months from November to April. The cycles of 6 and 9.4 years are representative of drought cyclicity since, as seen previously (section 2.3.6), there was a good agreement between the Fourier waves and the drought events that occurred in all clusters. Furthermore, in the years where a drought is installed, the December values of the SPI-12 reflected this situation through assuming highly negative values. This fact denoted the effect of the lack of precipitation in the precedent rainy months; the same occurred with the SPI-12 relative to January and February. Contrarily, in the rainy years,

the SPI12 from May to September reflected precipitation above normal that occurred in the precedent rainy and transition months. Therefore, the short cycles, which relate with precipitation above normal, were significant in the SPI values from May to September, while the medium cycles, which relate with drought, were significant for the months November to April.

The NAO plays a fundamental role in the Atlantic and European climate, in particular, the negative phase of the NAO regime is fundamental for the winter interannual variability of precipitation in Portugal (Santos et al. 2005), whereas positive phases of the NAO are usually associated with drought conditions (Santos et al. 2005, 2007). Various studies have shown that the NAO influences precipitation (Trigo et al. 2002; Pires et al. 2007) and streamflow (Trigo et al. 2004; Bierkens and van Beek 2009). Thus, it is reasonable to relate the cyclicity of drought events with large circulation patterns such as the NAO. Santos et al. (2007) studied the physical mechanisms responsible for the extremely dry winter of 2004/2005 in Portugal and concluded that the strengthening of the NAO toward its positive phase contributed to the extreme conditions of that particular winter. In addition, Sousa et al. (2011) showed significant correlations between dry periods, measured with the self-calibrated PDSI, and the positive phase of the NAO during winter on the region.

The 6 and 9.4-year cycles may be partially explained by the NAO periodicity index cycle. Polonskii et al. (2004) studied the cyclicity of the NAO index in Eurasia and stated that the characteristic period of fluctuations of the NAO index corresponding to the main spectral peak is 6–10 year. That hypothesis is also compatible with the assumptions of Trigo et al. (2004) relative to the influence of NAO on the precipitation in Portugal. However, García et al. (2002) associated of 2.4 and 7.7 years oscillations of NAO with the same patterns of interannual precipitation in the Iberian Peninsula. Moreover, these authors assumed multidecadal cycles, which were also observed in this study. Labat (2006) also assumed NAO influences on European surface water regimes in terms of multidecadal periods. Nevertheless, in agreement with conclusions by Santos et al. (2010), periodicity of more than 10 years, more frequent in the northern region, are difficult to relate with NAO. This is also concluded by Küçük et al. (2009) for Turkey. Following the results reported by Tsiropoula (2003) and Hathaway (2010), these multidecadal cycles may relate with solar cycles.

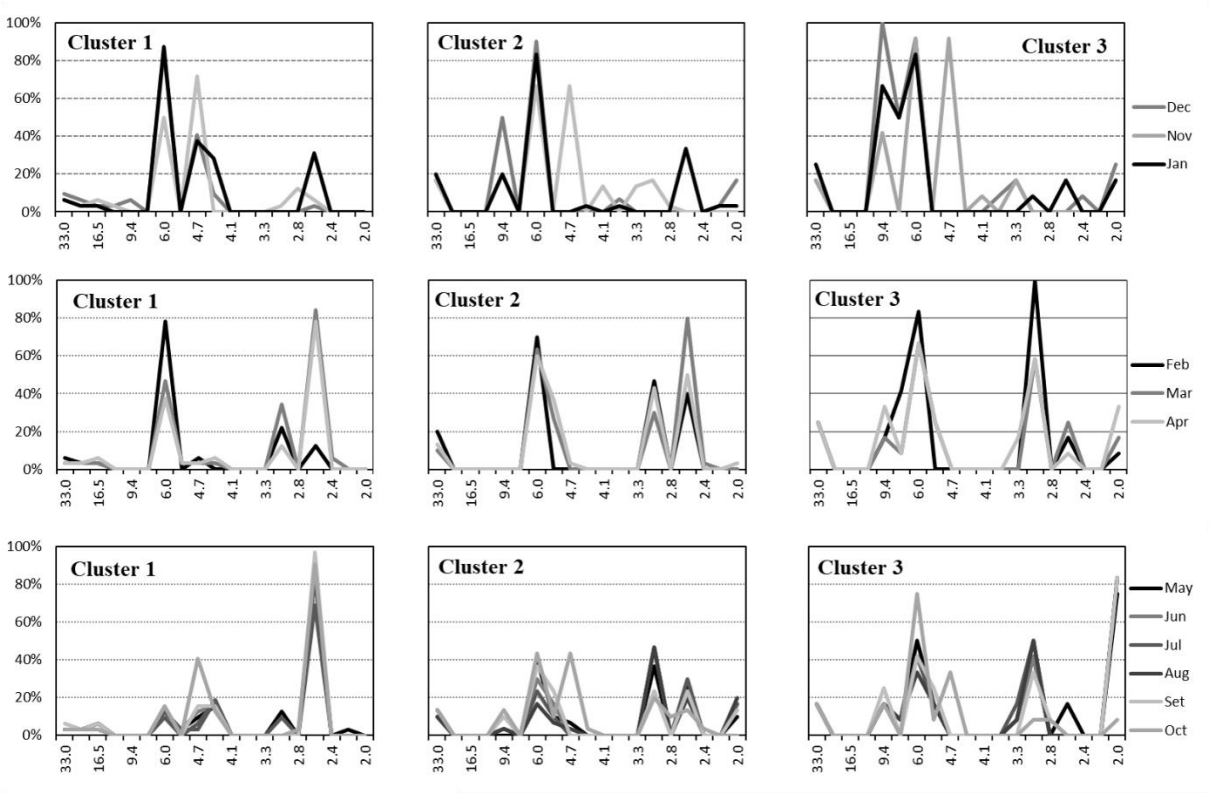

Figure 2-12 Frequency of significant cycles relative to each cluster per period cycle, gathered in three groups: November, December and January (wet season); February, March and April (transition months); and May–September (dry season)

2.4 Conclusions

The present study provided an insight regarding the temporal and spatial drought patterns of drought in Portugal using the Standardized Precipitation Index. The regional drought patterns were assessed with the S-Mode PCA with varimax rotation applied to the SPI on different time scales computed using the three precipitation data sets for the period 1950–2003. Results identified the northern and southern Portugal as the two main sub-regions of drought variability, considering all data sets and SPI time-scales. These two main sub-regions were considered stable, since they are quite similar for all cases and a spatial congruence test applied to the loadings of the PCA revealed an excellent spatial congruence between all data sets and time scales. In addition, a small sub-region in the mountainous inland of central-eastern Portugal was found for the 24-month time scale using the PT02 data set. The northern and southern sub-regions were identified with high positive rotated loading values. Similar spatial patterns were found using the three datasets and all considered SPI time scales, suggesting that the sub-regions are quite stable with respect to the changes in the SPI time scale. Differently, a third sub-region was observed for the PT02 data set referring to central-eastern Portugal, which was

sensitive to the SPI time scale and spatial resolution of the data set. Despite the third spatial mode explains a smaller percentage of the total variance, its position in the mountainous area of central Portugal and the statistically significant downward trend characterizing the associated RPC, suggest the need for further studies relative to that region using a dense network of observations.

Three different time windows were used in order to examine if the identified sub-regions are conditioned to the considered time window. The results showed that the southern sub-region is the most stable one, while the northern and central-eastern sub-regions are very sensitive to the selected time window.

The temporal analysis of drought in Portugal was assessed testing the linear trends of the principal components of all sub-regions identified, and searching for significant cycles of drought variability using a Fourier analysis. The linear trend analysis applied to all the rotated PC scores, showed no evidence for linear trends for either the increase or attenuation of drought conditions in the northern or southern sub-regions identified. However, the third sub-region captured by PT02 at longer time scales, showed a significant downward trend pointing to a possible drought aggravation in the central region of Continental Portugal.

The identification of significant drought cycles was conducted using a Fourier analysis applied to SPI-12 time series. To identify the groups of weather stations sharing similar drought characteristics, the PCA was combined with a K-means cluster analysis. With this methodology, three statistically distinct clusters of weather stations were identified in Portugal, then the Fourier analysis was applied individually to each SPI time series and the frequency of the significant cycles is analyzed for each cluster. The Fourier analysis, used to search for significant cycles that could relate to return periods of droughts, was performed using a SPI-12 time series respective to each month. The results of this analysis for the SPI-12 relative to December values are of particular interest since they are a good indicator for drought monitoring for the Portuguese climatic conditions. Results showed that drought periodicities varied among the three sub-regions and differ when different months were considered for the Fourier analysis. For the SPI-12 relative to December, the main cycles identified were:

- a cycle with a 6-year period compatible with NAO influences, doubtless the most frequent across the country and, that generally showed a good agreement with the range time of the drought events that occurred in each region;
- the cycle of 9.4 years, also partially related to the NAO, but that loses importance from south to north, where it was nearly non-existent;
- the cycle with a small period of 4.7 years that was frequent in the northern region but was not significant in the central and southern regions.

These results pointed to northern and southern Portugal having different climatic influences that cause the strong presence of cycles with periodicities in the range of 6–10 years in the time series of central/southern regions. As for the cycles of SPI-12 in the remaining months, the results showed that the 4.7, 6, 9.4-year cycles were also found but their frequency varied with latitude (cluster) and with the month that was considered.

From October to January, the 4.7-year cycle was present in all clusters; the 6-year cycle was also frequent, but it could not be found in the dry season in the north, cluster 1; the 9.4-year cycle was also quite frequent, but only in the rainy months. Shorter cycles, 2–3 years, were identified and were significant in the dry months in the south and in the transition months in the north and center. However, they seemed to be associated with cycles related to wetness, i.e. SPI > 1.0, instead of drought. The adopted methodology, simpler than other more complex techniques such as the wavelet transform analysis, allowed a good understanding and interpretation of the drought periodicity. Furthermore, the Fourier analysis may also be useful in longterm drought prediction as it may provide an estimative relative to the return periods of drought events.

Overall, results are in agreement with other studies applied to Portugal and the Iberian Peninsula despite differences in the methodological approaches. The spatial analysis allowed the identification of these sub-regions with similar drought variability and characteristics can be useful for drought risk management at a regional scale. The sub-regions identified include the most important river basins in Portugal, Tagus and Guadiana, in the Southern sub-region and the Douro basin inside the Northern sub-region. This means that the drought sub-regions here identified well represent the distinct drought variability characterizing these river basins, thus these results may be useful for drought risk management at a regional scale. However, the existence of a third sub-region identified with the PCA and with the cluster analysis should be further studied. Moreover,

the temporal analysis also showed that further studies are required to improve the understanding of teleconnections between drought indices and large-scale atmospheric circulation indices for Portugal and the Mediterranean to improve the predictability of droughts and supporting related risk management.

Chapter 3

Influence of climate variability on the SPI and PDSI. An analysis using long-term data series.

ANA A PAULO, DIOGO S MARTINS AND LUIS SANTOS PEREIRA (2016) INFLUENCE OF PRECIPITATION CHANGES ON THE SPI AND RELATED DROUGHT SEVERITY. AN ANALYSIS USING LONG-TERM DATA SERIES. WATER RESOURCES MANAGEMENT 30: 5737-5757.

AND

DIOGO S MARTINS, ANA A PAULO, CARLOS A PIRES, LUIS S PEREIRA (2017) LONG-TERM VARIATION OF PDSI AND SPI COMPUTED WITH REANALYSIS PRODUCTS. EUROPEAN WATER 60: 271-278.

Influence of climate variability on the SPI and PDSI. An analysis using long-term data series.

Abstract. Drought indices, such as the Standardized Precipitation Index (SPI) and the Palmer Drought Severity Index (PDSI) are used to quantify drought severity. Due to the SPI probabilistic and standardized nature, a given value of SPI computed in distinct time periods or locations indicates the same relative drought severity but corresponds to different amounts of precipitation. Likewise, the PDSI is also influenced by the calibration period used to compute the potential values for the definition of the climatically appropriate for existing conditions (CAFEC) of the local climate. Thus, the present study aims at contributing for a comprehensive analysis of the influence of long-term precipitation variability on drought assessment by the SPI and the combination of the variability of precipitation and evapotranspiration in the case of the PDSI. Long records of monthly precipitation, spanning from 1863 to 2007 in several locations across Portugal, were divided into 30 years sub-periods and the SPI with 12-month time scale (SPI-12) was computed for each sub-period and for the entire period of records. The same approach was followed to compute the SPI with 9-month time scale for comparison against the PDSI. The PDSI and SPI-9 were computed using weather data from the NOAA-CIRES Twentieth Century Reanalysis Project version 2c, which spans from 1851 to 2014 with a spatial coverage of 2.0º latitude x 2.0º longitude. For the PDSI, monthly evapotranspiration was computed using the FAO PM-ET_o method. Monthly data from reanalysis products consisted of maximum and minimum air temperature, net radiation, wind speed and relative humidity. Precipitation data was obtained from the same source. PM-ET_o was retrieved from the CRU TS3.21 database and was combined with the observed precipitation used to compute SPI-12. This allowed comparing and assessing the differences between the PDSI and SPI-9 computed with reanalysis against the PDSI and SPI-9 obtained with observed data sets. The probability distributions adjusted to precipitation in those different time periods were compared envisaging to detect the SPI sensitivity to the reference period and, therefore, to changes in precipitation. Precipitation thresholds relative to the upper limits of SPI-12 drought categories were obtained and the influence of the time period was investigated. For the PDSI, to assess how the long-term climate variability influences the identification of dry events in the drought indices, five different calibration periods were selected to estimate, the potential values of evapotranspiration, runoff, soil moisture recharge and percolation loss of the PDSI water

balance. Results have shown that when SPI values derived from the full data record for a recent time period were lower/higher than the SPI values derived from data of the considered time period in which a recent downward/upward shift of precipitation occurred. Coherently, a common pattern of drought aggravation from the initial until the more recent period was not detected. However, in southern locations, lower precipitation thresholds of the SPI drought categories were generally found in the more recent period, particularly for more severe drought categories, whereas in the northern locations Porto and Montalegre, an increase was detected. The impacts of the reference period on the computed SPI drought severity and frequency are shown, bringing to discussion the need for updating ´normal´ conditions when long-term precipitation records are available and precipitation changes are observed. Moreover, results showed that the adopted calibration period had a significant impact of the frequency of extreme events detected on both the PDSI and the SPI and highlight the importance of selecting an adequate calibration period when computing these drought indices.

Keywords: PDSI; SPI; long-term variability; 20th century reanalysis; precipitation thresholds; drought severity; reference periods.

3.1 Introduction

Drought is a natural temporary imbalance of water availability, consisting of a persistent lower-than-average precipitation, of uncertain frequency, duration and severity, of unpredictable or difficult to predict occurrence, resulting in diminished water resources availability and carrying capacity of the ecosystems (Pereira et al., 2009). There are numerous definitions for drought and its perception varies with the water sectors affected, and its frequency or severity may be aggravated by climate change.

Standardized drought indices computed from precipitation, evapotranspiration, streamflow or soil moisture have been used to monitor drought and to quantify drought severity. The standardized precipitation index (SPI) is the most widely used. SPI values quantify deviations from 'normal precipitation' (Mckee et al. 1993). SPI values are classified in drought (wetness) categories, with the more negative values indicating a more severe drought category (McKee et al. 1995). The World Meteorological Organization recommends its inclusion in drought monitoring systems since 2009 (World Meteorological Organization 2012). As a result of the evaluation of drought indices in the quantification of meteorological drought using a combined pool of criteria (Keyantash et

al. 2002), the SPI is surpassed by rainfall deciles in transparency and by cumulative precipitation anomalies in dimensionality. Transparency refers to the way an index of drought is understandable by the scientists, stakeholders and the public, and dimensionality refers to the link of the index to a physical quantity. The index is obtained from the adjustment of a probability distribution function (pdf) to the precipitation cumulated over a given number of months denoted as time scale. Shorter time scales are appropriate to monitor the effects of precipitation shortages in soil water storage and agriculture, while longer time scales are used to monitor drought effects on surface and ground water resources.

Despite the SPI being, possibly, the most used drought index in the world to characterize and monitor drought, historically, the Palmer drought severity index (PDSI) (Palmer 1965) continues to be highly in use, because instead of using solely precipitation it combines the latter with evapotranspiration (ET) in a simple water balance. The PDSI was introduced as a tool to determine regional moisture availability and it has been used to study drought/wet events and it measures the cumulative departure, compared to pre-determined mean conditions, in atmospheric moisture supply and demand at the surface (Dai et al. 2004). However, it has some important limitations (Alley 1984; Guttman 1998; Wells et al. 2004) related to the selection of the ET equation, the soil water balance procedure, the calculation of the climatic characteristic or the empirical coefficients in the duration factors, and the backtracking computation procedure. Several attempts were made to improve PDSI: a weighing calibration procedure generating the WPDSI (Heddinghaus and Sabol 1991), the self-calibrating procedure originating the Sc-PDSI (Wells et al. 2004), and changes in ET and the water balance to produce the MedPDSI which is explained in detail in Chapter 6.

Moreira et al. (2012) reviewed numerous studies aimed at detecting any possible aggravation of drought frequency and severity in Portugal and in the Iberian Peninsula showing non-increasing trends for northern Iberia and varied trends for central and southern regions. Those authors investigated the temporal drought aggravation applying generalized log-linear models and statistical inference to long time series and their decomposition into sub-periods using the SPI. Their results did not support the assumption of a trend of drought aggravation that could be related to climate change but cycles corresponding to the considered sub-periods where drought was more frequent and severe followed by others where frequency and severity were lower. However, comparing

the last period of 27 years with the precedent one they concluded that drought occurrence and severity increased during that last period with exception of the northern region. The studies by Santos et al. (2010), Martins et al. (2012), Paulo et al. (2012), and Raziei et al. (2015) did not reveal trends for either an increase or decrease of drought occurrence or severity in most of the country. de Lima et al. (2010) studied trends for precipitation in Portugal using long data sets, ranging between 88 and 145 years and did not found a generalized significant longterm pattern of change but a sequence of alternating periods of decreasing and increasing trends in both annual and monthly precipitation, which were sometimes statistically significant. The results by Moreira et al. (2012) were in the same line. The analysis of trends and correlation in annual extreme precipitation indices de Lima et al. (2015) led to conclude that there is an important but not statistically significant decrease in regional average annual precipitation. Studies relative to PDSI trends point to the same conclusions. Martins et al. (2012) and Paulo et al. (2012) did not find any evidence of drought increase or decrease in Portugal using the PDSI in the period 1941-2006. Sousa et al. (2011) using the self-calibrating PDSI observed significant negative trends of the PDSI in period 1901-1950 but did not observed such trends for period 1901-2000 or 1951-2000. Other authors have also studied PDSI trends related to the evapotranspiration input used to simulate the drought index water balance (van der Schrier et al. 2011; Dai 2011; Sheffield et al. 2012). Whereas van der Schrier et al. (2011) and Dai (2011) found no major differences in the trends of the PDSI computed with different evapotranspiration equations, a temperature based one, the Thorntwhaite equation (Thornthwaite 1948) and the physically based reference evapotranspiration (PM-ET_o). Contrarily, Sheffield et al. (2012) observed large differences in the global trends of the PDSI computed using these methods to estimates evapotranspiration. In that study, Sheffield et al. (2012) compared two global version of the Sc-PDSI computed using potential evapotranspiration (PET) from the empirical Thornthwaite equation and the PM-ET_o estimated using the FAO-PM equation (Allen et al. 1998) and results showed that the Sc-PDSI computed with the PM-ET_o had clear differences in the trends identified by both indices pointing to an overestimation of the trends to increased global dryness.. Furthermore, for the period 1980-2008 differences were even larger with the Sc-PDSI based on PET showing, again, significant drying trends, whereas the average trend of the PM-ET_o counterparts was not significant. These results showed the importance of selecting the appropriate evapotranspiration estimates to characterize climate variability and that temperature based equations like the Thornthwaite equation are not capable of

fully describe the climate and can produce unrealistic trends on drought indices. However, Dai et al (2011) and Van der Shrier et al. (2011) observed only small differences between the Sc-PDSI computed with both types of evapotranspiration estimation. Significant drying trends of the PDSI computed with PET have also been reported in other studies like Dai et al. (2004) reporting that very dry areas have increased from 12% to 30% from 1970 onwards. Although its impacts on droughts indices is not clear, temperature based methods are more influenced by global warming, and trends for the increase of evapotranspiration computed with this methods are usually more evident than when using ET_o estimation based on more variables than temperature (Chapter 4).

Due to its standardized nature, the same negative SPI value computed in different locations or time periods corresponds to the same relative drought severity but to different amounts of precipitation. The relative measure provided by the SPI would be more transparent if accompanied by an absolute value of the monthly precipitation thresholds relative to the SPI drought categories as shown by Paulo and Pereira (2008) and Portela et al. (2012). However, the SPI depends on the pdf adopted, on the method used for parameter estimation and on the reference time period used in the estimation. Although some authors advocate the Pearson III distribution (Guttman 1999; Vicente-Serrano 2006) the gamma distribution is the more common worldwide and has been adopted in various Portuguese studies following previous tests (Paulo et al. 2003; Paulo and Pereira 2006). However, the precipitation thresholds relative to the severity drought categories were already considered (Paulo and Pereira 2008) and may consist of a first step for the application of the SPI to future precipitation scenarios.

Impacts of future climates on aridity and drought have been addressed by several authors using the SPI and several modifications to this index (Loukas et al. 2008; Dubrovsky et al. 2009; Dai 2011; Sienz et al. 2011; Russo et al. 2013; Zargar et al. 2014; Jeong et al. 2014; Asadi Zarch and Sharma 2015). Louckas et al. (2008) computed the SPI in Thessaly-Greece with the gamma distribution adjusted separately for the base time period 1960-1990 and for two future periods, 2020–2050 and 2070–2100. These authors concluded that the annual drought severity increased for the future scenarios for all target hydrological areas. However, they did not consider possible differences in the precipitation deficits that are associated with the severity categories.

In the context of climate change, some alterations to the SPI were proposed in relation to impacts on drought, either with the objective of comparing present conditions and future

climates or to include trends in the probability model accounting for the non-stationarity in precipitation. Dubrovsky et al. (2009) proposed a relative SPI derived from a reference precipitation time series with the aim of between-stations comparison considering present climate conditions and future climates. However, the pdf obtained for the reference period used to compute the SPI in different time periods, e.g., periods with future climate data, may lead to errors due to lack of fit of the pdf to those various periods, namely relative to the tails of the pdf curves, as noted by the same authors. Russo et al. (2013) presented a new formulation of the SPI applied to model-simulated precipitation under greenhouse forcing gradual changes; precipitation outputs from climate models were modelled by a gamma distribution with the scale parameter varying linearly with time, and the modified SPI, denoted as nonstationary Standardized Precipitation Index (SnsPI), was compared with the SPI relative to the full period. Authors reported that SnsPI performed better than SPI to describe simulated precipitation changes. Zargar et al. (2014) modified the SPI calculation with the objective of modelling the effects of the shift in precipitation normals on drought frequency. The authors built confidence intervals for the parameters of the gamma distribution and applied an enhanced p-box method for studying climate change effects on SPI drought frequency. Assuming non-stationarity of at-site precipitation series, a time-dependent SPI (SPIt) was developed and applied to historical records of summer precipitation in the Luanhe River basin, China (Wang et al. 2015b). The mean is described by a polynomial function of time and, as a result, the scale parameter of the gamma distribution is time dependent. This approach is similar to the one proposed by Russo et al. (2013) replacing the linear variation of the scale parameter of the gamma distribution by a polynomial variation with time.

The PDSI, contrarily to the SPI, is not a standardized index, and because of that, it has great variation if computed for different locations. This occurs because the index has several empirical components that were used to calibrate it to local condition of the central plains of the United States of America (Palmer 1965). Chapter 6 provides a detailed description of the computational procedure of the PDSI, its limitations and suggestions to improve the index in this regard. Thus, this characteristic of the original PDSI limits its comparability among different locations and periods (Wells et al. 2004). In that study the empirical coefficients were modified to reflect the local conditions in which the PDSI is computed and, thus, improving its comparability between different regions and years. Nevertheless, even using the modifications proposed by Wells et al. (2004) the PDSI is

still sensible to changes in the calibration period used to estimate the potential values in the PDSI water balance. Karl (1986) showed significant changes in the PDSI when different calibration were selected to calibrate the potential values of the PDSI water balance and suggested using the complete time series to adjust these values. Mo and Chelliah (2006) developed a new drought index, the MPDSI, based on the PDSI, but using a regional reanalysis to provide all the input data for the water balance and their results suggested that the calibration of most of the PDSI parameters should be based upon the complete data series. This need for calibration of the PDSI is enhanced by climate change, since precipitation and temperature have changed significantly in the past 60 years. This option was also followed by Van Der Schrier et al. (2013) which stated that by using the complete record of data would include all the variability of precipitation and ET would guarantee that the PDSI values would be within the range established by Palmer, from -6 to 6. However, Dai and Zhao (2017) studied uncertainties in historical changes of drought using the PDSI with PM-ET_o and recommended not to use the years after 1980 for the calibration of the PDSI climatic potential so the impacts of climate change are not included in the PDSIs calibration. Using different calibration periods for the PDSI may be the answer for the differences in trends observed in these studies (Van der Schrier et al. 2013), since Dai (2011) used the period 1950-1979 to calibrate the PDSI whereas Shefield et al (2012) calibrated the PDSI using the period 1959-2008.

Considering the review above and the need to better understand the impact that climate variability has on drought indices such as the SPI and PDSI the present study aims to: (1) analyse the influence of precipitation changes on the SPI dynamics and on drought assessment and the variation of the precipitation thresholds associated with the SPI categories and (2) assess the impact of using different calibrations periods for the PDSI and SPI. For that purpose both the PDSI and the SPI were computed with long time series of data, using, respectively, a reanalysis data set and observed precipitation for continental Portugal.

3.2 Data

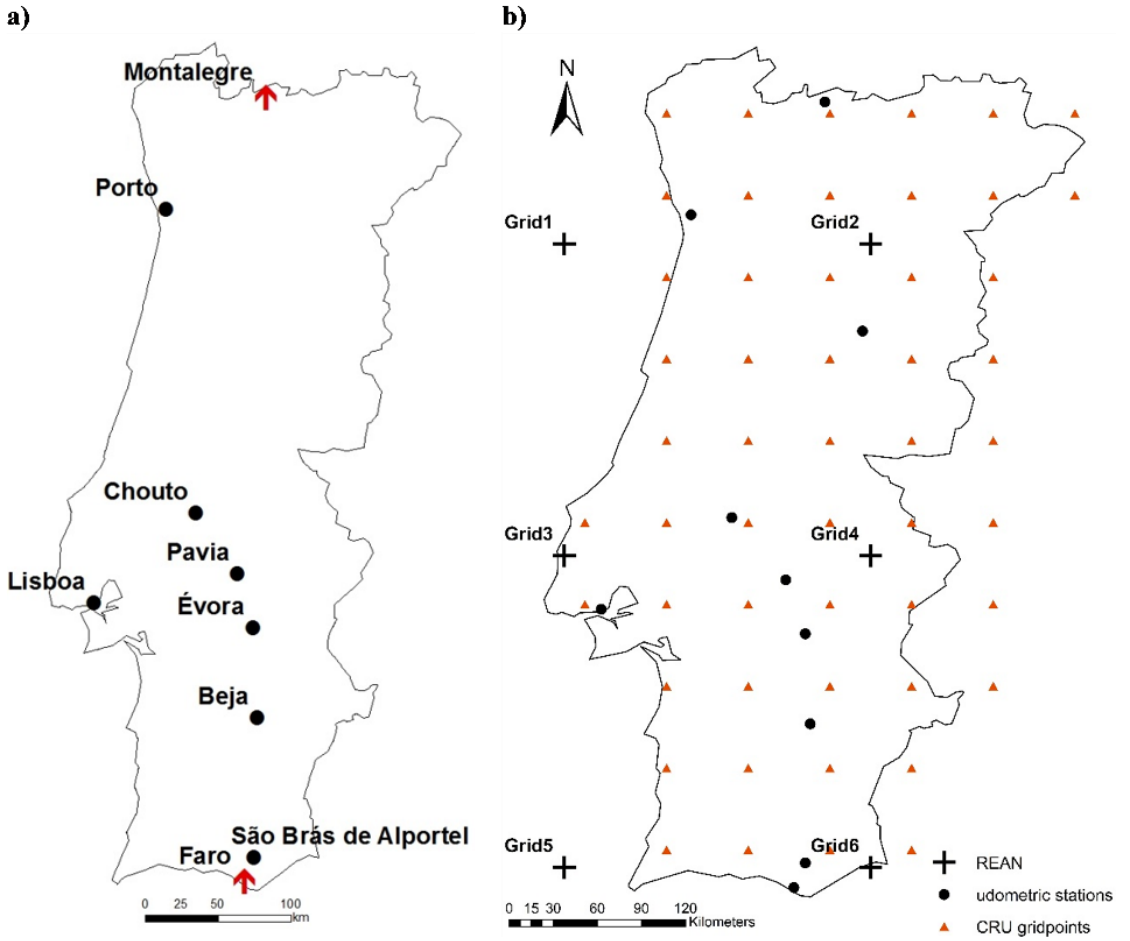

Figure 3-1 a) Location of the meteorological stations used for the SPI analysis, with the arrow representing significant trends for the increase of annual precipitation amount; b) Distribution of the 20th reanalysis gridpoints and, udometric stations and CRU gridpoints used for computing the PDSI.

Long records of monthly precipitation from 9 meteorological stations across Portugal (Figure 3-1a) were used to compute the SPI-12 in this study. These weather stations were the same used by Moreira et al. (2012) having monthly precipitation with at least 99 years. The data records were divided into sub-periods with a minimum record length of 30 years. The altitude and coordinates of the stations, dates of beginning and ending of precipitation records, record length and duration of the first sub-period preceding 1911, are presented in Table 3-1.

Annual precipitation was statistically examined for homogeneity. Linear trends, autocorrelation and changes in the median and in the variance were investigated through non-parametric tests. Due to the uncertainty and subjectivity involved in the adjustment of a single site (Rhoades and Salinger 1993) the original series were not corrected

similarly to the procedure adopted by Santos et al. (2010) in the analysis of spatial and temporal variability of droughts in Portugal based on 94 years of precipitation data. However, positive linear trends and changes in the median and in the variance of precipitation were detected in Montalegre and Faro; the first is the more northern station, located at high altitude and having annual median precipitation above 1000 mm, and the second is the more southern station, located by the coast and having an annual median precipitation below 500 mm.

Table 3-1 Location of the meteorological stations, date of records, record length and duration of the first sub-period used for the SPI analysis.

				Precipitation records		Record length (Years)	
Station	Latitude (North)	Longitude (West)	Altitude (m)	From	To	Total	before 1911
Montalegre	41.82	7.78	1005	Jan 1879	Dec 2007	128	32
Porto	41.13	8.60	93	Jan 1863	May 2012	148	48
Chouto	39.28	8.35	130	Jan 1911	Dec 2009	98	-
Pavia	38.90	8.02	192	Jan 1911	Dec 2011	100	-
Lisboa	38.72	9.15	77	Jan 1871	May 2012	140	40
Évora	38.57	7.90	309	Jan 1870	Jul 2012	141	41
Beja	38.02	7.87	246	Jan 1897	Dec 2007	110	14
S.Brás de Alportel	37.17	7.90	325	Nov 1908	Sep 2012	103	-
Faro	37.02	7.97	8	Jan 1896	Sep 2012	115	15

Precipitation time series were divided into sub-periods: prior to 1911, 1911 to 1943, 1944 to 1975 and 1976 to 2007. The criteria adopted for this partition was based on the time series length, on drought identification with SPI in the nine stations considering the full period of records, on results of a previous study with the same data (Moreira et al. 2012), and on previous drought studies applied to southern Portugal relative to the period 1932-1999 (Paulo et al., 2003, Paulo and Pereira, 2006) and to the entire country in various periods (Santos et al. 2010; Martins et al. 2012). Main droughts were identified in those studies for the years of 1944-1945, 2004-2006, 1949 and 1980-1981, all with a regional coverage of more than 60% of the area.

Box plots of annual precipitation (Figure 3-2) from October to September in 4 or 3 sub-periods according to the length of data records highlight differences between sub-periods and locations. The boxes range from the 1st to the 3rd quartile, the bold line represents de median and the plot whiskers the maximum and minimum values in each sub-period; the

outliers are not represented. Greater median values were observed in Montalegre, located at higher altitude, and Porto, in the northern region.

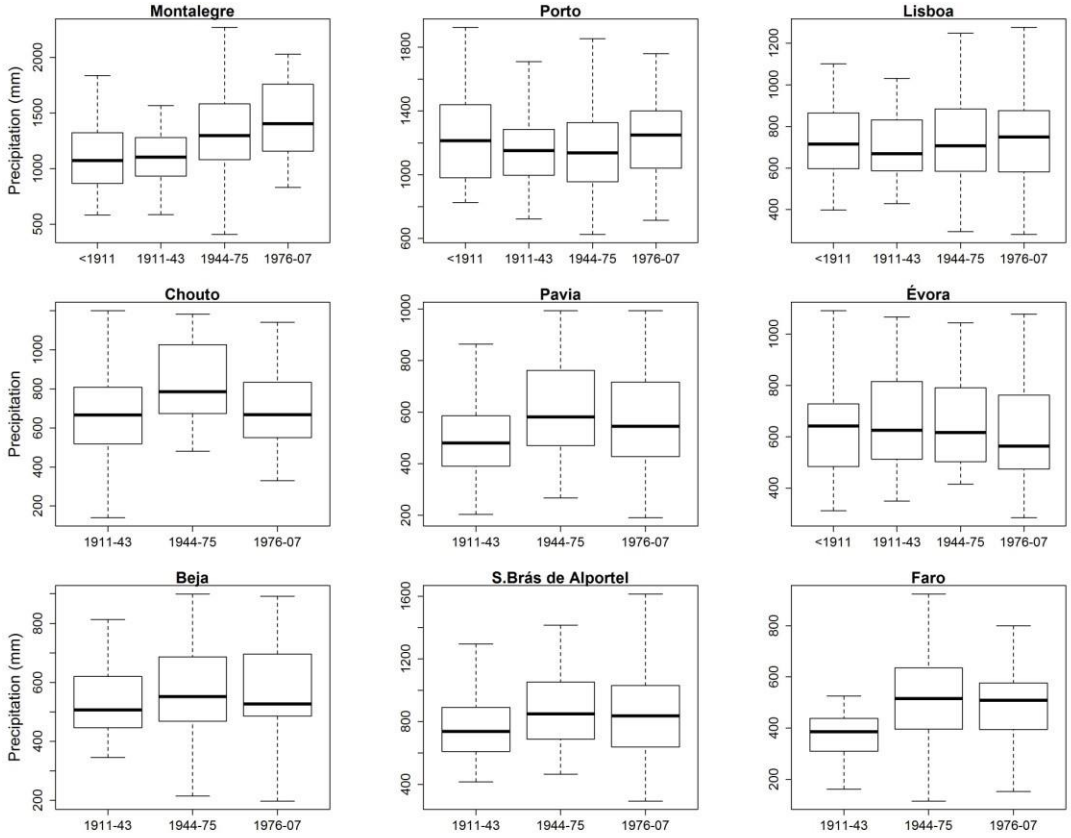

Figure 3-2 Annual precipitation (October to September) in 4 or 3 time sub-periods according to the length of data records

For the impacts of long-term variability of precipitation and PM-ET_o on drought assessment by the SPI and PDSI, monthly records of precipitation rate (kg m^2 s^{-1}), maximum and minimum temperature (K), downwards shortwave radiation (W m^{-2}), meridional (v) and zonal (u) wind components, both at 10 m height (m s^{-1}), specific humidity (kg kg^{-1}) and surface level pressure (kPa) from NOAA-CIRES Twentieth Century Reanalysis Project (hereafter 20th reanalysis) were retrieved for the period 1851-2014 (Compo et al. 2011). For this application the PDSI was computing using the FAO-PM equation (Allen et al. 1998) because previous studies have shown that evapotranspiration computed using the PM-ET_o equation better describes climate variability as discussed on the Introduction and tested in Chapter 4 and 5.

To assess the accuracy of the reanalysis based PDSI, the index was also computed with the same long records of precipitation from the weather stations used for the SPI analysis and with PM-ET_o from the CRU TS3.21 (Harris et al. 2014) with data from 1901 to 2012.

The spatial distribution of the three groups of data is depicted in Figure 3-1b. To match the observed precipitation and PM-ET_o from the CRU gridded data with the locations of the 20th reanalysis gridpoints, the average of precipitation and PM-ET_o from the udometric stations or gridpoints, respectively, in the gridded area of the 20th reanalysis was computed. The observed PDSI was computed for the common period of 1911-2007.

3.3 Methods

The SPI is a probabilistic drought index. A probability distribution is adjusted to the k-months cumulative precipitation, where k is the SPI time scale, for each calendar month. Therefore, twelve distribution functions are independently obtained. The cumulative probability associated with an observed precipitation amount is estimated from the adjusted distribution function and is then transformed into a standard normal quantile, the SPI, as described by McKee et al. (1993).

The calculation of the SPI requires the following steps (Mckee et al. 1993; Bordi and Sutera 2001; Sienz et al. 2012):

1) Estimation of the distribution $F(x;\hat{\lambda})$ where $\hat{\lambda}$ is the vector of estimated parameters. The two parameter gamma distribution was adopted with the probability density function defined by

$$f(x) = \frac{1}{\beta_l^{\alpha_l}\Gamma(\alpha_l)} x^{\alpha_l - 1} e^{-\frac{x}{\beta_l}}, \; x > 0 \qquad (3.1)$$

where Γ is the gamma function, and α_l and β_l are the shape and scale parameters. The parameters were estimated by the maximum likelihood method.

2) Calculation of the probability for each precipitation event PRE = $F(x; \hat{\alpha}_l; \hat{\beta}_l)$

3) Calculation of the standard normal quantile SPI $= \phi^{-1}$ (PRE) where $\phi(x;0,1)$ is the standard normal distribution.

Any SPI value can be back-transformed into precipitation by the inversion of the statistical and computational methods. The SPI value is transformed into non-exceedance probability through the normal distribution PRE $= \phi^{-1}$ (SPI) and the probability is transformed into precipitation x by the inversion of the gamma distribution, $x = F^{-1}(PRE; \hat{\alpha}_l; \hat{\beta}_l)$. This back-transformation assumes a perfect fit between the adjusted pdf and the empirical distribution of precipitation.

Drought is classified according to SPI values. McKee et al. (1995) proposed four drought categories: near normal/mild, moderate drought, severe drought and extreme drought (Table 3-2). The SPI is normalized, so the cumulative probabilities relative to the upper thresholds of SPI drought categories are obtained from the normal distribution.

Table 3-2 Upper thresholds of SPI drought categories and respective cumulative probabilities

Drought category	SPI (interval)	Cumulative probabilities
Mild/Near normal	[0,-1[	0.5000
Moderate	[-1,-1.5[	0.1587
Severe	[-1.5,2[	0.0668
Extreme	<-2	0.0228

The SPI provides a relative measure of drought severity, thus allowing comparisons between locations and between time periods for a given location. An SPI value in the interval [-1.5,-2[is classified everywhere as a severe drought. However, a given SPI value obtained in different locations or, in the same location using a different reference period, corresponds to different precipitation deficits, i.e., the difference between the observed and the median. Therefore, the SPI index should not be used for absolute drought comparisons between stations or, for a given station, between time periods if appropriate complementary information is not available. In the present study, the SPI is not only obtained with a pdf adjusted for the complete precipitation series but it is also computed separately for each time sub-period. This approach assumes the hypothesis of coherence between precipitation observed in a given time period and the probability laws governing the occurrence of precipitation during the same period.

A 12-month time scale identifies cumulated precipitation deficiencies over a large period, is well related with the impacts of drought in water resources and is more adequate in the present study than shorter time scales (Mishra and Singh 2010). Therefore, the SPI-12 was obtained for the nine locations and for the sub-periods defined above (Table 3-1 and Figure 3-2) and for the full period of records. The SPI-9 was also computed to be compared against the PDSI, using precipitation from the 20th reanalysis because it is time-scale that compares better with PDSI (Paulo et al. 2012). The normality of the SPI was verified in each period and calendar month through the Kolmogorov-Smirnov and the Shapiro-Wilk non-parametric tests (D'Agostino and Stephens 1986). As the Shapiro-Wilk normality test does not validate the parameters of the normal distribution the approach by Wu et al. (2007), which considers that a distribution is not normal when the

Shapiro-Wilk statistic is smaller than 0.96, the respective p-value is smaller than 0.10 and the absolute value of the median SPI is greater than 0.05, was also used.

The moments of the gamma distribution, expected value, variance and asymmetry were obtained from the shape and scale parameters

$$\mu = \alpha_l\beta_l;\ \sigma^2 = \alpha_l\beta_l^2;\ \gamma_l = \frac{2}{\sqrt{\alpha_l}} \quad (3.2)$$

and were estimated for the total period and the sub-periods. Differences in the parameter values between sub-periods relate to precipitation changes in the mean, variability and asymmetry, which are easier to interpret than comparing the shape and scale parameters of the gamma distribution.

The pdf curves and the histogram of precipitation for the total period and the sub-periods were plotted in the same graphics; similarly, the cumulative distribution functions (cdfs) were plotted in a companion graphic to support visual comparisons.

The precipitation depths corresponding to the thresholds of the SPI categories were estimated within each time sub-period and the full period. Therefore, the near normal or mild drought category (-1<SPI<0) corresponds to a precipitation depth below the median (SPI=0) and above the threshold of moderate drought (SPI=-1); similarly, for the moderate, severe and extreme drought. The inter-comparison of time periods was also performed by examining the precipitation thresholds corresponding to the same drought categories. If the precipitation threshold of a given drought category in the recent period is lower/higher than in the precedent time period it means that a decrease/increase in precipitation has occurred. Conversely, the precipitation thresholds in a given time period correspond to different cumulative probabilities in another time period and may be classified in a different drought category. The inter-comparison is therefore illustrated by a zoom of the lower tail of the cdf.

The frequency of SPI categories, for the total period and sub-periods was obtained by counting the number of months in those categories and values were tabled to support the comparison between the SPIs when computed for the full data record and for each sub-period.

The PDSI is based on a supply-and-demand concept of the soil water balance, which is applied to a two layer soil model (Palmer, 1965). The detailed computational procedure of the PDSI is on Chapter 6. Briefly, the index computes a moisture departure, i.e., is the

difference between actual precipitation and the precipitation expected to occur for the average conditions of the climate, which implies performing a monthly water balance and the calibration of local monthly coefficients for the various terms of the soil water balance (Paulo et al., 2012). Thus, four values related to the water balance, namely, evapotranspiration (ET), recharge (R), runoff (RO) and loss (L), and their potential values (α, β, γ and δ) are computed for each month of the year. These potential values of the water balance give the climatically appropriate for existing conditions (CAFEC). The selection of the period to estimate the CAFEC potential may affect the PDSI index. In this study, the water balance was computed considering a water holding capacity of 150 mm, 25 mm in the first layer and 125 in the second layer. In this application it was decided to compute the PDSI using the PM-ET_o instead of potential evapotranspiration to limit the temperature bias that this type of evapotranspiration estimators have, as discussed in Chapters 4 and 5 and in van der Schrier et al. (2011) and Dai (2011).

The PDSI and SPI-9, used to compare against the PDSI, were computed with the 20th Century Reanalysis time series (Compo et. al. 2011) for the period 1851-2014, using five different calibration periods: the total length of the time series and four periods of 40 years. This approach aimed at assessing the impact of the calibration period used to estimate the Gamma distribution parameters of the SPI-9 and the CAFEC potential values of the PDSI. Those periods were: 1851-2014, 1851-1891, 1892-1932, 1933-1973 and 1974-2014.

3.4 Results

3.4.1 Changes in the gamma distribution function

The goodness of fit tests applied to the SPI-12 showed a good agreement with the normal distribution. The Kolmogorov-Smirnov test did not reject the N(0,1) distribution of SPI in any time period, calendar month and location. The approach of Wu et al. (2007) led to only 2.9% rejections of SPI-12 normality, i.e., 14 rejections in 480 tests. These results supported the appropriateness of using the gamma distribution and the hypothesis of normality of the SPI-12.

Table 3-3 Mean, standard deviation and coefficient of asymmetry estimated from the gamma distribution fitted to the cumulated precipitation (October to September) for the full time period and the considered sub-periods

Estimates of	time period	Montalegre	Porto	Chouto	Pavia	Lisboa	Évora	Beja	S.Brás	Faro
Mean	Full records	1257	1236	728	556	737	640	566	816	471
	Before 1911	1104	1292	-	-	748	635	-	-	-
	1911-1943	1097	1182	679	504	708	665	548	773	402
	1944-1975	1376	1195	829	609	748	666	582	866	513
	1976-2007	1488	1276	706	579	732	610	567	853	509
Std. deviation	Full records	406	323	252	186	219	190	155	288	180
	Before 1911	302	363	-	-	211	193	-	-	-
	1911-1943	265	238	279	174	167	188	135	219	133
	1944-1975	479	314	215	176	224	171	158	267	192
	1976-2007	450	341	212	196	235	198	188	323	214
Coef. asymmetry	Full records	0.65	0.52	0.69	0.67	0.59	0.59	0.55	0.71	0.77
	Before 1911	0.55	0.56	-	-	0.56	0.61	-	-	-
	1911-1943	0.48	0.40	0.82	0.69	0.47	0.57	0.49	0.57	0.66
	1944-1975	0.70	0.53	0.52	0.58	0.60	0.51	0.54	0.62	0.75
	1976-2007	0.60	0.53	0.60	0.68	0.64	0.65	0.66	0.76	0.84

It is known that changes in precipitation affect the parameters and the moments of the gamma distribution. The resulting values for the mean, the standard deviation and the coefficient of asymmetry estimated for the annual precipitation cumulated from October to September are presented in Table 3-3. It can be observed that the highest mean precipitation refers to 1944-75 for all seven southern stations and to the later period in case of Montalegre and Porto, in the northern region. The lowest mean values were for 1911-43 except for Évora. The mean values computed with the full period of records were generally smaller than the mean relative to 1944-75. The differences in the precipitation

mean relative to the highest and lowest mean values relative to the considered sub-periods is quite large at Montalegre, 391 mm, and small in Beja, 32 mm. Large differences, 150 and 105 mm, were also present for Chouto and Pavia respectively. The standard deviation were often larger in the last period, 1976-2007 and not when the mean is larger. It could be observed that the coefficient of asymmetry is also more often larger in the sub-period 1976-2007.

The effects of the reference period on the gamma distribution relative to the 12 month cumulated precipitation October-September were observed in the gamma pdf and cdf curves presented in Figure 3-3 relative to the four stations with longer records, Montalegre, Porto, Évora and Lisboa. Necessarily, the above referred differences in behaviour reflected on the differences among pdf and cdf curves, as for the examples in Figure 3-3. The cases when the mean values had larger changes quite different cdf curves among sub-periods were detected.

The pdf curves (Figure 3-3) relative to the various sub-periods and the full period of records showed greater differences in the northern mountainous station of Montalegre, where differences in the mean value were larger in absolute and relative terms. Somewhat similar behavior were observed for Chouto and Pavia (not shown), where differences in the mean were large. Contrasting, smaller differences were observable for Évora, in the south and at low altitude. The other southern inland stations showed a behavior similar to Évora. Similarly, to Porto, Lisboa and Faro, other southern stations, excepting Chouto and Pavia, showed a behavior marked by the changes in pdf during 1911-43 (left panel of Figure 3-3). These differences also appeared in the cdfs, on the right panel of Figure 3-3. In the station of Montalegre, the cdf curves of the initial sub-periods were nearly superposed while the curves of the more recent sub-periods of 1944-75 and 1976-2007 were somewhat distant with the cdf relative to the full period lying in the middle, so reflecting the average conditions over the complete time of records. Differently, all other stations showed cdf curves closer than in Montalegre. This indicates a smaller variability of precipitation, which was also evident from Figure 2-2 and Table 3-3.

In Montalegre the median, i.e., the 12-month precipitation corresponding to a 0.5 cumulative probability was higher for recent conditions. Generally, with exception for Évora, precipitation with higher non-exceedance probabilities in 1911-43 were lower than for other sub-periods as shown by the cdfs on the right panel of Figure 3-3. However, as referred before, differences among sub-periods were smaller than for Montalegre.

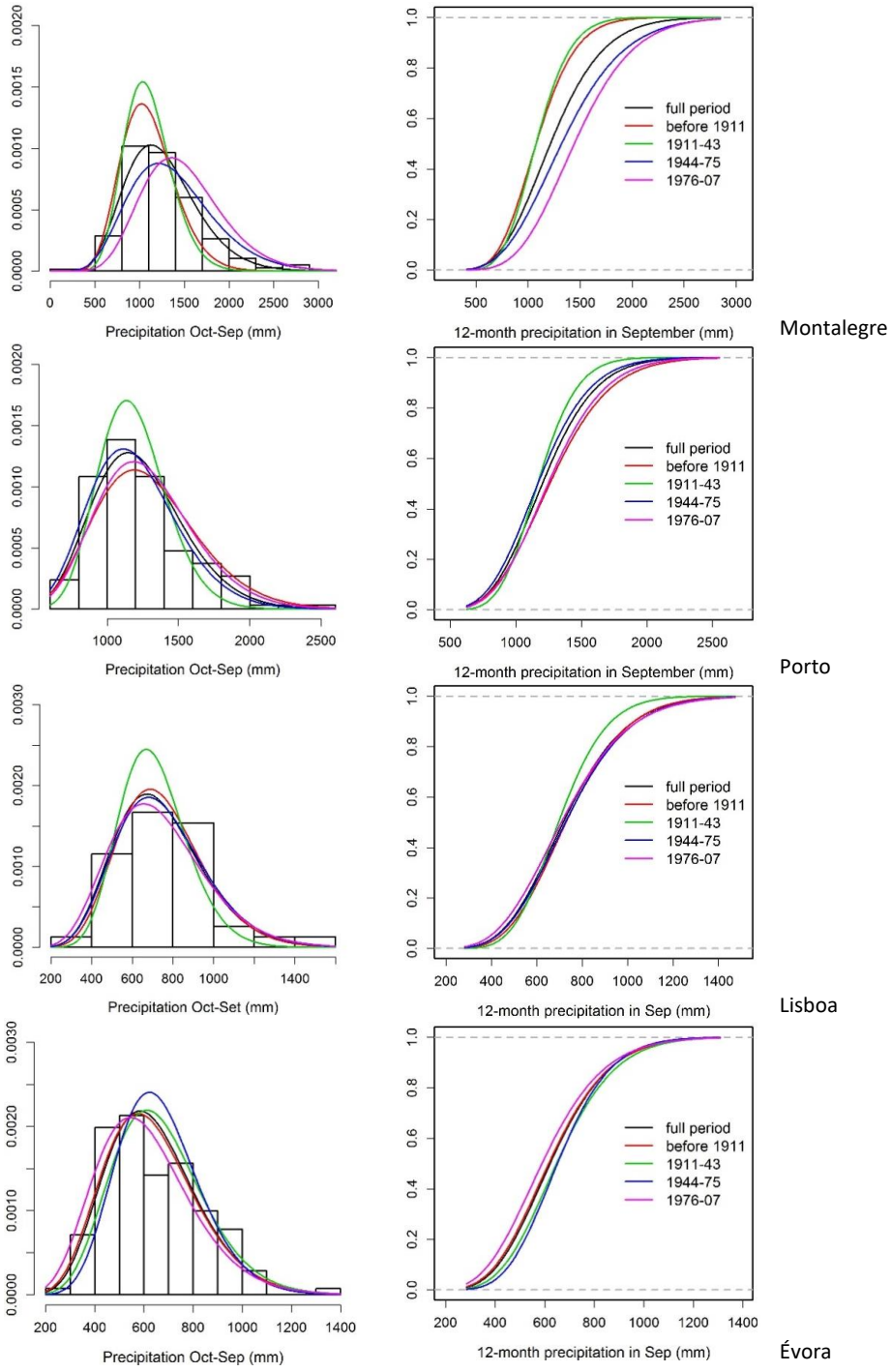

Figure 3-3 Gamma probability distribution functions (on left) and cumulative distribution functions (on right) of annual precipitation cumulated from October to September for the full data records and the four sub-periods for Montalegre, Porto, Lisboa and Évora. The histogram of the precipitation frequencies for the full period is also shown.

3.4.2. Changes in SPI precipitation thresholds

A zoom of the lower tail of the cdfs relative to October-September is presented in Figure 3-4 relative to the four stations having longer periods of records. The zoom allowed identifying the SPI precipitation thresholds relative to moderate, severe and extreme

droughts. These values corresponded to the interception of the SPI horizontal lines with the cdf curves relative to the full period and the sub-periods. For a given location, the horizontal distance between two interception points relative to the various drought categories corresponded to the difference in precipitation for the considered sub-periods relative to the SPI thresholds. When differences in precipitation among sub-periods were large than the difference of the thresholds were also large. When the precipitation threshold values increase (decrease) this meant that a given drought category was attained for a larger (smaller) precipitation than before.

The distances between cdf curves at the lower tail were higher in Montalegre (and Chouto, not shown). Conversely, differences were smaller in Lisbon and Porto (and Beja, not shown). Montalegre was the location where the cdf curves of the various periods show an increase in the SPI precipitation thresholds from the earlier to the last period. A moderate drought was identified for 806 mm in the period prior to 1911 while for the last period, 1976-2007, that amount increased to 1046 mm (Table 3-4). For the severe droughts, the threshold increased for the same periods from 690 to 878 mm. This behavior was due to an increase of precipitation as identified in Figure 3-2 and through trend analysis. Due to that increase, the month September 1989, with a 12-month cumulated precipitation of 832 mm, thus between the precipitation thresholds 731 and 878 mm (Table 3-4) relative to SPI=-1.5 and SPI=-1 and identified as severely dry, would be classified as a moderate drought month if the full period threshold interval, 711 mm to 859 mm, was applied. Differently, for Porto changes in precipitation thresholds among the four sub-periods were small (Figure 3-4). For Lisboa, Évora and Beja the precipitation thresholds increased and decreased through the considered sub-periods but the threshold relative to the last period was the smallest one. This may indicate a variable trend in annual precipitation depths. In Lisbon, a severe drought was identified for a threshold of 459 mm prior to 1911 while for the latest period that threshold decreased to 416 mm (Table 3-4); for Porto, there was a small increase, from 795 to 807 mm, and for Évora there was a decrease from 373 to 343 mm.

For all other stations, the smaller precipitation thresholds for the three drought categories generally referred to the period of 1911-43 and the larger ones referred to 1944-75. When considering the extreme drought category the comparison among sub-periods was generally similar to that for severe droughts. A possible interpretation is that droughts were probably not aggravating but they were somewhat responding to some cyclic

variation as per the analysis performed by Moreira et al. (2012), also in agreement with the trend analysis performed by Santos et al. (2010), Martins et al. (2012), Paulo et al. (2012) and Raziei et al. (2015). However, despite there was no evidence of aggravation of droughts in terms of SPI values, the meaning of the category of drought is certainly different when, for instance, a severe drought in Évora was attained when the precipitation was not above 408 mm, in 1911-43, and later was attained if precipitation did not exceed 343 mm. In fact, that difference of 65 mm may indicate that impacts of a severe drought have increased with the decrease of the precipitation. It is likely that instead of using a probabilistic and standardized drought index results could be different when using a deterministic index like PDSI or MedPDSI that determine the departure from normal conditions through a water balance using precipitation and evapotranspiration data.

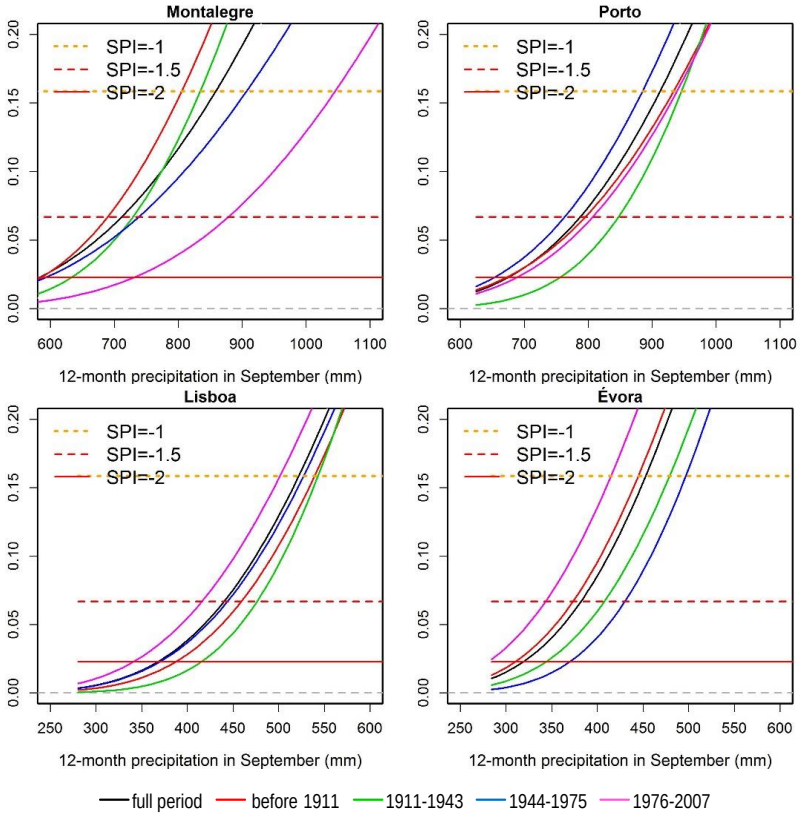

Figure 3-4 Zoom on the lower tail of the gamma cumulative distribution functions of Montalegre, Porto, Lisboa and Évora for the full period of records and four sub-periods with identification of the related SPI-12 thresholds of moderate, severe and extreme drought categories relative to the 12-month precipitation from October to September.

Table 3-4 Precipitation thresholds (mm) corresponding to SPI-12=0 (median), SPI-12=-1, -1.5, -2 (moderate, severe and extreme drought categories) computed for September with the full records and respective sub-periods for all weather stations.

		Meteorological stations								
SPI	Period	Monta	Porto	Chouto	Pavia	Lisboa	Évora	Beja	S.Brás	Faro
0	Total	1214	1208	699	536	716	621	552	782	448
	Before	1077	1258	-	-	728	615	-	-	-
	1911-43	1076	1167	641	485	695	647	537	752	387
	1944-75	1321	1168	810	593	725	651	567	839	489
	1976-07	1443	1246	685	557	707	588	546	812	479
-1	Total	859	916	481	374	522	453	413	534	295
	Before	806	934	-	-	539	445	-	-	-
	1911-43	835	946	408	334	543	479	415	556	272
	1944-75	907	885	616	436	527	497	425	603	325
	1976-07	1046	939	497	386	502	415	382	537	301
-1.5	Total	711	790	391	308	440	382	354	433	234
	Before	690	795	-	-	459	373	-	-	-
	1911-43	729	847	317	272	476	408	362	473	224
	1944-75	738	763	532	370	444	430	364	505	260
	1976-07	878	807	418	316	416	343	315	428	232
-2	Total	583	677	315	250	368	319	300	346	183
	Before	586	672	-	-	388	310	-	-	-
	1911-43	633	756	242	219	415	344	313	399	182
	1944-75	593	653	456	311	370	370	310	418	204
	1976-07	731	688	348	256	341	281	256	335	175

Observing the time series of SPI-12 in Montalegre, Porto, Évora and Lisboa (Figure 3-5) computed for the full period and for each sub-period it was possible to notice a disagreement between the SPI-12 computed for the full data set and for the sub-periods. At Montalegre, the first two sub-periods, prior to 1911 and 1911-1943, had higher SPI values when they were computed with the sub-periods data, inversely during the later sub-periods. This behaviour related with the referred changes in the drought (and wetness) precipitation thresholds as analysed before. This result highlighted an apparent increase of precipitation at Montalegre in the more recent time periods.

The SPI series for Porto behaved similarly but with less evidence of changes; differently, for Lisboa and Évora there was a better agreement between SPI computed from the pdf adjusted for the full period and for the sub-periods, meaning that normal precipitation patterns were similar in the full period and sub-periods. Briefly if the SPI values in recent periods were lower/higher when using the full period as reference period instead of the sub-periods then a recent downward/upward shift of precipitation may have occurred. The ´normal´ conditions were therefore changing and an update of the SPI calculation

should be considered. This could be particularly important when comparing past conditions with future if changes in precipitation are foreseen for future; it is then likely that SPI thresholds will be different, leading to possible biased interpretations of changes in droughts.

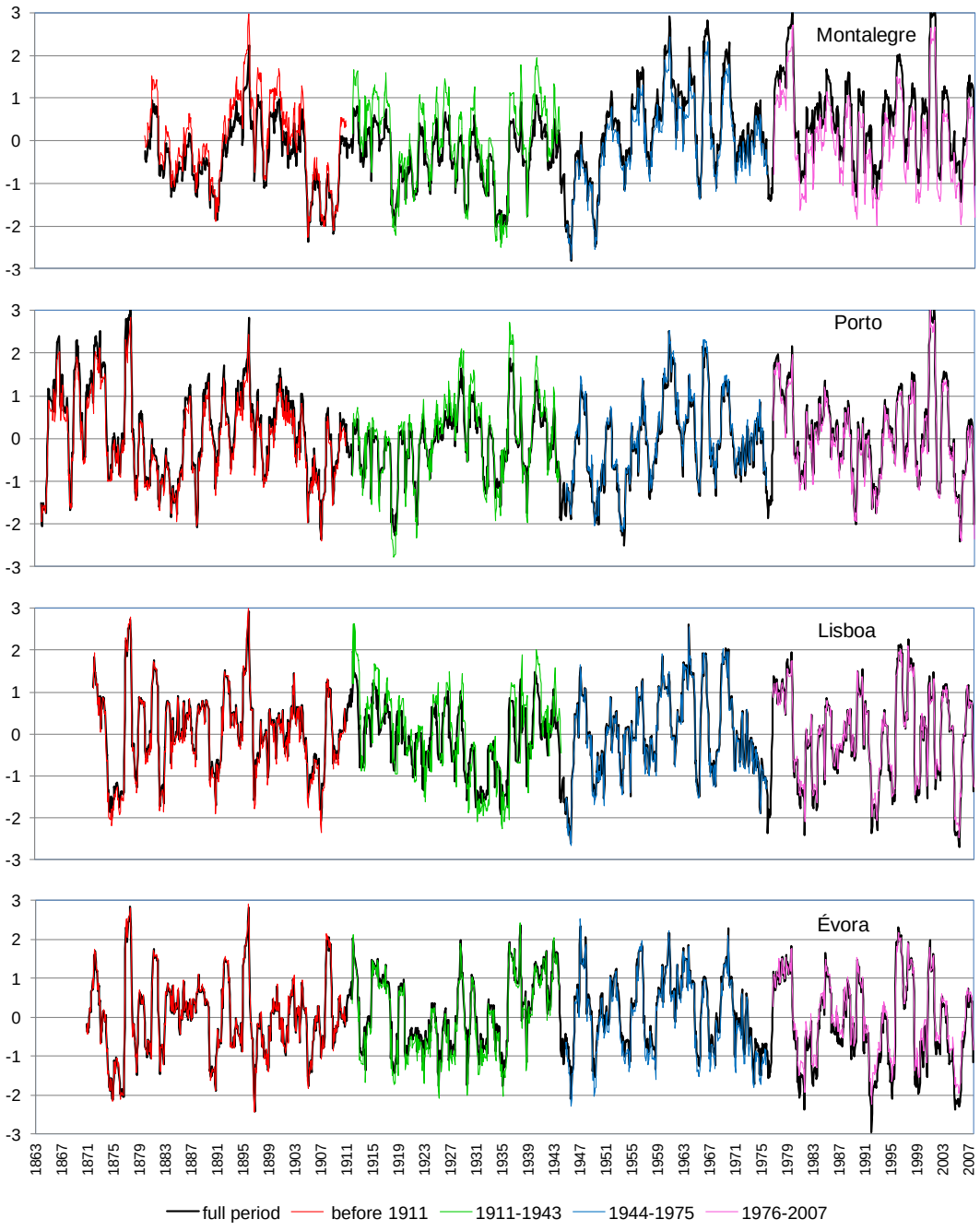

Figure 3-5 SPI-12 at Montalegre, Porto, Évora and Lisboa computed for the full data period and for the sub-periods.

3.5 Changes in the percentage of time in SPI categories

The percentage of time in moderate and more severe (combined severe and extreme) drought and wetness categories for each time period is shown in Table 3-5 for the nine stations using as reference period the full record and each sub-period. The 1911-43 and the more recent time period, 1976-2007 showed greater differences on the percentage of time in the SPI categories.

Table 3-5 Comparing the percentage of time in moderate, severe and extreme drought/wetness categories for the full period (full) of records and the various sub-periods (sub); Mont. is Montalegre; Extr+S is extreme plus severe and Moder is Moderate

Time	SPI category		Reference	Meteorological Stations								
				Mont.	Porto	Chouto	Pavia	Lisboa	Évora	Beja	Faro	S.Brás
1879-	Dry	Extr+S	Full	10%	5%	-	-	5%	6%	-	-	-
			Sub	9%	6%	-	-	8%	6%	-	-	-
1910		Moder	Full	12%	10%	-	-	9%	10%	-	-	-
			Sub	8%	12%	-	-	10%	9%	-	-	-
	Wet	Moder	Full	3%	12%	-	-	9%	5%	-	-	-
			Sub	12%	10%	-	-	8%	4%	-	-	-
		Extr+S	Full	1%	12%	-	-	6%	8%	-	-	-
			Sub	6%	7%	-	-	6%	9%	-	-	-
1911-	Dry	Extr+S	Full	10%	5%	10%	11%	5%	1%	5%	6%	5%
			Sub	11%	7%	7%	10%	10%	4%	6%	4%	6%
1943		Moder	Full	8%	7%	13%	10%	9%	8%	10%	16%	11%
			Sub	6%	8%	5%	4%	6%	17%	10%	11%	12%
	Wet	Moder	Full	0%	5%	7%	5%	8%	13%	10%	4%	6%
			Sub	13%	6%	10%	11%	10%	12%	11%	8%	10%
		Extr+S	Full	0%	2%	5%	3%	1%	8%	2%	3%	2%
			Sub	3%	7%	5%	5%	7%	6%	8%	8%	7%
1944-	Dry	Extr+S	Full	6%	8%	0%	2%	6%	2%	6%	5%	4%
			Sub	6%	6%	5%	6%	6%	5%	6%	7%	6%
1975		Moder	Full	5%	12%	2%	6%	10%	8%	8%	5%	7%
			Sub	8%	9%	13%	8%	8%	15%	10%	10%	9%
	Wet	Moder	Full	11%	9%	15%	15%	10%	15%	12%	17%	14%
			Sub	8%	11%	13%	12%	10%	11%	12%	14%	11%
		Extr+S	Full	13%	6%	9%	9%	9%	6%	7%	8%	7%
			Sub	9%	7%	7%	9%	9%	6%	6%	3%	6%
1976-	Dry	Extr+S	Full	0%	5%	3%	6%	13%	17%	15%	8%	7%
			Sub	4%	5%	8%	6%	7%	6%	8%	8%	7%
2007		Moder	Full	5%	10%	12%	8%	9%	10%	4%	7%	10%
			Sub	17%	12%	10%	11%	12%	12%	10%	8%	12%
	Wet	Moder	Full	16%	11%	10%	13%	13%	13%	10%	10%	13%
			Sub	8%	10%	11%	14%	11%	15%	9%	5%	10%
		Extr+S	Full	15%	8%	3%	10%	8%	6%	11%	10%	11%
			Sub	7%	6%	7%	6%	6%	6%	8%	7%	7%

In 1976-2007, a disagreement between the percentage of months in the more severe drought categories when using the full period and the sub-period as reference was observed in some stations. In Montalegre, when the gamma distribution was obtained from the centennial record, the frequency of severe and extreme drought months in the time period 1976-2007 was 0% and the percentage of time in moderate drought is 5%, corresponding to only 18 months in 32 years of the sub-period. From the perspective of present, when considering 1976-2007 as reference for the computation of SPI results were quite different with 4% of time under more severe drought and 17% with moderate drought. Using the full period as reference, 16% of time in moderate wetness and 15% in more wet categories were identified, thus contrasting with the drought conditions. These results, dictated by a 128 years long precipitation record having a significant positive trend, would identify 1976-2007 as a wet period. Differently, deriving the SPI from data relative to that period, a moderate wetness. This behaviour is coherent with issues discussed before and reflects the detected changes in precipitation. The behaviour for Faro, where an increased precipitation trend was detected, was somewhat similar but mitigated because changes in precipitation are smaller than at Montalegre.

For Porto, differences in the frequency of drought (wetness) events when the SPI was computed from full data or from sub-periods, data were relatively small. In the previous analysis it was observed that differences in precipitation thresholds were small, which may justify that behaviour.

In Évora, the SPI obtained from the full precipitation record identified as dry (moderate or more severe) 10% of the months in the time periods 1911-43 and 1944-75 and 27% in 1976-2007, very different from the balanced percentages of 21%, 20% and 18% relative to the SPI sub-period time series. Particularly in 1976-2007, 17% of months were identified as severe or extremely dry with the full record and that frequency decays to 6% under 1976-2007 gamma distribution of precipitation. The results obtained for the full record parametrization may be explained by the negative but not significant trends observed in precipitation (not shown). In Lisboa and Beja, in the later period, the SPI obtained from the full record identified 13% of the months as severe or extremely dry in Lisboa and 15% in Beja while for the sub-period those percentages diminish to 7% in Lisboa and 8% in Beja. An over estimation of drought frequencies in the later period by the full record distribution may indicate a recent precipitation decrease and was also concordant with the decrease of the precipitation thresholds of drought categories in 1976-2007. For Chouto, under the gamma distribution of the full record, a 2% frequency

of the moderate or more severely dry months in the second period, 1944-75, contrasted with the 23% in the period 1911-43 and 15% in the more recent period while it remained almost the same for the sub-periods distributions. Pavia presented approximately the same tendencies for the 1911-43 and 1944-75 sub-periods. In S. Brás de Alportel, in the south, there was a better agreement between the percentage of severely dry months for the full period and the sub-periods; however, the first period was characterized by a marked difference relative to the wettest months, 8% for the full record versus 17% for the sub-period. These results showed the drought frequency similarities between alternate sub-periods in Chouto and Pavia and the dissimilarities between the consecutive 1944-75 and 1976-2007 time periods in Évora, Beja and Lisboa relative to the percentage of severely dry months when considering a unique SPI time series, in the same line of the study conducted by Moreira et al. (2012).

3.6 Time variability of precipitation and PM-ET_O from the 20th Century reanalysis

Table 3-6 Comparison of mean (μ) and standard deviation (σ^2) of reanalysis precipitation and PM- ET_o in each grid-point for the five calibration periods.

	1851-2014		1851-1891		1892-1932		1933-1973		1974-2014	
	μ	σ^2	μ	σ^2	μ	σ^2	μ	σ^2	μ	σ^2
Precipitation (mm month^{-1})										
Grid1	70.8	70.5	70.8	71.2	74.2	68.6	74.7	73.9	63.3	67.6
Grid2	78.3	73.4	77.0	74.7	80.5	70.0	83.6	77.9	71.9	70.5
Grid3	60.4	68.3	60.4	70.2	62.3	67.1	64.5	69.7	54.5	65.8
Grid4	65.0	72.6	63.5	74.9	65.6	69.7	70.6	75.5	60.2	69.7
Grid5	45.7	57.2	45.8	59.7	46.8	55.1	49.0	57.3	41.2	56.3
Grid6	43.5	56.5	42.0	58.2	43.9	53.6	48.1	59.6	40.2	54.2
PM-ET_o (mm d^{-1})										
Grid1	2.8	1.3	2.7	1.3	2.7	1.2	2.8	1.3	2.8	1.2
Grid2	2.9	1.3	2.8	1.4	2.8	1.3	2.9	1.3	2.9	1.3
Grid3	3.2	1.3	3.2	1.4	3.2	1.3	3.3	1.3	3.3	1.3
Grid4	3.3	1.3	3.2	1.4	3.2	1.3	3.3	1.3	3.3	1.3
Grid5	3.6	1.3	3.6	1.4	3.6	1.3	3.7	1.3	3.7	1.3
Grid6	3.6	1.3	3.6	1.4	3.6	1.3	3.7	1.3	3.7	1.3

To search for changes in the longterm variability of time series of precipitation and PM-ET_o in the six grid-points (PRE_{REAN} and PM-$ET_{o\,REAN}$) used in this study, the mean value and the standard deviation were computed for the entire period of data (1851-2014) and to each period of 40 years (Table 3-6). Results in Table 3-6 showed a large variability of

PRE $_{REAN}$, with a variance close to the mean, while the variability of PM- $ET_{o\ REAN}$ is smaller. In the 164 years analyzed, the lowest values of both of the mean and variance of the precipitation were observed in the latest period (1974-2015) in all the grid-points, which was consistent with the negative precipitation trend over Iberian Peninsula related to more frequent North-Atlantic Oscillation (NAO) positive phases (Rodríguez-Puebla and Nieto 2009). The periods 1892-1932 and 1933-1973 were the wettest periods, both in terms of mean and variance of precipitation. PM-ET_o variability changes little throughout the period with a slow increase in both mean value and variability over the years.

3.7 Comparing the 20th century reanalysis with observations

PRE $_{REAN}$ was compared with their observations conterparts and PM-$ET_{o\ REAN}$ were compared with the respective grid-points obtained from the average of the observed precipitation and PM-ET_o (PRE $_{OBS}$ and $ET_{o\ OBS}$) in the gridded area of the 20th-century reanalysis, for the common period between 1911-2007 (Table 3-7) using a set of performance indicators. This set of indicators were used to assess the performance of the precipitation and reference evapotranspiration from the 20th century reanalysis in representing the amplitude and time variation of those climate variables. The comparison between the observed time series of precipitation and PM-ET_o, O_i, with corresponding reanalysis time series, P_i, was performed using the following statistical indicators: i) the regression coefficients, the slope of the linear regression (b) and respective intercept (a); ii) the slope of linear regression (b_0) of a linear regression forced to the origin (FTO); iii) the coefficient of determination (R^2); iv) the Root Mean Square Error (RMSE); iv) the Percent Bias (PBIAS) which is the ratio between reanalysis bias and mean observations, that measures the average tendency of the reanalysis data to be larger or smaller than corresponding observations; and vi) the efficiency of modelling, EF, (Nash and Sutcliff, 1970) that measures the relative magnitude of the mean square error ($MSE=RMSE^2$) and the observed data variance (Legates and McCabe Jr., 1999). These indicators were also applied to compare monthly and daily PM-ET_o estimated from reanalysis data with PM- ET_o estimated from observations (Chapter 5) and were defined therein in detail.

The comparison between the observed precipitation against the precipitation from reanalysis relative to the 6 gridpoints (identified in Figure 3-1) from the 20th Century reanalysis covering Continental Portugal revealed a general tendency for the underestimation of precipitation, with 4 out of 6 gridpoitns having large negative PBIAS,

with values ranging from -14.70% to -39.50%: and two gridpoints, Grid 3 and 4, with respective values of PBIAS of 0.10 and 22.60. b_0 values and the linear regression coefficients also followed the PBIAS values with a general pattern for underestimation of precipitation in almost all gripoints, except for Grid3 and Grid4, which had a good agreement between observations and reanalysis and a large overestimation of precipitation, respectively. R^2 was relatively high for all locations, ranging from 0.74 in Grid6 to 0.83 in Grid4. EF, however was lower than R^2 for all Grid points, starting with 0.55 for Grid2 and reached 0.78 for Grid5, but still showed adequate indicator values. These results indicated that precipitation provided by the reanalysis was able to explain the observed precipitation variability in most of the locations but the amplitude of the observed time series was not well explained by the reanalysis series, with large PBIAS values, in absolute terms, which were also reflected by large RMSE values that reached a maximum of 87.48 mm month^{-1} in Grid2 (Table 3-7).

Table 3-7 Performance indicators relative to the comparison between PRE_{REAN} and $PM\text{-}ET_{o\ REAN}$ against PRE_{OBS} and $PM\text{-}ET_{o\text{-}OBS}$

	b	a*	b_0	R^2	RMSE*	EF	PBIAS (%)
PRE_{OBS} vs PRE_{REAN} (mm month^{-1})							
Grid1	0.71	-0.51	0.71	0.82	49.30	0.70	-29.20
Grid2	0.52	11.73	0.56	0.82	87.48	0.55	-39.50
Grid3	0.94	3.48	0.97	0.80	30.22	0.78	0.10
Grid4	1.20	1.40	1.21	0.83	33.78	0.62	22.60
Grid5	0.72	6.49	0.76	0.76	34.64	0.74	-16.30
Grid6	0.80	2.55	0.82	0.74	31.67	0.72	-14.70
$PM\text{-}ET_{o\ OBS}$ vs $PM\text{-}ET_{o\ REAN}$ (mm day $^{-1}$)							
Grid1	0.93	0.41	1.07	0.72	0.70	0.62	9.30
Grid2	0.73	0.84	0.96	0.76	0.77	0.75	2.90
Grid3	0.83	0.94	1.09	0.77	0.81	0.66	16.00
Grid4	0.65	1.13	0.92	0.80	0.87	0.77	-0.60
Grid5	0.80	1.26	1.14	0.78	0.96	0.57	22.00
Grid6	0.68	1.38	1.00	0.79	0.87	0.75	8.30

b is the regression coefficient of a linear regression, a is the intercept of the linear regression, b_0 is the regression coefficient of a linear regression forced to the origin, R^2 is the coefficient of determination, RMSE is the Root Mean Square Error, EF is the efficiency of modelling, PBIAS is the Percent Bias. * indicates the same units as the variables.

Results relative to the $PM\text{-}ET_o$ analysis showed a tendency for overestimation of reference evapotranspiration estimated by reanalysis. b_0 was larger than 1 for Grid 1, 3 and 5 and PBIAS had maximum value of 22.00% for Grid5. However, these results

showed that the reanalysis PM-ET_o time series were more able to describe the amplitude of values of the observed counterparts, however, the variability of observed PM-ET_o was less well explained by reanalysis, with lower R^2, ranging from 0.72 to 0.80 and also lower EF values (Table 3-7).

Figure 3-6 shows the comparison between PDSI and SPI-9 obtained from the reanalysis data (PDSI $_{REAN}$, SPI-9 $_{REAN}$) and the respective PDSI and SPI-9 computed with the observed data (PDSI $_{OBS}$, SPI-9 $_{OBS}$) by comparing the frequency of each drought class. The different drought classifications relative to both indices were adopted. Results showed that the frequency of extreme and severe drought events were much larger when PDSI was computed from reanalysis data. Only for Grid4 the frequency of severe events of PDSI $_{REAN}$ was lower. However, the frequency of drought events detected by SPI-9 $_{REAN}$ was closer to SPI-9 $_{OBS}$. Extreme wet events were more frequent through the SPI-9 $_{OBS}$, and extreme and severe events were more frequent through SPI-9 $_{REAN}$ although the difference was smaller than when comparing PDSI $_{REAN}$ with PDSI $_{OBS}$.

Considering the nature of the drought indices, the underestimation of precipitation and the overestimation of PM-ET_o (Figure 3-6), were acceptable to analyze how PDSI and SPI changed with time and with the calibration period. Since PDSI combines precipitation and PM-ET_o through a water balance, if precipitation was greatly underestimated and PM-ET_o was overestimated, then drier, more frequent, events were expected. Differently, as the SPI is a probabilistic index that computes the deviation from average precipitation conditions, the underestimation of PRE $_{REAN}$ should not affect the frequency of dry events detected as long as the reanalysis time series are able to describe the variability of observed precipitation, which was the case for precipitation (Table 3-7).

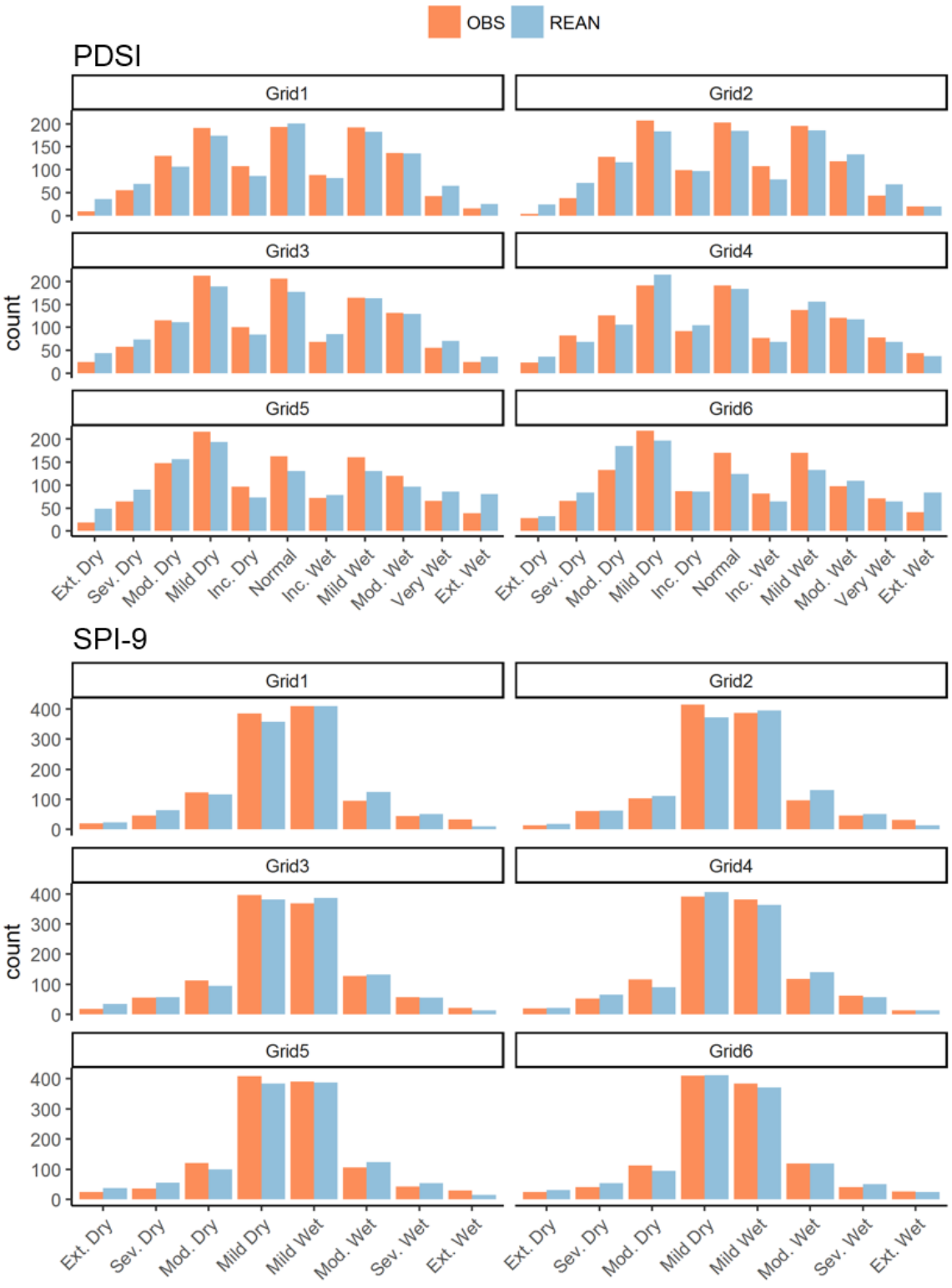

Figure 3-6 Comparison of the count of occurrences in each class of PDSI and SPI-9 computed reanalysis and observations (Ext. Dry: Extreme droughts; Sev. Dry: Severe droughts; Mod. Dry: Moderate droughts; Mild Dry: Mild droughts; Incip. Dry: Incipient drought; Incip. Wet: Incipiently wet; Mild Wet: Mildly wet; Mod. Wet: Moderately wet; Very Wet: Very wet; Ext. Wet: Extremely wet).

3.8 Analysing the long-term variability of the PDSI and the SPI-9

To assess how the climate variability affect both PDSI and SPI-9, different calibration periods (CP) were used to estimate the Gamma pdf parameters, for SPI-9, and the potential values of the water balance of the PDSI, using the 20th-century reanalysis data for the period 1851-2014.

Results showed that, despite no major changes occurred in the time variability of precipitation and PM-ET_o in the entire period, the selection of the reference period was important. Results were coherent for all grid-points and to both PDSI and SPI, and thus, in Table 3-8, only examples for Grid2 and Grid3 were shown. Focusing the analysis on the occurrence of extreme and severe events, there were clear differences between the PDSI time series calibrated for the five reference periods. The PDSI calibrated using the complete period (1851-2014), as suggested by many authors (Karl 1986; Mo and Chelliah 2006; Van Der Schrier et al. 2013), identified more extreme and severe drought events relative to calibration for the periods 1851-1891 and 1974-2014, and lesser number of extreme and severe wetness events than those identified when the PDSI was calibrated for those periods. In fact, the PDSI calibrated for 1974-2014 was the most different when compared to the other CP. Only 4 or 5 extreme dry events were identified in 164 years in Grid2 and Grid3, respectively, and 30 severe drought events were identified, which were much less than those identified for all other periods. The number of severe and extreme wet events increased significantly in this period, in all grid-points, when compared to the PDSI calibrated for the other periods. Similar results were found for SPI-9 for all grid-points. Lower occurrence of extreme and severe events were identified when the SPI-9 was calibrated for the period 1974-2014 and with the highest occurrence of extreme and severe wet events being identified for this CP as well. The highest occurrence of severe and extreme dry events occurred when both drought indices were calibrated using the wet periods 1892-1932 and 1933-1973 (Table 3-6). These results combined with the variation of the mean values of precipitation and reference evapotranspiration in each period showed that both drought indices were influenced by the climatology of the reference period selected, even if the magnitude of those changes are not considerably large. The selection of a drier period such as the period 1974-2014 resulted in drought indices with larger identification of wet events, whereas a wetter 30 year period produced drought indices more prone to detect more extreme and severe droughts (Table 3-6 and Table 3-8).

Table 3-8 Count of occurrences in each class of PDSI and SPI-9 using different calibration periods for Grid2 and Grid3

Index	Calibration Period	Ext. Dry	Sev. Dry	Mod. Dry	Mild Dry	Inc. Dry	Normal	Inc. Wet	Mild Wet	Mod. Wet	Very W.	Ext. W.
PDSI												
Grid2	1851-2014	35	137	200	323	150	304	149	322	209	98	41
	1851-1891	22	93	191	313	165	308	168	303	225	124	56
	1892-1932	100	167	246	320	173	297	141	285	160	56	23
	1933-1973	74	175	240	354	167	325	140	260	155	53	25
	1974-2014	4	30	161	256	136	305	135	353	263	197	128
Grid3	1851-2014	68	137	207	324	143	270	137	281	218	127	56
	1851-1891	62	134	220	320	150	266	151	265	223	123	54
	1892-1932	124	165	236	328	126	287	131	239	205	86	41
	1933-1973	128	163	261	345	150	290	115	266	162	56	32
	1974-2014	5	45	143	261	97	255	137	305	293	207	220
		Ext. Dry	Sev Dry	Mod Dry	Mild Dry	Mild Wet	Mod. Wet	Very Wet	Ext. Wet			
SPI-9												
Grid2	1851-2014	35	104	203	593	703	207	90	25			
	1851-1891	21	62	179	617	757	212	87	25			
	1892-1932	150	147	233	491	610	173	99	57			
	1933-1973	93	154	232	615	637	149	61	19			
	1974-2014	13	35	119	561	779	264	128	61			
Grid3	1851-2014	44	100	173	638	688	205	75	37			
	1851-1891	23	72	177	659	741	196	62	30			
	1892-1932	134	119	231	590	540	191	101	54			
	1933-1973	91	144	220	628	617	157	63	40			
	1974-2014	12	35	112	564	759	283	124	71			

The largest difference observed in Table 3-8 occurred in the last period, 1974-2014, which was drier than the previous periods and the calibration period that considered the complete time series (1851-2014). According to Dai and Zhao (2017) this was due to global warming observed since the 1980s which is caused by anthropogenic forcing and, thus, one should avoid considering calibration periods after the 1980 for the PDSI calibration, so the impacts of climate change are not included in the PDSI calibration. Even then, excluding the period after 1980, the selection of the calibration period should be discussed when using larger time series such as the ones used in this study of the PDSI, either using the period 1851-1980 or other possibilities, all of which, as observed by the results in Table 3-8 would have relevant impacts on the drought indices obtained. Thus, the establishment of the reference calibration period, when possible, would limit these effects and allow comparisons of the PDSI, and the SPI for that matter, among different studies

using different input data and for other locations. This is done by NOAA with their PDSI computational tool, using the reference period 1931-1990, although this options goes against the results obtained by Dai and Zhao (2017) that discourage the use of data after 1980 to calibrate the PDSI.

3.9 Conclusions

The influence of the reference period in the SPI and PDSI computation was explored using long time series of precipitation, for the case of the SPI and precipitation and reference evapotranspiration for the PDSI segmented into sub-periods. Results have shown that when SPI values derived from the full data record for a recent time period are lower/higher, than the SPI values derived from data of the considered time period a recent downward/upward shift of precipitation has occurred. The estimation of the precipitation thresholds for the moderate, severe and extreme drought categories, corresponding to SPI=-1, SPI=-1.5 and SPI=-2, complemented the information provided by the SPI. The joint plotting of the pdf and cdf computed for the full period and the different sub-periods allowed a visual comparison of the distributions and allowed to perceive that large differences in the SPI precipitation thresholds would be justified.

It was observed that long-term precipitation variability was reflected on the precipitation thresholds in different periods. The changes in precipitation from the initial until the more recent time period in locations where a positive trend existed, such as Montalegre, produced increasing drought severity precipitation thresholds meaning that a recent severe drought should be classified as moderate when the full period distribution is applied. For most stations, the precipitation thresholds relative to a given drought category in the more recent period 1976-2007 were lower than in the precedent period meaning that a downward shift in precipitation may have occurred, except for the northern stations of Porto and Montalegre. In some stations, an observed precipitation depth in the last period, classified by the SPI as moderate drought, could be classified as a severe drought if the SPI has been obtained from the probability distribution of the full data record. The differences between the severe precipitation thresholds in the more recent and in the precedent period range from -140 mm in Montalegre to 114 mm in Chouto showing positive values in the southern stations and thus reflecting a possible decrease in precipitation. An over estimation of drought frequencies in the later period by the full record distribution as verified in Lisboa, Évora and Beja may also indicate a recent decrease in precipitation.

The comparison of the drought indices computed with reanalysis compared against observations showed that SPI-9 $_{REAN}$ relates well with SPI-9 $_{OBS}$ for all grid-points. In all cases the frequency of events in each class of the SPI-9 $_{REAN}$ was very close to those of SPI-9$_{OBS}$. PDSI $_{REAN}$ related worst with PDSI $_{OBS}$ than for both SPI-9 because the frequency of extremely dry (wet) events identified with PDSI $_{REAN}$ was considerably larger (lower) then that identified by PDSI $_{OBS}$. This may be explained by the underestimation of PRE $_{REAN}$ and the overestimation of ET_o $_{REAN}$ resulting in less water availability when the water balance was performed, which lead to drier PDSI $_{REAN}$. With SPI-9, due to its probabilistic feature, the consistent underestimation of precipitation did not significantly affect its standardized values. Statistical downscaling techniques should be studied to correct the biases in precipitation and PM-ET_o to improve the accuracy of the PDSI from reanalysis.

The long-term variability precipitation and PM-ET_o had clear effects on the drought indices. Results showed very distinct index values depending on the calibration period considered. With the same patterns for all grid-points, when the PDSI and SPI-9 were calibrated with the most recent period (1974-2014) the amount of severe or extreme droughts were the lowest when compared to the PDSI $_{REAN}$ and SPI-9 $_{REAN}$ computed for other calibration periods; also, with this calibration period, the number of severe and extreme wet events were the highest. In contrast, if the calibration period selected was the period 1892-1932, the opposite occurred with a larger amount of dry events and fewer wet events detected. In conclusion, in general, wetter (dryer) calibration periods lead to an SPI and PDSI biased towards drier (wetter) classes. These results showed the importance that the selection of the calibration period has to both PDSI and SPI-9. Thus, for the specific case of the SPI, under persistent or cyclic changes in precipitation and when long precipitation time series are available, using the complete record as reference period to derive ´normal conditions´ for SPI computation masks the actual precipitation deficits/surplus. If precipitation changes are expected the parametrization of the precipitation distribution and the SPI computation using as reference a more recent period along with the estimation of precipitation severity thresholds should be considered. Precipitation thresholds relative to SPI drought categories can be useful information for water managers in the sense that a dimensionless value of SPI is translated into precipitation depths.

Chapter 4

Daily reference evapotranspiration for hyper-arid to moist sub-humid climates in Inner Mongolia, China: Assessing temperature methods, and spatial and temporal variability of PM-ET_o and weather variables.

XIAODONG REN, ZHONGYI QU, DIOGO S MARTINS, PAULA PAREDES AND LUIS S PEREIRA (2016) DAILY REFERENCE EVAPOTRANSPIRATION FOR HYPER-ARID TO MOIST SUB-HUMID CLIMATES IN INNER MONGOLIA, CHINA: I. ASSESSING TEMPERATURE METHODS AND SPATIAL VARIABILITY. WATER RESOURCES MANAGEMENT 30: 3769–3791

AND

XIAODONG REN, DIOGO S MARTINS, ZHONGY QU, PAULA PAREDES AND LUIS S PEREIRA (2016) DAILY REFERENCE EVAPOTRANSPIRATION FOR HYPER-ARID TO MOIST SUB-HUMID CLIMATES IN INNER MONGOLIA, CHINA: II. TRENDS OF ETO AND WEATHER VARIABLES AND RELATED SPATIAL PATTERNS. WATER RESOURCES MANAGEMENT 30: 3793-3814

Reference evapotranspiration for hyper-arid to moist sub-humid climates in Inner Mongolia, china: assessing temperature methods, and spatial and temporal variability of PM-ET_o and weather variables

Abstract. When weather data sets available for computing the reference evapotranspiration are incomplete or of questionable quality, there is the need to replace the FAO Penman-Monteith (PM-ET_o) method by approaches requiring reduced sets only, particularly maximum and minimum temperature. The Hargreaves-Samani (HS) equation and the PM-ET_o using only temperature data (PMT) were considered in this study and their results were compared with those of the PM-ET_o using full data sets. Daily data sets refer to the period 1981-2012 and to a network of 50 meteorological stations covering the wide range of climates of Inner Mongolia. For both the PMT and HS methods, the solar radiation coefficients k_{Rs} were calibrated and have shown to be similar for both methods and to vary with climate aridity. For the PMT, the estimation of the dew point temperature, T_{dew}, was performed using the minimum temperature corrected for site aridity or, for humid climates, from a value near the average temperature. This improved estimation of T_{dew} was essential for a good performance of the PMT method in arid conditions and when temperatures are extremely low. The principal components analysis (PCA) in R-Mode have shown that the spatial variability of reference evapotranspiration (ET_o) computed with PM-ET_o or with the HS and PMT methods were coherent. PCA supported the interpretation of reference evapotranspiration results. Overall, PMT performed better than HS for most locations. A temporal analysis was also conducted to understand the differences in trend detection between PM-ET_o, HS and PMT. Different methodologies were also tested to assess and quantify existing trends. Trends for PM-ET_o varied with aridity, with decreasing trends in the areas marked by aridity in the West and increased trends in less arid and sub-humid areas in the East and could be explained by the trends of the weather variables. Contrarily, results for the temperature methods, $ET_{o\ PMT}$ and $ET_{o\ HS}$ identified increased trends due to warming and, thus showing inappropriate to assess reference evapotranspiration trends.

Keywords: Grass reference evapotranspiration, Hargreaves-Samani (HS) equation, PM-ET_o method, PM temperature method (PMT), k_{Rs} radiation coefficient, Principal Component Analysis, Aridity index, global warming, wind speed decline, sunshine duration decrease.

4.1 Introduction

Evapotranspiration is among the most important components of the water cycle and related changes can have significant impacts on ecosystems and human activities. Thus, an accurate estimation of reference evapotranspiration, ET_o, is important in several domains. In agriculture, ET_o is essential to evaluate crop water and irrigation requirements, to assess crop water use, and to base crops and water management decisions as revised by Pereira et al. (2015). As defined by Allen et al. (1998), reference evapotranspiration, often called potential evapotranspiration in climate and hydrologic studies, not only provides appropriate estimates of the atmospheric evaporating capability but is a base to assess actual evapotranspiration of any cropped or natural vegetation surface (Yang and Zhou 2011; Cadol et al. 2012). It can be applied in a variety of studies and to support management in agriculture, environment, water resources as well as to assess impacts of climate change (Irmak et al. 2012; Saadi et al. 2015) or combined with precipitation to support drought management (e.g., Dai 2011; McEvoy et al. 2012) as recently reviewed by Pereira et al. (2015). Moreover, depending from a set of weather variables, ET_o integrates the effects of the driving variables – solar radiation (R_s), maximum and minimum air temperature (T_{max} and T_{min}), relative humidity (RH) and wind speed at 2.0 m height (u_2).

The reference crop evapotranspiration, ET_o, is defined in FAO-56 (Allen et al. 1998) as the rate of evapotranspiration from a hypothetical crop with an assumed fixed height (12 cm), surface resistance (70 s m−1) and albedo (0.23), closely resembling the evapotranspiration from an extensive surface of a disease-free green grass cover of uniform height, actively growing, completely shading the ground, and with adequate water and nutrient supply. This definition resulted from parameterizing the Penman-Monteith equation for grass, which was assumed as reference crop (Smith et al. 1991; Allen et al. 1994, 1998). The corresponding equation, the FAO Penman-Monteith ET_o equation (PM-ET_o) was well proved in many places and for a variety of climates. This has been demonstrated through comparative studies of PM-ET_o and local evapotranspiration measurements, e.g., Todorovic (1999), Ventura et al. (1999), particularly in locations marked by aridity (Lecina et al. 2003; Berengena and Gavilán 2005; López-Urrea et al. 2006). Various sensitivity analyses and regional studies confirm the applicability of PM-ET_o to various and diverse environments (Garcia et al. 2004; Nandagiri and Kovoor 2006; Gong et al. 2006; Ye et al. 2009; Estévez et al. 2009).

Procedures for parameter computation from these weather variables are well defined (Allen et al. 1994, 1998). Meanwhile, it was also demonstrated that the accuracy of the PM-ET_o estimates depends upon the procedures for its parameterization, e.g., Liu and Pereira (1997) and Nandagiri and Kovoor (2006). Hourly time steps calculation procedures and the alternative use of alfalfa reference crop are also well defined (Allen et al. 2006).

The lack of observations of weather variables relative to R_s, RH and u_2, and the limited availability of quality weather data limit the application of the PM-ET_o equation in many locations. As recently reviewed by Pereira et al. (2015), these limitations led to numerous studies comparing a variety of equations with the PM-ET_o (e.g., Mallikarjuna et al. (2014)) and to develop alternative methods to estimate ET_o, e.g., adopting artificial neural networks (Rahimikhoob 2014), or gene expression programming (Martí et al. 2015). Alternatives also include the use of daily weather forecast messages (Cai et al. 2007, 2009), gridded weather data (Thomas 2008; Raziei and Pereira 2013a), and reanalysis weather data (Srivastava et al. 2013). Other authors developed alternative equations for using remote sensed weather data (Zheng and Zhu 2015) or to use estimates of missing weather variables (Valiantzas 2013). However, alternative equations may do not follow the dynamics of ET_o when computed with the full data PM-ET_o. Differently, a comparison among various evapotranspiration equations was performed by (Vangelis et al. 2013) aiming at assessing impacts of the evapotranspiration equation on results relative to the reconnaissance drought index and not to just assess the superiority of any given equation.

Studies comparing the PM-ET_o with other equations using data sets reduced to T_{max} and T_{min}, are very numerous as reviewed by Todorovic et al. (2013) and (Raziei and Pereira 2013b). However, they rarely focus the use of the PM-ET_o equation with T_{max} and T_{min} only (PMT approach), which retains many of the dynamics of the full data PM-ET_o. The main focus is on the Hargreaves-Samani equation (HS), which is easier to compute than the PMT approach. In addition, the main objective of related comparative studies essentially consists of just obtaining an operational equation alternative to the PM-ET_o, thus, without considering the possible advantage of using the PM-ET_o with estimators of the missing variables, which may be lacking only temporarily. In China, a first study comparing favorably PMT against HS method was developed in the North China Plain (Liu and Pereira 2001; Pereira et al. 2003). Later, a study using daily weather forecast messages confirmed the appropriateness of using radiation estimates from temperature in

the PM-ET_o equation (Cai et al. 2009). However, recent studies developed in China focused on assessing if the HS equation could replace the PM-ET_o method, thus without considering the PMT approach (e.g., Yan et al. 2008; Wang et al. 2010). HS estimates of ET_o have been compared with PM-ET_o estimates by many authors. Results generally show that the HS method performs well in most climatic regions. However, in humid areas it tends to overestimate ET_o (Nandagiri and Kovoor 2006; Martinez and Thepadia 2010). Yoder et al. (2005) reported a poor correlation of HS results when compared with lysimeter data in a humid location and the HS equation ranked last in a study focusing humid regions (Trajkovic and Kolakovic 2009). Differently, various authors stated that the HS method underestimates ET_o for dry and windy locations due to not considering a wind term (Temesgen et al. 2005; Gavilán et al. 2006). Other studies have shown that the HS equation does not rank first when comparing temperature equations (Irmak et al. 2003). Thus, despite the HS equation performed well in most applications, many authors attempted to recalibrate the HS coefficients and exponents (e.g., Gavilán et al. 2006; Trajkovic 2007; Wang et al. 2010). This calibration approach resulted in a large number of versions of the HS equation corresponding to local calibrations. However, analyzing the applications of the HS equation, Hargreaves and Allen (2003) concluded that "recalibrating the exponents and coefficients of the HS equation only increased the complexity of the equation". Contrarily to the numerous calibrations of coefficients and exponents of the HS equation, only rare attempts to the calibration of the radiation adjustment coefficient (k_{Rs}) are reported, probably because it is inexplicitly included in the HS equation (Samani 2000, 2004; Hargreaves and Allen 2003). Nevertheless, very good results were reported by Todorovic et al. (2013) and Raziei and Pereira (2013b) relative to calibrating k_{Rs} for a wide range of climates. Meanwhile, there are no studies in China relative to the calibration of k_{Rs}.

Studies relative to the PMT approach provided accurate results, often better than using the HS equation, for various world regions (Liu and Pereira 2001; J. et al. 2002; Trajkovic 2005; Popova et al. 2006; Jabloun and Sahli 2008; López-Moreno et al. 2009). These studies also have shown that the use of alternative estimates of solar radiation, actual vapor pressure and wind speed could be an approach to overcome problems due to incomplete data sets when using the PM-ET_o method. Majidi et al. (2015) tested methodologies for estimating those variables when using the PM-ET_o. Gocic and Trajkovic (2010) proposed a software to estimate ET_o that includes the use of the PMT

when weather data are incomplete. Those studies, however, used a default k_{Rs} following the propositions by Allen (1997) and Allen et al. (1998). Attempts to calibrate k_{Rs} were only performed by Todorovic et al. (2013) and Raziei and Pereira (2013b) using monthly data sets. The latter have shown that k_{Rs} varies with climate aridity and is similar when obtained from calibrating the HS or the PMT approaches. An analysis using daily data still is lacking.

Recent PMT studies (Raziei and Pereira 2013b; Todorovic et al. 2013) have shown the need for correcting T_{min} for aridity when estimating the dew point temperature (T_{dew}) from T_{min}, thus following the propositions in FAO-56 (Allen et al. 1998) and Temesgen et al. (1999). A different approach for estimating T_{dew} for humid climates was used by Todorovic et al. (2013) and Raziei and Pereira (2013b). Its test for daily weather data was not yet performed. However, despite the study by Liu and Pereira (2001) to North China Plain was among the first worldwide studies relative to the PMT method, new approaches to this method using both a calibrated k_{Rs} and an improved estimation of T_{dew} still are lacking in China.

Alternative equations and estimation methods may not follow the dynamics of ET_o when it is computed with the full data PM-ET_o and may be biased when just based on temperature. Thus, by considering the effects of temperature in the evapotranspiration process, it may be expected that global warming lead evapotranspiration to increase. However, a clear distinction must be done: while ET_o is a climatic variable, depending upon the above referred weather variables when computed with the PM-ET_o equation, actual evapotranspiration (ET_{act}) also strongly depends on local environment conditions. These refer mainly to precipitation and water available for evaporation (Jung et al. 2010) and to the characteristics of the evaporative surfaces, namely the type of vegetation and its stomatal control and responsiveness to rising of CO_2 (Liu et al. 2013b). Thus, studying ET_{act} temporal variability and trends is quite complex and related trends are difficult to detect due to the number and type of driving variables influencing that variability. Results relative to the temporal variability and trends of ET_{act} may be coherent relative to those of ET_o (Gao et al. 2007; Wang et al. 2012) or may be contradictory (Calanca et al. 2006; Zhang et al. 2011b).

Studies analyzing the temporal variation of ET_o often aim at predicting its future changes as influenced by global warming. Global and regional circulation models (GCM and RCM) as well as ensemble models are then used. These predictions may use various

approaches to compute ET_o but the PM-ET_o equation is often used. Results of these modeling approaches often predict a rise of ET_o in the 21st century, e.g., various studies on Spain river basins, such as by (Rodríguez Díaz et al. 2007) relative to the Guadalquivir basin and Moratiel et al. (2011) for the Duero basin, as well as studies relative the Alpine region Calanca et al. (2006) and the Mediterranean basin (Saadi et al. 2015). Terink et al. (2013) also predicted an increase in ET_o for the Middle East and Northern Africa region but using the Hargreaves temperature equation. Modelling approaches have also been used in China, with results indicating an expected increase of ET_o in the Loess Plateau (Li et al. 2012), in the Haihe river basin (Xing et al. 2014) and in the Zhejiang Province (Xu et al. 2014). However, contrarily, Wang et al. (2007) detected a decreasing change of ET_o for the Yangtze River basin.

When performing a trend analysis, thus looking on the past weather dynamics instead of predicting future changes, results are quite diverse. On the one hand, several authors refer to the evapotranspiration paradox, i.e., a trend for ET_o to decrease when temperature increases (Peterson et al. 1995). However, since ET_o depends upon other weather variables in addition to temperature, it is less appropriate to refer to a paradox when ET_o tends to decrease. It resulted a number of studies, mainly in China, where the ET_o decrease is referred and associated with the decrease of other variables such as solar radiation and wind speed. Studies relative to China often refer to a decreasing trend of ET_o in large areas of China but to trends for increasing in other areas, particularly in the northeast and center north of China (Thomas 2000; Gao et al. 2006; Cong et al. 2009; Liu and McVicar 2012). Similarly, studies focusing selected river basins, regions and Provinces, also detected ET_o decreasing trends (Xu et al. 2006; Song et al. 2010; Yin et al. 2010; Tang et al. 2011a) and for some cases, negative trends were detected in large part of the reported study areas while other parts have shown an increasing trend (Wang et al. 2007, 2012; Liang et al. 2010; Zhang et al. 2011b; Yang et al. 2011). Differently, Zuo et al. (2012) reported a positive trend for the Wei river basin. Nevertheless, changes in trends, namely from negative to positive, were also reported by some authors (Liang et al. 2010; Yin et al. 2010).

Studies focusing on ET_o trends in India identified decreasing trends whose seasonality refers to the monsoon (Bandyopadhyay et al. 2009; Jhajharia et al. 2012). Shadmani et al. (2012) and Kousari et al. (2013) reported that a majority of weather stations in Iran present a negative trend but others show an increase in ET_o trends. A study for Northern

Eurasia detected significant decreasing trends as more important than the positive ones (Liu et al. 2014). For Romania (Croitoru et al. 2013) positive trends were detected for most of locations. Similarly, studies relative to southern France (Chaouche et al. 2010), southern Spain (Espadafor et al. 2011) and the whole Spain (Vicente-Serrano et al. 2014) also show positive trends for ET_o. Abtew et al. (2011) also reported a negative trend to southern Florida while (Cohen et al. 2002) did not report significant trends in Israel.

Results are affected by various factors. Han et al. (2012) referred to the weather station environment reporting that the decrease in ET_o is favored in weather stations located in agricultural areas, particularly in regions influenced by aridity, which may relate to the fact that those weather stations respect better the conditions desirable for ET_o reference weather stations (Allen et al. 1998). Similarly, (Zhang et al. 2011a) referred the possible influences of urbanization on various weather variables such as wind speed. This issue also relates with the problems of weather data quality as discussed by Allen et al. (1998) and Pereira et al. (2015). The appropriateness of the equations used was discussed by Irmak et al. (2012) who considered ET_o more appropriate than the ASCE alfalfa reference ET_r, and by Vicente-Serrano et al. (2014) that questioned the use of simplified and temperature equations for analysis that refer to global warming impacts. Thomas (2008) used gridded ET_o data and referred to possible limitations related with the arbitrary begin and end of the time series.

Studies referred above generally searched explanations for the observed ET_o trends and mostly include an analysis of the variability of the climatic variables used in computations. In addition, studies revealed a diverse seasonal variability. Generally, particularly the Chinese studies, they refer to a decrease in solar radiation all over China. A few articles analyze that decrease, which could be due to increased aerosols and greenhouse gases (Che et al. 2005; Liang and Xia 2005; Qian et al. 2006). A decrease in wind speed is also often referred as contributing to the observed negative trends. However, few studies are available on the causes of that decrease, which may relate with changes in atmospheric circulation (Guo et al. 2011). Other authors refer to an increase or a decrease in relative humidity with contradictory results mostly depending of the magnitude of global warming (Dai 2006; Vicente-Serrano et al. 2014).

Considering the above referred advances and limitations in ET_o estimation and the lack of information regarding the spatial and temporal variability of ET_o, in the region a study was developed in Inner Mongolia, China, using a 30 years set of daily weather data,

whose objectives were: (1) to test the PMT and HS methods for a wide range of climates, from hyper-arid to sub-humid, thus with consideration of aridity impacts on ET_o while evaluating the relative advantage of adopting the PMT or the HS temperature methods when available weather data are limited; (2) test the calibration of the radiation adjustment coefficient k_{Rs} and checking the procedures for estimating dew point temperature, T_{dew}; (4) Assess the spatial variability of ET_o using principal component analysis and assess its temporal variability in combination with the climatic driving variables used to compute PM-ET_o with possible relations with ET_o trends; (5) Compare trends of ET_o temperature methods with those of PM-ET_o, assessing the differences in trend detection between the FAO-PM equation and the temperature based alternatives.

4.2 Data and Methods

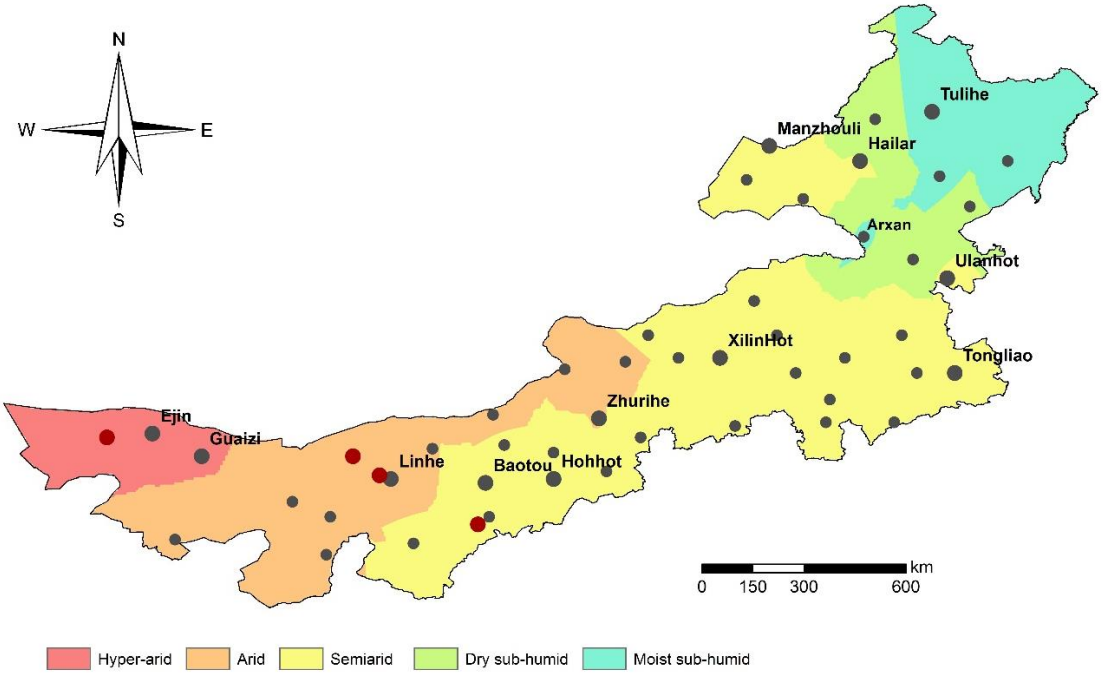

Figure 4-1 Climatic aridity map of Inner Mongolia and spatial distribution of the weather stations. In red are the station that were not used for trend analysis.

The climate in Inner Mongolia, following the Köppen classification (Kottek et al. 2006), varies from BWk (arid, desertic and cold) in the East, BSk (arid, steppe and cold) in the middle area and Dwb (winter dry and warm summer) and Dwc (winter dry and cool summer) in the East. It corresponds to a variety of aridity climates (Figure 4-1), from hyper-arid in the West to moist sub-humid in the East. The UNEP aridity index (AI) (UNEP 1997) was used to characterize the climate of each weather station. This index is

the ratio between the mean annual precipitation and the mean annual potential climatic evapotranspiration (Thornthwaite 1948).

Table 4-1 Coordinates and aridity index (AI) of the 50 weather stations of Inner Mongolia used in the current study.

Weather stations	Lon. (° E)	Lat. (° N)	Elevation (m.a.s.l.)	AI	Start year[1]	Weather stations	Lon. (° E)	Lat. (° N)	Elevation (m.a.s.l.)	AI	Start year[1]
Hyper-arid						**Semiarid**					
Ji Kede	99.9	41.9	965.6	0.01	-	Ongniud	119.0	42.9	634.3	0.33	1957-
Ejin	101.1	42.0	940.5	0.02	1960-	Xin Barag L.	118.3	48.2	642.0	0.33	1959-
Guaizi	102.4	41.4	960.0	0.02	1960-	Manzhouli	117.4	49.6	661.7	0.34	1957-
Arid						Tongliao	122.3	43.6	178.7	0.34	1951-
Jartai	105.8	39.8	1031.8	0.07	1955-	Dongsheng	110.0	39.8	1461.9	0.35	1957-
Bayan knoll	104.8	40.2	1323.9	0.08	1958-	Chifeng	118.9	42.3	568.0	0.36	1951-
Alxa R.	101.7	39.2	1510.1	0.09	1960-	Jarud	120.9	44.6	265.0	0.37	1953-
Hailisu	106.4	41.4	1509.6	0.10	-	Xi Ujimqin	117.6	44.6	1000.6	0.37	1955-
Erenhot	112.0	43.7	964.7	0.11	1956-	Jining	113.1	41.0	1419.3	0.38	1954-
Hanggin	107.1	40.9	1056.7	0.12	-	Bairin	119.4	44.0	486.2	0.39	1953-
Linhe	107.4	40.8	1039.3	0.14	1957-	Bao Guotu	120.7	42.3	400.5	0.39	1957-
Mandula	110.1	42.5	1225.2	0.14	1958-	Linxi	118.1	43.6	799.5	0.39	1953-
Sonid	113.6	43.9	1036.7	0.16	1959-	Hohhot	111.7	40.8	1063.0	0.41	1952-
Zhurihe	112.9	42.4	1150.8	0.16	1953-	Siziwangqi	111.7	41.5	1490.1	0.41	1959-
Alxa L.	105.7	38.8	1561.4	0.17	1953-	Duolun	116.5	42.2	1245.4	0.42	1953-
Urat	108.5	41.6	1288.0	0.19	1954-	Huade	114.0	41.9	1482.7	0.44	1953-
Semiarid						Ulanhot	122.1	46.1	274.7	0.46	1951-
Damao	110.4	41.7	1376.6	0.24	1954-	Hailar	119.8	49.2	610.2	0.47	1951-
Naranbulag	114.2	44.6	1181.6	0.24	1955-	**Dry sub-humid**					
Otog	108.0	39.1	1380.3	0.24	1955-	Sauron	121.2	46.6	499.7	0.53	1958-
Xilin Hot	116.1	44.0	1003.0	0.27	1953-	Eji Guna	120.2	50.3	581.4	0.54	1957-
Xin Barag R.	116.8	48.7	554.2	0.27	1958-	Zhalantun	122.7	48.0	306.5	0.62	1953-
Dong	117.0	45.5	838.9	0.28	1956-	**Moist sub-humid**					
Kailu	121.3	43.6	241.0	0.30	1953-	Arxan	119.9	47.2	997.2	0.69	1953-
Abag	115.0	44.0	1126.1	0.31	1953-	Bugt	121.9	48.8	739.7	0.69	1951-
Baotou	109.9	40.7	1067.2	0.31	1951-	Tulihe	121.7	50.5	732.6	0.77	1957-
Ejin Horo	109.7	39.6	1329.3	0.32	-	Xiaoer Gou	123.7	49.2	286.1	0.79	1957-

The data sets consist of maximum and minimum temperature (T_{max} and T_{min}, °C), sunshine duration (SD, h) used to estimate the shortwave incoming radiation, relative humidity (RH, %) and wind speed (WS, m s^{-1}), which was measured at 2 m height, from 50 surface meteorological stations distributed over Inner Mongolia and referring to the

[1] Start year is the first year of the monthly data used for used for trend analysis, spanning to 2013 for all weather stations. The four stations without starting year were not considered for the trend analysis on the account of having less than 30 years of consecutive data.

period of 1981 to 2012 and that were used to compute ET_o with the PM-ET_o equation. ET_o computed with the HS and PMT procedures used only T_{max} and T_{min}. However, only 46 out of those 50 weather stations were used for the temporal analysis to ET_o and each weather variable, since only 46 weather stations had more than 30 years of data, all reaching the end of 2013. The four stations that were not used are marked in Figure 4-1 and the starting year of each weather station is in Table 4-1. Data provided by the China Meteorological Organization have been controlled for quality (Feng et al. 2004). All stations are listed in Table 4-1 ordered according to AI.

4.2.1 ET_o computation methods

The FAO PM-ET_o equation relative to daily grass reference evapotranspiration (Allen et al. 1998) is given as:

$$ET_o = \frac{0.408\Delta(R_n - G) + \gamma_c \frac{900}{T+273} u_2 (e_s - e_a)}{\Delta + \gamma_c (1 + 0.34 u_2)} \quad (4.1)$$

where ET_o is the grass reference evapotranspiration (mm day^{-1}), R_n is the net radiation at the surface (MJ m^{-2} day^{-1}), G is the soil heat flux density (MJ m^{-2} day^{-1}), T is the mean air temperature (℃) at 2 m height, u_2 is the wind speed at 2 m height (m s^{-1}), e_s is the saturation vapor pressure (kPa), e_a is the actual vapor pressure (kPa), (e_s - e_a) is the vapor pressure deficit (VPD, kPa), Δ is the slope of vapor pressure curve (kPa $℃^{-1}$), and γ_c is the psychometric constant (kPa $℃^{-1}$). The standard calculation procedures were given by Allen et al. (1998) and are detailed, herein, in Chapter 5. Annual PM-ET_o in Inner Mongolia is mapped in Figure 4-2.

If radiation or sunshine duration measurements are not available, when using the PMT method, solar radiation may be estimated with the Hargreaves radiation equation (Allen 1997; Allen et al. 1998):

$$R_s = k_{Rs} \sqrt{(T_{max} - T_{min})} R_a \quad (4.2)$$

where R_s is short wave incoming radiation (MJ m^{-2} day^{-1}), T_{max} and T_{min} are respectively maximum and minimum temperature (℃), R_a is the radiation on the top of the atmosphere (MJ m^{-2} day^{-1}), and k_{Rs} is the empirical radiation adjustment coefficient ($℃^{-0.5}$). Differently to former recommendations by Allen (1997) and Allen et al. (1998), k_{Rs} needs to be adjusted locally as reported by Todorovic et al. (2013) and Raziei and Pereira (2013b). A trial and error procedure was used to obtain the k_{Rs} value that

minimizes the root mean square error (RMSE) relative to comparing ET_o estimates with the PMT approach with the PM-ET_o computed with full data.

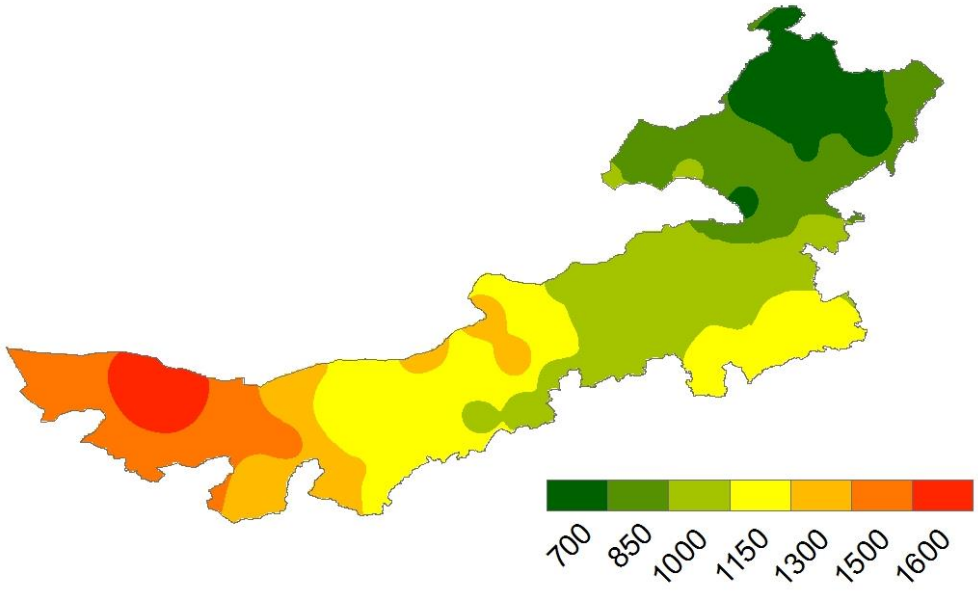

Figure 4-2 Annual PM-ET_o (mm) in Inner Mongolia

When RH data are not available, the actual vapor pressure (e_a, kPa) may be estimated with the PMT method assuming that the daily T_{dew} is close to the daily T_{min}. In previous studies performed with data from various reference weather stations (Liu and Pereira 2001; Popova et al. 2006; Jabloun and Sahli 2008) it was assumed $T_{dew} = T_{min}$, resulting that e_a was computed as:

$$e_a = e^0(T_{min}) = 0.611 exp\left(\frac{17.27 T_{min}}{T_{min}+273.3}\right) \quad (4.3)$$

Meanwhile, it was observed that for non-reference weather stations, without appropriate green grass soil cover, and where local advection occurs, temperature observations were overestimated resulting that $T_{min} > T_{dew}$ and it was required to adopt a temperature correction (Allen 1996; Allen et al. 1998; Temesgen et al. 1999). Thus, Todorovic et al. (2013) and Raziei and Pereira (2013b) successfully adopted $T_{dew} = T_{min} - a_T$, where the correction factor a_T varies with the climate aridity of the station. Based upon these former studies, the following a_T values were adopted:

1) Hyper-arid, AI <0.05, a_T = 4 ℃,
2) Arid, AI from 0.05 to 0.20, a_T = 2 ℃,
3) Semiarid, IA from 0.20 to 0.5, a_T = 1 ℃,
4) Dry Sub-humid, AI from 0.5 to 0.65, a_T = 1 ℃,

For humid climates, and when the mean temperature is very low, T_{dew} was estimated following Todorovic et al. (2013) and Raziei and Pereira (2013b):

$$T_{dew} = \left(\frac{T_{max}+T_{min}}{2}\right) - a_T \quad (4.4)$$

where a_T = 2 ℃ when 0.8 < PRE/ET_o< 1.0 and a_T = 1 ℃ if PRE/ET_o> 1.0 and PRE is precipitation (mm).

When wind speed observations are lacking, the world average value u_2 = 2 m s^{-1} is generally adopted with PMT. However, for very windy hyper-arid and arid locations it could be appropriate to adopt a local or regional average value.

The Hargreaves and Samani (1985) equation (HS) is a quite common alternative to PM-ET_o. As proposed by Todorovic et al. (2013), it writes:

$$ET_o = 0.0135 K_{RS} \frac{R_a}{\lambda} \sqrt{T_{max} - T_{min}} \, (T_{mean} + 17.8) \quad (4.5)$$

where ET_o is the estimate of grass reference ET (mm day^{-1}), 0.0135 is a conversion factor from the American to the International system of units, T_{max}, T_{min} and T_{mean} are respectively maximum, minimum and mean daily temperature (℃), R_a is the radiation on the top of the atmosphere (MJ m^{-2} day^{-1}), k_{Rs} is the empirical radiation adjustment coefficient ($℃^{-0.5}$), and λ is the latent heat of vaporization, generally estimated for 20 °C, thus resulting λ = 2.45 MJ kg^{-1}. k_{Rs} = 0.17$℃^{-0.5}$ was formerly used (Samani 2004) but Todorovic et al. (2013) and Raziei and Pereira (2013b) proposed a calibration of k_{Rs} using a trial and error procedure to find the k_{Rs} value that minimizes RMSE when comparing ET_o estimated with the HS equation with estimates of the PM-ET_o.

4.2.2 Evaluation procedure

As referred above, a trial and error procedure was applied to find the best k_{Rs} values for all locations and for both the PMT and HS method; this was performed by comparing the ET_o estimates by PMT and HS, herein referred as $ET_{o\,PMT}$ and $ET_{o\,HS}$, with those obtained with PM-ET_o using full data sets. The trial and error procedure was applied to PMT after T_{dew} estimation as described above. To assess the performance of HS and PMT methods with respect to the PM-ET_o method, various statistical performance indicators were used as referred by Todorovic et al. (2013) and are explained in detail in Chapter 5. Considering the data set O_i relative to the PM-ET_o data computed with full data sets and

the predicted temperature based data sets, P_i, relative to both temperature methods, which mean values are $\bar{O}$ and $\bar{P}$, the considered statistical performance indicators are:

a) The coefficient of regression, b_0, of the regression forced to the origin (FTO) (Eisenhauer 2003), which is given by:

$$b_0 = \frac{\sum_{i=1}^{n}(O_i * P_i)}{\sum_{i=1}^{n} {O_i}^2} \tag{4.6}$$

This FTO regression ($y=b_0x$, with predicted (y) and observed (x) values) assumes the proportionality between $ET_{o\ PMT}$ or $ET_{o\ HS}$ and PM-ET_o, where the slope b_0 is the constant of proportionality with $b_0>1$ suggesting overestimation and $b_0<1$ indicating underestimation.

b) The coefficient of determination R^2 computed with the ordinary least squares (OLS) defined as

$$R^2 = \frac{\sum_{i=1}^{n}(\hat{P}_i - \bar{P})^2}{\sum_{i=1}^{n}(P_i - \bar{P})^2} \tag{4.7}$$

R^2 represents the proportion of the variance of the P_i values that is explained by their regression on the observed values O_i. When R^2 is close to 1.0 it denotes that the variances of both compared methods are similar.

c) The root mean square error (RMSE), computed as

$$RMSE = \sqrt{\frac{\sum_{i=1}^{n}(O_i - P_i)^2}{n}} \tag{4.8}$$

that measures the overall discrepancies between PM-ET_o and $ET_{o\ PMT}$ or $ET_{o\ HS}$ values. As small is RMSE better is the performance of the alternative method.

d) The modeling efficiency EF (Nash and Sutcliffe 1970; Legates and McCabe 1999) that was computed as

$$EF = 1 - \frac{\sum_{i=1}^{n}(O_i - P_i)^2}{\sum_{i=1}^{n}(O_i - \bar{O})^2} \tag{4.9}$$

EF is the ratio between the mean square error ($MSE=RMSE^2$) of $ET_{o\ PMT}$ or $ET_{o\ HS}$ estimates and the variance of PM-ET_o. The maximum value EF = 1.0 can only be achieved if there is a perfect match between all observed and predicted values, thus a value close

to 1.0 indicates that MSE is much smaller than the PM-ET_o data variance; contrarily, a very low EF means that MSE is close to the reference data variance.

4.2.3 Spatial variability of ET_o

Using the three sets of ET_o - PM-ET_o, $ET_{o\ PMT}$ and $ET_{o\ HS}$ - for each weather station, ten variables were defined to characterize the variability of ET_o throughout Inner Mongolia: the annual ET_o amount, four seasonal ET_o amounts; four seasonal percentages of total annual ET_o and the aridity index. The season variables were created considering four 3-month periods: December–January–February (DJF, winter), consisting of the cold and dry season, when air temperatures are very low, negative, and precipitation is very small; March-April-May (MAM, spring) corresponding to the transition from the cold winter to the hot summer, yet before the monsoon rains; June-July-August (JJA, summer) that consists of the warm and monsoon rainy season, wet in the east but dry in the arid western areas; and September-October-November (SON, autumn), when temperature highly decrease to become negative by December and with reduced precipitation.

The spatial patterns of ET_o were extracted by applying the principal components analysis (PCA) in R-Mode (Richman 1986) to these ten variables relative to each ET_o estimation method and all locations. This procedure follows those adopted by Raziei et al. (2008) and Martins et al. (2012), when analyzing the spatial patterns of precipitation and differs from the PCA analysis performed in Chapter 2 in which the S-Mode was adopted.

The R-Mode PCA is used to search for interrelationship among variables or parameters, in which each row correspond to the weather stations and the columns to the variables considered. As defined in Chapter 2, PCA is a dimension reduction technique that forms a new set of uncorrelated variables based on a linear combination of the original input time series (Sharma 1996). The method consists of computing the covariance matrix of the considered variables with the corresponding eigenvalues and eigenvectors. The eigenvalues provide information regarding the explained variance of each component, which is used to decide how many components to retain for Varimax rotation. The number of components retained was based on the scree plot and the North's rule of thumb (North et al. 1982). With R-Mode PCA, the PC scores were used to depict the spatial patterns of ET_o. The Varimax rotation was applied to the loadings to find areas with independent ET_o patterns.

4.2.4 Temporal variability of ET_o

Two methodologies appropriate to search for significant positive or negative trends were applied to all time series of ET_o - PM-ET_o, PMT and HS – as well as to the time series of the climatic - variables used for the respective computation, i.e., T_{max}, T_{min}, SD, RH and WS. They consisted of the Modified Mann-Kendall test (Hamed and Rao 1998) and the Deterministic Trend Scheme (DTS) as described by Fatichi et al. (2009) and Barbosa (2011).

The Mann-Kendall is a non-parametric test used to search for randomness of a time series against time (Kendall 1975). It tests the null hypothesis that a given time series does not have a monotonic trend; hence it may have a significant positive or negative trend. The Mann-Kendall (MK) test is performed under the assumption that data are independent and randomly ordered, which is often not true for auto-correlated time series such as for hydro-meteorological data series (Hamed and Rao 1998). Therefore, these authors proposed a modification of the original MK test to consider the effects of autocorrelation, thus resulting the modified Mann-Kendall test (MMK). The MK and MMK tests indicate the signal of the trend, positive or negative, when selecting a given significance level; in this study, it has been assumed a p-value < 0.05, i.e., a confidence level of 95%. The MK and MMK tests are generally associated with the Sen slope (Sen 1968) to estimate the magnitude of the trend. The MK test and the Sen slope methods are described in numerous studies, namely relative to ET_o trends quoted herein, e.g., Zuo et al. (2012) and Huo et al. (2013). Good descriptions of the MMK approach were provided by Hamed and Rao (1998) and Yue and Wang (2004). The MMK test and the Sen slope were computed using the fume package (Santander Meteorology Group 2012).

The Deterministic Trend Scheme (DTS) applies two statistical tests: the PP test (Phillips and Perron 1988) and the KPSS test (Kwiatkowski et al. 1992) to search for significant deterministic trends in time series. The first tests for the null hypothesis that a time series has a unit root, i.e., red noise time series that are difference stationary (stationary after a first order integration). In hydrometeorological time series that null hypothesis is generally rejected, which has been confirmed in this study. The KPSS test is applied to test the null hypothesis that a time series is trend stationary and the respective results refer to a calculated p-value. When both tests are rejected the possible occurrence of a deterministic trend is identified considering a selected significance level using the generalized least square linear model (GLS) (Aitken 1936). In this study a highly

significance level was associated with a confidence level of 99% and a common significance level was 95%. The results of the linear model refer to both the trend and to its uncertainty. The DTS methodology is well described by Fatachi et al. (2009) and Barbosa (2011) in which the definition of trend was reviewed as well as the possible causes for non-stationary time series. Both the PP-test and the KPPS-test were explained there with good detail. The statistical tests were performed using the *tseries* package (Trapletti and Hornik 2018).

Prior to apply both trend methodologies a decomposition technique, STL (Cleveland et al. 1990), was used to remove the seasonal component from all the monthly time series, thus reducing the intra-annual autocorrelation.

4.3 Results

4.3.1 Performance of the PMT method

Table 4-2 presents the statistical indicators relative to comparing $ET_{o\,PMT}$ with PM- ET_o. The calibrated k_{Rs} values for each location are also included. Results showed that the b_0 values were close to 1.0 for all locations, varying in a short range, from 0.97 to 1.01, mostly 0.99 and 1.0. This indicated that $ET_{o\,PMT}$ and the PM-ET_o were statistically similar. R^2 range from 0.77 to 0.92, meaning that a high proportion of the variance of $ET_{o\,PMT}$ was explained by their regression on the PM-ET_o. R^2 was generally smaller when the range of variation of ET_o was larger, which occurred more often for arid climates contrarily to sub-humid locations. A larger dispersion of ET_o values around the regression line occurred for the higher ET_o values corresponding to windy and dry days. The ET_o values being compared varied in a quite wide range, from near 0 mm d^{-1}, during the very cold winter, up to ET_o > 10 mm d^{-1} in very arid and windy western locations. The spatial distribution of b_0 and R^2 (Figure 4-3a and b) indicated that b_0 values did not show any spatial pattern but R^2 showed a slight trend to be higher in the eastern region where aridity is lesser and the range of ET_o values was smaller.

Errors of estimates (Table 4-2) were higher where the range of variation of ET_o was higher, thus in the hyper-arid and arid locations. RMSE ranges 0.90-1.62 mm d^{-1} for the hyper-arid locations, and 0.64-1.13 mm d^{-1} for the arid ones. RMSE decreased to 0.51-0.90 mm d^{-1} for the semiarid locations and to 0.44-0.68 mm d^{-1} in sub-humid ones. The corresponding spatial pattern was well evidenced in Figure 4-3c. Larger errors were

related with the size of ET_o and are influenced by various other factors such as temperature variations, wind speed intensity and the occurrence of dust in the atmosphere, which affects the incoming radiation available at the surface and is due to the occurrence of wind erosion, very strong in most of Inner Mongolia.

The Nash and Sutcliffe modeling efficiency EF followed a pattern similar to that of RMSE, varying from 0.76 to 0.86 and 0.80 to 0.89 for respectively hyper-arid and arid climates, from 0.77 to 0.92 in semiarid climates, and increasing to 0.86 to 0.91 in sub-humid climates. This was depicted in Figure 4-3d. These results indicated that the $ET_{o\ PMT}$ had smaller MSE values for the sub-humid climates, with lower variance of PM-ET_o, i.e., where the variability of factors influencing ET_o was smaller. Differently, $ET_{o\ PMT}$ had higher MSE in arid areas where the range of variation of ET_o was larger; nevertheless, since the EF values were all quite high, MSE values were much smaller than the variance of PM-ET_o.

The k_{Rs} values (Table 4-2) tended to be higher for the hyper-arid climates (0.20 - 0.23ºC$^{-0.5}$) and smaller for the sub-humid locations (0.14 - 0.18 °C$^{-0.5}$). Values for the arid and semiarid climates varied in large ranges, respectively 0.16 – 0.23 and 0.13 – 0.21 °C$^{-0.5}$. This behavior was visible through the respective spatial pattern presented in Figure 4-4, which agreed with that observed by Raziei and Pereira (2013b) for Iran. However, despite it was evident that k_{Rs} values were, in average, smaller when aridity was lower, the variability of k_{Rs} values within each climate region was large and it was not possible to find an appropriate relationship between k_{Rs} and the aridity index. There are other factors influencing the variation of k_{Rs}, mainly the transparency of atmosphere that highly varies with the occurrence of dust due to wind erosion. Nevertheless, users may infer local values through interpolation from nearby locations using data in Table 4-2.

Table 4-2. Calibrated k_{Rs} coefficient and statistical performance indicators when comparing the $ET_{o\ PMT}$ with the PM-ET_o.

Stations	k_{Rs} ($°C^{-0.5}$)	b_0	R^2	RMSE (mm d^{-1})	EF	Stations	k_{Rs} ($°C^{-0.5}$)	b_0	R^2	RMSE (mm d^{-1})	EF
Hyper-arid						**Semiarid**					
Ji Kede	0.23	0.99	0.86	1.21	0.86	Ongniud	0.20	1.00	0.81	0.90	0.79
Ejin	0.20	0.98	0.87	1.00	0.86	Xin Barag L	0.18	0.98	0.93	0.57	0.92
Guaizi	0.23	0.97	0.77	1.62	0.76	Manzhouli	0.19	1.00	0.90	0.68	0.89
Arid						Tongliao	0.21	1.00	0.83	0.88	0.81
Jartai	0.19	0.99	0.87	0.90	0.86	Dongsheng	0.21	0.97	0.89	0.66	0.89
Bayan knoll	0.22	1.00	0.85	0.99	0.85	Chifeng	0.18	1.00	0.84	0.80	0.83
Alxa R.	0.24	0.98	0.81	1.13	0.80	Jarud	0.17	0.98	0.84	0.77	0.83
Hailisu	0.24	0.97	0.88	0.93	0.88	Xi Ujimqin	0.18	1.00	0.87	0.74	0.86
Erenhot	0.22	0.98	0.90	0.83	0.89	Jining	0.17	1.00	0.85	0.71	0.84
Hanggin	0.17	1.00	0.87	0.76	0.86	Bairin	0.16	0.98	0.79	0.90	0.78
Linhe	0.16	0.98	0.90	0.64	0.90	BaoGuotu	0.19	1.00	0.80	0.90	0.77
Mandula	0.20	0.98	0.86	0.92	0.86	Linxi	0.17	0.98	0.81	0.83	0.80
Sonid.	0.23	0.98	0.89	0.85	0.89	Hohhot	0.16	1.00	0.89	0.64	0.88
Zhurihe	0.22	0.99	0.85	1.01	0.85	Siziwangqi	0.20	1.00	0.89	0.68	0.88
Alxa L.	0.23	0.98	0.84	0.90	0.84	Duolun	0.16	0.99	0.84	0.73	0.83
Urat	0.20	1.00	0.89	0.74	0.89	Huade	0.20	1.00	0.87	0.71	0.87
Semiarid						Ulanhot	0.19	1.00	0.86	0.77	0.85
Damao	0.19	0.98	0.87	0.77	0.86	Hailar	0.17	1.01	0.91	0.57	0.91
Naranbulag	0.20	1.00	0.92	0.64	0.92	**Dry sub-humid**					
Otog	0.18	0.98	0.86	0.75	0.86	Sauron	0.15	1.00	0.87	0.68	0.86
XilinHot	0.20	1.00	0.90	0.73	0.89	EjiGuna	0.18	0.97	0.91	0.53	0.91
Xin Barag R	0.19	0.98	0.91	0.65	0.91	Zhalantun	0.16	0.98	0.87	0.65	0.87
Dong Ujimqin	0.17	0.97	0.90	0.68	0.90	**Moist sub-humid**					
Kailu	0.21	0.99	0.84	0.88	0.82	Arxan	0.18	0.99	0.90	0.53	0.89
Abag	0.13	1.00	0.92	0.51	0.92	Bugt	0.19	0.99	0.88	0.58	0.87
Baotou	0.16	0.98	0.88	0.66	0.88	Tulihe	0.14	1.00	0.92	0.44	0.91
EjinHoro	0.19	0.98	0.84	0.83	0.83	Xiaoer Gou	0.16	0.99	0.90	0.54	0.89

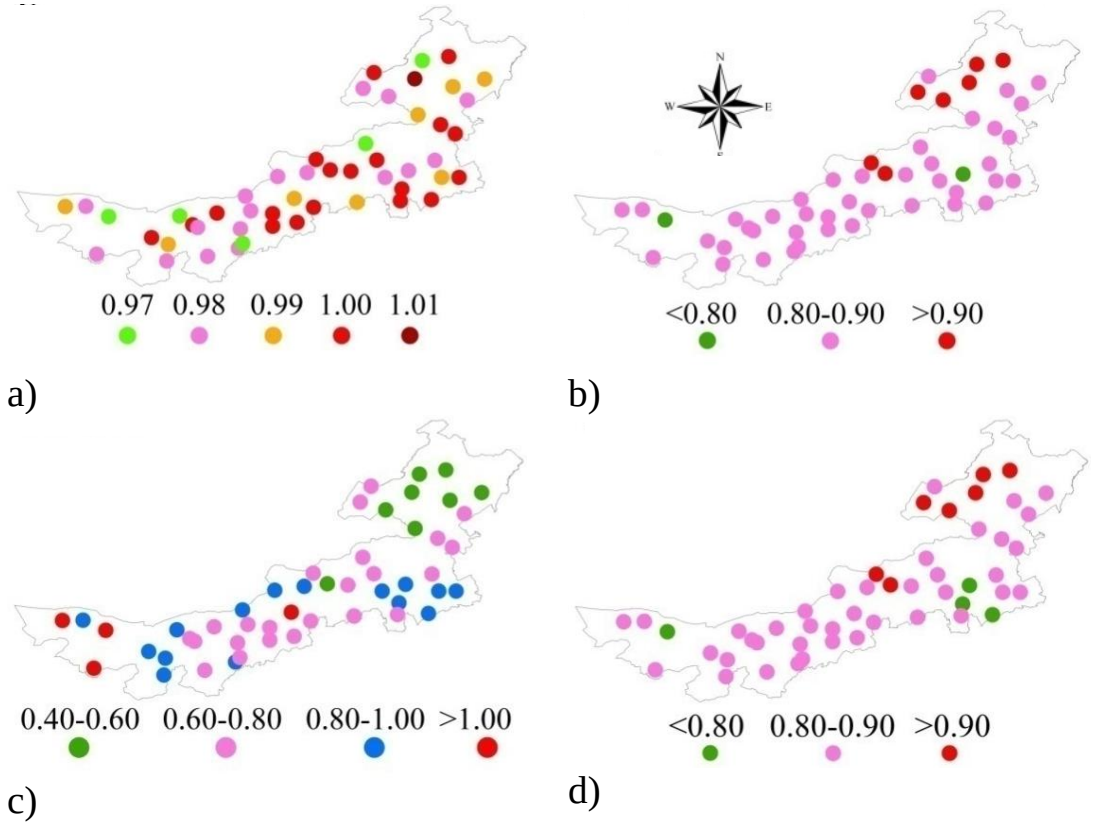

Figure 4-3 Spatial distribution of the statistical performance indicators comparing $ET_{o\ PMT}$ with PM-ET_o: a) regression coefficient, b_0, b) coefficient of determination, c) root mean square error, and d) modeling efficiency (aridity increases from east to west, Figure 4-1).

The temperature correction for aridity was highly important for locations with hyper-arid and arid climates. It was observed (data not shown) that the k_{Rs} values tended to highly increase for locations in hyper-arid and arid climates when temperature was not corrected to estimate T_{dew}. Several values then obtained were out of the range analyzed by Samani (2004). All k_{Rs} values were reduced by 0.03 - 0.02 $°C^{-0.5}$ in case of hyper-arid and arid locations when the temperature correction was performed. Differently, the b_0 slope values changed very little and the coefficients of determination R^2 also had negligible changes due to temperature correction. However, the RMSE values were decreased by 2 to 5% similarly to what observed by Raziei and Pereira (2013b). EF also increased a few points, more in case of hyper-arid climates and few for semiarid locations. These results for EF indicate that MSE decreased when improved estimations of T_{dew} were produced. For humid climatic zones and stations with low mean temperature, T_{dew} estimates with Equation 4.4 led to improved performance. These results agree with those reported by Todorovic et al. (2013) and Raziei and Pereira (2013b).

It is well known that wind speed strongly affects ET_o in climates marked by aridity (Allen et al. 1998). The studies by Jabloun and Sahli (2008) for Tunisia and Raziei and Pereira (2013b) applied to Iran clearly identified the effects of wind speed on $ET_{o\ PMT}$. The impacts of the average wind speed values used as alternative to observations on the performance of the $ET_{o\ PMT}$ were assessed. Relatively poor correlations were observed when comparing $ET_{o\ PMT}$ with PM-ET_o in stations where high wind speed occurs throughout the year, in western hyper-arid and arid regions (Figure 4-1). Adopting the default value of 2 m s^{-1} in $ET_{o\ PMT}$ computations did not lead to under-estimate PM-ET_o but k_{Rs} values were above the range reported by Samani (2004) and out of the range of values obtained for the other stations in Inner Mongolia (Table 4-2 and Figure 4-4). Differently, selecting a higher average wind speed resulted k_{Rs} values in the range of those obtained for the other stations and to slight improvements in the statistical performance indicators (data not shown). Similar conclusions were reported by Raziei and Pereira (2013b) for Iran.

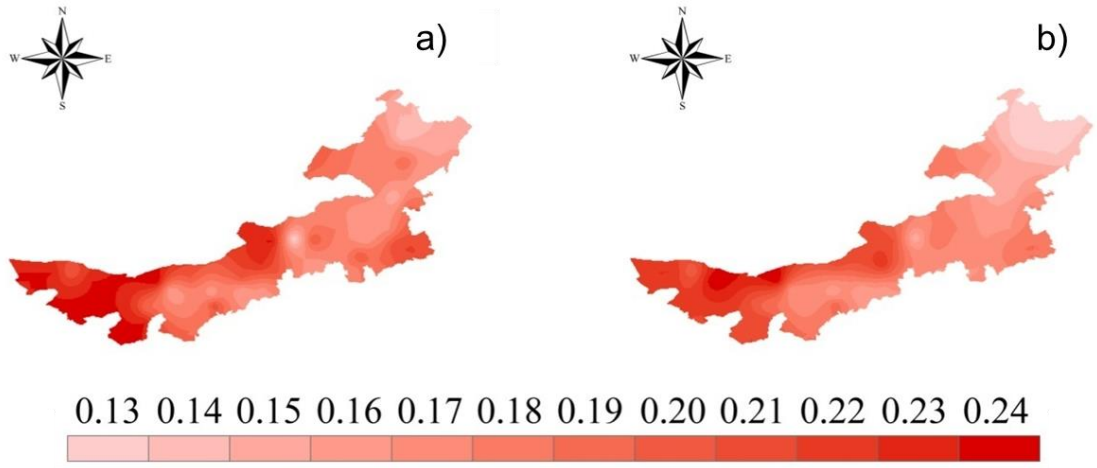

Figure 4-4 Spatial patterns of the optimal kRs (°C-0.5) over Inner Mongolia for: (a) PMT and (b) HS methods (aridity increases from east to west, Figure 4-1).

4.3.2 Performance of the HS method

The statistical indicators relative to $ET_{o\ HS}$ when compared with the PM-ET_o and the calibrated k_{Rs} were shown in Table 4-3 for all weather stations. Similarly, with $ET_{o\ PMT}$, results showed that the performance of $ET_{o\ HS}$ was influenced by climate aridity. $ET_{o\ HS}$ tended to slightly underestimate daily PM-ET_o under arid conditions, with b_0 ranging from 0.96-0.98 in hyper-arid climates and 0.97-1.01 in arid climate locations.

Table 4-3 Calibrated k_{Rs} coefficient and statistical performance indicators when comparing the $ET_{o\ HS}$ with the PM-ET_o.

Stations	k_{Rs} (°C$^{-0.5}$)	b_0	R^2	RMSE (mm d^{-1})	EF	Stations	k_{Rs} (°C$^{-0.5}$)	b_0	R^2	RMSE (mm d^{-1})	EF
Hyper-arid						**Semiarid**					
JiKede	0.23	0.97	0.87	1.21	0.86	Ongniud	0.18	0.96	0.82	0.90	0.79
Ejin	0.20	0.98	0.87	1.03	0.86	Xin Barag L	0.18	1.00	0.92	0.60	0.92
Guaizi	0.25	0.98	0.78	1.64	0.75	Manzhouli	0.18	0.98	0.90	0.69	0.89
Arid						Tongliao	0.19	0.99	0.84	0.90	0.80
Jartai	0.19	0.96	0.87	0.92	0.86	Dongsheng	0.20	0.98	0.89	0.68	0.88
Bayan knoll	0.21	0.97	0.85	1.00	0.84	Chifeng	0.17	0.96	0.85	0.79	0.83
Alxa R.	0.22	0.98	0.81	1.15	0.79	Jarud	0.17	0.98	0.85	0.72	0.84
Hailisu	0.25	0.99	0.88	0.99	0.87	Xi Ujimqin	0.18	1.00	0.87	0.92	0.77
Erenhot	0.21	1.01	0.90	0.87	0.88	Jining	0.17	0.97	0.85	0.91	0.76
Hanggin	0.18	1.01	0.87	0.79	0.85	Bairin	0.17	0.99	0.81	0.85	0.79
Linhe	0.17	0.98	0.90	0.65	0.90	BaoGuotu	0.18	0.99	0.81	0.63	0.89
Mandula	0.22	0.99	0.87	0.96	0.85	Linxi	0.17	0.96	0.82	0.70	0.88
Sonid	0.21	0.97	0.89	0.86	0.88	Hohhot	0.16	0.96	0.89	0.76	0.82
Zhurihe	0.23	0.99	0.86	1.06	0.83	Siziwangqi	0.19	0.98	0.89	0.73	0.86
Alxa L.	0.22	1.00	0.84	0.93	0.83	Duolun	0.17	0.98	0.85	0.79	0.84
Urat	0.19	0.97	0.89	0.74	0.89	Huade	0.19	0.98	0.87	0.58	0.91
Semiarid						Ulanhot	0.18	0.99	0.86	0.79	0.84
Damao	0.19	0.99	0.87	0.81	0.85	Hailar	0.17	1.00	0.91	0.58	0.91
Naranbulag	0.19	0.99	0.92	0.66	0.91	**Dry sub-humid**					
Otog	0.18	0.98	0.87	0.76	0.86	Sauron	0.16	0.97	0.87	0.72	0.84
XilinHot	0.19	1.00	0.90	0.74	0.89	EjiGuna	0.15	0.99	0.91	0.55	0.90
Xin Barag R	0.18	0.97	0.91	0.66	0.91	Zhalantun	0.16	0.95	0.88	0.67	0.86
Dong Ujimqin	0.18	1.00	0.90	0.70	0.89	**Moist sub-humid**					
Kailu	0.19	0.98	0.84	0.91	0.81	Arxan	0.15	0.98	0.90	0.55	0.88
Abag	0.15	0.98	0.94	0.45	0.93	Bugt	0.15	0.96	0.88	0.61	0.86
Baotou	0.16	0.96	0.89	0.65	0.89	Tulihe	0.13	0.98	0.92	0.46	0.91
EjinHoro	0.19	1.01	0.84	0.86	0.82	Xiaoer Gou	0.14	1.01	0.90	0.53	0.89

Most b_0 values were close to 1.0 but generally $b_0 < 1.0$. These results expressed that a statistical similarity exists between $ET_{o\ HS}$ and PM-ET_o. The R^2 values were generally

greater than 0.80 but very few are larger than 0.90. R^2 range 0.75 to 0.86 for hyper-arid climates, 0.79 to 0.89 in arid climates, 0.77 to 0.91 in semiarid locations and 0.84 to 0.91 in sub-humid locations. These results indicated that $ET_{o\ HS}$ was able to explain a large fraction of the variability of the PM-ET_o values for all climates. As for $ET_{o\ PMT}$, R^2 results related to the range of ET_o values, with a larger dispersion for higher daily ET_o values when wind speed was high since u_2 is not considered when computing $ET_{o\ HS}$. The spatial distribution of b_0 values did not show any specific pattern (Figure 4-5a); contrarily, the R^2 values showed a clear trend to increase from east to west similarly with $ET_{o\ PMT}$ results (Figure 4-5b).

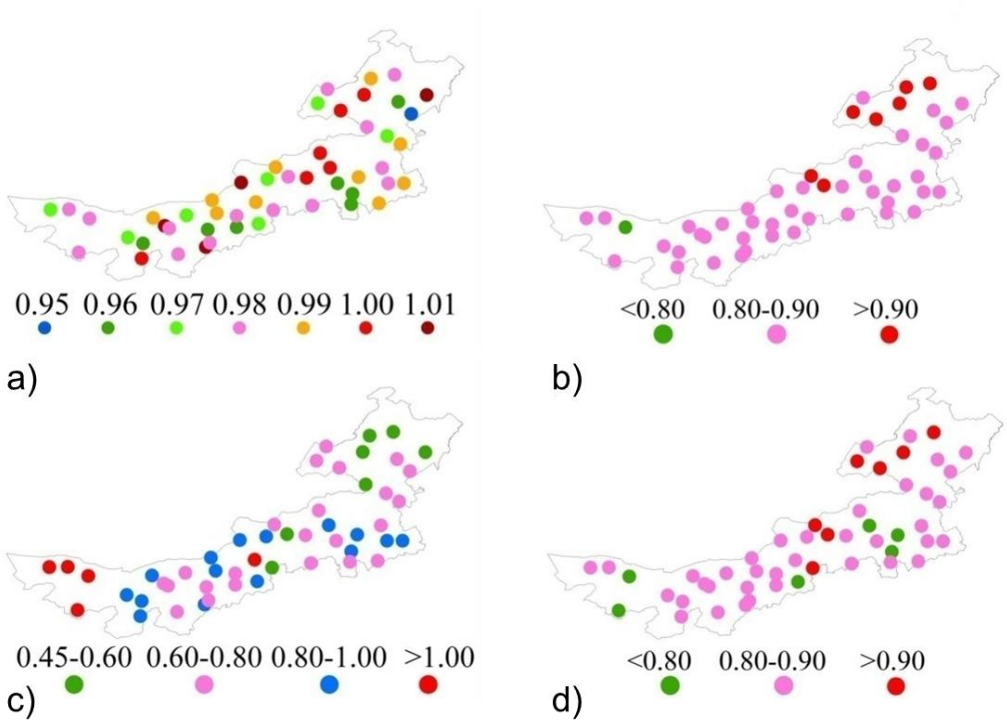

Figure 4-5 Spatial distribution of statistical performance indicators comparing ETo HS with PM-ET_o: a) regression coefficient, b) coefficient of determination, c) root mean square error, and d) modeling efficiency (aridity increases from east to west as per Figure 4-1).

RMSE values (Table 4-3) were much higher for hyper-arid climates (1.03-1.64 mm d^{-1}) and tended to decrease when aridity decreases: RMSE varied from 0.65 to 1.13 mm d^{-1} in arid areas and 0.46 to 0.61 mm d^{-1} in the moist sub-humid region. The size of errors clearly relate to the range of ET_o values, higher in more arid climates and smaller in moist sub-humid locations, and also relate with b_0 and R^2 distribution, which may be observed in Table 4-3 and Figure 4-5c. The EF values were generally high, greater than 0.75 but rarely above 0.90 (Table 4-3), thus indicating that MSE values relative to comparing $ET_{o\ HS}$ with the standard PM-ET_o were much smaller than the variance of the PM-ET_o values.

As expected, EF tended to be higher for the moist sub-humid climates. These results, similarly to $ET_{o\ PMT}$, indicated that the $ET_{o\ HS}$ was a good estimator of ET_o. The spatial distribution of EF values (Figure 4-5d), as already observed for $ET_{o\ PMT}$ (Figure 4-3), closely followed those of R^2 because both indicators refer to the variance of PM-ET_o values and to the errors of estimate.

Overall, acceptable results were obtained for the windy and arid locations, e.g., Guaizi, Ji Kede, Alxa and Zhurihe (Table 4-3). Because wind speed is not considered in the $ET_{o\ HS}$ computations, it resulted that the calibrated values for k_{Rs} were then higher relative to the nearby stations, thus indicating that the effect of wind speed in increasing ET_o was considered in $ET_{o\ HS}$ through increasing the k_{Rs} value.

The k_{Rs} factor tended to be higher in the more arid climates varying from 0.20 to 0.25 $°C^{-0.5}$ in the hyper-arid locations and decreasing to 0.13 to 0.15 $°C^{-0.5}$ in the moist sub-humid locations (Table 4-3). Their spatial pattern followed that trend (Figure 4-4), with k_{Rs} increasing from east to west, i.e., from sub-humid to hyper-arid climates. Results were similar to those obtained for $ET_{o\ PMT}$ (Table 4-2 and Figure 4-4) The values for k_{Rs} showed to be related with the aridity index but were also influenced by other factors such as turbidity of the atmosphere, influencing the energy available for evaporation, and wind speed as referred above. Operationally, because it was not possible to find a k_{Rs} estimation equation, users may just interpolate k_{Rs} values from the nearby stations referred in Table 4-3.

4.3.3 Spatial variability of ET_o in relation to the computational method

The spatial variability of ET_o in Inner Mongolia was studied for the three data sets relative to the PM-ET_o, $ET_{o\ PMT}$ and $ET_{o\ HS}$. For each method, 10 variables were created to characterize ET_o: four seasonal ET_o amounts, the respective ET_o percentages in the year, the annual ET_o amount, and the aridity index. Figure 4-6 shows the spatial variability of PM-ET_o, $ET_{o\ PMT}$ and $ET_{o\ HS}$ for each season. All three computation methods provided similar results with ET_o decreasing from West to East, in agreement with Figure 4-2. The spatial variability of ET_o was higher in the summer warm season and lower in the cold winter season (Figure 4-6). Moreover, the spatial pattern of ET_o in the warm season followed closely the aridity spatial pattern shown in Figure 4-1.

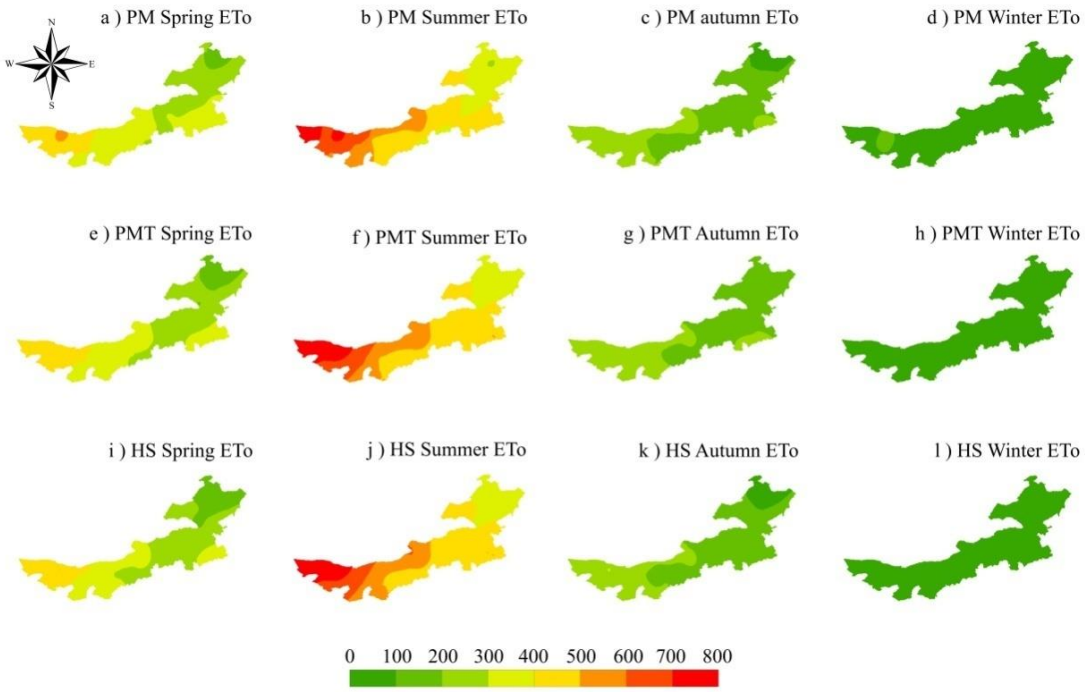

Figure 4-6 Spatial distribution of seasonal ET_o computed with FAO-PM (a-d), PMT (e-h) and HS (i-l).

The three data sets including the 10 variables relative to all locations were submitted to PCA in R-Mode to determine which variables mainly influence the spatial variability of ET_o in the region. For each data set of 10 climate variables used to explain ET variability a factor analysis analysis, the principal component analysis, in R-Mode (Richman, 1986) was performed to classify the data and reduce the 10 variables with new, fewer, and uncorrelated variables which are able to explain maximum possible information of the original data. In this application, from each data set, a matrix of 50 rows (weather stations) and 10 columns (variables) was constructed. Then, the respective covariance matrix were computed and the respective eigenvalues and eigenvectors were retrieved. The significant principal components, which explain the majority of the variance were retained using the North's rule of thumb (North et al. 1982) and the rotated PC scores represent, in this application, the most important spatial patterns of ET in the region. Furthermore, the rotation used herein, the varimax rotation, is an orthogonal rotation method used to obtain clear separation between the factor loadings and therefore more spatially localized and uncorrelated PCs.

The contribution of each variable to the construction of Principal Components (PC) is presented in Table 4-4. Results showed that two PCs were retained for all three cases with a cumulative explained variance by both PCs larger than 90%, thus showing that those

two PCs were enough to characterize the ET_o patterns. After Varimax rotation of the two retained components, PC1 explained more variance when $ET_{o\ PMT}$ variables were considered, 53% (Table 4-4). Differently, the difference between the explained variance by both components was the smallest with PM-ET_o since then PC1 represented 49% of the variance and PC2 represented 42% (Table 4-4). The ET_o amounts relative to the spring, summer and autumn and the aridity index (with a high negative correlation) were the main variables contributing to PC1 (Table 4-4) for all three sets of variables.

Table 4-4 Explained variances of the rotated principal components corresponding to the three sets of ET_o variables.

Variables	PM-ET_o		$ET_{o\ PMT}$		$ET_{o\ HS}$	
	PC1	PC2	PC1	PC2	PC1	PC2
Winter (DJF) ET_o amount	0.57	0.78	0.74	0.63	0.66	0.68
Spring (MAM) ET_o amount	**0.80**	0.55	**0.97**	0.20	**0.91**	0.39
Summer (JJA) ET_o amount	**0.96**	0.22	**0.99**	-0.06	**0.98**	0.13
Autumn (SON) ET_o amount	**0.82**	0.55	**0.92**	0.37	**0.88**	0.46
Annual ET_o amount	**0.88**	0.46	**0.98**	0.16	**0.94**	0.32
Percentage of winter ET_o	0.25	**0.93**	0.33	**0.91**	0.43	**0.85**
Percentage of spring ET_o	**-0.77**	0.43	0.10	0.74	0.11	**0.86**
Percentage of summer ET_o	0.00	**-1.00**	-0.17	**-0.98**	-0.34	**-0.94**
Percentage of autumn ET_o	0.30	0.77	-0.06	**0.93**	0.27	**0.90**
Aridity index	**-0.89**	-0.26	**-0.92**	-0.07	**-0.89**	-0.23
Percentage of explained variance	48.77	41.68	52.87	38.02	50.82	41.52
Cumulative percentage of explained variance		90.45		90.88		92.34

Among them, the summer ET_o amount is the variable that most contributes to PC1. This result was well explained when comparing Figures 4-6 and 4-7 showing that the spatial patterns depicted for PC1 were very close to those of the summer ET_o amount. The differences among the three data sets on the relative importance of each variable for PC1

were very small and results in Figure 4-7 showed very similar patterns for PC1. It may be concluded that $ET_{o\ PMT}$ and $ET_{o\ HS}$ had spatial distributions similar to PM-ET_o.

Table 4-4 also showed that winter and summer ET_o percentages were the main variables relative to PC2, which were common to all three data sets. The autumn percentage was also relevant for the PC2 relative to $ET_{o\ PMT}$ and $ET_{o\ HS}$ data sets, and the spring percentage was also added for the $ET_{o\ HS}$ data set. These differences in contributing variables may be responsible for a less similar behavior found for the spatial patterns identified for PC2 (Figure 4-7).

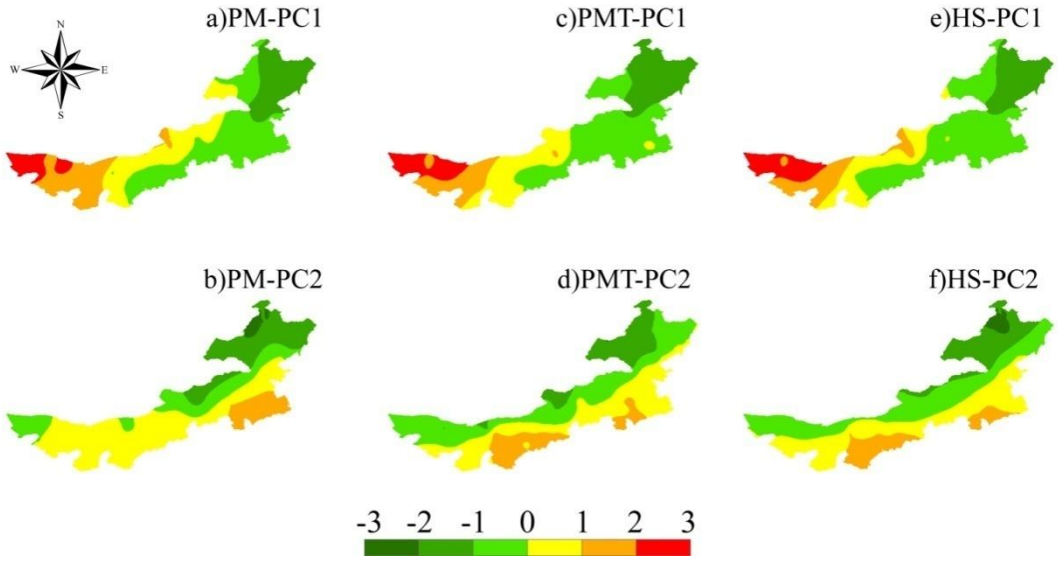

Figure 4-7 Spatial distribution of the rotated PC-scores of ET_o variables.

The spatial patterns obtained with the PC-scores (Figure 4-7) showed a good agreement between the three ET_o estimation methods. The spatial pattern relative to PC1 was more stable because the same sub-regions were identified with PM-ET_o, $ET_{o\ PMT}$ and $ET_{o\ HS}$ data sets, with the PC-scores variability close to that found for the aridity index (Figure 4-1). Differently, for PC2 some differences were evident (Figure 4-7 b, d, and f): a sub-region was identified in the south-east, more significant when using the PM-ET_o derived data set, and another was identified in the southwest when using the temperature methods but it was not identified with the PM-ET_o. PC-scores varied from south to north. Results for PC2 showed that $ET_{o\ PMT}$ and $ET_{o\ HS}$ had a similar behavior (Figure 4-7d and f) that was different from that of PM-ET_o (Figure 4-7b), thus indicating that it was not indifferent to use a full data set or only temperature data for computing ET_o.

4.3.4 Comparison of HS and PMT methods

Results analysed above showed that the performance of HS and PMT methods are good and very similar. However, when comparing the respective statistical indicators, there were differences which allowed assessing advantages of a method compared to the other. To ease this comparison, main performance indicators are paralleled in Table 4-5 where indicators showing the superiority of the PMT method are highlighted. b_0 values were often equal but RMSE and EF values referring to the PMT method were often better. Errors were generally smaller with PMT as also depicted in Figure 4-8. Nevertheless, there was no evidence of a spatial pattern of RMSE since locations having better RMSE with the HS method were scattered throughout Inner Mongolia.

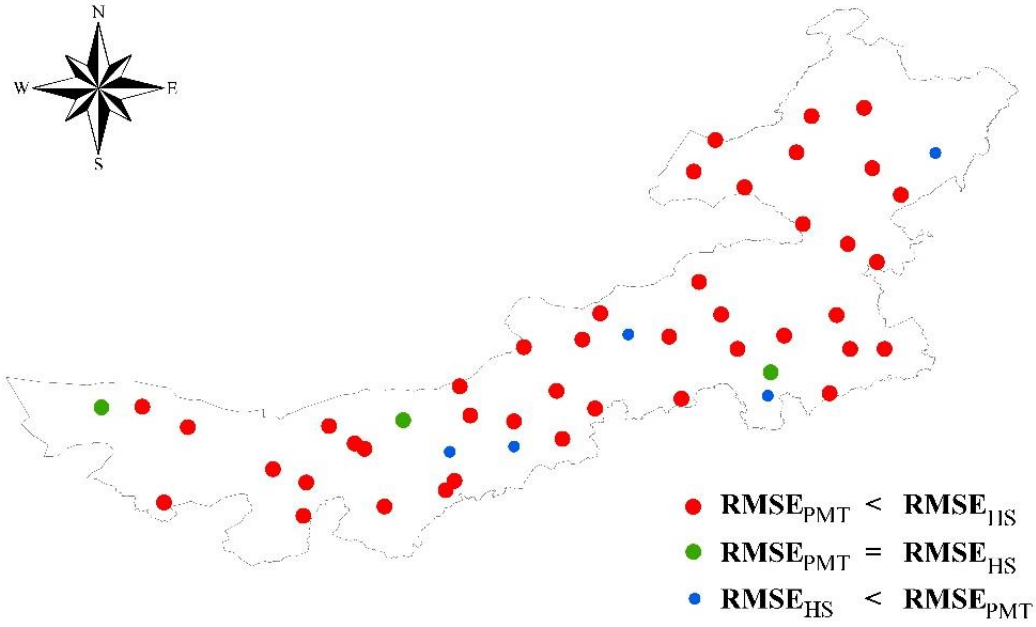

Figure 4-8 Spatial distribution of RMSE results when comparing PMT and HS methods throughout Inner Mongolia.

The PMT method had also the advantage of following the conceptual approach of the PM-ET_o method because variables lacking were replaced by their estimators. Therefore, it is advisable to use the PMT when data sets lack one or two variables, particularly when this occurs temporarily. This advantage was already analysed in former studies, e.g. Liu and Pereira (2001) for North China, Popova et al. (2006) for Bulgaria and Jabloun and Sahli (2008) for Tunisia. This type of approach is however rare because, on the one hand, computations are more demanding with PMT and, on the other hand, most authors just look for computations alternative to PM-ET_o.

Table 4-5 Comparing the performances of HS and PMT methods (highlighted cells refer to better results).

Stations	PMT performance indicators			HS performance indicators		
	b	RMSE (mm d^{-1})	EF	b	RMSE (mm d^{-1})	EF
Hyper-arid						
Ji Kede	**0.99**	1.21	0.86	0.97	1.21	0.86
Ejin	0.98	**1.00**	0.86	0.98	1.03	0.86
Guaizi	0.97	**1.62**	**0.76**	**0.98**	1.64	0.75
Arid						
Jartai	**0.99**	**0.90**	0.86	0.96	0.92	0.86
Bayan knoll	**1.00**	**0.99**	**0.85**	0.97	1.00	0.84
Alxa R.	0.98	**1.13**	**0.80**	0.98	1.15	0.79
Hailisu	0.97	**0.93**	**0.88**	**0.99**	0.99	0.87
Erenhot	0.98	**0.83**	**0.89**	**1.01**	0.87	0.88
Hanggin	**1.00**	**0.76**	**0.86**	1.01	0.79	0.85
Linhe	0.98	**0.64**	0.90	0.98	0.65	0.90
Mandula	0.98	**0.92**	**0.86**	**0.99**	0.96	0.85
Sonid	**0.98**	**0.85**	**0.89**	0.97	0.86	0.88
Zhurihe	0.99	**1.01**	**0.85**	0.99	1.06	0.83
Alxa L.	0.98	**0.90**	**0.84**	**1.00**	0.93	0.83
Urat	**1.00**	0.74	0.89	0.97	0.74	0.89
Semiarid						
Damao	0.98	**0.77**	**0.86**	**0.99**	0.81	0.85
Naranbulag	**1.00**	**0.64**	**0.92**	0.99	0.66	0.91
Otog	0.98	**0.75**	0.86	0.98	0.76	0.86
Xilin Hot	1.00	**0.73**	0.89	1.00	0.74	0.89
Xin Barag R.	**0.98**	**0.65**	0.91	0.97	0.66	0.91
Dong Ujimqin	0.97	**0.68**	**0.90**	**1.00**	0.70	0.89
Kailu	**0.99**	**0.88**	**0.82**	0.98	0.91	0.81
Abag	**1.00**	0.51	0.92	0.98	**0.45**	**0.93**
Baotou	**0.98**	0.66	0.88	0.96	**0.65**	**0.89**
Ejin Horo	0.98	**0.83**	**0.83**	**1.01**	0.86	0.82
Ongniud	**1.00**	0.90	0.79	0.96	0.90	0.79
Xin Barag L.	0.98	**0.57**	0.92	**1.00**	0.60	0.92
Manzhouli	**1.00**	**0.68**	0.89	0.98	0.69	0.89
Tongliao	**1.00**	**0.88**	**0.81**	0.99	0.90	0.80
Dongsheng	0.97	**0.66**	**0.89**	**0.98**	0.68	0.88
Chifeng	**1.00**	0.80	0.83	0.96	**0.79**	0.83
Jarud	0.98	**0.77**	**0.83**	0.98	0.80	0.82
Xi Ujimqin	1.00	**0.74**	**0.86**	1.00	0.76	0.85
Jining	**1.00**	**0.71**	0.84	0.97	0.72	0.84
Bairin L.	0.98	**0.90**	**0.78**	**0.99**	0.92	0.77
Bao Guotu	**1.00**	**0.90**	**0.77**	0.99	0.91	0.76
Linxi	**0.98**	**0.83**	**0.80**	0.96	0.85	0.79
Hohhot	**1.00**	0.64	0.88	0.96	**0.63**	**0.89**

Table 4-5 (continued).

Siziwangqi	**1.00**	**0.68**	0.88	0.98	0.70	0.88
Duolun	**0.99**	**0.73**	**0.83**	0.98	0.76	0.82
Huade	**1.00**	**0.71**	**0.87**	0.98	0.73	0.86
Ulanhot	**1.00**	**0.77**	**0.85**	0.99	0.79	0.84
Hailar	1.01	**0.57**	0.91	**1.00**	0.58	0.91
Dry sub-humid						
Sauron	**1.00**	**0.68**	**0.86**	0.97	0.72	0.84
Eji Guna	0.97	**0.53**	**0.91**	**0.99**	0.55	0.90
Zhalantun	**0.98**	**0.65**	**0.87**	0.95	0.67	0.86
Moist sub-humid						
Arxan	**0.99**	**0.53**	**0.89**	0.98	0.55	0.88
Bugt	**0.99**	**0.58**	**0.87**	0.96	0.61	0.86
Tulihe	**1.00**	**0.44**	0.91	0.98	0.46	0.91
Xiaoer Gou	0.99	0.54	0.89	1.01	**0.53**	0.89

4.3.5 Annual trends of PM-ET_o computed with full data sets

The MMK test associated with the Sen's slope analysis (Sen 1968) and the DTS trend analysis were applied to the monthly ET_o series cumulated to the year and computed with the PM-ET_o, PMT and HS methods. Results for the PM-ET_o series are shown in Table 4- 6 where the weather stations are listed according the rank of the aridity index. Tables include the Sen's slope when the MMK test was significant with a confidence level of 95% and the GLS linear trend when a deterministic trend was considered with the KPSS test also for a confidence level of 95%. Results for the MMK test showed that 23 out of the 46 time series revealed significant trends, 14 for an increase of ET_o and 9 for a decrease of ET_o (Table 4-6).

The PP test was performed for the null hypotheses of a unit root and was rejected for all stations, which is a result common in geophysical time series. The KPSS test was applied to test for the null hypotheses that the time series was trend stationary, which was rejected for 34 time series, thus indicating that a deterministic trend could be possible for these time series. The GLS linear model was then fitted to these 34 time series to estimate the respective regression coefficients. For the confidence level of 95% 19 series have shown significant increasing trends and significant decreasing trends were detected for 11 series.

Table 4-6 Trends (mm yr^{-1}) for PM- ET_o computed with full data sets using both the MMK test associated with the Sen slope and the KPSS test associated with the GLS linear trend. Significant results were assumed for a confidence level of 95%.

Stations	MMK test Sen slope (mm yr^{-1})	KPSS test Linear trend and uncertainty (mm yr^{-1})	Stations	MMK test Sen slope (mm yr^{-1})	KPSS test Linear trend and uncertainty (mm yr^{-1})
Hyper-arid			**Semiarid**		
Ejin	-2.49	-2.44 ± 0.94	Manzhouli	2.09	2.07 ± 0.88
Guaizi	4.43	4.55 ± 1.00	Tongliao	1.19	0.90 ± 0.70
Arid			Dongsheng	-	-
Jartai	-1.12	-0,81 ± 0.63	Chifeng	-	-
Bayan knoll	-	-	Jarud	-1.35	-1.05 ± 0.69
Alxa R.	-	-1.81 ± 0.96	Xi Ujimqin	-	-
Erenhot	-	-	Jining	-2.00	-1.74 ± 0.66
Linhe	-	-*	Bairin	-	0.93 ± 0.72
Mandula	-	-	Bao Guotu	-2.52	-2.57 ± 0.67
Sonid	-	1.28 ± 0.85	Linxi	-	-
Zhurihe	-	1.04 ± 0.97	Hohhot	1.33	1.43 ± 0.55
Alxa L.	-	-*	Siziwangqi	-1.08	-0.95 ± 0.76
Urat	-	-	Duolun	-	0.60 ± 0.60
Semiarid			Huade	-	-
Damao	-1.84	-1.47 ± 0.83	Ulanhot	-	-*
Naranbulag	-	-	Hailar	1.09	1.07 ± 0.51
Otog	-1.72	-1.40 ± 0.71	**Dry sub-humid**		
Xilin Hot	2.50	2.49 ± 0.73	Sauron	1.48	1.39 ± 0.60
Xin Barag R.	0.56	-	Eji Guna	1.21	1.04 ± 0.59
Dong Ujimqin	-	-	Zhalantun	-	0.59 ± 0.58
Kailu	1.10	0.99 ± 0.71	**Moist sub-humid**		
Abag	1.34	1.34 ± 0.74	Arxan	1.10	1.20 ± 0.49
Baotou	-3.11	-2.45 ± 0.95	Bugt	1.00	1.04 ± 0.43
Ongniud	-	-*	Tulihe	1.14	1.07 ± 0.41
Xin Barag L.	-1.24	-1.25 ± 0.73	Xiaoer Gou	-	0.66 ± 0.49

Thus, the DTS approach detected more significant trends than the MMK. For the locations where a trend was identified with DTS but not with MMK, the uncertainty associated with the detected trend value was high, i.e., the uncertainty value was close to the trend value itself (Table 4-6). MMK detected only one significant trend for a location (Xin Barag R.) where no trend was detected with DTS, although it was the smallest trend observed, 0.56 mm yr^{-1}. Despite the differences in the number of time series identified with significant trends, both methods provided coherent results since for all the commonly identified stations the trend signals were always the same and the trend

magnitudes were not very different (Table 4-6). The largest difference (0.66 mm yr^{-1}) was found for the station of Baotou, in the Yellow River basin, where the decreasing trends detected with MMK and DTS were high, -3.11 and -2.45 mm yr^{-1} respectively.

The spatial patterns of the GLS computed linear trends of PM-ET_o are shown in Figure 4-9. The trend magnitudes represented correspond to two confidence levels, 99% and 95%, the first corresponding to a larger trend, with p-value < 0.01, the latter representing a smaller but significant trend for p-values < 0.05. Results in Figure 4-9a did not show a clear spatial pattern for the PM-ET_o time series but it was noticeable that the increasing trends were concentrated in the East, in the more humid areas of Inner Mongolia, while the decreasing trends were detected for the stations where the climate varies from hyper-arid, in the west, to semi-arid. However, one contradictory exception was observed with a positive trend for Guaizi, in the hyper-arid area, which may be due to local station characteristics and site conditions.

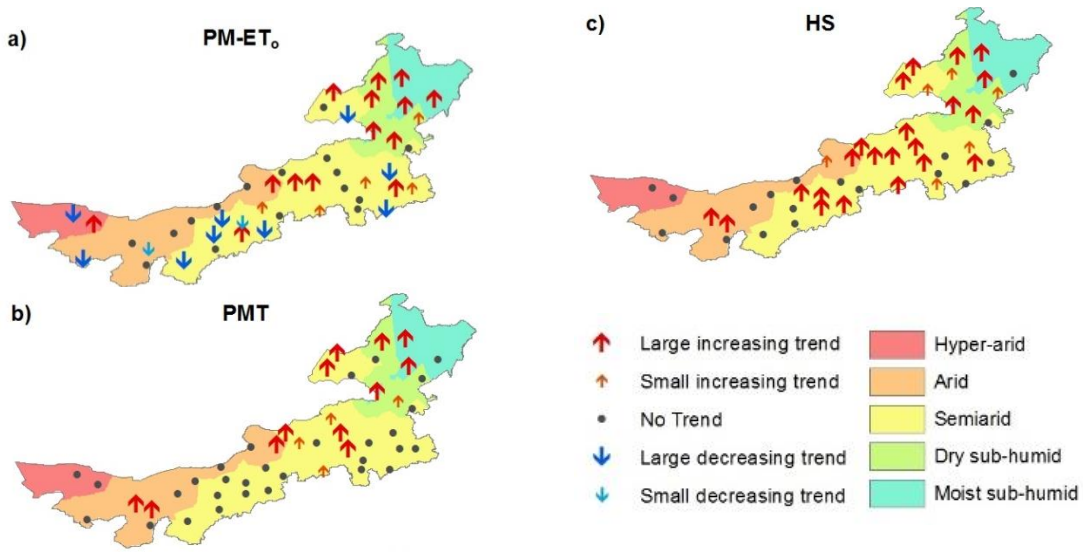

Figure 4-9 Spatial distribution of deterministic linear trends of annual ET_o in Inner Mongolia.

The spatial pattern of PM-ET_o trends (Figure 4-9a) was generally in agreement with literature. The western regions, where climate is arid to hyper-arid, trends were generally for a decrease of ET_o despite one location exhibited a contradictory positive trend. These results agreed with those referred for northwest China by Thomas (2000), Yin et al. (2010) and Huo et al. (2013); however, contradictory results were reported by Liu and Zhang (2013) who have shown that the decreasing trend has been inverted in the last two decades. Relative to the west-central area, with arid to semiarid climate, the trend detected

herein is mainly for a decrease of ET_o. Studies relative to the middle Yellow River basin, which is partly located in this area, are somewhat opposed: Liu et al. (2010) and Yang et al. (2011) reported both positive and negative trends, while Wang et al. (2012) referred to a decreasing trend in this area. For the east-central semiarid area both positive and negative trends were detected, which apparently agree with results reported by Liang et al. (2010). Trends identified herein for the western region, of sub-humid climate, were mostly positive, in agreement with the increasing ET_o trends referred by Thomas (2000), Gao et al. (2006), Liang et al. (2010) and Yin et al. (2010).

It may be concluded that ET_o trends were influenced by the aridity of the climate, with increased trends in sub-humid areas and decreasing trends in the areas highly marked by aridity. In the semiarid areas both positive and negative trends were observed, with increasing trends predominating in the western area, where aridity tends to be higher, and decreasing ones in the eastern one, close to the sub-humid areas. However, it was apparent that significant increases in temperature were overcoming the influence of other meteorological factors and a direct relation between ET_o trends and aridity is likely not possible to fully assume.

4.3.6 Trends for ET_o computed with the HS and PMT temperature methods

The application of the MMK test and of the corresponding Sen slope to the ET_o time series obtained from the computations with the HS and PMT approaches, respectively $ET_{o\,HS}$ and $ET_{o\,PMT}$, led only to significant increasing trends, 24 for $ET_{o\,HS}$ and 13 for $ET_{o\,PMT}$, i.e., decreasing trends for ET_o were not detected when temperature methods were applied. The application of the KPSS test followed by the computation of the GLS linear trend led to detect 28 cases of positive trend for $ET_{o\,HS}$ and 16 for $ET_{o\,PMT}$ (Table 4-7), also without identification of decreasing trends. It resulted that, for a few cases in arid and semiarid areas, increasing trends were detected for $ET_{o\,HS}$ and $ET_{o\,PMT}$ when descending trends were detected for PM-ET_o, e.g., Jartai and Xin Barag L..

Table 4-7 Trends in ET_o (mm yr^{-1}) computed with temperature methods, HS and PMT using both the MMK test associated with the Sen slope and the KPSS test associated with the GLS linear trend. Significant results were assumed for a confidence level of 95%. All columns are in mm yr^{-1}

Stations	ET_o from HS		ET_o from PMT		Stations	ET_o from HS		ET_o from PMT	
	MMK test Sen slope	KPSS test Linear trend and uncertainty	MMK test Sen slope	KPSS test Linear trend and uncertainty		MMK test Sen slope	KPSS test Linear trend and uncertainty	MMK test Sen slope	KPSS test Linear trend and uncertainty
Hyper-arid					**Semiarid**				
Ejin	-	-*	-	-*	Manzhouli	1.06	1.03 ± 0.51	0.82	0.82 ± 0.51
Guaizi	-	-	-	-*	Tongliao	-	-	-	-
Arid					Dongsheng	-	-	-	-
Jartai	0.92	0.90 ± 0.43	0.72	0.73 ± 0.40	Chifeng	-	0.57 ± 0.46	-	-
Bayan knoll	-	0.90 ± 0.50	-	0.91 ± 0.48	Jarud	-	0.48 ± 0.46	-	-
Alxa R.	-	-	-	-*	Xi Ujimqin	1.09	1.10 ± 0.51	0.87	0.88 ± 0.50
Erenhot	-	0.54 ± 0.50	-	-	Jining	0.65	0.62 ± 0.42	-	-
Linhe	-	-	-	-*	Bairin	-	-*	-	-
Mandula	-	-	-	-*	Bao Guotu	-	-*	-	-*
Sonid	1.70	1.77 ± 0.57	1.72	1.84 ± 0.57	Linxi	1.06	1.03 ± 0.49	0.91	0.86 ± 0.47
Zhurihe	0.53	-*	-	-	Hohhot	0.59	0.52 ± 0.37	-	-
Alxa L.	-	-	-	-	Siziwangqi	0.76	0.75 ± 0.53	-	-*
Urat	-	-	-	-*	Duolun	0.83	0.80 ± 0.43	-	0.45 ± 0.44
Semiarid					Huade	-	-	-	-
Damao	0.74	0.71 ± 0.47	-	-*	Ulanhot	-	-	-	-*
Naranbulag	1.04	1.00 ± 0.39	0.67	0.64 ± 0.40	Hailar	0.68	0.51 ± 0.41	-	-
Otog	-	-	-	-*	**Dry sub-humid**				
Xilin Hot	0.91	0.84 ± 0.51	-	-*	Sauron	0.82	0,86 ± 0.48	-	0.54 ± 0.49
Xin Barag R.	0.98	0.90 ± 0.53	0.79	0.71 ± 0.53	Eji Guna	1.27	1.19 ± 0.44	1.12	1.03 ± 0.43
Dong Ujimqin	0.92	1.04 ± 0.53	-	0.67 ± 0.52	Zhalantun	-	0.48 ± 0.42	-	-
Kailu	0.66	0.65 ± 0.45	-	-*	**Moist sub-humid**				
Abag	0.96	0.85 ± 0.49	0.57	0.48 ± 0.47	Arxan	0.91	0.84 ± 0.34	0.72	0.69 ± 0.32
Baotou	-	-	-	-	Bugt	0.86	0.86 ± 0.37	0.81	0.81 ± 0.33
Ongniud	-	-*	-	-*	Tulihe	0.85	0.79 ± 0.37	0.84	0.81 ± 0.38
Xin Barag L.	0.8	0.69 ± 0.53	0.55	-*	Xiaoer Gou	-	-	-	-

*identifies the weather stations where the KPSS Test is rejected but the linear trend was not significant

Contradictory results also refer to several stations where trends were not detected for PM-ET_o series but positive trends were detected with the temperature methods. These opposed trends were often of small magnitude and, when detected with the DTS approach, the linear trends had high uncertainty.

There are no cases where a trend was identified for $ET_{o\ PMT}$ and was not identified for $ET_{o\ HS}$. When significant trends were identified for the same $ET_{o\ PMT}$ and $ET_{o\ HS}$ time series the magnitude of the trend was larger for ET_o computed with HS with two exceptions, Bayan and Sonid, both having an arid climate (Table 4-7). Trends relative to PM-ET_o (Table 4-6) that agreed with those of $ET_{o\ PMT}$ and $ET_{o\ HS}$ were few and those relative to stations having sub-humid climates have PM-ET_o trends larger than those of $ET_{o\ PMT}$ and $ET_{o\ HS}$ (Table 4-7). Results indicated that trends of ET_o when it was estimated by the temperature methods were likely highly influenced by trends in temperature, mainly in case of HS equation because it was only a function of temperature while PMT uses estimates of shortwave radiation and actual vapor pressure, however temperature dependent.

Comparing ET_o trends relative to the temperature methods, those for $ET_{o\ PMT}$ showed less trend results contradicting those of PM-ET_o than $ET_{o\ HS}$, respectively two and five cases. In addition, less increasing trends were detected for $ET_{o\ PMT}$ when no significant trends were observed for PM-ET_o. Trends detected for $ET_{o\ HS}$ time series were larger than those identified for $ET_{o\ PMT}$ time series with one exception, Sonid (Table 4-7).
DTS identified more significant increasing trends for both $ET_{o\ PMT}$ and $ET_{o\ HS}$ than those identified with the MMK test (Table 4-7). All trends detected with MMK were also detected with the DTS methodology. When DTS was applied to the $ET_{o\ PMT}$ time series, the KPSS test identified 15 time series having a deterministic trend but whose slopes were not significantly different from zero (marked * in Table 4-7), which mostly refer to the PMT estimation method.

Results in Figure 4-9b, relative to $ET_{o\ PMT}$ time series, showed that the increasing trends generally followed those identified for PM-ET_o (Figure 4-9a) and mostly occurred in the eastern areas, where climate is sub-humid or semiarid. Increasing trends relative to the $ET_{o\ HS}$ time series were detected for most of Inner Mongolia, excepting the western regions where climate is hyper-arid (Figure 4-9c). Comparing the spatial patterns of the linear trends of $ET_{o\ PMT}$ and $ET_{o\ HS}$ with those of PM-ET_o (Figure 4-9) and considering the discussion above, it was clear that those relative to $ET_{o\ PMT}$ approach better those of

the PM-ET_o than those relative to $ET_{o\ HS}$. However, neither HS of PMT methods were able to reproduce the negative ET trends observed for many locations when ET was estimated with the PM-ET_o equation. This superiority results from the fact that, in addition to the consideration of solar radiation estimated from T_{max} and T_{min} used in both PMT and HS, the use of estimates of actual vapor pressure and wind speed in PMT improves the respective calculation and supports a better approach to the base physics of the PM-ET_o equation.

It may then be concluded that ET_o trends should not be assessed when ET_o is computed with temperature methods because these ones do not capture all climate features but are biased by the influence of temperature. Moreover, in case of the HS equation, because it does not consider wind speed effects, that bias is likely larger, particularly when the radiation adjustment coefficient k_{Rs} is not calibrated since its value is depending on local wind speed as reported above in section 4.3.2. Our conclusions are supported by McVicar et al. (2012) when they advocate that assessing evaporative demand trends requires consideration of all four primary weather variables - radiation, air temperature, wind speed and air humidity.

4.3.7 Annual trends of weather variables

Trends relative to the weather variables used to compute PM-ET_o - maximum and minimum temperature (T_{max} and T_{min}, °C), sunshine duration used as estimator of shortwave incoming radiation (SD, h), relative humidity (RH, %) and wind speed (WS, m s^{-1}) were performed using the DTS methodology. The resulting linear trends, computed after the KPSS test revealed a possibly non-null slope, are presented in Table 4-8.

The linear trends for T_{max} and T_{min} were significantly positive for all cases (Table 4-8 and Figure 4-10a) and b). T_{max} trends varied from 0.20 to 0.39 ^oC $decade^{-1}$ in the regions having hyper-arid and arid climates, from 0.15 to 0.38 ^oC $decade^{-1}$ in the semiarid area and range 0.20 to 38 ^oC $decade^{-1}$ in the sub-humid areas. Differently, T_{min} values ranged from 0.20 to 0.85 ^oC $decade^{-1}$ when the climate is arid and hyper-arid, from 0.09 to 0.66 ^oC $decade^{-1}$ in the semiarid region and from 0.17 to 0.70 ^oC $decade^{-1}$ when the climate is sub-humid. The effect of global warming was therefore well visible in all Inner Mongolia, particularly through the increase of the minimum temperature, which generally exceeded that of T_{max} (Table 4-8). The magnitude of trends could not be attributed to climate aridity since their ranges are not distinct among climates. However, that magnitude was likely influenced by the local station characteristics.

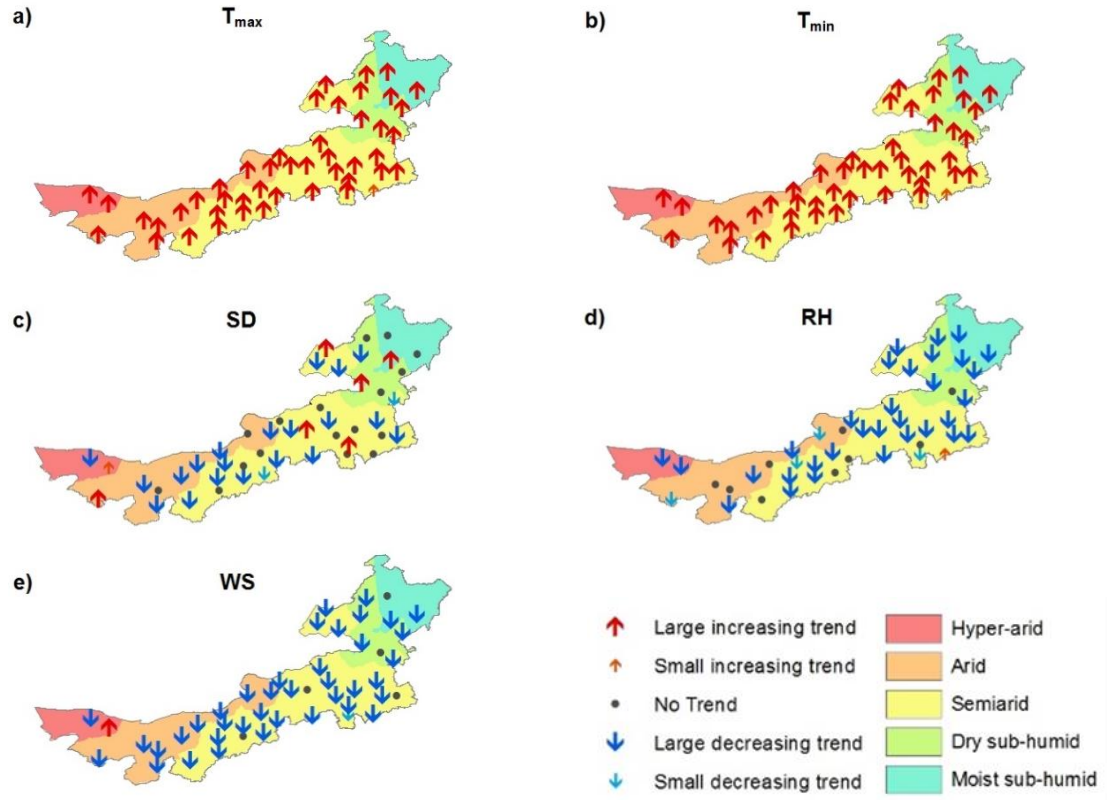

Figure 4-10 Spatial distribution of annual trends of the climatic variables in Inner Mongolia: a) maximum temperature (T_{max}), b) minimum temperature (T_{min}), c) sunshine duration (SD), d) relative humidity (RH) and e) wind speed (WS).

In line with large global warming detected in north hemisphere (IPCC 2014), significant trends for temperature rising in China have been reported by numerous authors, e.g., (Wang and Gaffen 2001), Cong et al. (2009) and Yin et al. (2010) for the entire China, Liu et al. (2010) and Wang et al. (2012) for the Yellow River Basin, Huo et al. (2013) for the arid north-western area. Some authors as Liu and Zhang (2013) referred that the influence of temperature rising was overcoming the influence of other weather variables and changing the ET_o trend signal from negative to positive in the last decade.

The sunshine duration trends were significantly negative for most locations (Table 4-8 and Figure. 4.10c). Most SD trends detected in the semiarid region were negative, ranging -0.05 to -0.24 h decade^{-1}. In more arid areas, SD trends were also predominantly negative. Differently, for the stations located in sub-humid areas SD trends were not significant or were positive but small (0.08-0.09 h decade^{-1}). The spatial distribution did not reveal any special pattern (Figure 4.10c). Likely, the characteristics of local weather stations, including those of the measuring equipment used, may have influenced the cases where trends are contradictory in neighboring locations.

Table 4-8 Linear trends of the weather variables maximum and minimum temperature (T_{max} and T_{min}, ^{o}C $decade^{-1}$), solar duration (SD, h $decade^{-1}$), relative humidity (RH, % $decade^{-1}$) and wind speed (WS, m s^{-1} $decade^{-1}$). The confidence level of 95% was assumed.

Station	Deterministic trend					Station	Deterministic trend				
	T_{max}	T_{min}	SD	RH	WS		T_{max}	T_{min}	SD	RH	WS
Hyper-arid						**Semiarid**					
Ejin	0.27	0.72	-0.08	-0.76	-0.27	Manzhouli	0.24	0.36	0.19	-0.86	-0.09
Guaizi	0.20	0.69	0.05	-0.69	0.09	Tongliao	0.18	0.42	-0.07	-0.91	-
Arid						Dongsheng	0.28	0.66	-*	-1.25	-0.23
Jartai	0.24	0.33	-*	-	-0.19	Chifeng	0.20	0.35	-*	-0.44	-0.05
Bayan knoll	0.29	0.20	-0.07	-	-0.14	Jarud	0.24	0.55	-0.12	-1.39	-0.31
Alxa R.	0.20	0.52	0.18	-0.61	-0.34	Xi Ujimqin	0.28	0.35	-0.06	-0.76	-0.27
Erenhot	0.28	0.63	-*	-0.55	-0.17	Jining	0.26	0.53	-0.05	-	-0.39
Linhe	0.30	0.85	-0.07	-1.64	-0.27	Bairin	0.21	0.51	-*	-1.11	-0.10
Mandula	0.19	0.51	-0.06	-0.74	-0.22	BaoGuotu	0.15	0.09	-*	0.40	-0.36
Sonid	0.39	0.27	-0.06	-	-0.11	Linxi	0.25	0.28	-*	-0.83	-0.11
Zhurihe	0.23	0.52	-*	-0.93	-0.15	Hohhot	0.29	0.66	-0.20	-1.58	-
Alxa L.	0.23	0.64	-0.06	-1.36	-0.13	Siziwangqi	0.30	0.50	-*	-0.99	-0.46
Urat	0.22	0.76	-0.07	-	-0.11	Duolun	0.25	0.46	-0.13	-0.90	-0.08
Semiarid						Huade	0.21	0.57	-0.09	-	-0.31
Damao	0.29	0.58	-0.17	-0.61	-0.32	Ulanhot	0.21	0.62	-*	-1.31	-0.16
Naranbulag	0.38	0.59	-*	-1.19	-0.11	Hailar	0.24	0.61	-0.19	-1.07	-0.11
Otog	0.19	0.52	-0.17	-	-0.20	**Dry sub-humid**					
XilinHot	0.27	0.53	0.07	-1.01	-	Sauron	0.19	0.35	-*	-	-
XinBarag R.	0.24	0.39	-0.10	-1.27	-0.39	EjiGuna	0.35	0.38	-*	-0.97	-0.19
Dong Ujimqin	0.30	0.58	-*	-1.02	-0.23	Zhalantun	0.25	0.55	-*	-1.14	-0.17
Kailu	0.21	0.41	-*	-0.96	-0.15	**Moist sub-humid**					
Abag	0.32	0.60	-0.10	-1.14	-0.12	Arxan	0.30	0.34	0.09	-1.03	-0.09
Baotou	0.27	0.55	-0.17	-0.78	-0.33	Bugt	0.29	0.17	0.08	-0.86	-0.04
Ongniud	0.20	0.30	0.08	-	-0.11	Tulihe	0.38	0.25	-*	-0.89	-
Xin Barag L.	0.22	0.45	-0.24	-0.91	-0.43	Xiaoer Gou	0.20	0.70	-*	-0.98	-0.11

* identifies the stations where the KPSS test is not rejected but the slope is not significant.

Che et al. (2005), relative to China as a whole, reported that over the second half of the 20th century, there have been significant decreases in global radiation, direct radiation and relative sunshine duration. These authors assumed that increased aerosol loadings

contributed for those observed decreases in R_s. Differently, Qian et al. (2006) referred to the contradictory decrease in cloud cover and the decrease in radiation observed throughout China, then assuming this could be the consequence of air pollution. Liang and Xia (2005) reported a decrease in solar radiation and sunshine duration over China; however, relative to the northern and northeastern part of China (Inner Mongolia) their study has shown that most SD trends were negative but that a few locations presented trends for increased SD. The analysis by Shi et al. (2008), after a detailed analysis on data quality, confirmed negative trends in R_s however with a trend inversion after 1990. These authors also accepted the hypothesis of increase in aerosols as a cause for that decline in R_s. Tang et al. (2011b) also referred a possible inversion of R_s trends, from negative to positive, for several weather stations during the last two decades. Their results refer to a majority of negative trends in Inner Mongolia for the last decades. The assumed influence of aerosols loading is well discussed by Streets et al. (2006) and Norris and Wild (2009). In agreement with the study by Tang et al. (2011b), it may be concluded that there is uncertainty in the detection of R_s and SD trends due to quality of available data and to methodologies used for trend analysis; however, it is likely that an overall trend for SD and R_s decrease characterizes climate in Inner Mongolia although with variation.

Trends of relative humidity were always negative when the KPSS trend analysis detected a trend, however with an opposed result for Bao Guotu, where a positive but small trend of 0.40% decade^{-1} was found (Table 4-8 and Figure 4-10d). RH trends varied from -0.86 to -1.14% decade^{-1} for the stations located in sub-humid climates, from -0.76 to -1.58% decade^{-1} in the semiarid areas and from -0.55 to -1.64% decade^{-1} in the areas having hyper-arid and arid climates. Small and large trends were spread through the Inner Mongolia but larger RH decreasing trends occurred in areas marked by aridity.

Wang and Gaffen (2001) analysed trends for air humidity for China as a whole. For the Inner Mongolia area they mostly found increasing trends for specific humidity, but decreasing trends for relative humidity, due to global warming, however detecting positive trends of RH spread throughout the Province. The global analysis on air humidity by Dai (2006) pointed out large positive and statistically significant RH trends over western China and that these RH increases resulted from large specific humidity increases that exceeded those in saturation humidity associated with moderate warming. Results were different for northeastern China where warming is important, which may justify why negative RH trends were found in this study. In the western arid area, our trend results

contradicted those of other authors, e.g., Huo et al. (2013) referred to a significant increase of RH in the arid NW region. However, in the middle Yellow River basin, in the central semiarid Inner Mongolia, a decreasing RH is reported by Liu et al. (2010) and both decreasing and increasing trends were referred by Wang et al. (2012). Zhang et al. (2011b) reported a majority of cases where decreasing trends were detected in the entire Province; nevertheless, increasing trends were detected for various locations spread over the whole area.

Trends for wind speed are all negative with exception of Guaizi, where a small positive trend of 0.09 m s^{-1} $decade^{-1}$ was detected. Smaller trends referred to sub-humid climates, where WS trends range from -0.04 to -0.19 m s^{-1} $decade^{-1}$, and larger trends were detected for the semiarid areas, varying from -0.09 to -0.43 m s^{-1} $decade^{-1}$.

McVicar et al. (2012) reported that declining rates of observed near-surface WS, which they called terrestrial stilling, is widespread across the globe and contributed to declining rates of evaporative demand. Their review included a number of Chinese studies that highlighted the contribution of terrestrial stilling to decreasing trends of ET_o. Various authors reported on WS decrease interesting Inner Mongolia, e.g., Huo et al. (2013) relative to the arid western areas, (Liu et al. 2010, 2013b) and Wang et al. (2012) for the Yellow River basin, in the center-western area, Zhang et al. (2011b) relative to the whole Inner Mongolia. The study by Guo et al. (2011) relative to the whole country allowed to perceive a generalized trend for WS decrease in Inner Mongolia, with larger trends for the semiarid areas like the one relative to the Yellow River basin. Meanwhile, Liu and Zhang (2013) reported an inversion of the WS decrease in recent decades in NW China, which included the most arid areas of Inner Mongolia and a consequence trend for ET_o to increase, which was not detected but for the Guaizi station in the current study.

The relationships among trends of PM-ET_o and trends of the weather variables are not easy to interpret and define. The increasing trends of PM-ET_o in the eastern areas, mainly in the sub-humid ones, corresponded to large positive trends of T_{max} (and T_{min}) combined with large decreasing trends of RH, thus with increased vapor pressure deficit. For several locations in this eastern area where ET_o trends were positive it was observed that the SD trends were either for increasing, do not exist or point for a small decrease, thus the contribution of a decreasing R_s was not enough to make ET_o to decrease. Moreover, the decreasing trends in WS were relatively small. It may be concluded that the increase in

ET_o in the eastern Inner Mongolia, mainly where the climate is sub-humid, are likely a consequence of climate change, particularly related to global warming.

In the western areas, clearly marked by aridity, trends for ET_o were mostly for decreasing, or no trends were detected. Warming was similar to other areas but the trends for RH decrease are often smaller than in the eastern areas. Trends for WS decrease are also more often larger than in the East while no clear differences were observable relative to the SD decrease. The combinations of such trends likely resulted in less frequent trends for ET_o to increase in the arid western Inner Mongolia.

4.3.8 Seasonal trends of ET_o

To understand the contribution of intra-annual changes on the long-term trends of ET_o in Inner Mongolia the DTS tests were applied to all the climatic variables and ET_o estimation procedures (PM-ET_o, PMT and HS) by creating four trimestral time series. Four seasons were considered: (a) December–January–February (DJF, winter), consisting of the cold and dry season, when air temperatures are very low, generally negative; (b) March-April-May (MAM, spring) corresponding to the transition from the cold winter to the hot summer; (c) June-July-August (JJA, summer) that consists of the warm and wet season; and (d) September-October-November (SON, fall), which corresponds to the transition from the summer to the cold and dry winter. ET_o showed increasing trends in spring (MAM) in the eastern areas (Figure 4-11), mainly those having sub-humid climates, but the majority of locations did not show trends. In the western area, no trends were detected except for Guaizi. In this season, the T_{max} increasing trends were often not high or are not detected mainly in the western area; however, T_{min} rises were detected for all locations (Figure 4-12). Opposing to annual results, no trends or small trends were detected for SD for most locations. Relative to RH, small trends for declining were identified for most locations, with no significant trends in the remaining stations. A decline in WS was quite often observed (Figure 4-12). These trends in weather variables, likely resulting from large impacts of global warming in the sub-humid areas, explain why ET_o was more often increasing in the eastern areas and no trends were detected in the central and western areas.

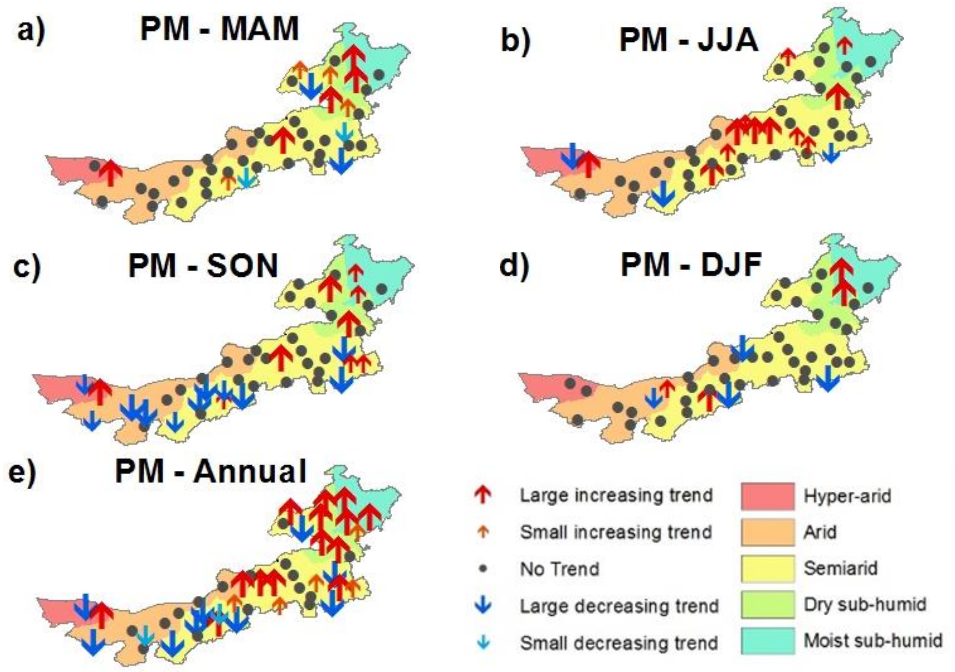

Figure 4-11 Spatial distribution of the seasonal trend analysis applied to PM-ET_o: a) MAM (March, April and May), b) JJA (June, July and August), c) SON (September, October and November), d) DJF (December, January and February) and e) annual.

In summer (JJA), trends for ET_o increase were mainly detected in the central semiarid areas and no trends or contradictory trends were detected in the eastern and western areas (Figure 4-11). Positive trends for T_{max} were now generalized, with smaller trends in the arid West (Figure 4-12). T_{min} increases were identified everywhere. Due to global warming influences, RH decreased for the majority of locations, without identification of trends mainly in the arid western area. Relative to SD, most locations did not show trends or trends were contradictory. WS decreased were identified in all areas but mixed with no trends. Positive trends for ET_o were therefore clearly a consequence of global warming in the central semiarid area.

In the fall season (SON) most ET_o trends were for declining in the arid central and western areas and for increase in the sub-humid eastern areas (Figure 4-11); several locations have shown no trends. Increasing trends of T_{max} were identified in all Inner Mongolia but with less significance in the East; differently, T_{min} increased everywhere with few exceptions (Figure 4-12). RH shows a negative trend everywhere but no trends were detected in the West. The majority of identified trends for SD were for decrease, mostly in the central area. Trends for WS were generally to decrease. Trends for ET_o were therefore compatible with the fact that temperature rises are often overcome by the decreases in SD and WS, which

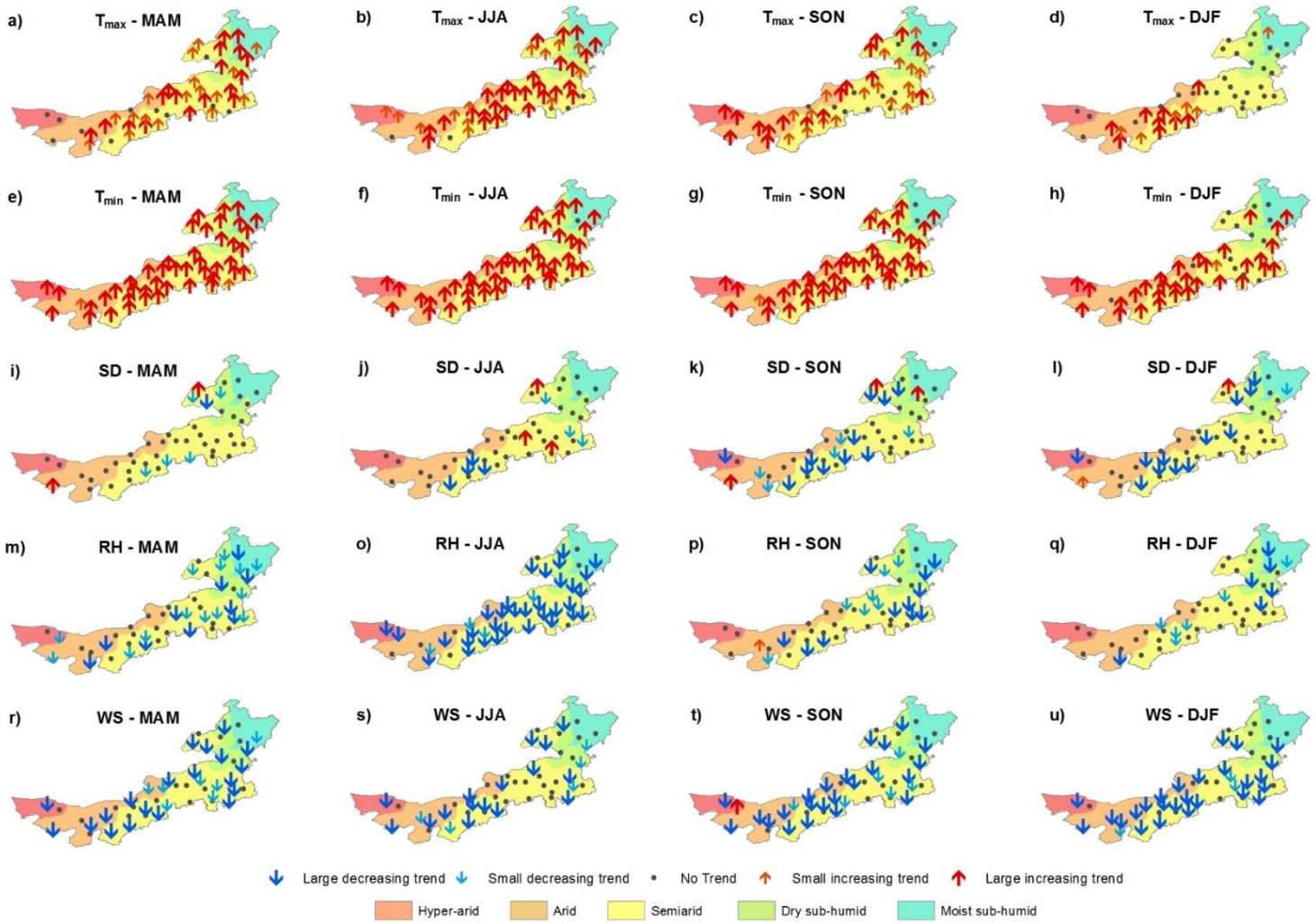

Figure 4-12 Spatial distribution of the trend analysis of seasonal climatic variables in Inner Mongolia

caused a decrease in ET_o mainly in the area extending between the arid and the dry sub-humid areas.

ET_o trends in winter were not clear (Figure 4-11). T_{max} showed to increase only in the central-western area without showing any trend in the East. T_{min} showed to increase for most locations but the northeastern area. SD showed to decrease in many locations but no trends were detected in most stations. A decrease in RH was identified mainly in the eastern areas while WS showed to decrease for most stations. The increase in ET_o in the East (Figure 4-11) is likely due to the combined effect of the T_{min} increase combined with the decrease of RH (Figure 4-12).

The results in this study were compatible with those of other studies applied to China (e.g., Zhang et al. 2011b) or to the middle Yellow River (Wang et al. 2012). However, in most studies the seasonality of trends were addressed through average values and not through spatially distributed values as it was used in the present study (e.g., Gao et al. 2006; Cong et al. 2009). In addition, different definitions of seasons were adopted (Liang et al. 2010; Zhang et al. 2011b).

4.4 Conclusions

The performance of HS and PMT temperature methods to estimate ET_o at a daily time scale was assessed for Inner Mongolia, covering a variety of climates, by comparing $ET_{o\ PMT}$ and $ET_{o\ HS}$ with PM-ET_o. Relative to the PMT method, good results were obtained when a correction of T_{min} was adopted to estimate T_{dew} in locations marked by aridity and using an empirical equation to calculate T_{dew} from T_{max} and T_{min} in moist sub-humid areas and locations with extremely low temperature. Impacts of strong wind speed in arid locations could be overcome by using a local or regional wind speed average instead of the common default value of 2 m s^{-1}. However, this approach did not decrease the estimation errors at all locations because other factors associated with high wind speed also contributed to high RMSE values, e.g., extreme temperatures, low relative humidity, and changes in the transparency of the atmosphere due to dust produced by wind erosion.

Results have shown that an appropriate calibration of the radiation adjustment coefficient (k_{Rs}) is essential for appropriately using both the PMT and HS methods. The k_{Rs} values calibrated for both temperature methods have shown to decrease from the hyper-arid to the moist sub-humid climates and were quite similar for both the HS and PMT methods. Because the HS equation does not include a wind speed term, it was observed that the

calibrated values for k_{Rs} were higher in windy locations, hence indicating that k_{Rs} played a main role in adjusting HS results for arid and windy locations.

The spatial patterns of PM-ET_o, $ET_{o\ PMT}$ and $ET_{o\ HS}$ were analyzed by applying PCA with R-Mode and Varimax rotation to the sets of 10 variables derived from the three ET_o estimation methods. The spatial pattern relative to PC1 identified nearly the same sub-regions with PM-ET_o, $ET_{o\ PMT}$ and $ET_{o\ HS}$ data sets, with the PC-scores variability close to that found for the aridity index. Differently, results for PC2 show that $ET_{o\ PMT}$ and $ET_{o\ HS}$ have a different behavior from that of PM-ET_o, thus indicating that it is not indifferent to use a full data set or only temperature data for computing ET_o.

It was observed that, comparing the $ET_{o\ PMT}$ and $ET_{o\ HS}$, $ET_{o\ PMT}$ was superior to $ET_{o\ HS}$ for most locations and throughout all climates. The advantages resulting from using the $ET_{o\ PMT}$ refer to obtain a smaller RMSE, to follow the conceptual approach of the PM-ET_o method and to have the possibility for replacing the missing variables by their alternative estimators while using all other observed variables. Further detailed studies are advisable for humid climates and for high elevation conditions.

The temporal analysis applied to the varied climates of Inner Mongolia led to conclude that ET_o trends are influenced by the aridity of the climate, with increased trends in sub-humid areas and decreasing trends in the areas highly marked by aridity. In the semiarid areas both positive and negative trends were observed, with increasing trends predominating in the western area, where aridity tends to be higher, and decreasing ones in the eastern one, close to the sub-humid areas. It was apparent that significant increases in temperature are often overcoming the influence of other meteorological factors and a direct relation between ET_o trends and aridity was not possible to fully assume. Results were compatible with most of those in literature.

Trends detected for ET_o computed with the PMT and HS temperature approaches were only positive, thus contradicting the trends detected for PM-ET_o. These results reflect a bias for trends estimation because $ET_{o\ PMT}$ and $ET_{o\ HS}$ were computed with only T_{max} and T_{min}. Nevertheless, the PMT approach revealed better than the HS equation because trends relative to $ET_{o\ PMT}$ time series led to much less contradictory trends relative to PM-ET_o comparatively to $ET_{o\ HS}$. However, the fact that the PMT and HS methods base upon temperature data only make them inappropriate to detect trends in ET_o when it is known that other variables, such as solar radiation and wind speed are main driving variables of PM-ET_o.

The relationships among trends of PM-ET_o and trends of the weather variables explain the spatial features of detected trends. The increasing trends of PM-ET_o in the eastern areas, mainly in the sub-humid ones, correspond to large positive trends of temperature combined with large decreasing trends of RH, thus with increased vapor pressure deficit. On the other hand, the the global warming impacts were not affected by the decreases in SD and WS. In the western areas, clearly marked by aridity, trends for ET_o were mostly for decreasing, or no trends were detected because trends for temperature and RH are insufficient to overcome the decreasing trends of SD and WS. The combinations of such behaviors likely resulted in less frequent trends for ET_o to increase in the arid western Inner Mongolia. The consideration of seasonality of trends in weather variables helped to explain the seasonal behavior of ET_o.

Chapter 5

Assessing montlhy and daily reference evapotranspiration estimation from reanalysis weather products.

DIOGO S MARTINS, PAULA PAREDES, TAYEB RAZIEI, CARLOS PIRES, JORGE CADIMA, AND LUIS S PEREIRA (2017) ASSESSING REFERENCE EVAPOTRANSPIRATION ESTIMATION FROM REANALYSIS WEATHER PRODUCTS. AN APPLICATION TO THE IBERIAN PENINSULA INTERNATIONAL JOURNAL OF CLIMATOLOGY 37 2378–2397

AND

PAULA PAREDES, DIOGO S MARTINS, LUIS S PEREIRA, JORGE CADIMA, AND CARLOS PIRES (2018) ACCURACY OF DAILY ESTIMATION OF GRASS REFERENCE EVAPOTRANSPIRATION USING ERA-INTERIM REANALYSIS PRODUCTS WITH ASSESSMENT OF ALTERNATIVE BIAS CORRECTION SCHEMES. AGRICULTURAL WATER MANAGEMENT 210:340-353

Assessing monthly and daily reference evapotranspiration estimation from reanalysis weather products.

Abstract. Computing crop reference evapotranspiration (ET_o) with the FAO Penman-Monteith method (PM-ET_o) requires maximum and minimum air temperature, shortwave radiation, relative air humidity and wind speed. These data are often not available, thus requiring alternative computation procedures. Although some proposed approximations may provide ET_o values with small estimation errors, the physics of the evapotranspiration processes may then not be well described. The use of reanalysis data, which is common in climate studies, represents an alternative to observation data for the weather variables referred above, when these are not available. The present study focus on the use of the National Center for Environmental Prediction/National Center for Atmospheric Research (NCEP/NCAR) blended reanalysis products with gridded data sets for the computation of PM-ET_o in the Iberian Peninsula considering that a monthly time-step was adopted. The PM-ET_o time series computed with the blended reanalysis data sets were compared with those obtained using observations for 130 weather stations in the Iberian Peninsula. Results showed that the PM-ET_o computed with blended reanalysis compared well with the series computed from observation data (average root mean square error, RMSE=0.49 mm d^{-1}). The weather variables derived from reanalysis were also compared with observation data. Results supported the quality of ET_o computations because, overall, there was a good match between solar radiation (average RMSE = 1.76 MJ m^2d^{-1}) and maximum temperature (average RMSE=1.48 ˚C) derived from reanalysis and *in situ* observations. By contrast, the wind speed from reanalysis highly over-estimated observations and this is likely a reason for the slight over-estimation of ET_o computed from reanalysis (percentage bias, PBIAS>20% in 89% of cases). In addition, the reanalysis products are apparently influenced by modelled warming, which contributes to over-estimation of the minimum temperature and, to a lesser extent, of the relative humidity. The spatial pattern of accuracy indicators revealed that poorer results corresponded to the southern and south-eastern coastal areas of Iberia, where climate is semi-arid. The compatibility of the PM-ET_o computed with monthly inputs and of the daily ET_o cumulated to the month, using the PM-ET_o equation was confirmed, thus allowing to extend conclusions of this study to daily computations. Alternative reanalysis products were also assessed. Tests for ERA-Interim reanalysis products revealed over-estimation of ET_o and those for NCEP/NCAR Reanalysis II have shown large under-

estimation. Results suggested that the blended reanalysis products are suitable for the estimation of ET_o in Iberia since they integrate an appropriate correction of radiation and temperature, which proved essential for the good estimation results obtained. ERA-Interim data products were also used to assess the accuracy of daily PM-ET_o and comparing 3 levels of bias-corrections approaches to adjust PM-ET_o to local conditions in Portugal using 24 weather stations: (i) an (uncorrected) PM-ET_o based on the individual weather variables for the nearest grid point to the weather station; (ii) the previously calculated PM-ET_o corrected for bias with a simple bias-correction rule based only on the nearest grid point; and (iii) the PM-ET_o corrected for bias with a more complex rule involving all grid points in a 100 km radius of the weather stations. Cross-validation was used to allow evaluating the uncertainties that are modelled independently of any forcing. Results showed that PM-ET_o from reanalysis, without bias correction, is strongly correlated with PM-ET_o (R^2>0.80) but tends to over-estimate PM-ET_o, with the slope of the regression forced to the origin $b_0 \geq 1.05$, a mean RMSE of 0.79 mm day^{-1}, and with EF generally above 0.70. Cross-validation results showed that using both bias correction methods improved the accuracy of estimations, in particular when a monthly aggregation was used. In addition, results showed that using the multiple regression correction method outperforms the additive bias correction leading to lower RMSE, with mean RMSE of 0.57 and 0.64 mm day^{-1} respectively.

Keywords: FAO Penman-Monteith ET_o; NCEP/NCAR reanalysis; ERA-Interim; accuracy indicators; statistical bias-corrections; cross-validation

5.1 Introduction

Evapotranspiration (ET) is a key variable in both the atmospheric and terrestrial branches of the hydrological cycle and plays a major role in quantifying the water balance at various scales, from the crop field to the hydrological basin. Knowledge of ET is essential in water resources management, for both natural and agricultural ecosystems, particularly for irrigation (Allen et al. 1998). There are various approaches for measuring and estimating ET at those scales, depending upon the available data and the goals (Pereira et al. 1999; H. J. Farahani et al. 2007; Allen et al. 2011; Glenn et al. 2011; Wang and Dickinson 2012; Liou and Kar 2014).

The Penman-Monteith equation (Monteith 1965) can be applied directly to estimate ET (one-step approach) when purposefully parameterized for the specific vegetation and environment conditions but requirements for parameterization may be challenging;

hence, the most common approach to estimating evapotranspiration from vegetation is adopting the two-step approach (K_c – ET_o), where a crop coefficient (K_c) for the considered vegetation multiplies the crop reference evapotranspiration (ET_o) to estimate crop (vegetation) evapotranspiration (Jensen 1968; Doorenbos and Pruitt 1977; Allen et al. 1998). As revised by Pereira et al. (2015), the use of the K_c – ET_o approach continues to be the most important in agricultural applications, both because it is less demanding for accurate use relative to the one-step method, and due to its accuracy, particularly when adopting the dual K_c approach (Allen et al. 2005; Allen and Pereira 2009; Rosa et al. 2012). In addition to agriculture, ET_o is used for other hydrologic purposes and in drought indices combining precipitation and evapotranspiration data (Dai 2011; Paulo et al. 2012; Vicente-Serrano et al. 2015).

The definition of reference evapotranspiration is traceable to Jensen et al. (1970). Doorenbos and Pruitt (1977) adopted grass as the reference crop. Later, FAO adopted the Penman-Monteith equation parameterized for cool season grass to describe ET_o that resulted in the standardized grass reference crop (ET_o) equation, generally referred to as the PM-ET_o equation (Allen et al. 1998). The PM-ET_o equation has become the reference ET_o equation (Pereira et al. 2015).

The computation of the PM-ET_o equation requires observation of various climate variables: solar radiation (R_s) or sunshine duration, air relative humidity (RH), maximum and minimum temperature (T_{max} and T_{min}) and wind speed at 2 m height (u_2). While T_{max} and T_{min} are reasonably well observed at most networks of weather stations in all countries, records of the other variables are usually only available for a limited number of stations, generally over short time spans and/or with many missing values. When observed, they are often expensive if meteorological services commercialize them. In addition to gaps in the data, the quality of observed data is often not appropriate for accurate calculations (Allen 1996).

The various problems with data availability led researchers to develop alternative ways of estimating ET_o or different approaches to obtaining data. Temperature based equations, such as the Hargreaves-Samani (HS) equation (Hargreaves and Samani 1985), and the adoption of alternative estimators of the parameters of the PM-ET_o equation using temperature data (Allen et al. 1998), often called the PMT approach, have been analyzed by many authors (Paredes et al., 2018a; Pereira et al. 2003; Popova et al. 2006; Jabloun and Sahli 2008; Trajkovic and Kolakovic 2009; Gocic and Trajkovic 2010; Todorovic et

al. 2013; Raziei and Pereira 2013b). Also, adopting temperature-based methods may lead to biased results due to the effects of global warming as analyzed in Chapter 4. However, most recent papers refer to a panoply of equations and do not consider the PMT approach (e.g., Tabari et al. 2013; Vicente-Serrano et al. 2014). Alternative approaches to compute ET_o include the use of artificial neural networks (ANNs), fuzzy and neuro-fuzzy systems, genetic algorithms, and multiple regression analyses (e.g., Partal 2009; Martí et al. 2011; Shiri et al. 2012; Cristea et al. 2013; Kisi and Cengiz 2013; El-Shafie et al. 2013). Nevertheless, there is no replacement for basic physics as represented in the PM-ET_o formulation, and the estimation of individual weather inputs to the PM equation has the merit of allowing an explicit review of the estimates and their accuracies prior to computations (Pereira et al. 2015). The issue of unavailability of observation data is often resolved by interpolating the values of surrounding observations, using gridded data, remote sensing or mesoscale model-based downscaled data sets (McVicar et al. 2007; Hart et al. 2009; De Bruin et al. 2010, 2012, 2016; Martí and Zarzo 2012; Raziei and Pereira 2013a; Srivastava et al. 2016). Nevertheless, applications of reanalysis products for the computation of ET_o are lacking, which will be dealt in this paper.

Global atmospheric reanalysis data sets can provide the required variables for ET_o estimation. However, reanalysis data may not be an adequate surrogate for weather data influencing hydrological processes as referred by Trenberth et al. (2014) who used reanalysis data for drought analysis but clearly identified the need for free access to observation data for more accurate drought analysis and global warming influences.

Several sources for global reanalysis products are available for ET_o estimation, in particular those from the European Centre for Medium-range Weather Forecasts, ECMWF, such as ERA-40 (Uppala et al. 2005) and ERA-Interim (Dee et al. 2011), and from the National Center for Environmental Prediction–National Center for Atmospheric Research, namely the NCEP/NCAR Reanalysis I (Kalnay et al. 1996) or the NCEP–DOE AMIP-II Reanalysis (Kanamitsu et al. 2002). The main advantages of the reanalysis products are their spatial and temporal consistency over 3 or more decades, the fact that several variables are available with free access to the data, and steadily improved model resolution and biases (Sheffield et al. 2006). Limitations are the coarse spatial resolution of the reanalysis products and the fact that their reliability seems to vary with the location, time period, and variables considered. Nevertheless, reanalysis products have already

been successfully used by many authors to represent the spatio-temporal variability of surface climate variables (Sheffield et al. 2004; Srivastava et al. 2013; Hwang et al. 2014).

Few studies focused on ET_o computation with reanalysis, comparing computed values with observed data. Generally, their use implied adopting downscaling models, e.g., Ishak et al. (2010) used the MM5 numerical weather model and (Srivastava et al. 2013, 2015) adopted the WRF mesoscale model for downscaling weather variables ERA-40, ERA-Interim and NCEP reanalysis products. Srivastava et al. (2014) used the WRF model coupled with the Noah Land Surface Model for rainfall-runoff modeling purposes and found that the ET_o derived from ECMWF compared well with the observed data sets. However, differently from the current study, these applications refer to a small catchment area and to a short time step computation approach.

Sheffield et al. (2006) used a combination of the NCEP/NCAR Reanalysis I with observation-based data sets, which resulted in a blended product that retains the consistency and continuity of the reanalysis but constrains it to the best available global observation data sets. This data set adjusts the short-term (daily and diurnal) variations to match observations where they are available and maintains interrelations between the variables (Sheffield et al. 2012). These reanalysis products were also used to assess spatial variation and temporal trends of drought over the globe using the Palmer Drought Severity Index, with ET computed from that data set (Sheffield et al., 2012).

The main objective of the present study is to assess the performance of the above referred reanalysis products, hereafter called blended reanalysis, in estimating monthly PM-ET_o for the Iberian Peninsula. This approach is innovative and necessary for computing the PM-ET_o equation in terms of estimating ET_o when full data sets are not available. The objective encompasses the quality assessment of estimating each reanalysis variable used to compute PM-ET_o by comparing the reanalysis and observed variables. A comprehensive set of statistical indicators was used to assess how monthly computed reanalysis weather variables and PM-ET_o compared to corresponding values of *in situ* observations. Moreover, two additional sections were added to this study: (1) to better understand the differences in ET_o between other reanalysis productions, with and without bias correction and (2) to evaluate the performance of computing daily ET_o, with reanalysis weather data relative to the PM-ET_o, to support irrigation management, while testing for efficient bias correction procedures.

5.2 Data

A global blended reanalysis data set of near-surface meteorological data for the period 1948-2008, with a spatial resolution of 0.5 degrees (Sheffield et al. 2006), was used to estimate PM-ET_o. This data set was selected because (1) it incorporates several corrections implemented to temperature and radiation data, which are key variables for estimating ET_o; (2) it spans more than 60 years of gridded global data, (3) it is available at different spatial resolutions (0.25^ox0.25^o, 0.5^ox0.5^o and 1.0^ox1.0^o), and (4) it is suitable for drought climate studies (Sheffield et al. 2012). The 0.5^ox0.5^o spatial resolution was used in the current study because the 291 grid-points available for the Iberian Peninsula, with that resolution to compare well with the 130 observed weather stations in Portugal and Spain (Figure 5-1).

The monthly time-scale was selected because the ET_o formulation for the monthly and the daily time steps is the same (Allen et al. 1994) with differences only in the computation of soil heat flux density (Allen et al. 1998). Moreover, this reanalysis application was mainly oriented to develop alternative approaches to accurately compute monthly ET_o for use in drought indices like the Palmer Drought Stress Index (PDSI) (Palmer 1965) and its modification for Mediterranean environments (Chapter 6). To better support this assertion, monthly ET_o estimated with monthly averaged values of the full set of variables (R_s, RH, u_2, T_{max} and T_{min}) were compared with the monthly totals of daily ET_o computed with the same variables. This comparison is presented in Section 5.3.

The blended reanalysis data set results from combining several global observation-based data sets with the NCEP/NCAR Reanalysis I (hereafter NCEP1). The blended reanalysis data set was corrected for biases in the precipitation and other near-surface meteorological variables (Sheffield et al. 2006) to avoid producing significant errors when estimating surface water balances and energy budgets. Such bias corrections were applied to the 3-hour time scale values of temperature and shortwave radiation so that their monthly mean were consistent with the monthly values of the observed data sets (Sheffield et al. 2006). Although no bias correction was considered for specific humidity, air pressure and wind speed, adjustments were made to the specific humidity and air pressure gridded data sets, to also make them consistent with the corrected temperature values (Sheffield et al. 2006).

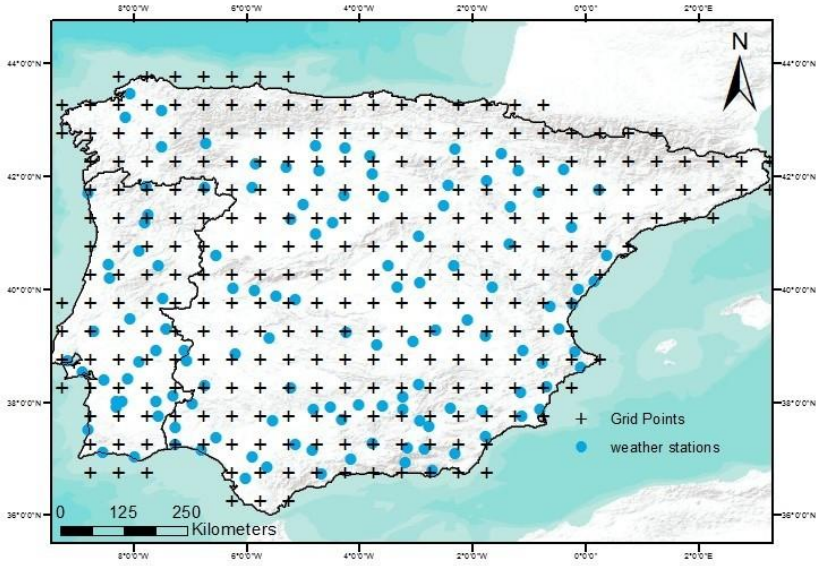

Figure 5-1 Spatial distribution of the reanalysis grid points (at each 0.5°) and the 130 Portuguese and Spanish weather stations over the Iberian Peninsula

Monthly means of T_{max} and T_{min} (K), wind speed (u_{10}, m s^{-1} at 10 m height) and R_s (W m^{-2}) were retrieved from the blended data set at a 0.5º x 0.5º spatial resolution for the Iberian Peninsula (Figure 5-1), available at http://hydrology.princeton.edu/. The retrieved u_{10} was adjusted for 2 m (u_2) using a logarithmic wind speed profile (Allen et al. 1998). Monthly reanalysis RH (%) values were estimated from daily blended reanalysis data sets relative to specific humidity (kg kg^{-1}), surface level pressure (kPa) and T_{max} and T_{min} with a spatial resolution of 1.0º x 1.0º degree. The use of this coarser resolution was due to inconsistencies in the downscaling of the specific humidity in the 0.5º x 0.5º grid. These RH values were then accumulated to the monthly time scale and downscaled to the 0.5º x 0.5º grid by ordinary kriging, in order to match the resolution of the other variables. The flow-chart of the procedure used to retrieve the reanalysis data and to compare them with observations is shown in Figure 5-2. That comparison is dealt with in Section 5.3.

To evaluate the performance of computations using the blended reanalysis data set, observation data of 130 Portuguese and Spanish weather stations, geographically distributed over Iberia (Figure 5-1), were used. The stations were selected based on the availability of all the weather variables required for estimating PM-ET_o. Data for 21 stations in Portugal was provided by the 'Instituto Português do Mar e da Atmosfera' (IPMA) relative to periods from 19 to 60 years, starting from 1948 to 1976 and ending between 1991 and 2008. For southern Portugal, data for 10 other stations were provided

by the ‘Centro Operativo e Tecnológico de Regadio’ but covering only 3 to 8 years and all ending by 2008. Data relative to the Spanish stations were provided by the ‘Sistema de Información Agroclimática para el Regadío’ for a time span of 3 to 10 years, in most cases starting in 2000 and ending in 2008.

The gridded reanalysis data sets do not coincide with the weather stations used for the evaluation (Figure 5-1). An interpolation applied to the gridded data set was therefore required. Ordinary kriging was used for the ET_o computed by reanalysis and to downscale RH from the 1^o x 1^o to the 0.5^o x 0.5^o grid. Ordinary kriging was selected because it was previously used to interpolate local temperatures and precipitation to regular gridded data sets applied to Spain and Portugal (Belo-Pereira et al. 2011; Herrera et al. 2012).

For each month (January to December) and every year, a variogram model was fitted. For each fit, four different variogram models were considered: exponential, spherical, Gaussian and power models. The most adequate variograms were selected by comparing the sum of squared errors associated with the fitted model. Then the selected variogram model was applied to predict the values of each weather variable at every weather station. The retrieval of the gridded data sets was done using the *ncdf* package (Pierce 2014) for the **R** programming language (R Core Team 2014) and the interpolation procedure was performed using the *gstat* package (Pebesma 2004).

Briefly speaking, the ET_o was obtained here from a three-step sequential algorithm: a) monthly averaging of inputs; b) calculation of ET_o from input data; c) kriging from reanalysis grid points to observation points (Figure 5-2). Any of the six possible step combination sequences of a), b) and c) would be possible, though not interchangeable.

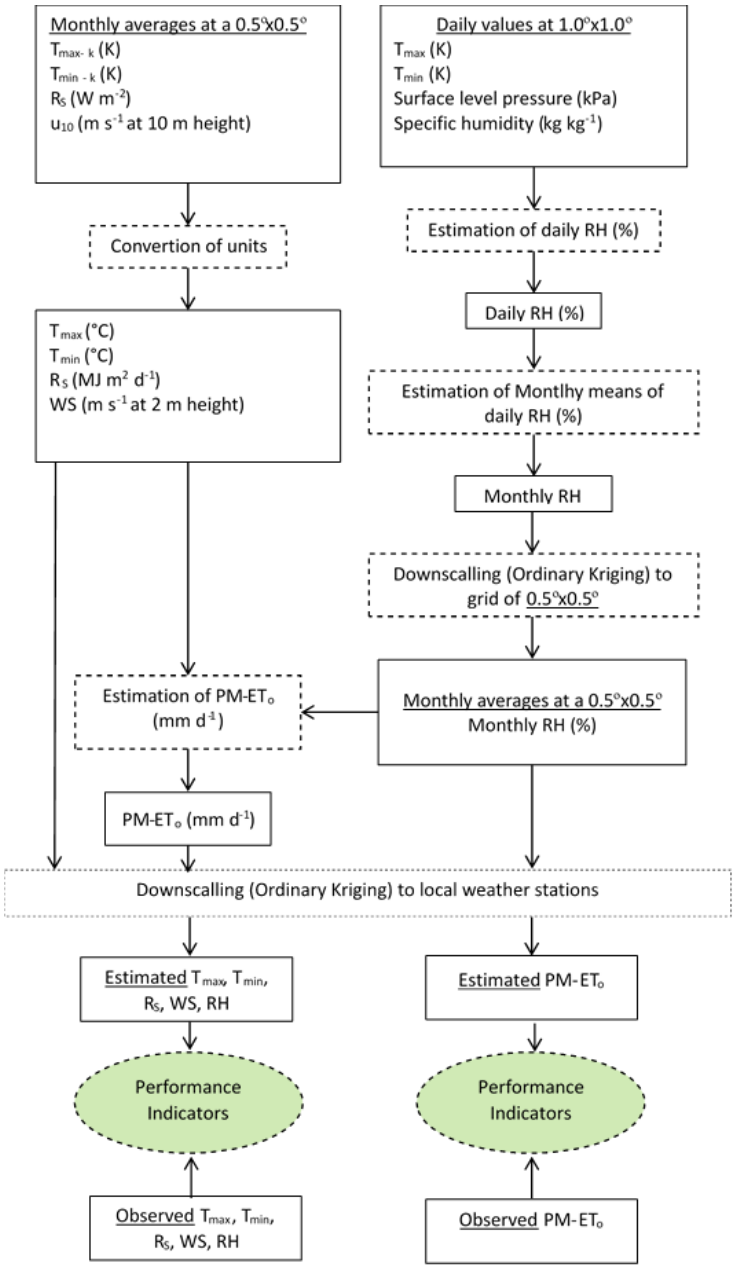

Figure 5-2 Flow chart of the procedure to estimate PM-ET_o from reanalysis data and comparing with observations.

5.3 Methods

5.3.1 Reference Evapotranspiration

The PM-ET_o equation describes grass reference evapotranspiration, i.e., the rate of evapotranspiration from a hypothetical crop with an assumed fixed height (12 cm), daily surface resistance (70 s m^{-1}) and albedo (0.23), approximately resembling the evapotranspiration from an extensive surface of a disease-free green grass cover of uniform height, actively growing, completely shading the ground, and with an adequate

water and nutrient supply (Allen et al. 1998). The PM-ET_o equation for the calculation of daily ET_o is:

$$ET_o = \frac{0.408\Delta(R_n - G) + \gamma_c \frac{900}{T+273} u_2 (e_s - e_a)}{\Delta + \gamma_c (1 + 0.34 u_2)} \quad (4.1)$$

where ET_o is the grass reference evapotranspiration (mm day^{-1}), R_n is the net radiation at the crop surface (MJ m^{-2} day^{-1}), G is soil heat flux density (MJ m^{-2} day^{-1}), T is the mean daily air temperature at 2 m height (°C), u_2 is wind speed at 2 m height (m s^{-1}), e_s is saturation vapor pressure (kPa), e_a is actual vapor pressure (kPa), e_s-e_a is vapour pressure deficit (kPa), Δ is the slope of the vapor pressure curve (kPa $°C^{-1}$), and γ_c is the psychrometric constant (kPa $°C^{-1}$).

The PM-ET_o equation (4.1) can be re-written as a function of the standard meteorological variables R_s, RH, T_{max}, T_{min} and u_2 see Allen et al. (1998) for details. To ensure the integrity of computations, the weather measurements should be made at 2 m (or converted to that height) above an extensive surface of green grass, shading the ground and not short of water. The parameters of equation (4.1) are preferably estimated from the observed climatic variables following the standard methods proposed by Allen et al. (1998). When the shortwave radiation R_s (MJ m^{-2} day^{-1}) is not measured, it can be estimated from the observed sunshine duration with the Angström (1924) equation:

$$R_s = \left(a_s + b_s \frac{n_s}{N_s}\right) R_a \quad (5.1)$$

where n_s is actual duration of sunshine (hour), N_s is maximum possible duration of sunshine or daylight hours (hour), R_a is the downwelling shortwave extraterrestrial radiation (MJ m^{-2} day^{-1}), a_s is the coefficient expressing the fraction of R_a reaching the earth on overcast days (n_s = 0), and a_s+b_s is the fraction of extraterrestrial radiation reaching the earth on clear sky days (n_s = N_s). The values a_s = 0.25 and b_s= 0.50 are recommended when these fractions are not calibrated (Allen et al. 1998; Azorin-Molina et al. 2015). Extraterrestrial radiation R_a and daylight hours N_s are computed for any given day as a function of the latitude of the site (Allen et al. 1998).

Vapor pressure deficit (VPD) was estimated as the difference between the saturation and the actual vapor pressure (e_s and e_a respectively). e_s is computed as the average of $e_s(T_{max})$ and $e_s(T_{min})$. When using mean relative humidity (RH_{mean}, %), the actual daily vapor pressure e_a is computed as Allen et al. (1998):

$$e_a = \frac{RH_{mean}}{100}\left[\frac{e_s(T_{min})+e_s(T_{max})}{2}\right] \quad (5.2)$$

In the present study, the PM-ET_o was estimated for all considered grid points over the area using full weather variables provided by the blended reanalysis. These equations (5.1 and 5.2) were used with observation data when R_s and e_a were not available.

5.3.2 Statistical assessment of reanalysis variables and ET_o

To evaluate the performance of the data sets in representing the amplitude and time variation of ET variable inputs and evapotranspiration, we compared reanalysis variables with observations over the Iberian Peninsula and the PM-ET_o series estimated using reanalysis variables with those computed from observations at all stations.

The comparison of a set of in situ observations O_i with a set of corresponding values P_i obtained by an alternative method has been addressed in numerous papers, among which Nash and Sutcliffe (1970), Legates and McCabe (1999) and (Moriasi et al. (2007) and, for the specific context of assessing the quality of ET_o computations, Todorovic et al. (2013 and Raziei and Pereira (2013b). Various statistical performance indicators have been suggested, as means of assessing the quality of the P_i estimates. In this study, seven indicators were used to measure the quality of M values based on reanalysis data (P_i) as estimates of the in situ (O_i) values. These indicators are defined below.

In an Ordinary Least Squares (OLS) regression of the ET_o values resulting from computations with reanalysis data ($y_i = P_i$) on ET_o values computed with observations ($x_i = O_i$) the fitted regression line has equation y=a+bx ($\hat{P} = a + bO$) with the regression coefficient (slope) given by:

$$b = Cov_{OP}/s_O^2 \quad (5.3)$$

and the intercept by $a = \overline{P} - b\overline{O}$, where Cov_{OP} is the covariance between the values O_i and P_i, s_O^2 is the variance of O_i, and $\overline{P}$ and $\overline{O}$ are the mean values of P_i and O_i. The overall quality of the regression line fit over the n available samples can be measured by the coefficient of determination, R^2:

$$R^2 = \frac{\sum_{i=1}^{n}(\widehat{P_i}-\overline{P})^2}{\sum_{i=1}^{n}(P_i-\overline{P})^2}. \quad (4.7)$$

Ideally, the fitted line would be $\hat{P}_i = O_i$, i.e. (b=1 and a=0) and R^2 would be equal to its maximum value of 1. But, as Legates and McCabe Jr. (1999) correctly point out, it is possible to have a very high value of R^2, but with a different regression line, so that a high value of R^2 is, in itself, insufficient to state that there is good overall agreement between observed and estimated values. Likewise, the interpretation of the parameters values a and b is not always straightforward. If b is very close to 1, a>0 indicates overestimation and a<0 indicates underestimation. Nevertheless, for regression coefficients b further from 1, the meaning of a is not always clear. Since the OLS regression line will always cross the sampling average $(\overline{O},\overline{P})$ of the scatterplot, b>1 suggests underestimation for smaller values of O_i but overestimation for larger O_i.

An alternative is to use a linear regression Forced To the Origin (FTO) (Eisenhauer 2003), with equation $y=b_0x$ between predicted (y) and observed (x) values. This model assumes proportionality between reanalysis-based and in situ values, the slope b_0 being the constant of proportionality. The regression coefficient (b_0) is now

$$b_0 = \frac{\sum_{i=1}^{M} O_i P_i}{\sum_{i=1}^{M} O_i^2}. \qquad (4.6)$$

The FTO regression line is less flexible than the OLS line as a model, since there is only a single free parameter; it is sensitive to additive changes of scale (such as those involved in converting from ^oF to ^oC); and it is forced to cross the origin, which may well be a convention, rather than an absolute reference point. Despite these important drawbacks, our experience indicates that the FTO slope b_0, being an overall constant of proportionality between the values, can often be better interpreted as a measure of bias than the OLS slope b, with $b_0>1$ suggesting overestimation and $b_0<1$ underestimation. The standard OLS regression line is also a proportionality model, but between the deviations of each set of values from their means rather than between the values themselves, since its equation can be re-written as $(y - \bar{y}) = b(x - \bar{x})$.

Other accuracy indicators used to compare the weather variables obtained from reanalysis (P_i) with observed data (O_i) are:

the Root Mean Square Error (RMSE)

$$\mathrm{RMSE} = \sqrt{\frac{\sum_{i=1}^{n}(O_i - P_i)^2}{n}} \qquad (4.8)$$

which has the same units as the variable under analysis. RMSE measures overall discrepancies between observed and estimated values and the smaller, the better.

The normalized RMSE (NRMSE) (Janssen and Heuberger 1995) that is defined as the ratio between RMSE and the mean of observations $\overline{O}$,

$$\mathrm{NRMSE} = \frac{\mathrm{RMSE}}{\overline{O}} \tag{5.4}$$

Since it is normalized, NRMSE is dimensionless, making it easier to compare its values for different variables.

The Percent Bias (PBIAS) (Gupta et al. 1999), which is a bias indicator that measures the average tendency of the simulated data to be larger or smaller than their corresponding observations. It is simply a normalized difference between the means of both sets of values:

$$\mathrm{PBIAS} = \frac{\sum_i^n (P_i - O_i)}{\sum_{i=1}^n O_i} \mathrm{x}\ 100\% = \frac{\overline{P} - \overline{O}}{\overline{O}} \mathrm{x}\ 100\% \tag{5.5}$$

PBIAS = 0 denotes a prediction with no mean bias. Positive values indicate an over-estimation bias, and negative values indicate an under-estimation bias.

The efficiency of modelling (EF) (Nash and Sutcliffe 1970) that provides an indication of the relative magnitude of the mean square error (MSE=RMSE^2) and the observed data variance (Legates and McCabe 1999):

$$\mathrm{EF} = 1 - \frac{\sum_{i=1}^n (O_i - P_i)^2}{\sum_{i=1}^n (O_i - \overline{O})^2} \tag{4.9}$$

i.e., compares "noise" with "information" (Moriasi et al. 2007). The maximum value EF = 1.0 can only be achieved if there is a perfect match between all observed (O_i) and predicted (P_i) values, a case in which RMSE=0, R^2=1 and both fitted regression lines have equation y=x. For values of EF close to 1, the "noise" is negligible relative to the "information", implying that reanalysis-based values of ET_o are a good reflection of the in situ values. Negative values of EF are possible, indicating that MSE is larger than the observed data variance. As Legates and McCabe Jr. (1999) correctly stressed, this means that it would be better to use the mean $\overline{O}$ of observed values, rather than the predicted values P_i.

The joint assessment of this set of indicators provides a good understanding of the quality of prediction of weather variables and ET_o when using the reanalysis based data. In addition, scatterplots and the regression lines between observations and reanalysis data were also analyzed for every variable set. In the following, the subscripts REAN and OBS are used to identify the variables and ET_o relative to, respectively, the reanalysis and observation data sets.

5.3.3 Montly vs. daily ET_o computations

Following Allen et al. (1998), the monthly ET_o (mm day $^{-1}$) was computed with Equation 4.1 using the monthly averages of the weather variables with G (MJ m^{-2} d^{-1}) estimated as G = 0.14 ($T_{month} - T_{previous\text{-}month}$). This results from the fact that the linearized version (first order Taylor expansion) of the PM-ET_o equation around the monthly values of wind, temperature, pressure, vapor pressure and shortwave radiation is quite accurate on a daily basis if the daily anomalies with respect to monthly-means are not extreme. This was assumed when developing the FAO-56 guidelines (Allen et al. 1994). To verify that assumption in the current study, ET_o computed using 30-day average weather data was compared with the daily ET_o cumulated to the month in 15 weather stations representing the range of climates of the Iberian Peninsula. Equation 4.1 was used for both scales. Results in Table 5-1 and Figure 5-3 support the above mentioned assumption. This assumption is made, although not explicitly, in studies relative to assessing alternative ET_o equations by comparing them with the FAO reference PM-ET_o using monthly computations (McVicar et al. 2007; Todorovic et al. 2013; Vicente-Serrano et al. 2014; Azorin-Molina et al. 2015). Results showed b_0 and b close to 1.0, R^2=1.0, RMSE close to 0.10 mm d^{-1}, very small PBIAS and EF=1.0.

Table 5-1 Performance indicators relative to the comparison between ET_o computed with monthly averages of the weather variables and daily ET_o cumulated to the month (both expressed in mm d^{-1}).

Weather Stations	Performance indicators*						
	b_0	b	a (mm d^{-1})	R^2	RMSE (mm d^{-1})	EF	PBIAS (%)
Vila Real	1.00	0.99	0.04	1.00	0.09	1.00	0.30
Bragança	1.01	1.00	0.02	1.00	0.10	1.00	0.80
Lerma	0.99	0.98	0.03	1.00	0.10	1.00	-0.20
Monte Julia	1.00	1.01	-0.03	1.00	0.11	1.00	0.20
Castelo Branco	1.01	1.00	0.03	1.00	0.11	1.00	0.80
Aldehuela del Jerte	0.99	0.99	0.02	1.00	0.11	1.00	-0.50
Puig	0.98	0.98	0.00	1.00	0.10	0.99	-1.50
Lisboa	1.00	0.99	0.04	1.00	0.08	1.00	0.50
Portalegre	1.00	0.99	0.10	1.00	0.13	1.00	1.10
Barajas de Melo	1.00	0.99	0.05	1.00	0.16	1.00	0.40
Chiclana de Segura	1.00	1.00	0.03	1.00	0.13	1.00	0.40
Altea	0.99	0.98	0.06	1.00	0.10	1.00	-0.40
Faro	1.00	0.99	0.06	1.00	0.09	1.00	0.40
Cabezas de S. Juan	1.00	1.00	0.03	1.00	0.10	1.00	0.50
Tabernas	1.00	0.99	0.01	1.00	0.10	1.00	-0.10

*described in section 5.3.2

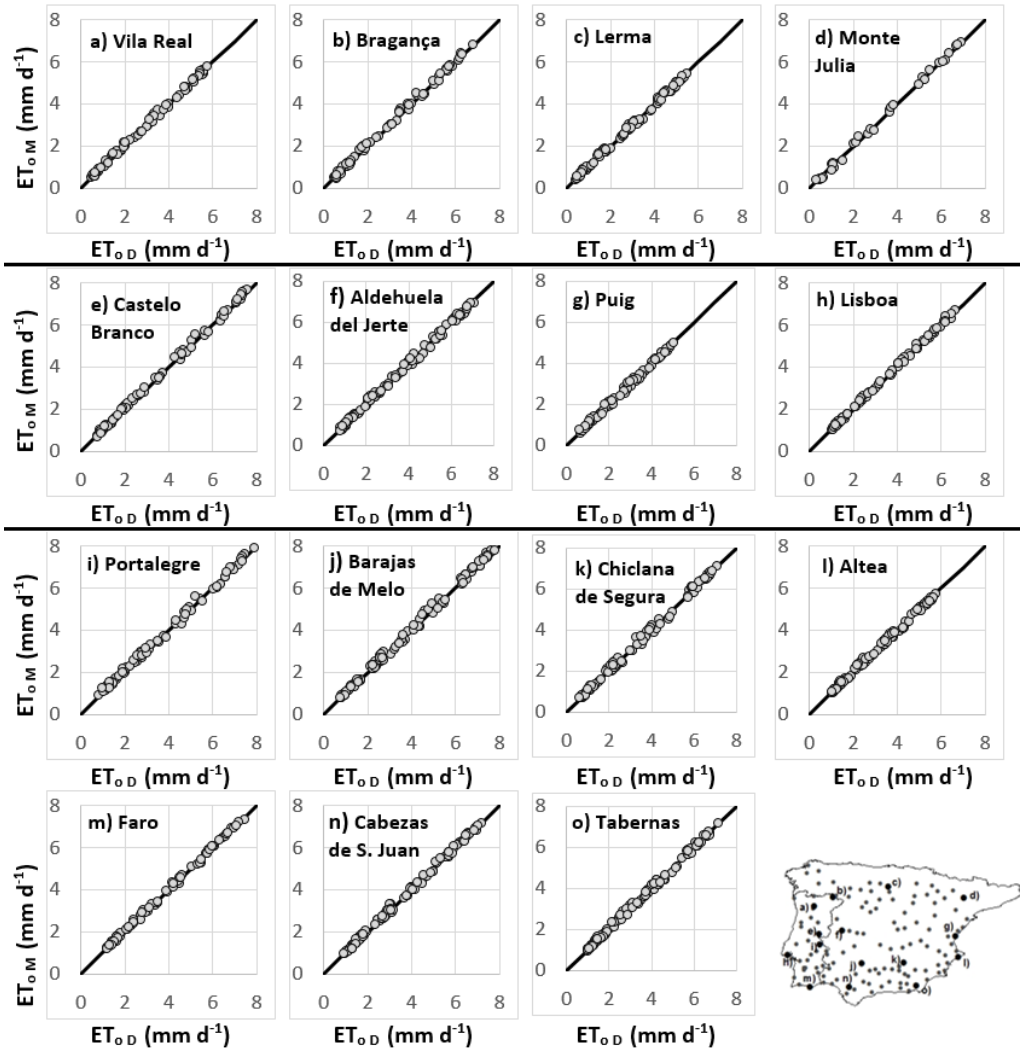

Figure 5-3 Examples of linear regressions between ET_o computed with monthly averages of the weather variables and daily ET_o cumulated to the month when computed with daily values of the same variables ($ET_{o\,D}$). The map identifies the locations of the selected weather stations.

5.4 Results and Discussion

5.4.1 Evaluating ET_o estimates using reanalysis products

The statistical indicators described in 5.3.2 were used to compare the PM-ET_o (Equation 4.1) derived from blended reanalysis products with those computed with weather variables observed at 130 weather stations across the Iberian Peninsula. In addition to comparisons focusing on the blended reanalysis products, other comparisons were also performed for 15 selected weather stations using the NCEP–DOE AMIP-II Reanalysis (NCEP2) and ERA-Interim aiming at a comparative assessment of the three sets of reanalysis products. Results are discussed in Section 5.4.4. Furthermore, the same set of

statistical indicators were used to assess the accuracy of daily ET_o using ERA-Interim reanalysis compared to 24 weather stations located in continental Portugal (Section 5.4.5)

Table 5-2 shows the frequency distributions (among the 130 cases) of the indicators. Results showed that indicators for ET_o were overall very good, i.e., the values of $ET_{o\ REAN}$ were generally close to $ET_{o\ OBS}$. R^2 values were very close to 1.0, with $R^2 > 0.90$ for all cases and $R^2 > 0.95$ for most (97%). In nearly 40% of sites, the OLS coefficient of regression, b, was in the interval 0.95-1.05 and for 70% of stations in the interval 0.85-1.15. However, 75% of the b values were greater than 1.0. The b_0 FTO slope behaved in a similar way to b (Table 5-2), with most b_0 values in the interval 0.95-1.15 and with the highest frequency in the interval 1.05-1.15.

Table 5-2 Frequency (%) distribution of the performance indicators comparing ET_o computed with reanalysis products with ET_o computed from observed weather data.

Intervals of R^2	(%)	Intervals of b	(%)	Intervals of b_0	(%)
]0.95, 1.00]	96.9	]1.30, [	0.0	]1.30, [	1.5
]0.90, 0.95]	3.1	]1.15, 1.30]	11.5	]1.15, 1.30]	20.0
]0.80, 0.90]	0.0	]1.05, 1.15]	32.3	]1.05, 1.15]	36.9
]0.70, 0.80]	0.0	]0.95, 1.05]	38.5	]0.95, 1.05]	33.1
]0.60, 0.70]	0.0	]0.85, 0.95]	13.9	]0.85, 0.95]	6.9
]0.50, 0.60]	0.0	]0.70 ,0.85]	3.0	]0.70 ,0.85]	0.8
[0.00, 0.50]	0.0	], 0.70]	0.8	], 0.70]	0.8
Intervals of PBIAS (%)	(%)	Intervals of RMSE (mm d^{-1})	(%)	Intervals of EF	(%)
],-20.0]	0.7	[0.00, 0.20]	0.0	] , 0.00]	0.0
]-20.0, -10.0]	0.8	]0.20, 0.35]	24.6	]0.00, 0.50]	0.0
]-10.0, -2.5]	8.5	]0.35, 0.50]	31.5	]0.50, 0.70]	3.9
]-2.5 0.0]	6.9	]0.50, 0.60]	13.8	]0.70, 0.80]	8.5
]0.0, 2.5]	10.8	]0.60, 0.75]	19.2	]0.80, 0.90]	21.4
]2.5, 10.0]	33.9	]0.75, 1.00]	6.3	]0.90, 0.95]	16.2
]10.0, 20.0]	29.2	]1.00, [	4.6	]0.95, 1.00]	50.0
]20.0, [	9.2				

R^2 is the coefficient of determination of the OLS regression; b is the regression coefficient of the OLS; b_0 is the regression coefficient of the FTO; PBIAS is the Percent Bias; RMSE is the Root Mean Square Error; EF is the efficiency of modelling

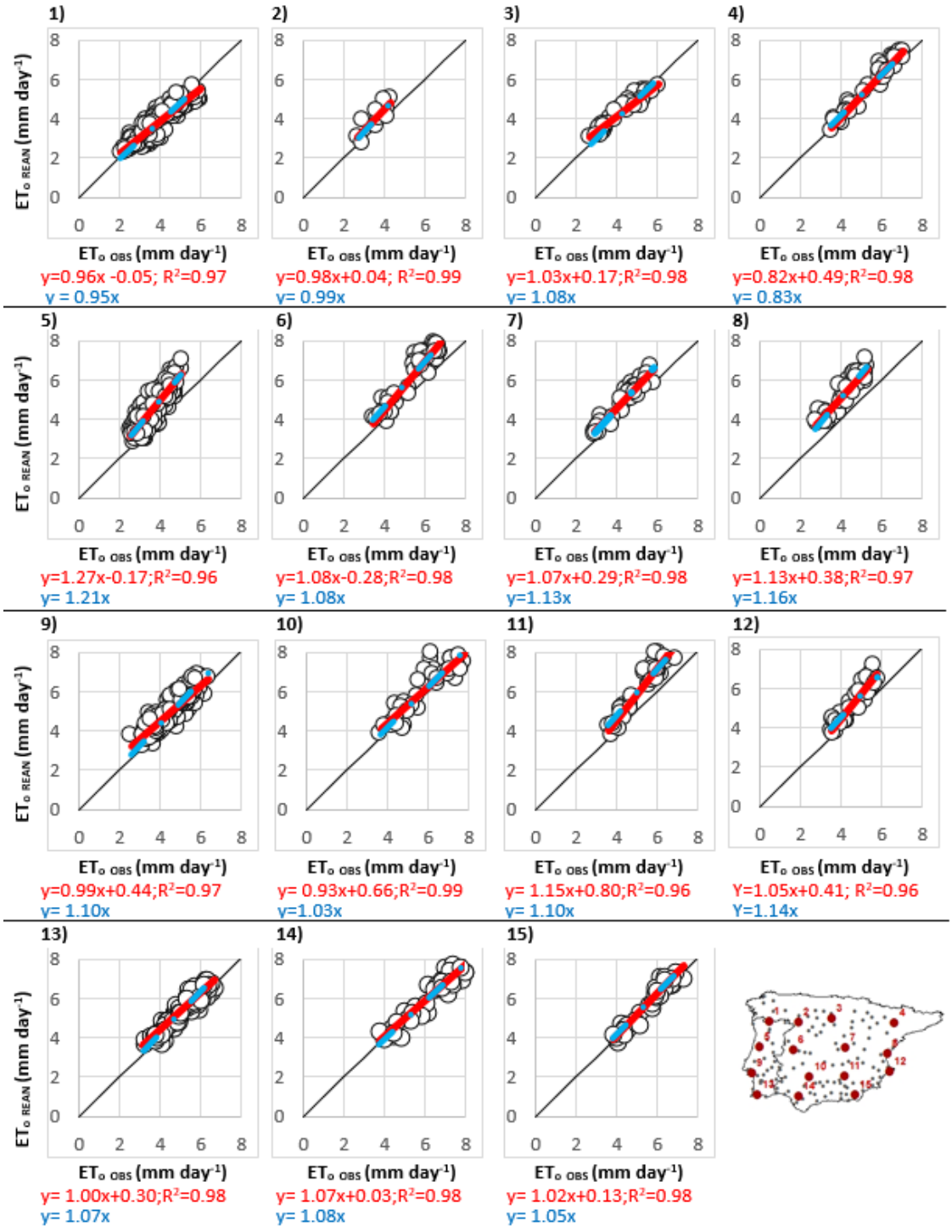

Figure 5-4 Examples of linear regressions of $ET_{o\ REAN}$ relative to $ET_{o\ OBS}$ using both the ordinary least squares and the regression forced to the origin. The map identifies the locations of the selected weather stations.

Figure 5-4 shows examples of scatter plots comparing $ET_{o\ REAN}$ with $ET_{o\ OBS}$ using both OLS and FTO regression lines. Weather stations were selected on four west to east transepts, covering the full range of conditions observed. Both OLS and FTO regression lines were very similar in most locations, thus confirming that b and b_0 behaved similarly.

In most cases, $ET_{o\ REAN}$ was slightly larger than $ET_{o\ OBS}$, with a 7% overestimation. Reflecting this, most PBIAS values are positive, with the highest frequency in the interval 2.5 to 10%.

RMSE estimation errors (Table 5-2) were generally small, with nearly 60% of the weather stations having RMSE<0.50 mm d^{-1} and nearly 50% with RMSE between 0.30 and 0.50 mm d^{-1}. Less than 20% of locations had RMSE > 0.70 mm d^{-1}. EF values were large, with almost 90% of the weather stations having EF > 0.80 and 50% of the locations with EF > 0.95. In addition, the smallest EF values were greater than 0.50. Thus, EF results indicated that the mean square errors were smaller or much smaller than the variance of ET_o obtained from observations, hence the "noise" was small. The referred accuracy indicators suggest that the use of reanalysis data to overcome the lack of observation data for computing ET_o is encouraging.

The spatial variability of the statistical indicators over the Peninsula (Figure 5-5) shows that large R^2 values covered Iberia well, with lower values in the eastern part of inland Spain. The distribution of b and b_0 values were similar. Larger b and b_0 values, indicating larger over-estimation of $ET_{o\ REAN}$ relative to $ET_{o\ OBS}$ occurred in regions close to, or not far from, the coast in southern and south-eastern parts of Iberia; by contrast, b_0 values indicating less over-estimation or even under-estimation were scattered in the inland and northern areas of the Peninsula. However, the scattering of b and b_0 values likely denotes differences in observation data sets, which have different sources and lengths. The larger positive PBIAS values correspond to the coastal areas, so that the distribution of PBIAS values was coherent with that of the regression coefficient b_0. There were better results for RMSE in the northern and inland areas, where $ET_{o\ REAN}$ slightly over-estimated $ET_{o\ OBS}$. Larger RMSE were obtained in the southern coastal area of Andalusia. EF results follow a spatial distribution similar to the bias indicators, with best results in inland and northern areas and poorer ones in southern and south-eastern coastal areas.

Limited information is available on the use of reanalysis data for ET_o computations. The studies for the Brue catchment (Ishak et al. 2010; Srivastava et al. 2013, 2014, 2016) used different sources and various models to downscale reanalysis data and focused on spatial and time scales much smaller than those in the current study; mainly they used hourly data and aimed at supporting catchment hydrologic modelling. Those studies inspired the current one but the enormous differences in spatial and time scales make it inappropriate to compare the quality of both applications.

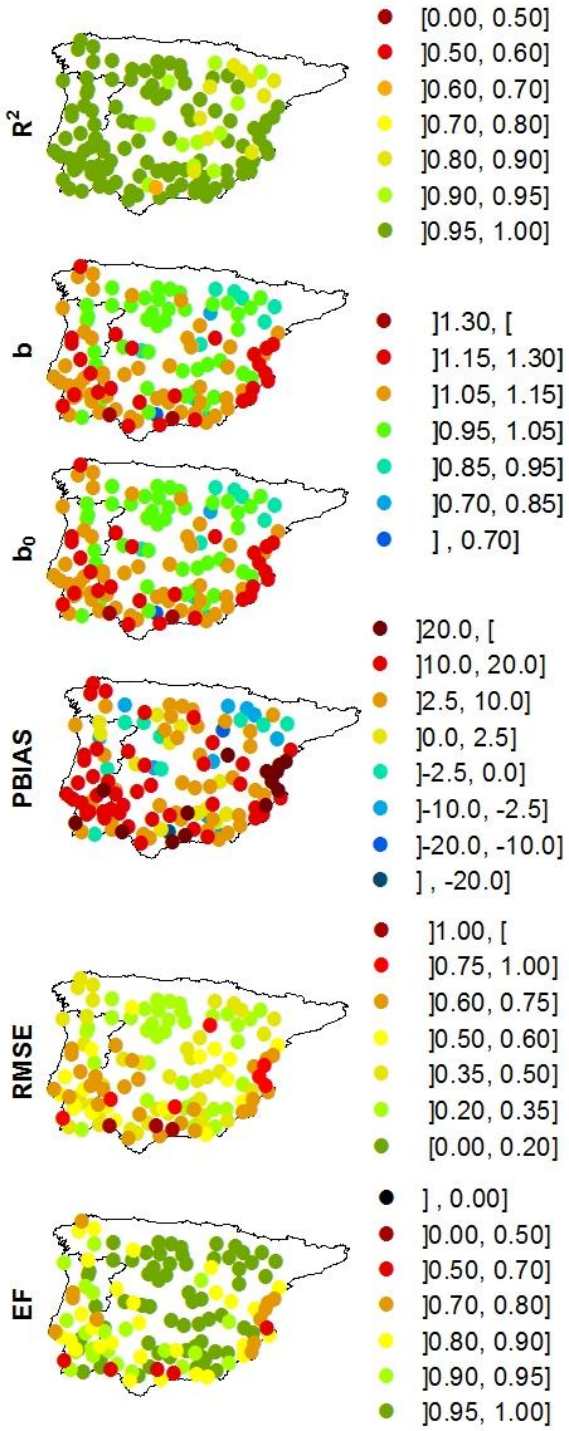

Figure 5-5 Spatial distribution of the statistical indicators measuring the performance of ET_o estimation with blended reanalysis data sets.

These are a few studies for Portugal and Spain relative to the use of alternative methods to compute ET_o when available data are limited to temperature. Gavilán et al. (2006) compared daily HS with PM-ET_o in Andalusia, Spain, and found RMSE ranging from 0.39 to 1.22 mm d^{-1}. For the same region, López-Urrea et al. (2006) reported an average RMSE of 0.9 mm d^{-1} when using HS, but with a strong over-estimation trend. As reported

by Todorovic et al. (2013) for the Mediterranean region, the HS equation produced an average RMSE of 0.57 mm d^{-1} while PMT led to averages of 0.36 mm d^{-1} in humid climates and 0.49 mm d^{-1} in dry sub-humid climates. Results in Table 5-2 indicate RMSE values that are generally smaller than those reported. The study by Vicente-Serrano et al. (2014) relative to Spain, which does not include RMSE, showed worse R^2 results than those in this study, but a similar spatial distribution of R^2. For Portugal, using the PMT approach with calibrated radiation coefficients, Paredes and Rodrigues (2010) found RMSE averages varying from 0.47 to 0.87 mm d^{-1} while in the current study RMSE ranged from 0.27 to 0.70 mm d^{-1} for the same locations, thus indicating a better accuracy of the reanalysis ET_o computations.

Other alternatives to estimate ET_o refer to the use of remote sensed data. Cruz-Blanco et al. (2015) used radiation data from the Land Surface Analysis - Satellite Applications Facility combined with forecast data of ECMWF (LAS SAF/ECMWF) in Andalusia, southern Spain. They reported RMSE averaging 0.69 mm d^{-1} in a range of 0.43 to 1.04 mm d^{-1}. That average was smaller, 0.50 mm d^{-1}, when observations were used instead of ECMWF data Cruz-Blanco et al. (2014). In the present study, RMSE for the Andalusia region ranged from 0.22 to 1.00 mm d^{-1}, with an average value of 0.55 mm d^{-1}, thus showing that reanalysis provides for similar or better ET_o results. Using artificial neural networks (ANN) to estimate ET_o for the Basque region, northern Spain, Landeras et al. (2008) reported RMSE averages ranging 0.57 to 0.65 mm d^{-1} when computations were performed with temperature data only. For the same region, Shiri et al. (2012) reported RMSE averages from 0.53 to 0.78 mm d^{-1} when using gene expressing programming with only T_{max} and T_{min}, and from 0.49 to 0.65 mm d^{-1} when estimations were performed with a neuro fuzzy model, also with T_{max} and T_{min} only. In a later study, Shiri et al. (2013) reported a wider range for non-humid locations than for humid ones. In the present study, RMSE ranging 0.22 to 0.38 mm d^{-1} were obtained for the same region.

In conclusion, the estimation errors for $ET_{o\ REAN}$ (Table 5-2) were low, usually better or similar to ET_o values observed by other authors when using different methodologies. RMSE were higher in drier climates and smaller in more humid and higher elevation areas (Figure 5-5). Coastal areas also had relatively large RMSE and positive bias. Nevertheless, it is important to understand how the various climatic variables obtained as reanalysis products and downscaled to observations locations compare with *in situ*

observations, in order to possibly explain the observed over-estimation trend of $ET_{o\ REAN.}$ This issue was addressed in the subsequent sections.

Table 5-3 Frequency (%) distributions of the performance indicators for shortwave radiation (R_S), maximum temperature (T_{max}) and minimum temperature (T_{min}) when comparing reanalysis products with observed values

Intervals of R^2	(%)	Intervals of b	(%)	Intervals of b_0	(%)	Intervals of PBIAS (%)	(%)	Intervals of NRMSE	(%)	Intervals of EF	(%)
Short wave radiation											
]0.95, 1.00]	80.0	]1.30, [	0.0	]1.30, [	0.0	] , -20.0]	0.0	]0.50, 1.00]	0.0	] , 0.00]	0.0
]0.90, 0.95]	16.9	]1.15, 1.30]	0.0	]1.15, 1.30]	0.0	]-20.0, -10.0]	3.1	]0.30, 0.50]	0.0	]0.00, 0.50]	0.0
]0.80, 0.90]	1.5	]1.05, 1.15]	12.3	]1.05, 1.15]	13.8	]-10.0, -2.5]	43.1	]0.20, 0.30]	0.8	]0.50, 0.70]	0.8
]0.70, 0.80]	0.8	]0.95, 1.05]	49.3	]0.95, 1.05]	55.4	]-2.5, 0.0]	16.2	]0.15, 0.20]	7.7	]0.70, 0.80]	0.8
]0.60, 0.70]	0.8	]0.85, 0.95]	36.9	]0.85, 0.95]	30.8	]0.0, 2.5]	12.2	]0.10, 0.15]	46.9	]0.80, 0.90]	8.5
]0.50, 0.60]	0.0	]0.70, 0.85]	1.5	]0.70, 0.85]	0.0	]2.5, 10.0]	23.1	]0.05, 0.10]	43.8	]0.90, 0.95]	48.4
[0.00, 0.50]	0.0	] , 0.70]	0.0	] , 0.70]	0.0	]10.0, 20.0]	2.3	[0.00, 0.05]	0.8	]0.95, 1.00]	41.5
						]20.0, [	0.0				
Maximum temperature											
]0.95, 1.00]	96.2	]1.30, [	1.5	]1.30, [	0.8	],-20.0]	0.0	]0.50, 1.00]	0.8	] , 0.00]	0.8
]0.90, 0.95]	1.5	]1.15, 1.30]	3.1	]1.15, 1.30]	1.5	]-20.0, -10.0]	4.7	]0.30, 0.50]	0.0	]0.00, 0.50]	1.5
]0.80, 0.90]	2.3	]1.05, 1.15]	10.0	]1.05, 1.15]	12.3	]-10.0, -2.5]	17.8	]0.20, 0.30]	0.0	]0.50, 0.70]	0.8
]0.70, 0.80]	0.0	]0.95, 1.05]	51.5	]0.95, 1.05]	70.0	]-2.5, 0.0]	14.7	]0.15, 0.20]	5.4	]0.70, 0.80]	3.8
]0.60, 0.70]	0.0	]0.85, 0.95]	32.4	]0.85, 0.95]	13.9	]0.0, 2.5]	23.9	]0.10, 0.15]	7.7	]0.80, 0.90]	8.5
]0.50, 0.60]	0.0	]0.70 ,0.85]	1.5	]0.70 ,0.85]	1.5	]2.5, 10.0]	33.2	]0.05, 0.10]	49.2	]0.90, 0.95]	16.9
[0.00, 0.50]	0.0	], 0.70]	0.0	], 0.70]	0.0	]10.0, 20.0]	4.8	[0.00, 0.05]	36.9	]0.95, 1.00]	67.7
						]20.0, [	0.9				
Minimum temperature											
]0.95, 1.00]	79.2	]1.30, [	0.0	]1.30, [	9.2	] , -20.0]	0.8	]0.50, 1.00]	17.7	] , 0.00]	1.5
]0.90, 0.95]	16.9	]1.15, 1.30]	1.5	]1.15, 1.30]	35.4	]-20.0, -10.0]	3.8	]0.30, 0.50]	20.8	]0.00, 0.50]	14.6
]0.80, 0.90]	2.3	]1.05, 1.15]	6.2	]1.05, 1.15]	26.2	]-10.0, -2.5]	6.9	]0.20, 0.30]	13.9	]0.50, 0.70]	16.2
]0.70, 0.80]	0.8	]0.95, 1.05]	54.6	]0.95, 1.05]	20.0	]-2.5, 0.0]	1.5	]0.15, 0.20]	19.2	]0.70, 0.80]	14.6
]0.60, 0.70]	0.0	]0.85, 0.95]	36.2	]0.85, 0.95]	6.9	]0.0, 2.5]	5.4	]0.10, 0.15]	16.1	]0.80, 0.90]	14.7
]0.50, 0.60]	0.0	]0.70, 0.85]	0.0	]0.70, 0.85]	1.5	]2.5, 10.0]	13.1	]0.05, 0.10]	10.8	]0.90, 0.95]	16.9
[0.00, 0.50]	0.8	] , 0.70]	1.5	] , 0.70]	0.8	]10.0, 20.0]	20.0	[0.00, 0.05]	1.5	]0.95, 1.00]	21.5
						]20.0, [	48.5				

R^2 is the coefficient of determination of the OLS regression; b is the regression coefficient of the OLS; b_0 is the regression coefficient of the FTO; PBIAS is the Percent Bias; NRMSE is the Normalized Root Mean Square Error; EF is the efficiency of modelling

5.4.2 Evaluating the blended reanalysis variables shortwave radiation and temperature

Table 5-3 shows the frequency distributions of the statistical indicators for the weather variables R_s, T_{max} and T_{min}. Results showed that the reanalysis-based values were generally fairly close to the observed ones. To be noted that in Table 5-3, instead of RMSE used to assess $ET_{o\ REAN}$ estimation, the normalized NRMSE values were used since NRMSE is better suited for comparing the performance of the different variables.

Results for R_s revealed that R^2 were generally not far from the optimal value 1.0, with $R^2 > 0.95$ in 80% of cases and only some 3% of stations having $R^2 < 0.90$. These results suggest that the reanalysis data sets $R_{s\ REAN}$ reflect well the time variability of the observed R_s in the overwhelming of locations. The OLS coefficient of regression, b (Table 5-3), was in 49% of cases very close to 1.0, ranging 0.95 to 1.05. The next most frequent occurrence was that for the interval 0.85 to 0.95 (37%), which indicates a slight tendency for under-estimation. Furthermore, $R_{s\ REAN}$ results have shown that the FTO slope b_0 generally does not deviate much from 1.0, with 55% of values within the interval 0.95-1.05 and 31% in the interval 0.85 to 0.95. The examples presented in Figure 5-6, which refer to the same weather stations selected for the ET_o example in Figure 5-3, illustrate that b and b_0 slopes were similar, with a possible under-estimation trend, i.e., $R_{s\ REAN}$ was under-estimated relative to $R_{s\ OBS.}$ However, the estimation bias was small with 43% of cases having a PBIAS ranging -2.5 to -10% (Table 5-3) and 23% of cases with a positive PBIAS in the interval 2.5 to 10%. The magnitude of the estimation error was generally small, since NRMSE < 0.15 in 91.5% of cases. As with previous results, it was observed that EF was greater than 0.90 in 90% of stations with most values greater than 0.80. Thus, it can be concluded that excellent results for $R_{s\ REAN}$ contributed to the very good results obtained with $ET_{o\ REAN}$.

The coefficient of determination for $T_{max\ REAN}$ was also not far from the optimal value 1.0, with $R^2 > 0.95$ in 96% of the cases and only 2.3% of stations having $R^2 < 0.90$. The regression coefficient b had similar frequencies to those observed for R_s, with b usually close to 1.0 and in 52% of cases in the interval 0.95 to 1.05. The next most frequent class was that for the interval 0.85 to 0.95, indicating a slight tendency to under-estimate.

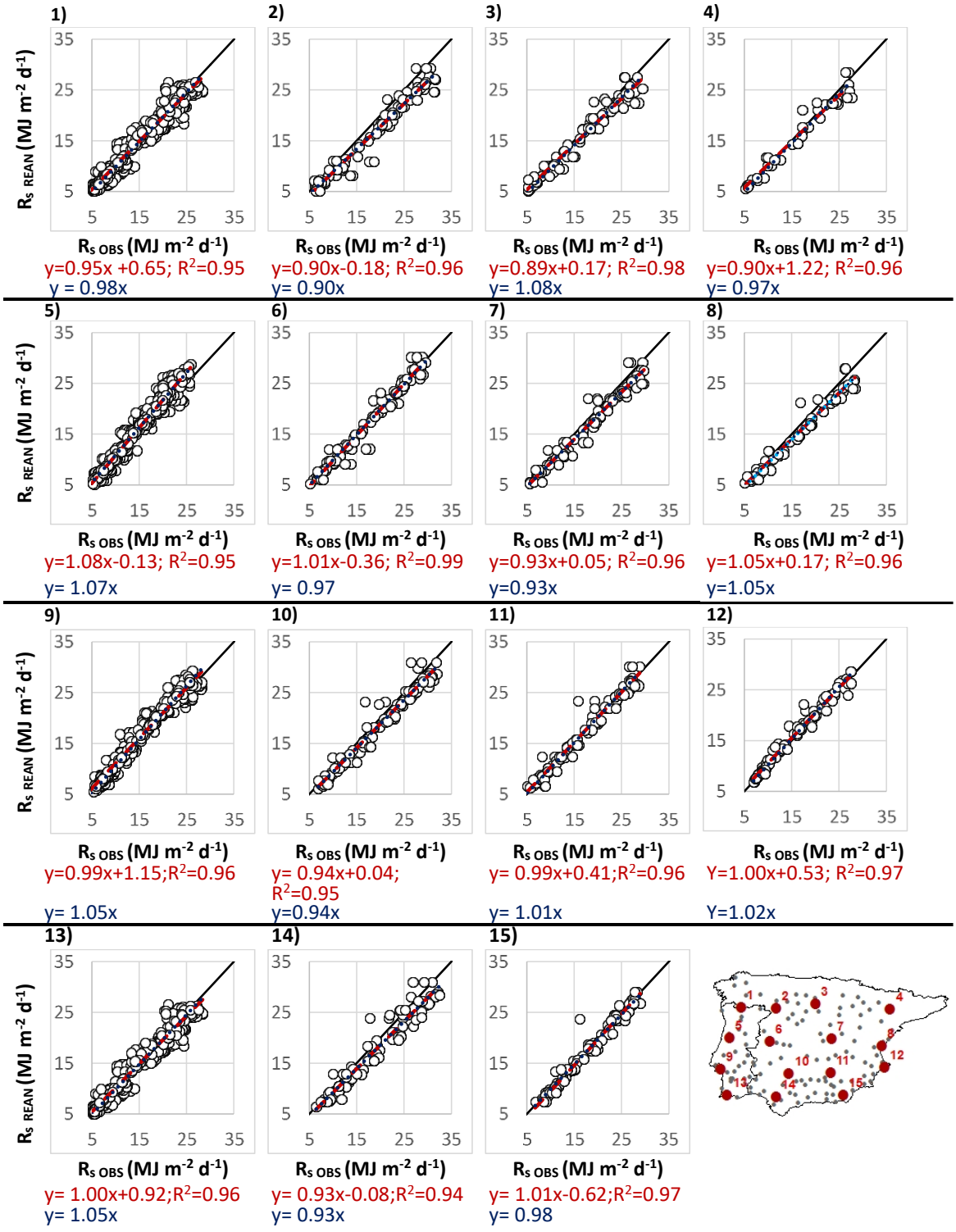

Figure 5-6 Examples of linear regressions of $R_{S\ REAN}$ over $R_{S\ OBS}$ using both the ordinary least squares and the regression forced to the origin. The map identifies the locations of the selected weather stations.

Results for T_{max}, in Table 5-3 showed that the slope b_0 generally did not deviate much from 1.0 with most values, 70%, within the interval 0.95-1.05. The frequency of cases

with b_0 between 0.85-0.95 or 1.05-1.15 was approximately the same, i.e., 14 and 12%. Consequently, the estimation of T_{max} had little bias with an average PBIAS of 1.2% and only 10% of cases with PBIAS > 10% or PBIAS < -10%. The magnitude of the estimation error is quite small, with NRMSE < 0.10 in nearly 86% of stations and NRMSE < 0.20 in 99% of cases. EF results were very good, higher than 0.95 for 68% of the locations and larger than 0.80 in 93% of cases.

R^2 for the OLS regression of $T_{min\ REAN}$ vs. $T_{min\ OBS}$ (Table 5-3) was greater than 0.95 in 79% of cases, with less than 4% of stations having $R^2 < 0.90$. As for the variables analyzed before, those high R^2 values suggest that reanalysis products follow well the time variability of observations. The distribution pattern of b values was similar to that for T_{max}. Differently, for b_0 the majority of stations show an over-estimation of T_{min} with only 20% of cases having b_0 values between 0.95 and 1.05. This over-estimation was well identified by the values of PBIAS, with 68.5% of cases with PBIAS > 10% and almost 50% with PBIAS larger than 20%. The errors associated with $T_{min\ REAN}$ were higher than those for T_{max} and R_s (Table 5-3) as could be expected considering the over-estimation trend identified above. 12% of cases had NRMSE < 0.10 but NRMSE > 0.5 in 18% of stations. In contrast to the results of EF for $T_{max,}$ those for T_{min} show that only half of the stations had EF > 0.80, with EF < 0.5 in few cases (16%). The examples shown in Figure 5-7, referring to two west to east transepts illustrating the full range of conditions observed, show that b and b_0 values for T_{max} were quite close, but were different in the case of T_{min}.

The spatial variability of the statistical performance indicators over the Peninsula (Figure 5-8) confirmed that overall, very good performance results were obtained for R_s and T_{max}. For these variables, b and b_0 coherently present a similar spatial distribution. Differently, for T_{min} a high over-estimation was observed with $b_0 > 1$ in southern Portugal and Castilla-León region, Spain. High PBIAS and b_0 values for T_{min} were also widely distributed, with special incidence in southern Portugal and Castilla-León and in the coastal areas of Spain. The poorest results for EF were identified for the same locations. These results may be influenced by the shorter data sets used for southern Portugal (<7 years) and could be stemming from inaccuracies of the meteorological network. Results in Figure 5-8 help understanding the spatial distribution of the performance indicators for ET_o. While distribution patterns for R_s and T_{max} were generally similar to those for ET_o (Figure 5-5),

particularly for R^2, b and RMSE, a tendency to over-estimate T_{min} likely influenced the distribution patterns of b_0 and PBIAS relative to ET_o.

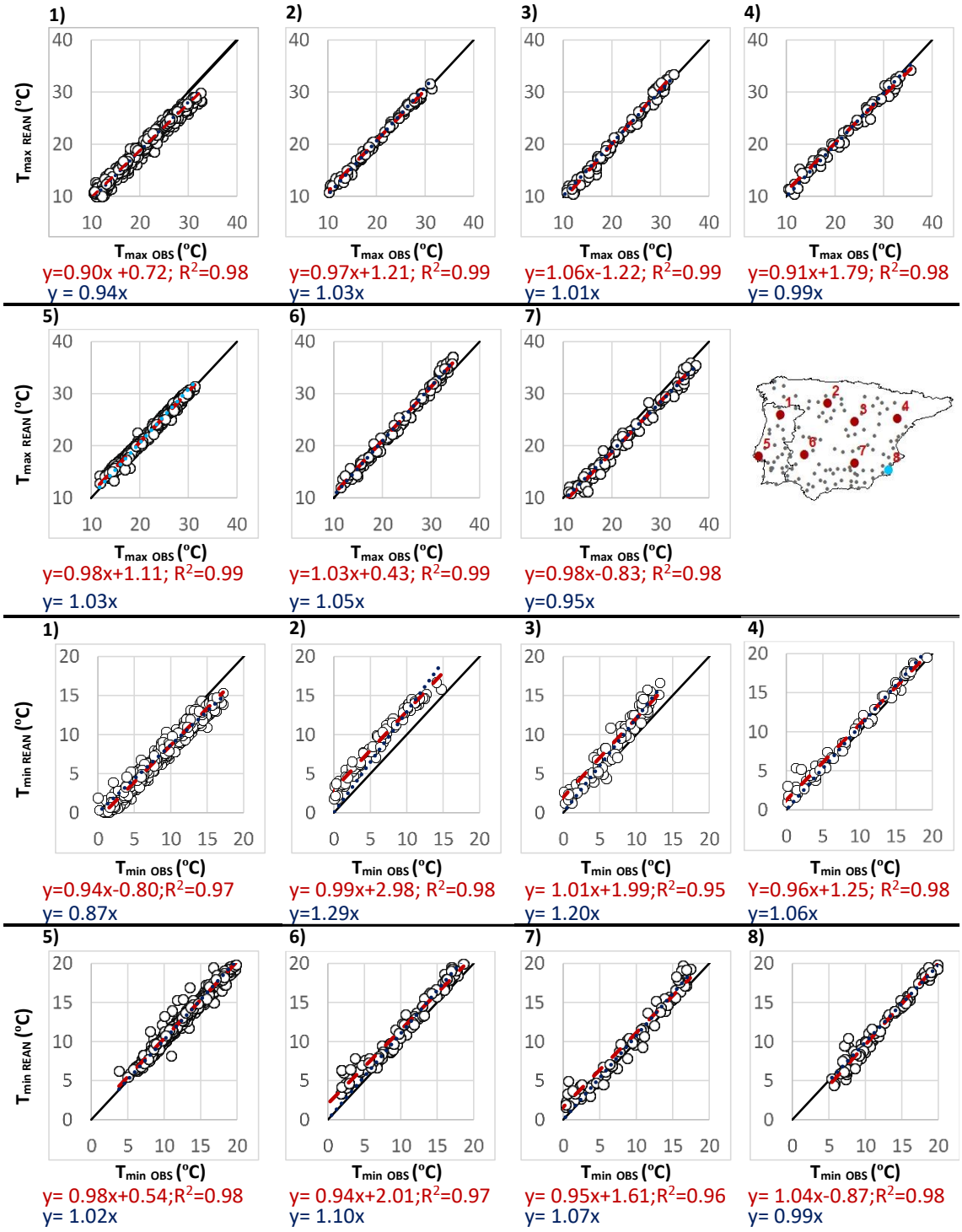

Figure 5-7 Examples of linear regressions of $T_{max\ REAN}$ over $T_{max\ OBS}$ and $T_{min\ REAN}$ relative to $T_{min\ OBS}$ using both the ordinary least squares and the regression forced to the origin. The map identifies the locations of the selected weather stations

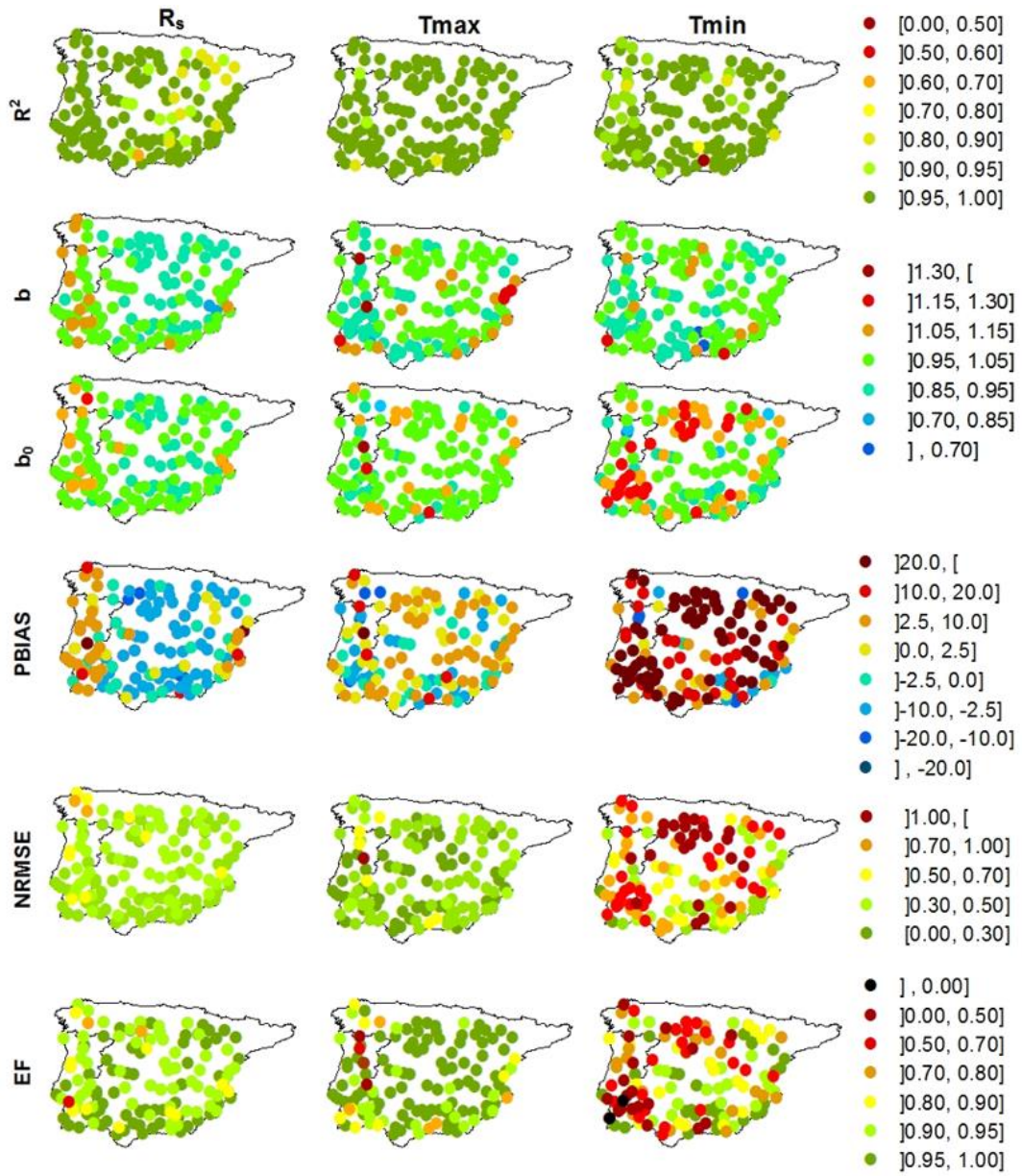

Figure 5-8 Spatial distribution of statistics measuring the association between observed and blended reanalysis data sets over the Iberia for shortwave radiation (R_s) and maximum and minimum temperature (T_{max} and T_{min})

Results on solar radiation reported in the literature indicate that R_s from reanalysis is often over-estimated when using NCEP/NCAR reanalysis products with daily or smaller time scales (Xia et al. 2006; Lohmann et al. 2006; Decker et al. 2012; You et al. 2013; Srivastava et al. 2015). Sheffield et al. (2006) reported overestimation of global radiation for NCEP1 associating this behavior with the fact that the NCEP model does not produce enough clouds to block shortwave radiation. The bias corrections applied by those authors to adjust shortwave radiation in the blended reanalysis data sets are likely the main reason

for the good agreement between Rs_{REAN} and $R_{s\ OBS}$, observed in this study. In addition, these good results may be related to the large time scale used.

Assessments of temperature from NCEP1 reanalysis products are available from various studies reporting on spatial and seasonal variability of T_{max} and T_{min}. Rusticucci et al. (2002) for Argentina, Halenka et al. (2006) for the Czech Republic, Fujihara et al. (2008) for the Seyhan River Basin, in Turkey, and Nastos et al. (2011) for Greece, reported under-estimation of T_{max} and over-estimation of T_{min}. A detailed study by Sillmann et al. (2014) relative to the globe reported good results for T_{min}, with a slight under-estimation bias and a consistent under-estimation bias for T_{max}. (Fu et al. 2016) for Australia reported that both T_{max} and T_{min} were generally over-estimated with NCEP1. For the Brue catchment, Srivastava et al. (2015) reported an over-estimation trend for T_{min} from NCEP/NCAR reanalysis products. As analyzed by (Simmons et al. 2010) for the ERA-40 and ERA-Interim, a possible explanation for the referred over-estimation of T_{min} is that reanalysis is capturing warming over land more than over sea, and that warming affects nighttime temperatures more, thus T_{min} becomes larger than station data.

5.4.3 Evaluating the blended reanalysis variables relative humidity and wind speed

The accuracy of estimating RH and WS based on reanalysis is presented in Table 5-4. R^2 values relative to comparing RH_{REAN} with RH_{OBS} show that 48% of stations have $R^2 > 0.80$ and only 15% of the sites have $R^2 < 0.50$. This indicates that, in most cases, the variance of RH_{REAN} was relatively well explained by the OLS regression on RH_{OBS}. The OLS regression coefficient b varied in a wide range (Table 5-4) with $b < 1.0$ in most cases (74%). Differently, for the FTO regression, b_0 was closer to 1.0, with b_0 in the range 0.95 to 1.05 for 59% of locations. However, 34% of cases had b_0 ranging 1.05 to 1.15, which indicated a slight trend for over-estimation, which averages 3%. Coherently, PBIAS results indicated a slight over-estimation bias, with PBIAS between 0 and 10% in 70% of locations and 9% of cases with PBIAS from -2.5 to -10 %. Results in Figure 5-9 relative to two west to east transepts, clearly showed differences between b and b_0, with a tendency to over-estimate. It was observed (Table 5-4) that NRMSE < 0.15 in 92% of the stations, thus indicating that RMSE values were relatively small. Coherently, the EF values were generally high, with EF > 0.70 in 43% of cases. However, 21% of the stations had negative EF values.

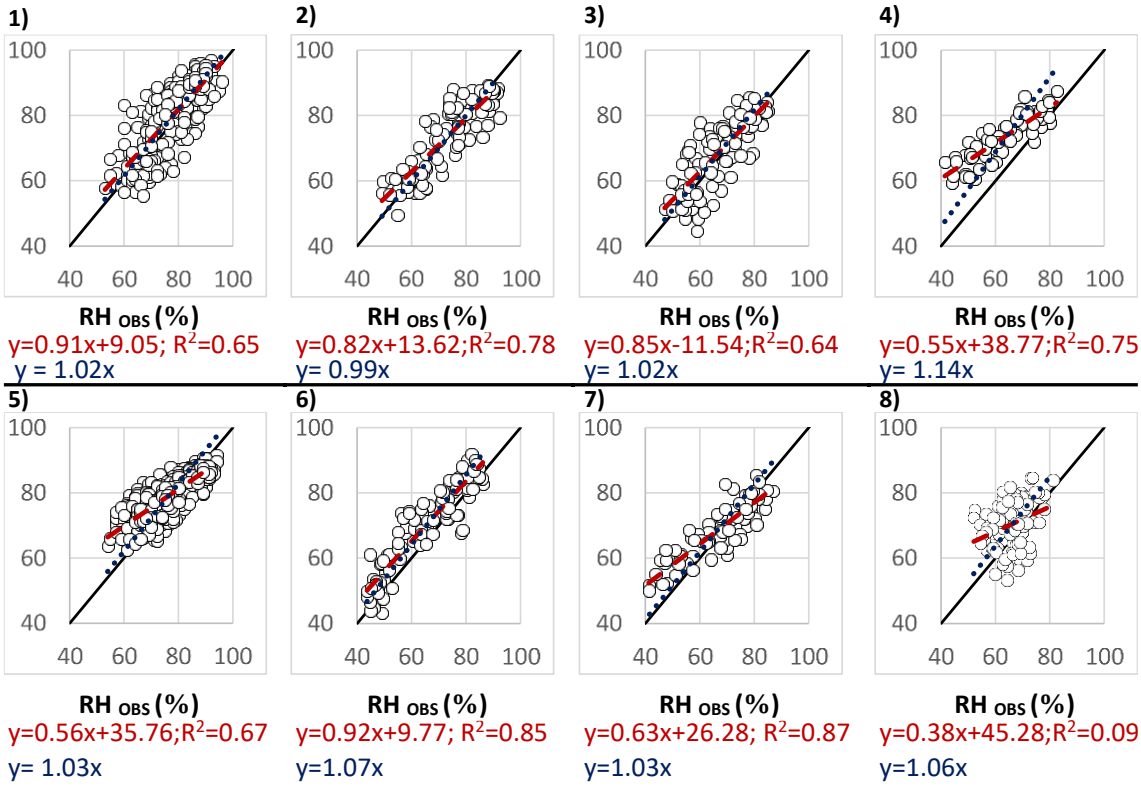

Figure 5-9 Examples of linear regressions of RH $_{REAN}$ over RH $_{OBS}$ using both the ordinary least squares and the regression forced to the origin. Locations are the same as for minimum temperature.

Results clearly showed a very large over-estimation of wind speed. $R^2 < 0.50$ in most stations (87%) and $b_0 > 1.30$ in 81% of locations (Table 5-4). A very large difference between the OLS and FTO regression lines was observed for WS, with very different values of b and b_0, as illustrated in Figure 5-10, considering the same locations of Figure 5-3 for ET_o. Biases were very large, with PBIAS > 20% in 89% of cases. Consequently, errors of estimation were also very large, with NMRSE > 0.5 in 75% of cases. Moreover, there was no gain in using WS $_{REAN}$ over using the mean observed WS since 96% of cases had EF < 0.0.

The spatial variability of the performance indicators relative to RH (Figure 5-11) shows that the worst results of R^2, b_0 and EF, were found in the east and south east coastal areas of Spain, which is an area of semiarid climate. The best indicator values were scattered through the Peninsula. In contrast, the poor results for WS were spread out throughout most of the Iberian Peninsula (Figure 5-11).

Few studies comparing RH $_{REAN}$ and RH $_{OBS}$ are available. Zhao et al. (2006) reported under-estimation trends in VPD when using NCEP1 reanalysis data sets for USA, with a

likely over-estimation of actual vapor pressure and relative humidity. The analysis by Simmons et al. (2010) relative to ERA reanalysis has shown that there was a reduction in RH at low and mid-latitudes. Also Fu et al. (2016) considered that RH from NCEP1 was slightly under-estimated in Australia. Our results using the blended NCEP/NCAR reanalysis products show both over- and under-estimation of RH, however small.

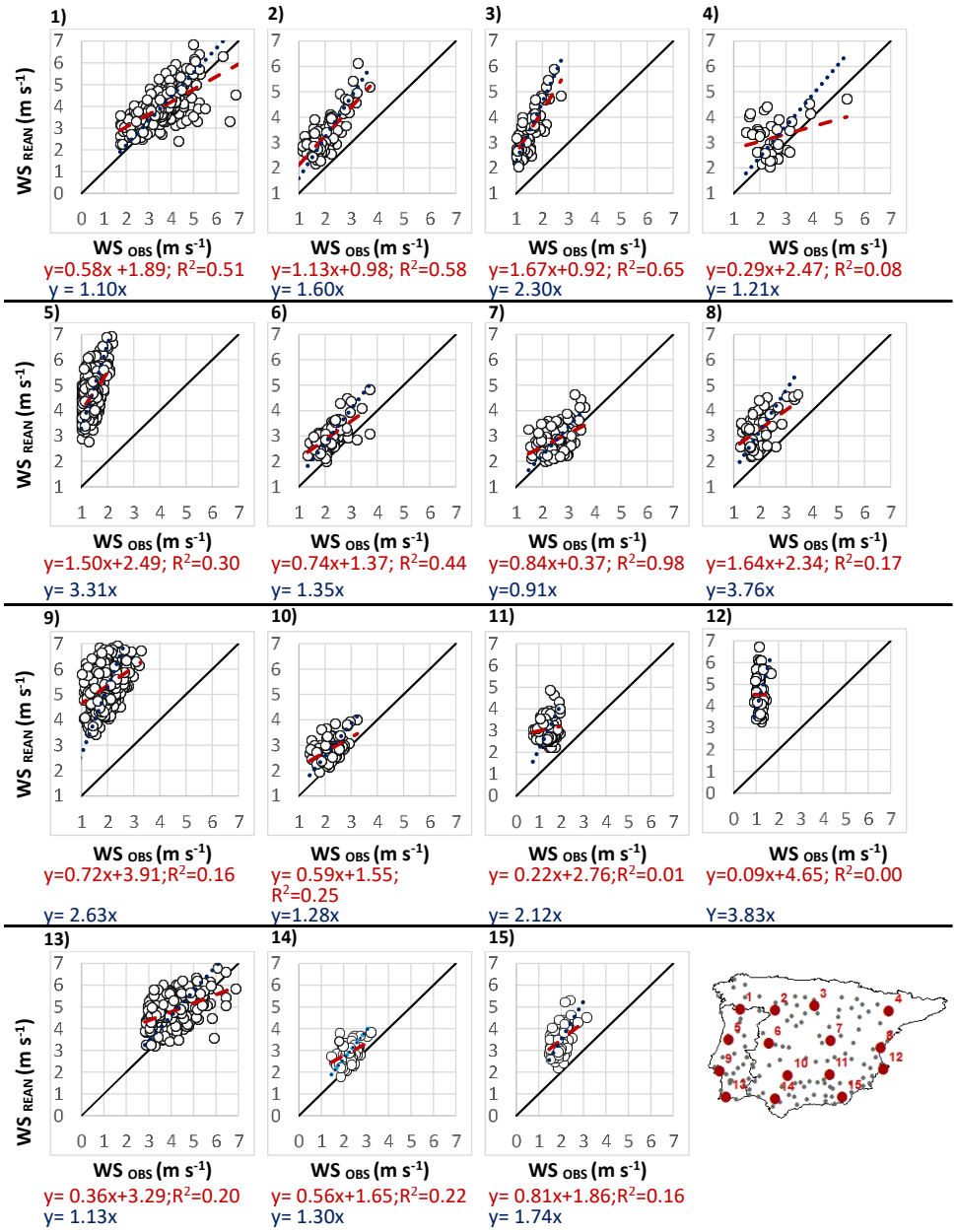

Figure 5-10 Examples of linear regressions of WS $_{REAN}$ over WS $_{OBS}$ using both the ordinary least squares and the regression forced to the origin. The map identifies the locations of the selected weather stations.

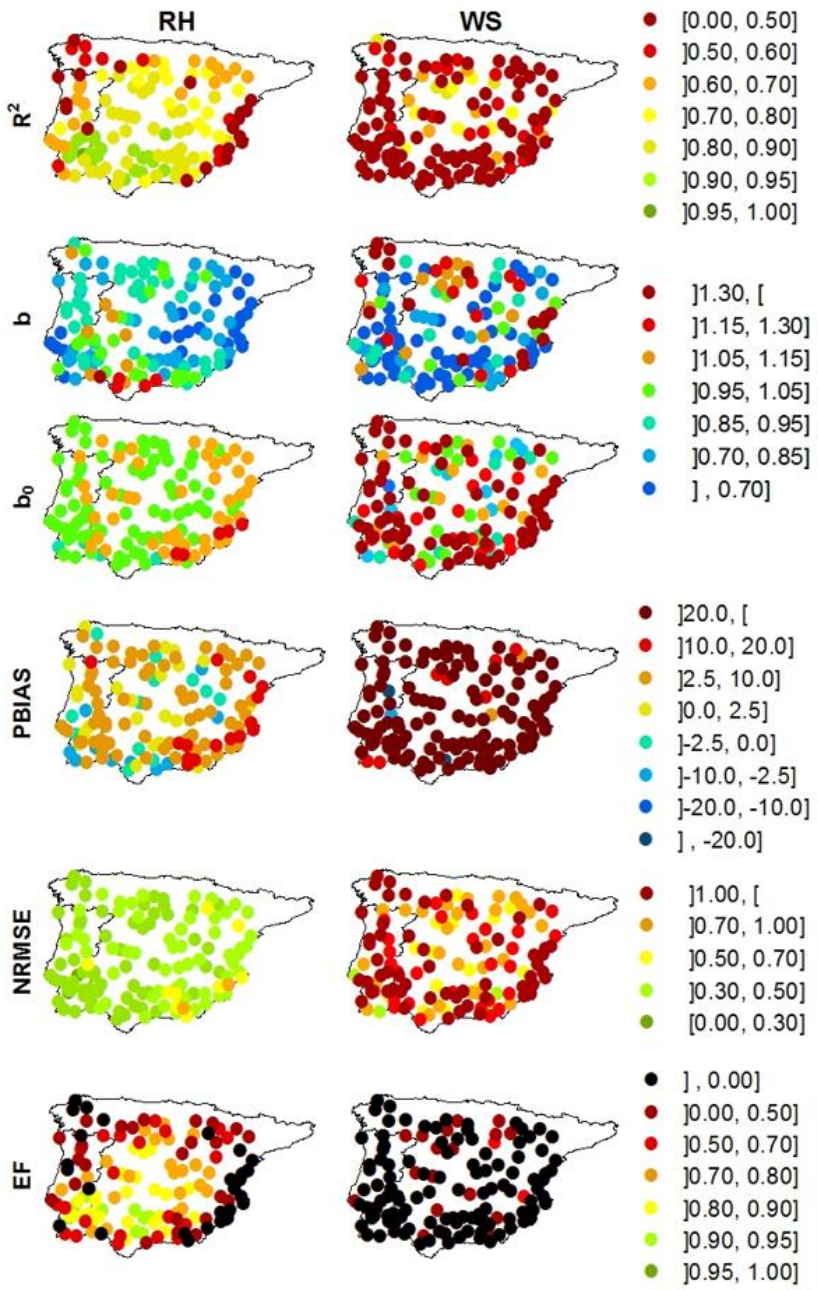

Figure 5-11 Spatial distribution of statistics measuring the association between observed and blended reanalysis data sets over the Iberia for relative humidity (RH) and wind speed (WS).

The comparison between WS reanalysis and observation data is dealt with in few studies. Low accuracy of WS reanalysis products is often reported, even when mesoscale models were used, which may be explained by the difficulty in assimilating the high variability of WS due to local environment influences. Ishak et al. (2010) reported a large over-estimation of WS, with a bias ranging from 200 to 400%, when using ERA-40 downscaled with the MM5 model for the Brue catchment. McVicar et al. (2008) reported a large over-estimation of WS from NCEP1 and 2 in Australia. For the Tibetan Plateau, You et al. (2010) reported WS over-estimation using NCEP1 and Decker et al. (2012)

also reported over-estimation of WS for USA with NCEP1. Lorente-Plazas et al. (2015), for the Iberian Peninsula using ERA-40 and the model MM5, found a trend for over-estimation of daily WS. Our results are therefore in agreement with the over-estimation trends reported in literature.

The identified over-estimation bias for WS is likely to contribute to the over -estimation of $ET_{o\ REAN}$ relative to $ET_{o\ OBS}$. However, wind speed impacts on ET_o are mainly important in dry and hot climates (Allen et al. 1998; Gong et al. 2006; Raziei and Pereira 2013b). Thus, when estimating ET_o for large regions in which simple or hybrid mesoscale models are not an option, alternatives may consist of using the average value of WS_{OBS} or to use the global average of 2.0 m s^{-1} as suggested by Allen et al. (1998). To check the impacts of these alternatives, PM-ET_o was computed with both approaches and compared with results when using WS_{REAN} for various sets of data relative to stations having poor WS_{REAN} performance. Results have not shown improvements on the statistical performance indicators of $ET_{o\ REAN}$, particularly on RMSE, or these improvements were not relevant. It may be concluded that results for WS_{REAN} do not greatly affect the quality of $ET_{o\ REAN}$.

Table 5-4 Frequency (%) distribution of the performance indicators for humidity (RH) and wind speed (WS) , when comparing reanalysis products with observed values.

Intervals of R^2	(%)	Intervals of b	(%)	Intervals of b_0	(%)	Intervals of PBIAS (%)	(%)	Intervals of NRMSE	(%)	Intervals of EF	(%)
Relative Humidity											
]0.95, 1.00]	0.8	]1.30, [	0.8	]1.30, [	0.0	] , -20.0]	0.0	]0.50, 1.00]	0.0	] , 0.00]	20.8
]0.90, 0.95]	16.2	]1.15, 1.30]	3.1	]1.15, 1.30]	3.8	]-20.0, -10.0]	0.0	]0.30, 0.50]	0.0	]0.00, 0.50]	19.2
]0.80, 0.90]	30.8	]1.05, 1.15]	6.2	]1.05, 1.15]	33.8	]-10.0, -2.5]	9.2	]0.20, 0.30]	0.0	]0.50, 0.70]	16.9
]0.70, 0.80]	16.9	]0.95, 1.05]	16.2	]0.95, 1.05]	58.5	]-2.5, 0.0]	8.5	]0.15, 0.20]	8.5	]0.70, 0.80]	16.9
]0.60, 0.70]	13.8	]0.85, 0.95]	26.9	]0.85, 0.95]	3.8	]0.0, 2.5]	16.9	]0.10, 0.15]	43.1	]0.80, 0.90]	19.2
]0.50, 0.60]	6.9	]0.70, 0.85]	28.5	]0.70, 0.85]	0.0	]2.5, 10.0]	53.1	]0.05, 0.10]	46.9	]0.90, 0.95]	6.9
[0.00, 0.50]	14.6	] , 0.70]	18.5	] , 0.70]	0.0	]10.0, 20.0]	12.3	[0.00, 0.05]	1.5	]0.95, 1.00]	0.0
						]20.0, [	0.0				
Wind speed											
]0.95, 1.00]	0.0	]1.30, [	11.5	]1.30, [	80.8	] , -20.0]	2.3	]0.50, 1.00]	75.4	] , 0.00]	96.2
]0.90, 0.95]	0.0	]1.15, 1.30]	8.5	]1.15, 1.30]	8.5	]-20.0, -10.0]	0.0	]0.30, 0.50]	16.2	]0.00, 0.50]	3.8
]0.80, 0.90]	0.0	]1.05, 1.15]	8.5	]1.05, 1.15]	6.9	]-10.0, -2.5]	0.8	]0.20, 0.30]	4.6	]0.50, 0.70]	0.0
]0.70, 0.80]	2.3	]0.95, 1.05]	6.9	]0.95, 1.05]	0.8	]-2.5, 0.0]	0.0	]0.15, 0.20]	3.1	]0.70, 0.80]	0.0
]0.60, 0.70]	3.1	]0.85, 0.95]	8.5	]0.85, 0.95]	0.8	]0.0, 2.5]	0.0	]0.10, 0.15]	0.8	]0.80, 0.90]	0.0
]0.50, 0.60]	7.7	]0.70, 0.85]	12.3	]0.70, 0.85]	0.8	]2.5, 10.0]	1.5	]0.05, 0.10]	0.0	]0.90, 0.95]	0.0
[0.00, 0.50]	86.9	] , 0.70]	43.8	] , 0.70]	1.5	]10.0, 20.0]	6.2	[0.00, 0.05]	0.0	]0.95, 1.00]	0.0
						]20.0, [	89.2				

R^2 is the coefficient of determination of the OLS regression; b is the regression coefficient of the OLS; b_0 is the regression coefficient of the FTO; PBIAS is the Percent Bias; NRMSE is the Normalized Root Mean Square Error; EF is the efficiency of modelling

5.4.4 Brief comparison of ET_o computed with various reanalysis products

The statistical indicators described in 5.3.3 were also used to compare the PM-ET_o (Equation 4.1) derived from NCEP2 and ERA-Interim reanalysis data with those computed with weather variables observed at 15 selected weather stations across the Iberian Peninsula. NCEP/NCAR blended reanalysis outperforms NCEP2 and ERA-Interim in the performance indicators obtained for the same 15 locations (Table 5-1).

Results for the ERA-Interim estimations revealed a tendency to overestimate: all regression coefficients of the FTO regression are larger than 1.0 and averaged 1.11; with 4 exceptions, OLS slopes b are greater than 1.0, with an average value of 1.07; the PBIAS, with one exception, ranged from 4.1% up to 33.6% averaging 12.9%. Differently, NCEP2 based estimates tended to strongly underestimate ET_o: b_0 averaged 0.76, b averaged 0.53 with a=1.02, and PBIAS, with 2 exceptions, ranged from -6.4 to -26.0% averaging -15.1%. For the blended reanalysis, the b_0 and b values are close to 1.0 and PBIAS averages 7.72%. Results in Table 5-5 also showed that RMSE for the blended reanalysis estimates in the same 15 stations compared favorably with the other two reanalysis products: the average RMSE= 0.45 mm d^{-1} is smaller than those for ERA-Interim (RMSE=0.71 mm d^{-1}) and of NCEP2 (RMSE=1.15 mm d^{-1}), while the average Nash and Sutcliff efficiency is larger for the blended reanalysis products (EF = 0.93) than for ERA-Interim (EF=0.83) or for NCEP2 (0.65).

These results suggest the selection of the reanalysis products for estimating ET_o when observed weather data are unavailable. However, the comparison made is insufficient: on the one hand, daily weather data are required in irrigation management and, on the other hand, real time data is also required. ERA-Interim data may be a solution for daily irrigation management simulations as used in irrigation scheduling, especially when seasonal weather forecasts as provided by ECMWF are also used (Paredes et al. 2015). Further studies are required to understand the behavior of the weather variables (R_s, T_{max}, T_{min}, RH and u_2) and maybe decrease the estimation errors obtained with ERA-Interim products when using daily time steps. Moreover, studies are required to combine past data with seasonal forecasts for real time operation in irrigation scheduling models. Likely, these reanalysis products may be used to compute drought indices when adjusted for the month time scale.

Table 5-5 Comparing the performance indicators relative to the estimation of ET_o by ERA-Interim, NCEP2 and blended NCEP/NCAR Reanalysis for 15 weather stations in the Iberian Peninsula. *units in mm d^{-1}

Weather Stations	ERA-Interim							NCEP2							Blended NCEP/NCAR Reanalysis						
	b_0	b	a*	R^2	RMSE*	EF	PBIAS (%)	b_0	b	a*	R^2	RMSE*	EF	PBIAS (%)	b_0	b	a*	R^2	RMSE*	EF	PBIAS (%)
Vila Real	1.25	1.20	0.18	0.94	0.97	0.70	26.6	0.82	0.55	1.03	0.89	0.87	0.76	-6.4	1.02	1.02	0.01	0.98	0.26	0.97	2.3
Braganca	1.10	1.04	0.26	0.92	0.71	0.87	12.5	0.74	0.50	1.03	0.89	1.14	0.67	-15	0.97	0.96	0.06	0.98	0.27	0.98	-2.1
Lerma	1.30	1.23	0.24	0.94	1.02	0.60	32.9	0.90	0.62	0.98	0.91	0.69	0.82	1.5	1.09	1.04	0.18	0.98	0.35	0.95	11.3
Monte Julia	1.00	0.89	0.50	0.96	0.49	0.95	4.6	0.66	0.44	1.08	0.89	1.52	0.54	-23.5	0.94	0.83	0.50	0.98	0.44	0.96	-1.6
Castelo Branco	1.06	1.01	0.24	0.94	0.67	0.91	8.1	0.66	0.44	1.13	0.89	1.61	0.51	-24.8	0.99	0.99	-0.02	0.99	0.26	0.99	-1.1
Aldehuela del	1.09	1.05	0.19	0.93	0.66	0.89	10.2	0.72	0.49	1.07	0.88	1.28	0.60	-19.4	1.03	1.09	-0.28	0.98	0.38	0.97	0.3
Puig	1.32	1.27	0.18	0.96	1.03	0.43	33.6	0.96	0.74	0.74	0.88	0.52	0.85	1.7	1.13	1.13	0.38	0.96	0.96	0.78	35.8
Lisboa	1.22	1.31	-0.44	0.97	0.96	0.72	18.9	0.75	0.55	0.89	0.90	1.12	0.62	-19.7	1.05	1.06	-0.02	0.95	0.72	0.73	16.9
Portalegre	1.06	1.06	-0.02	0.93	0.69	0.90	5.5	0.67	0.46	1.07	0.87	1.60	0.48	-26	1.03	1.09	-0.24	0.97	0.42	0.95	15.2
Barajas de Melo	0.94	0.84	0.52	0.94	0.63	0.93	-1	0.66	0.42	1.19	0.88	1.62	0.53	-23.2	0.91	0.84	0.37	0.98	0.51	0.95	-5.3
Chiclana de	1.03	0.90	0.59	0.93	0.62	0.91	8.6	0.77	0.49	1.29	0.89	1.18	0.69	-10.5	1.08	0.99	0.44	0.99	0.47	0.95	12.4
Altea	1.19	1.15	0.14	0.96	0.77	0.76	20	0.87	0.67	0.76	0.89	0.68	0.81	-8.3	1.16	1.06	0.41	0.96	0.68	0.82	18.7
Faro	1.05	1.06	-0.06	0.96	0.43	0.95	4.2	0.74	0.55	0.91	0.89	1.22	0.59	-20.9	0.99	0.99	0.01	0.98	0.28	0.98	-0.8
Cabezas de S.	1.03	0.98	0.24	0.95	0.48	0.94	4.7	0.75	0.52	1.12	0.89	1.22	0.63	-17.7	1.08	1.07	0.04	0.98	0.46	0.95	8.0
Tabernas	1.03	1.00	0.15	0.94	0.48	0.94	4.1	0.79	0.58	0.97	0.89	1.03	0.70	-14.7	1.05	1.02	0.13	0.98	0.32	0.97	5.8
Average	1.11	1.07	0.19	0.95	0.71	0.83	12.9	0.76	0.53	1.02	0.89	1.15	0.65	-15.1	1.04	1.01	0.13	0.98	0.45	0.93	7.7

Table 5-6 Average goodness-of-fit indicators relative to the estimation of ET_o and the weather variables by the NCEP-NCAR Reanalysis II products for the period 1998 - 2008 and 1998 -2014 for 94 Spanish weather stations

NCEP2 - 1998 - 2008								
	b_0	b	a*	R^2	RMSE*	NRMSE	EF	PBIAS
ET_o (mm d^{-1})	0.81	0.52	1.19	0.87	1.09	0.36	0.69	-7.30
T_{max} (ºC)	0.82	0.33	11.36	0.41	6.41	0.31	0.19	-12.21
T_{min} (ºC)	1.08	0.69	4.67	0.69	4.13	0.63	0.33	39.48
R_s (MJ m^{-2} d^{-1})	1.15	0.99	3.10	0.90	3.80	0.23	0.69	17.92
RH (%)	1.25	-0.28	103.56	0.40	24.81	0.39	-5.36	30.37
WS (m s^{-1})	2.46	0.26	3.46	0.03	3.37	2.20	-151.49	156.48
NCEP2 - 1998 - 2014								
ET_o (mm d^{-1})	0.81	0.54	1.13	0.87	1.05	0.35	0.71	-7.21
T_{max} (ºC)	0.81	0.32	11.55	0.41	6.52	0.31	0.18	-12.71
T_{min} (ºC)	1.08	0.67	4.85	0.68	4.15	0.62	0.32	38.70
R_s (MJ m^{-2} d^{-1})	1.14	0.98	3.26	0.90	3.78	0.23	0.70	17.51
RH (%)	1.25	-0.25	101.47	0.32	24.56	0.38	-5.08	29.72
WS (m s^{-1})	2.46	0.70	2.71	0.04	3.33	2.21	-135.23	155.73

R^2 is the coefficient of determination of the OLS regression; b is the regression coefficient of the OLS; b_0 is the regression coefficient of the FTO; PBIAS is the Percent Bias; RMSE is the Root Mean Square Error; EF is the efficiency of modelling. *indicators in the same units as the variables.

Because blended reanalysis products ended in 2010 while NCEP2 products are available in almost real time, we assessed how NCEP2 products performed up to the present. Thus, monthly values of ET_o were computed for all Spanish weather stations (n=94) for both the period 1998-2008 used in the current study and the period 1998-2014, i.e., extending the assessment to the present. A substantial agreement in average results was observed (Table5-6), with only minor improvements when using the longer data sets. ET_o is under-estimated with average RMSE > 1.0 mm d^{-1} for both periods under consideration, which is larger than RMSE values obtained with the alternative approaches referred in Chapter 1 and Section and 4.1. Therefore, NCEP2 reanalysis products are not yet suitable for the estimation of ET_o when weather data are lacking without proper bias correction to local conditions. The high quality of estimates with NCEP/NCAR blended reanalysis calls for the continuity of these products, which would be beneficial for potential users interested in the post-2010 period.

5.4.5 Accuracy of daily ET_o estimation using ERA-Interim and test of alternative bias correction schemes

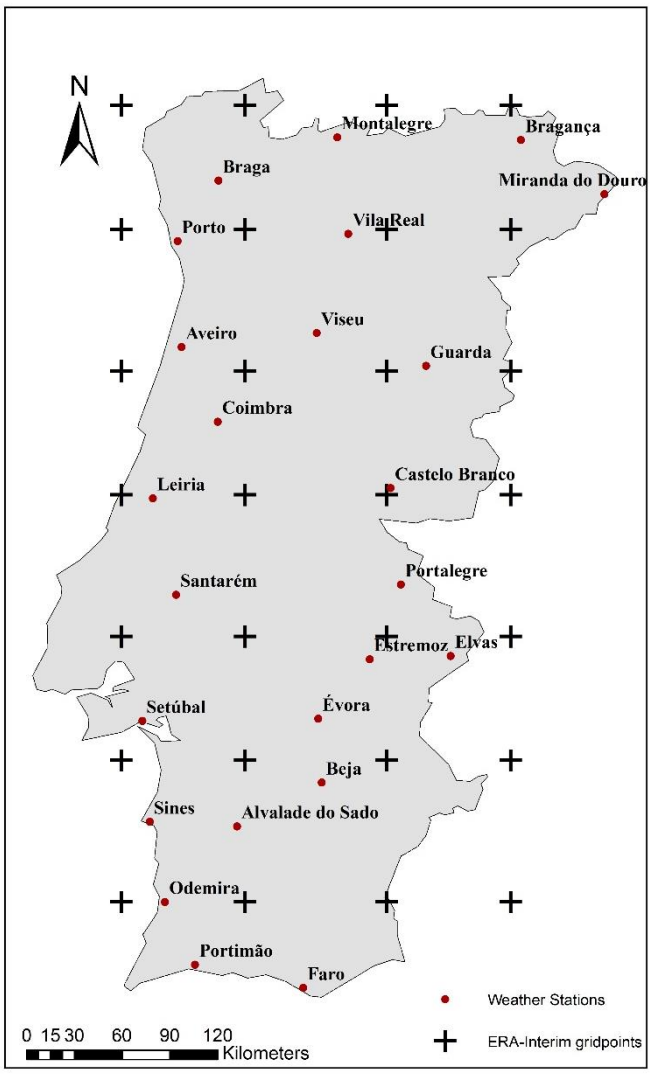

Figure 5-12 Spatial distribution of the ERA-Interim reanalysis grid points (at each 0.75°) in Continental Portugal and location of the 24 weather stations used in the current analysis.

Results from section 5.4.4 revealed that ERA-Interim monthly data produced relative good estimations of ET_o when compared to selected weather stations, even though no bias correction was implemented. For that reason, and aiming at using reanalysis data to support irrigation management, daily ET_o estimates from ERA-Interim were also compared against ET_o computed with observed data relative to 24 weather stations (Figure 5-12) in continental Portugal and different bias corrections schemes were tested to reduce the differences between ET_o computed with reanalysis data and with observation data.

Observed data, relative T_{max} and T_{min}, measured at 2 m height, RH, u_2, and solar radiation (R_S) or sunshine duration (h), were provided by IPMA and the Centro Operativo e de Tecnologia de Regadio. Most weather stations had daily data relative to the period 2003-2013 with in some location having longer time series, from 1979-2013 in two locations and from 1998 to 2013 in two other locations. The smaller time series ranges from 2009 to 2003 for the weather station of Miranda do Douro with 1572 observations. The ERA-Interim reanalysis products selected for the current study cover the period from 1979 to present on a regular grid with a spatial resolution of 0.75ºx0.75º latitude-longitude, corresponding to an approximately uniform spacing of 79 km (Dee et al. 2011). Data referred to eight 3-h forecasts for every day. All grid points located in Continental Portugal (Figure 5-12) were considered for retrieving daily weather products on maximum and minimum air temperature ($T_{max,}$ T_{min}, K), dew point temperature (T_{dew}, K), wind speed at 10 m height (u_{10}, m s^{-1}), and solar radiation (R_s, W m^{-2}).

ET_o from ERA-Interim was computed with Equation 4.1 using the following procedures: (a) the daily $T_{max\ REAN}$ and $T_{min\ REAN}$ were selected, respectively, as the maximum and minimum values from the eight daily available 3-h forecasts of T_{max} and T_{min} series; (b) the daily $T_{dew\ REAN}$ were obtained by computing the 24-h average of the eight 3-h forecasts of T_{dew}; (c) the daily $R_{s\ REAN}$ values were obtained by computing the 24-h cumulative value of the 12-h R_s forecasts; (d) the wind speed $u_{2\ REAN}$ were computed first as the 24-h average of the eight 3-h forecasts of u_{10}, and then these values were converted to 2 m height using using the logarithmic wind speed profile proposed in FAO56 (Allen et al. 1998). Then, all units of variables were converted into the units used in Equation 4.1, that is, K were converted into ºC and W m^{-2} into MJ m^{-2} day^{-1}. In addition, all temperature data were corrected for elevation relative to the target location where to be used. Following Soares et al. (2012), a fixed lapse rate of 6.5 ºC km^{-1} was adopted (Berg et al. 2003; Zhao et al. 2008; Grouillet et al. 2016; De Bruin et al. 2016), which is an intermediate value between the dry and wet adiabatic lapse rate.

5.4.5.1 Bias correction schemes

The use of the ERA-Interim reanalysis products may be carried out adopting several approaches, with or without bias correction of the calculated $ET_{o\ REAN}$. The simpler approach consists on using the data of the nearest grid point of the target location, while a possibly more precise approach considers multiple nearby grid points. Usable grid

points were selected: (a) at a distance <100 km of the target location; and (b) when the regression coefficient b_0 and the determination coefficient R^2 of the regression between $T_{max\ REAN}$ and $T_{max\ OBS}$, as well as between $T_{min\ REAN}$ and $T_{min\ OBS}$ satisfy respectively the conditions $0.70 \leq b_0 \leq 1.30$ and $R^2 \geq 0.70$.

ET_o may be computed with the referred reanalysis data ($ET_{o\ REAN}$) with or without bias correction of the computed $ET_{o\ REAN}$. Bias correction seeks to reduce the differences between ET_o computed with reanalysis data and with observations data, since reanalysis products are often biased due to errors in the host weather forecast models as discussed by Berg et al. (2003) for a hydrologic application of ECMWF reanalysis products. Hwang et al. (2014) reported on bias correction of reanalysis precipitation and temperature data used in hydrologic simulations. Various bias correction methods have been used and assessed in several studies (Maraun 2013; Fang et al. 2015).

Aiming at an accurate but simple bias correction procedure, it was applied to the computed $ET_{o\ REAN}$ and not to the individual reanalysis variables used to compute it. Nevertheless, bias correction applied to reanalysis computed ET_o is rarely reported in literature (Srivastava et al. 2015); differently, bias corrections of weather variables are adopted when these variables are used in model computations (Baigorria et al. 2007; Maurer et al. 2013).

Two bias corrections schemes were applied:

a) a simplified correction consisting in adding a constant c(t) to the uncorrected $ET_{o\ REAN\ unc}$ computed for the nearest grid point, where t denotes a time period and

$$c(t) = \overline{ET_{o\ REAN\ unc}(t)} - \overline{ET_{o\ OBS}(t)} \quad (5.6)$$

Thus, c(t) is the difference between the mean daily values of the uncorrected $ET_{o\ REAN\ unc}$ and of the $ET_{o\ OBS}$ computed with the observed variables at the target location. These mean values were computed grouping the daily data available (for all the years used to fit the model) for different periods of time (t): (1) twelve monthly averages (January, February,…, December); (2) four quarterly averages (JFM, AMJ, JAS and OND); and (3) a single overall average. A similar approach was used in various studies (Terink et al. 2010; Hofer et al. 2012; Hempel et al. 2013).

b) a combined approach, also for to the same periods t, which uses the multiple regression relating $ET_{o\ OBS}$ computed with observed data at the target location with the

nearby $ET_{o\ REAN\ unc}$ computed at M nearby grid points that satisfy the conditions on b_0 and R^2 that were mentioned above.

The multiple linear regression equation may be expressed as

$$ET_{o\ OBS}(t) = \rho_{0,t} + \sum_{i=1}^{i=M} \rho_{i,t}\ ET_{o\ REAN,i}\ (t) + \varepsilon_t \quad (5.7)$$

where the multiple regression coefficients ρ_0, ρ_1, ρ_2,… ρ_n are estimated relating the $ET_{o\ OBS}$ with the $ET_{o\ REAN,i}$ computed for each of n reanalysis grid points i. Using the estimated multiple regression coefficients, $\widehat{\rho_j}$, it is possible to obtain new values for $ET_{o\ REAN}$:

$$\widehat{ET}_{o\ REAN}(t) = \hat{\rho}_{0,t} + \sum_{i=1}^{i=M} \hat{\rho}_{i,t}\ ET_{o\ REAN,i}\ (t) \quad (5.8)$$

As with the bias correction scheme a) Equations 5.7 and 5.8 were fitted for monthly, quarterly and a single overall aggregated data.

A major uncertainty of bias correction refers to how well it performs for conditions different from those used at calibration. Thus, a cross-validation procedure was applied (e.g., Arlot and Celisse 2010; Hempel et al. 2013). The cross-validation procedure consisted in providing a validation of model fit with a set of data that is independent of the model fitting set. In the present study, the models were fitted individually for each weather station location and validated on independent data sets from the same location. The cross-validation procedure consisted in dividing each data set into two groups of the same size. For each cross-validation iteration, one group was used for training and the other was reserved for validation. In a first step, the correction parameters were obtained from the first set of data (training) and the same correction parameters were used with the second set of data (validation). Subsequently, the second set of data was used for deriving the correction parameters (training) and the first one for verification. The assessment of the performance of each bias correction procedure was performed on the validation/verification sets. The performance results of the cross-validation were averaged over the two validation sets.

5.4.5.2 Results

The performance indicators for each weather variable showed similar results to those showed previously using monthly data:

(1) There a good correlation between reanalysis temperature variables, like T_{max} and T_{min}, however after proper correction for altitude differences. Results for b_0 and PBIAS showed a clear tendency for under-estimation of both T_{max} and over-estimation of T_{min}. R^2 are high, mainly for T_{max}, indicating that that a large fraction of the variance of observations is explained by the reanalysis estimated variables. Coherently, EF were generally high for T_{max} but low EF were obtained for T_{min}. Consequently, errors were relatively small for T_{max}, with more frequent NRMSE ranging from 5 to 15%, while errors for T_{min} are larger, mainly in the interval 20 to 50%.

(2) T_{dew}, also corrected for altitude differences, was used in this comparison, since RH was not available in the ERA-Interim data sets, and results revealed an underestimation of this variable, $b0 \leq 0.95$ in 75% of locations, but with relatively high R^2, between 0.70 and 0.9 for most locations. Studies comparing e_a derived from reanalysis RH products also reported a tendency for under-estimation of e_a. (Berg et al., 2003; Simmons et al. 2010)

(3) $R_{s\ REAN}$ agrees well with $R_{s\ OBS}$, with b_0 ranging 0.95 to 1.05 in 79% of cases, and most PBIAS between 2.5 and 10%, thus with a slight tendency for under – estimation.

(4) Wind speed, like as for the monthly analysis, was the worst variable estimated by ERA-Interim, in this data set, with a general tendency for overestimation, with only 8% of locations with b0 ranging 0.95-1.05, with NRMSE > .30 for all 25 locations.

$ET_{o\ REAN}$ was compared against observations, considering both bias corrections schemes, applied to the three periods considered and using the original $ET_{o\ REAN}$, i.e., without bias correction. This approach allowed for comparing the relative improvements of each of the bias correction implemented and also how the bias correction improve upon the uncorrected ET_o estimated using the ERA-Interim data.

Figure 5-13 compares the indicators RMSE and absolute PBIAS, obtained with cross-validation, in order to understand the differences between the two bias corrections schemes, computed for the three periods (month, quarter and annual). Results showed that the monthly bias correction outperforms the other studied periods (quarterly and entire period). However, differences of using the various periods for estimating the

additive bias correction are not generally high. Comparing the cross-validation results relative to correcting reanalysis using both the additive and multiple regression bias correction (Figure 5-13) showed that the monthly multiple regression outperformed the other aggregation periods and all the additive correction periods tested. However, the differences in RMSE and absolute PBIAS are not appreciably better, and that the quarterly aggregation period appears to be a good aggregation scheme, capable of explaining the seasonality of ET_o. Moreover, differences between the multiple regression and the additive bias corrections are evident in Figure 5-13, with lower RMSE values and PBIAS. Furthermore, bias correction computed from a multiple regression associating various nearby grid points may provide better results. However, due to its simple usage and since related accuracy indicators compare well with those due to the multiple regression calculation, the use of the additive bias correction computed with the quarterly aggregation may also be appropriate.

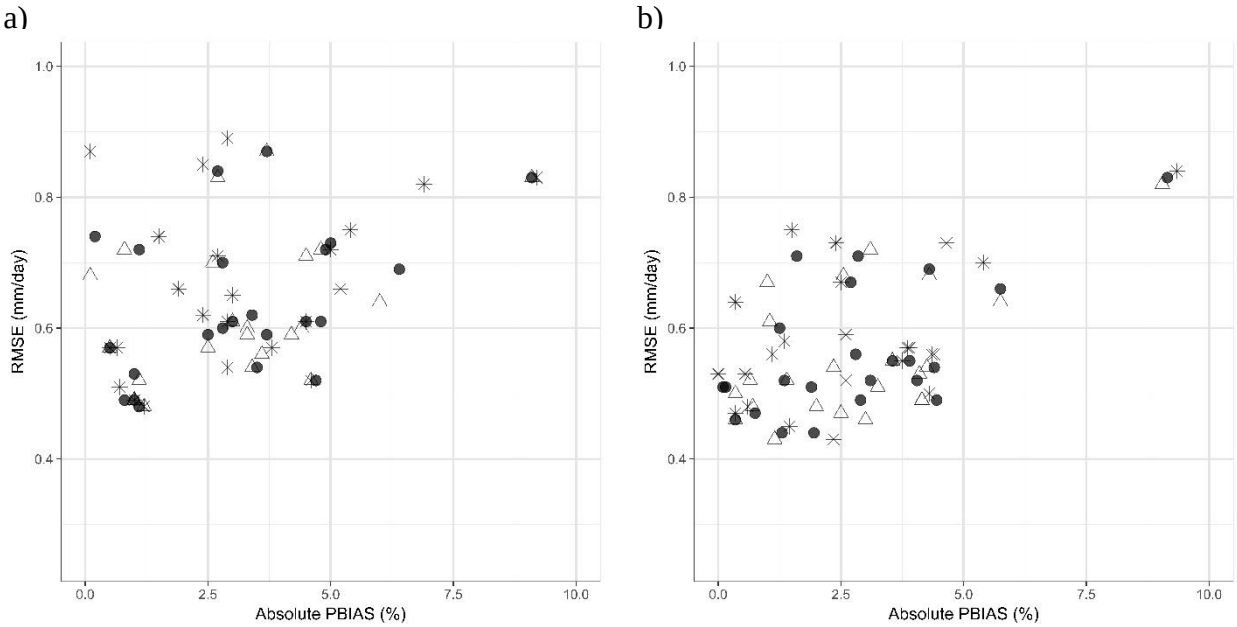

Figure 5-13 Cross-validation daily $ET_{o\ REAN}$ mean performance indicators relative to the (a) additive bias correction and (b) multiple regression using the different aggregation periods monthly (Δ), quarterly (•), and entire period (*)

The selection of the bias correction approach and related bias correction parameters was then based upon the accuracy of the validations sets when using the recent base-period sets for calibration. Results of comparing the uncorrected with the additive correction and multiple regression using the quarterly aggregation are presented in Figure 5-14. According to the computed performance indicators, both ET_o-bias correction approaches improved the uncorrected $ET_{o\ REAN}$ simulations to some extent. Results in Figure 5-14

clearly show the accuracy improvement of both bias correction methods relative to the use of the uncorrected daily $ET_{o\ REAN}$. Both correction approaches present no clear tendency for under and over-estimation of $ET_{o\ OBS}$ with b_0 generally ranging from 0.95 to 1.05. Both bias correction approaches performed well for the validation sets since the PBIAS ranged from -10% to 10% in 96% of locations. R^2 are high, indicating that a large fraction of the variance of $ET_{o\ OBS}$ was explained by the $ET_{o\ REAN}$. Coherently, EF were generally high (EF>0.80). Consequently, errors were relatively small with RMSE<0.75 mm day^{-1} in 88% and 92% of locations respectively when using the additive bias correction and the multiple regression.

However, results of both bias correction approaches did not highly differ and, therefore, because the additive bias correction is more straightforward to be applied in irrigation scheduling, operationally the use of the additive correction is preferable. These results, even using daily data, were generally better than those observed for the monthly data using the blended reanalysis data set, which shows that these bias correction schemes were adequate and that bias correcting the final ET_o series may be better than correcting the weather variables used for its computation. However, the bias correction used for the daily ET_o from ERA-Interim was performed with the same observed time series used to assess its performance, even though a cross-validation scheme was used. Contrarily, the observed data used for the bias correction by Sheffield et al. (2006) was independent from the observed weather data used for comparing $ET_{o\ REAN}$ and $ET_{o\ OBS}$ in the previous sections. Thus, this may help explain how the monthly ET_o analysis showed worst performance indicators than the daily data analysis.

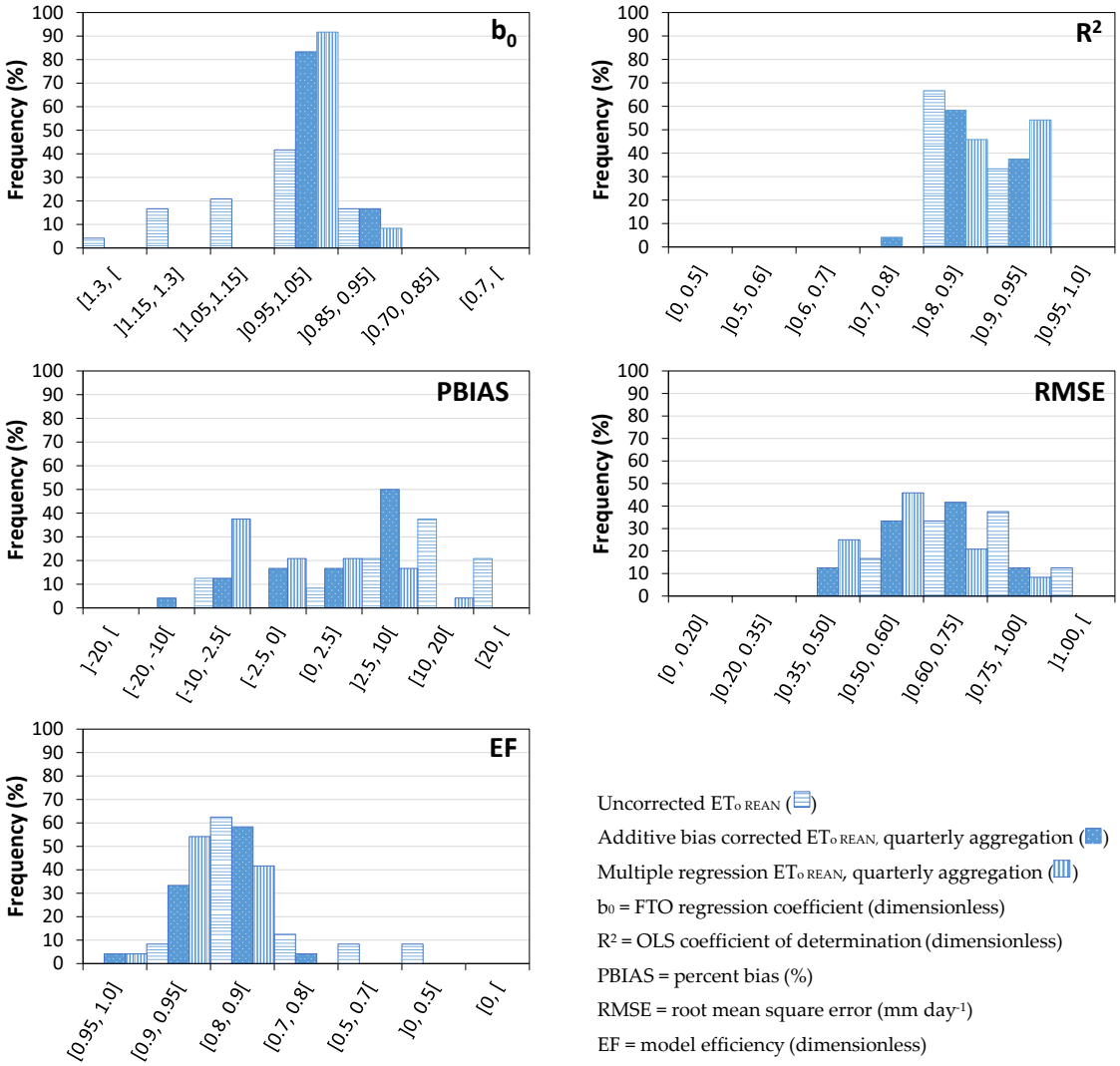

Figure 5-14 Frequency (%) distribution of the statistical indicators measuring the performance of ET_o estimation using uncorrected reanalysis data, additive bias correction and multiple regression with quarterly aggregation

5.5 Conclusions

The full sets of weather data required for ET_o computation are often not available or are not free, leading many users to adopt ET_o estimation alternatives that require less weather data, such as only temperatures. Easily accessible and continually updated reanalysis weather products supply all weather variables required to compute ET_o in various spatial resolutions. Monthly data were used to compare $ET_{o\ REAN}$ with $ET_{o\ OBS}$ for 130 weather stations covering the various climates of the Iberian Peninsula. Monthly data were used because the PM-ET_o equation for both daily and monthly data produces similar results. Our tests for 15 weather stations distributed over the Iberian Peninsula have shown that

monthly ET_o computed with monthly weather variables is almost identical to the monthly totals of daily ET_o.

Results revealed that $ET_{o\ REAN}$ reproduces well the spatial and temporal variability of $ET_{o\ OBS}$, as reflected in various statistical accuracy indicators. For 95% of the weather stations RMSE was smaller than 0.8 mm d^{-1} and only a slight over-estimation bias was detected, which was more noticeable in the southern and eastern areas of the Peninsula, including the drier coastal areas. When the computed RMSE values were compared with those obtained with a variety of methods alternative to the PM-ET_o procedure, it was observed that they were generally similar to the smaller ones reported by various authors, i.e., errors of estimates of ET_o computed with NCEP/NCAR blended reanalysis products are likely smaller than those obtained with alternative computation procedures. Results suggest that the use of reanalysis products is advantageous relative to alternative methods because, in addition to small estimation errors, it allows consideration of the physics of the processes described by the ET_o equation.

All reanalysis weather variables were also compared with those observed at the same 130 weather stations of the Iberian Peninsula in order to assess their possible influence on the quality of ET_o calculation. Results for solar radiation, the main driving variable of ET_o, are very good, with very small estimation errors and a slight under-estimation bias. Similarly, good results were obtained for maximum temperature. However, $T_{min\ REAN}$ revealed less agreement with observations, with an over-estimation bias but small errors of estimate. Results for relative humidity have also shown a small over-estimation bias. For all these variables, EF was generally high, with only few exceptions for RH_{REAN}, thus indicating that the mean square errors of estimates were generally much smaller than the variance of the observed variables. Contrarily, results for wind speed were poor, generally showing overestimation and negative values for EF. The good results for radiation and temperature likely reflect the corrections made to these variables in the blended reanalysis data set used in this study, while the lack of corrections for specific humidity and wind speed are a reason for less good estimates of RH and, mainly, poor results for the WS.

Good results for shortwave radiation and temperature and reasonably good ones for relative humidity, whose performance varied spatially, helped to obtain good results for $ET_{o\ REAN}$. The large overestimation of WS_{REAN} may have contributed to the slight over-estimation of $ET_{o\ REAN}$ that mainly affects stations in arid and semi-arid locations;

however, testing impacts of alternative estimation of WS did not show significant improvements in $ET_{o\ REAN}$.

Overall, the quality of estimates of weather variables from blended reanalysis products favors the adoption of reanalysis to estimate ET_o when full observation data sets are not available. In particular, our approach is useful for drought studies when using drought indices combining precipitation and evapotranspiration.

A set of 15 weather stations were used to assess the goodness of the NCEP2 reanalysis products using monthly data. Results revealed a consistent under-estimation of ET_o and errors more than doubled those of the blended reanalysis products used in this study. The same set of 15 weather stations was used to assess the quality of the ERA-Interim reanalysis products. Results show a consistent but small over-estimation of ET_o and errors larger than for the blended monthly reanalysis products.

An additional analysis evaluated the potential of the daily ERA-Interim reanalysis data sets in reproducing the temporal variability of the different climatic variables used to compute PM-ET_o as well as daily $ET_{o\ REAN}$ across continental Portugal. In addition, two approaches for bias correcting ET_o computed from reanalysis using different aggregation periods (month, quarter, entire period) were assessed. Results showed that, despite the limitations in representing the different variables used for computing daily PM-ET_o, the uncorrected $ET_{o\ REAN}$ results results were acceptable, with estimation errors lower than 1 mm day^{-1} in most locations and showing a tendency for over-estimation with 48% of stations having a positive bias. Thus, it appears that the uncorrected ERA-Interim reanalysis data set can be a useful tool although it should be used with caution.

The use of the additive bias correction and multiple regression approaches using month, quarter and entire period aggregation improved ET_o estimations. As expected using the month aggregation outperformed the other studied periods. However, cross-validation results did not show noticeable accuracy differences between using the different periods. Selection between approaches was based upon easiness of use, good quality of its results and ability of capturing the intra-annual seasonality of ET_o. Thus, aiming at irrigation scheduling operational purposes we propose the use of the additive bias correction using the quarter aggregation was proposed.

Chapter 6

MedPDSI, a modification of the Palmer drought severity index focusing on Olive Groves with their comparison for various climates.

LUIS S. PEREIRA, DIOGO S. MARTINS, ANA A. PAULO, PAULA PAREDES, RICARDO ROSA, CARLOS A. L. PIRES (2019) MEDPDSI, A MODIFICATION OF THE PALMER DROUGHT SEVERITY INDEX FOCUSING ON OLIVE GROVES WITH THEIR COMPARISON FOR VARIOUS CLIMATES (IN PREPARATION)

MedPDSI, a modification of the Palmer drought severity index focusing on Olive Groves with their comparison for various climates

Abstract. An adaptation of the Palmer Drought Severity Index (PDSI) for Mediterranean climate was here proposed assuming dry land olives as drought reference crop, which resulted in a revised index, the MedPDSI. It differs from the original PDSI because the olive crop, a typical Mediterranean perennial resistant to water stress, is assumed as drought reference crop aiming at the application of the soil water balance. A new soil water balance is proposed with the actual evapotranspiration computed with the FAO-PM reference evapotranspiration and a crop coefficient obtained from the FAO dual K_c approach, thus $K_c = K_{cb} + K_e$. The basal crop coefficient K_{cb} refers to transpiration and is parameterized at the month scale for a typical rainfed olives grove. The soil evaporation coefficient K_e is estimated every month as a function of soil evaporation, thus depending on monthly precipitation, evaporative atmospheric demand and the soil evaporation characteristics following FAO-PM. The self-calibrating methodology proposed to the PDSI was adopted for the MedPDSI. The MedPDSI was compared against the PDSI for selected locations in Portugal considering different climates. Comparing results of the water balance with MedPDSI and PDSI results showed relevant differences in actual evapotranspiration (ET_{act}), mainly in the transition from the dry to wet months, with a more realistic variability of ET_{act} computed with MedPDSI than with PDSI during the rainy months. PDSI and MedPDSI are similar, recognizing the same wet and dry events, with similar severity; however, droughts are identified earlier with the MedPDSI and are, generally, longer and more severe.

Keywords: Drought Indices, MedPDSI, PDSI, SPI, soil water balance, evapotranspiration, dual K_c approach

6.1 Introduction

Drought is a natural but temporary imbalance of water availability, consisting of persistent lower-than-average precipitation of uncertain frequency, duration and severity, of unpredictable or difficult to predict occurrence, resulting in diminished water resources availability and carrying capacity of the ecosystems (Pereira et al. 2009). Droughts are natural hazards, often with drastic and social environmental consequences, affecting all branches of society, from agriculture to hydropower generation and industry and can

seriously affect human activities and health (Wilhite et al. 2007; Pereira et al. 2009; Mishra and Singh 2010). Therefore, droughts may be grouped into various categories, namely, meteorological, agricultural, hydrological, water supply or groundwater drought referring to both the time when a precipitation deficit is observed and the lag time for the impacts of the water shortage being noticed across different sectors (Pereira et al. 2009).

Many different approaches have been developed to characterize the different drought types. The primary tools for drought monitoring and characterization are drought indices, which are numerical representations that measure drought characteristics such as, intensity, duration, severity, magnitude or spatial extent (Heim 2002; Keyantash et al. 2002; Mishra and Singh 2010). Among the most used indices are the Palmer Drought Severity Index (PDSI) (Palmer 1965) and its variants (Heddinghaus and Sabol 1991; Wells et al. 2004; Ma et al. 2014), or even the PDSI intermediary terms, such as the Z index (Karl 1983, 1986). Another group of indices frequently used include the Standardized Precipitation Index (SPI) (Mckee et al. 1993), the Reconnaissance Drought Index (RDI) (Tsakiris et al. 2007) and the Standardized Precipitation Evapotranspiration Index (SPEI) (Vicente-Serrano et al. 2010).

The SPI, SPEI and RDI are easy to compute, standardized and multiscalar indices, meaning that they can be computed for different time-scales and, thus, may be better suited to capture different types of droughts (Mckee et al. 1993). Moreover, these indices are standardized and normalized making them spatial and temporally comparable. The SPI uses monthly precipitation (PRE) to quantify drought severity by assessing deviations from normal precipitations amounts. The SPEI and RDI are based on the computational procedure of the SPI but consider the effect of temperature, by relating monthly precipitation with evapotranspiration (ET) either using potential evapotranspiration (PET) or reference evapotranspiration (PM-ET_o) (Vangelis et al. 2013; Beguería et al. 2014). While RDI considers the ratio PRE/PET, SPEI applies a so-called climatic water balance, which results from the difference between PRE and ET. Although SPEI and RDI incorporate the effect of global warming, by adding a temperature component, they are unable to truly reflect the relationship between precipitation and evapotranspiration, which can be accomplished by using a water balance. Moreover, studies have shown that actual evapotranspiration (ET_{act}) and ET are often anticorrelated or have decoupled relationships which reinforce the need to use of actual evapotranspiration to assess and monitor drought conditions (Hobbins et al. 2004; Brutsaert 2006; Zhang and He 2016).

In this regard, Kim and Rhee (2016) proposed a methodology to compute a drought index, the SEDI, computed solely with ET_{act}, using the Bouchet hypotheses (Bouchet 1963), without performing a water balance and without accounting for precipitation, which considers an empirical relation between ET_{act} and ET. Their results showed that the PDSI and the SEDI, computed with 9 month time scale, are comparable, although PDSI outperforms the SEDI when comparing these indices with remoted sensing vegetation indices (Kim and Rhee 2016).

The PDSI standouts from the above mentioned drought indices because it was developed with a physical background, which is necessary for the accurate estimation of moisture conditions in the soil (Dai 2011). Despite being one the first drought indices proposed, the Palmer drought severity index continues to be highly in use for drought studies (e.g.:Wells et al. 2004; Burke et al. 2006; Sousa et al. 2011; van der Schrier et al. 2011; Dai 2011; Martins et al. 2012; Paulo et al. 2012; Trenberth et al. 2014; Ma et al. 2014; Vicente-Serrano et al. 2015) and is used as an operational tool for drought monitoring, for example, in the USA and in Portugal. Despite many successful applications of the PDSI reported in the aforementioned studies, the majority of those researchers did not comment on the assumptions upon which the water balance calculation is based, which has some shortcomings in its formulation. Alley (1984) pointed to several limitations of the Palmer water balance method, including:

1. The Thornthwaite's method is a simplified procedure to estimate potential evapotranspiration (PET) as it depends only to monthly average temperature and the latitude of the considered site, ignoring aerodynamic and crop resistance factors, humidity and even the altitude of the site;
2. The attribution of 25 mm to the storage capacity of the soil's surface layer is rather arbitrary. This value will affect the PET rate, because the potential ET rate only occurs when the water is still available in the surface layer;
3. The method assumes that, whenever, monthly precipitation (PRE) is greater than monthly potential evapotranspiration (PET), the actual ET rate equals the potential ET rate for the entire month. However, as in the late summer of the Mediterranean region, the soil water content at the beginning of the month is often very low, but yet, if PRE > PET the model erroneously assumes that PET occurs at its potential rate for the entire month;

4. It is assumed that runoff do not occur until the soil's maximum holding water capacity is reached, which according to Rushton and Ward (1979) conduces to an estimation of runoff of about 25% less than that estimated when daily water balances are adopted;
5. The method fails to consider seasonal and annual changes in vegetation and root development.

Evapotranspiration is driven by more variables than temperature, such as radiation, wind speed and relative humidity, and the use of physical based equations such as the FAO-PM equation (Allen et al. 1998) improves the estimation of evapotranspiration. However, how the choice of the evapotranspiration input affects the variability of the PDSI in identifying and charactering drought must be understood. Hu and Willson (2000) studied the effect of variability of precipitation and temperature on the PDSI, using the Thornthwaite equation to compute potential evapotranspiration, and found that the index is equally affected by both precipitation and temperature if the variables have similar magnitudes of anomalies. The use of the Thornthwaite's method (Thornthwaite 1948) to estimate PET (potential evapotranspiration) as input for the PDSI, as criticized by Alley (1984), was compared against the FAO-PM Penman-Monteith reference evapotranspiration (PM-ET_o) (Allen et al. 1998) in order to access the impacts on the PDSI index (van der Schrier et al. 2011; Dai 2011; Sheffield et al. 2012). Both Dai (2011) and van der Schrier et al. (2011) did not find significant changes in the PDSI computed with both evapotranspiration equations, however, Sheffield et al. (2012) did observe an overestimation of negative PDSI trends, when computed with PET, which was not present when the PDSI was computed using PM-ET_o decreasing trends over large areas of the world. The results from Sheffield et al. (2012) are in agreement with many studies that reported a decrease in reference evapotranspiration, even though temperatures are rising (Espadafor et al. 2011; Vicente-Serrano et al. 2014), which revealed that, despite the complex computational procedure of the PDSI, the index is sensitive to the evapotranspiration input used, and thus its selection need to be carefully considered. Moreover, results from Chapter 4, with studies conducted for Inner Mongolia, from hyper-arid to humid locations, showed that there are significant differences in the temporal variability of evapotranspiration when computed with temperature methods and FAO-PM equation. The temperature methods, Hargreaves-Samani (Hargreaves and Samani 1985), or the Penman-Monteith temperature only method (Allen et al. 1998)

showed consistent trends for the increase of evapotranspiration for all types of climates, whereas decreasing trends were often observed with PM-ET_o, despite the increase of both minimum and maximum temperature observed in all locations in those studies. Reasonable good results were observed, when compared to local computed PM-ET_o, and the errors of estimation were, in average, lower with the PM-ET_o computed with reanalysis than when evapotranspiration was computed with temperature methods.

Despite the importance of the selection of ET estimation to be used for PDSI computations, other studies have analysed drought trends. Sousa et al. (2011) studied the temporal variability of droughts in the Mediterranean region with the PDSI and the Sc-PDSI from the CRU (Climate Research Unit) data sets, regarding the period (1901-2002). Both indices were computed using precipitation and temperature, thus using the Thornthwaite equation for estimation of PET. Results showed a clear drying trend in the 20^{th} century, with exception of the northwestern region on the Iberian Peninsula and concluded that the main driver of drought variability in the region was the NAO (North Atlantic Oscillation), most relevant in the winter. However, for the period 1941-2006, Martins et al (2012) found no significant trends for drought aggravation using the PDSI, computed with PET from Thornthwaite, in Mainland Portugal. Other studies have used climate projections to understand drought variability and extreme events occurrence in the future using different climate models to predict future climate conditions (Burke and Brown 2008; Sheffield and Wood 2008; Wehner et al. 2011; Im et al. 2012; Tian-Jun and Tao 2013; Liu et al. 2013a; Bonsal et al. 2013). All studies point to an increased drought frequency with the PDSI, usually more significant than the SPI changes (Burke and Brown 2008; Bonsal et al. 2013; Lui et al. 2013a). Im et al. (2012) emphasized the importance of temperature trends on the PDSI since the same PDSI computed with detrended time series of temperature did not revealed the decreasing trends present when the PDSI was computed with the original temperature data. Moreover, Bonsal et al. (2013) concluded that bias corrections are important when using climate models to better reproduce the observed statistics of the PDSI.

Another issue of the PDSI model was addressed by Wells et al. (2004) with the creation of the self-calibrating PDSI (Sc-PDSI). These authors tackled the issue of the lack of comparability of the PDSI between diverse climatological regions (Alley 1984; Guttman et al. 1992). This was related with the fact that Palmer introduced empirical constants in the PDSI algorithm from limited amount of data and specific to the US Great Plains,

which resulted in inconsistent behaviors of the PDSI when computed for other locations. This resulted in PDSI with a larger frequency of extremes larger than expected and with an apparent bimodal distribution for locations with different climates (Wells et al. 2004; van der Schrier et al. 2006). The methodology proposed to solve this issue replaces the climatic characteristic and duration factors, derived empirically by Palmer with values computed for each location, which are based upon the climate of the data. This implementation improved the index performance, with consistent results for different climates and allowing for more accurate comparisons of the PDSI for different locations (Wells et al. 2004; van der Schrier et al. 2006; Dai 2011).

A different approach to standardize the PDSI was suggested by Ma et al. (2014) in which a new methodology, also based on procedures of the PDSI and the SPI was developed. The authors proposed a new index, the standardized Palmer drought index (SPDI) which used the moisture departure index, D, computed using the PDSI soil water balance and then transforms it into a standard normal variable by fitting the observed moisture departures to a General Extreme Value distribution while avoiding the empirical constants of the PDSI and simplifying the index computation.

Heddinghaus and Sabol (1991) also identified an additional potential problem regarding the original PDSI computation. The authors discussed that the backtracking procedure proposed by Palmer in the original PDSI was not adequate for real-time monitoring of drought, since the values of several previous months could change according to the value of the current month. So, the authors developed a weighing calibration tool that removes backtracking, which creates more subtle transitions from dry to wet spells.

The Z_{index} was considered a better indicator of short-term agricultural drought because it is sensible to variations in soil-moisture (Karl 1986). Dai et al. (2004) compared both the PDSI and the corresponding Z_{index} against mean monthly soil moisture, in the first 1 m depth of soil, and found the PDSI values were more consistently correlated with soil moisture than the Z_{index}, in many locations in China. Concordantly a study by Wang et al. (2015) for China, revealed that the PDSI was better to capture soil moisture variability in deeper layers of the soil (from 0.9 to 1 m depth) whereas, the Z_{index} performed better than the PDSI and the Sc-PDSI in characterizing soil moisture in most surface layers (0 to 5 cm). Another interesting result is that the PDSI was better correlated with soil moisture in the first 1 m of soil than the Sc-PDSI. However, Quiring and Papakryiakou (2003)

found that the Z_{index} was better suited to measure agricultural drought in the Canadian prairies than the PDSI or the SPI. The performance of Z_{index} could, however, improve if the methodologies for the local calibration of the climatic characteristic were implemented (Wells et al. 2004), since the original parameters of the PDSI were calibrated for the central United States of America conditions, as discussed by Dai et al. (2004). The MedPDSI, using an updated water balance, purposely developed to better capture the Mediterranean climate and by applying, the self-calibrating methodology could improve the capabilities of its Z_{index} in capturing more accurately agricultural drought and the variation of soil moisture in the soil.

To face some of deficiencies regarding the PDSI water balance Mo and Chelliah (2006) used the National Centers for Environmental Prediction (NCEP) North American Regional Reanalysis (RR) data to create a version of the PDSI, the MPDSI, and replaced the input data in the soil water balance to include more accurate fields from the RR itself, eliminating the assumptions of a two-layered soil and the need to define an available water capacity, although maintaining most of the Palmer's original procedures. Such data included: potential evapotranspiration, evaporation, runoff, total soil moisture, and soil moisture change were used from the RR and thus ET computed with the Thornthwaite is not necessary. Moreover, the potential recharge is obtained, as the total soil moisture required to achieve total soil moisture in a given grid point for each month of the year and the potential precipitation is the maximum precipitation at each grid point for a given calendar month.

Drought indices have been studied to assess drought impacts on crops, to understand how droughts relate with crop yields and to understand crop vulnerability to droughts (e.g.: Mavromatis, 2007, Tunalıoğlu and Durdu, 2012 and Popova et al. 2014). Popova et al 2014 assessed the vulnerability of the maize crop to droughts in Bulgaria, and compared the SPI-2 relative to July and august against the relative yield decrease (RYD) and found strong correlations between the drought index and the yield. Mavromatis (2007) tested the SPI, PDSI, Sc-PDSI and PDSI computed using Priestlay–Taylor's as the evapotranspiration estimate, combined with climate change scenarios provided by Hadley Centre regional climate model HadRM3, in order to assess rainfed wheat vulnerability to climate change in two pilot crop regions in north and central Greece. These authors found that PDSI and Sc-PDSI were better at predicting wheat yields; however the relationship between the drought indices and the crop yields was weak when soil moisture was not an

important yield limiting factor. This study also showed that using the Priestlay–Taylor's to compute PET did not improve the yield predicting capabilities of the PDSI. Moreover, the yield projections showed significant decreases, up to 3.14 tn yr^{-1} in the region. Another study conducted by Tunalıoğlu and Durdu (2012) used a variety of drought indices to test which was more appropriate to assess olive (O. europaea L.) yield productions in Turkey and its vulnerability to climate change using future projections. Results showed that the Sc-PDSI was the index that explained most of variability of the olive crop yields in majority of the locations tested, followed by the PDSI. Likewise, McCarl et al. (2008) tested for changes in mean and variance of crop yields of corn, cotton, sorghum soybeans and winter wheat with data from 1960 to 2007 in the USA to assess the stationarity in these crop yields time series. Furthermore, the PDSI was compared against these time series and, except for cotton which as less affected by drought occurrence, the drought index was positive and significantly correlated with the crops. The authors also studied the impacts of changes in precipitation and temperature and results showed that precipitation intensity and drought have larger impacts on crop yields than annual precipitation amount and that a higher variability in temperature have significant negative impacts on crop yields. These results suggested, then, that the variability of precipitation temperature and PDSI have significant impacts of crop yields and that stationarity should not be assumed without caution in models that use weather data that is subject to climate change (McCarl et al. 2008).

The present study aims to test how the new soil water balance, developed for the MedPDSI, changes and affects the drought index and all its intermediate outputs, when compared to the original PDSI. The performance of the MedPDSI's water balance is also tested for different locations in mainland Portugal comparatively to the PDSI. For that matter: (1) the water balance results from both methods were compared; (2) The coefficients potentials, climatic characteristic and the Z_{index} were also compared, to evaluate how the index behaves for different climate conditions; (3) the new duration factors, computed using the self-calibrating procedure were analyzed and (4) the drought indices were compared, so its main differences may be analyzed to understand how the MedPDSI may improve drought detection and characterization in the Mediterranean conditions.

6.2 Data and Climate

For this study, monthly precipitation time series for the period 1941-2006 from 26 meteorological stations distributed along Continental Portugal (Figure 6-1), were used in combination with potential evapotranspiration (PET) using the Thornthwaite equation (Thornthwaite 1948) and the FAO-PM Penman-Monteith reference evapotranspiration (Allen et al. 1998) both estimated using a global blended reanalysis data set (Sheffield et al. 2006) to compute, respectively the PDSI and the MedPDSI. The PDSI was computed with the Thornthwaite equation to maintain the original methodology proposed by Palmer.

The data retrieved from the reanalysis data set consisted on maximum and minimum temperature (ºC) wind-speed (m s^{-1}), downwards shortwave radiation (MJ m^2 d^{-1}) and relative humidity (%). PET was computed with maximum and minimum temperature and PM-ET_o was computed with all 5 variables. This data set, which as a spatial resolution of 0.5º x 0.5º (Figure 6-1), and spans from 1948-2008, was used to assess the accuracy of monthly ET_o estimations for the Iberian Peninsula in a previous study (Chapter 5). The PDSI and MedPDSI were computed for the common period of both data sets, 1948-2006.

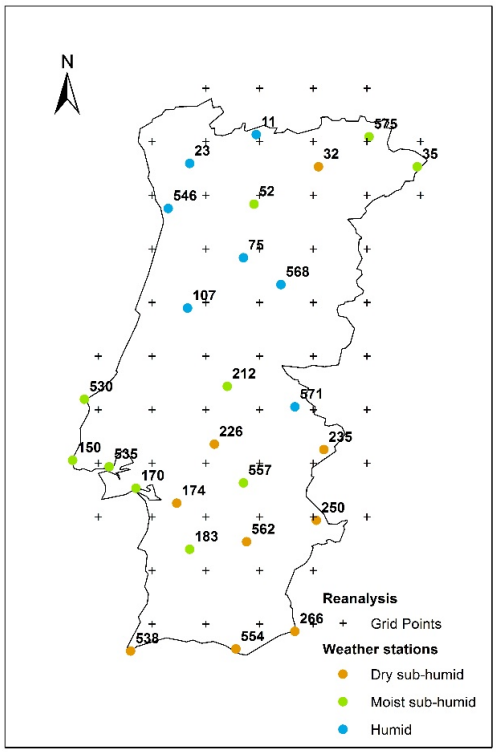

ID	Station	Latitude	Longitude	Aridity index
266	Vila Real S. António	37.19	-7.42	0.53
250	Amareleja	38.22	-7.22	0.55
554	Faro	37.02	-7.97	0.55
538	Sagres	37	-8.95	0.56
32	Mirandela	41.52	-7.2	0.57
235	Elvas	38.88	-7.15	0.59
226	Mora	38.93	-8.17	0.61
562	Beja	38.02	-7.87	0.62
174	Alcacer do Sal	38.38	-8.52	0.63
183	Alvalade do Sado	37.95	-8.4	0.65
150	Cabo da Roca	38.78	-9.49	0.67
557	Évora	38.57	-7.9	0.70
530	Cabo Carvoeiro	39.35	-9.38	0.75
35	Miranda do Douro	41.52	-6.28	0.75
535	Lisboa	38.72	-9.15	0.82
212	Alvega	39.47	-8.05	0.83
170	Setúbal	38.52	-8.9	0.86
52	Régua	41.17	-7.8	0.91
575	Bragança	41.8	-6.73	0.92
571	Portalegre	39.28	-7.42	1.03
107	Coimbra	40.2	-8.42	1.07
75	Viseu	40.67	-7.9	1.26
546	Porto	41.13	-8.6	1.57
23	Braga	41.55	-8.4	1.80
11	Montalegre	41.82	-7.78	2.10
568	Penhas Douradas	40.42	-7.55	2.36

Figure 6-1 Map with the location of the reanalysis gridpoints used and the weather stations classified by aridity (on the left) with the coordinates of the weather stations the respective aridity index on the right. Highlighted locations were selected to depict the behaviour of the drought indices for different climates.

To homogenize the precipitation data with the reanalysis data set, used for computing PM-ET_o and PET, the nearest reanalysis grid-point to each weather station was selected, and maximum and minimum temperature (T_{max} and T_{min}) were bias corrected for those locations using observed time series, and following a methodology approach similar to the one proposed in Chapter 5. Firstly, T_{max} and T_{min} were corrected for the difference in elevation between the grid-point selected and the location with the observed data, considering a lapse rate of 6.5 ºC km^{-1} (Soares et al. 2012b and Chapter 5). Temperature was bias corrected using an additive correction scheme that corrects the mean value of the reanalysis time series to match the mean value of the observed time series. For this study, following the results of Chapter 5 regarding the daily data analysis, the time series were divided into four trimesters to better capture the interannual variability of temperature for both the observations and the reanalysis data. Moreover, to correct T_{min} and T_{max}, the temperature range (TR), was computed for both the observed and the reanalysis data. Then the bias correction scheme was applied to T_{max} and TR with T_{min} =

T_{max} -TR. This approach links the correction of both temperatures, thus avoiding $T_{min} > T_{max}$.

The aridity index was computed for all the 26 locations to represent the country different types of climate, from dry sub-humid in the south to humid climate in the North-western regions according to the Aridity Index (UNEP 1997). The Aridity Index was computed from the ratio between precipitation and PET, computed for the 30 year period of 1976-2006. Furthermore, from the 26 stations used in this study, 6 were selected to demonstrate the behavior of the drought indices and the differences between the PDSI and MedPDSI according to the climate, and are highlighted in Figure 6-1. Those stations are Faro and Elvas representing the dry sub-humid climate, Alvalade do Sado and Miranda do Douro representing the moist sub-humid locations, Viseu, and Montalegre relative to the humid locations.

Figure 6-2 shows the 59 year mean of the intraanual variability of precipitation, PM-ET_o and PET on the 6 weather stations selected to describe the different climates in Mainland Portugal. There was a high variability of the average annual precipitation amount in the selected locations. Precipitation increased from the dry sub-humid locations to the humid locations with average annual amounts of 513 mm in Faro to 1490 mm in Montalegre. Moreover, the majority of the rainfall occurred in the autumn and winter with very dry summer months, especially in the dry and moist sub-humid locations.

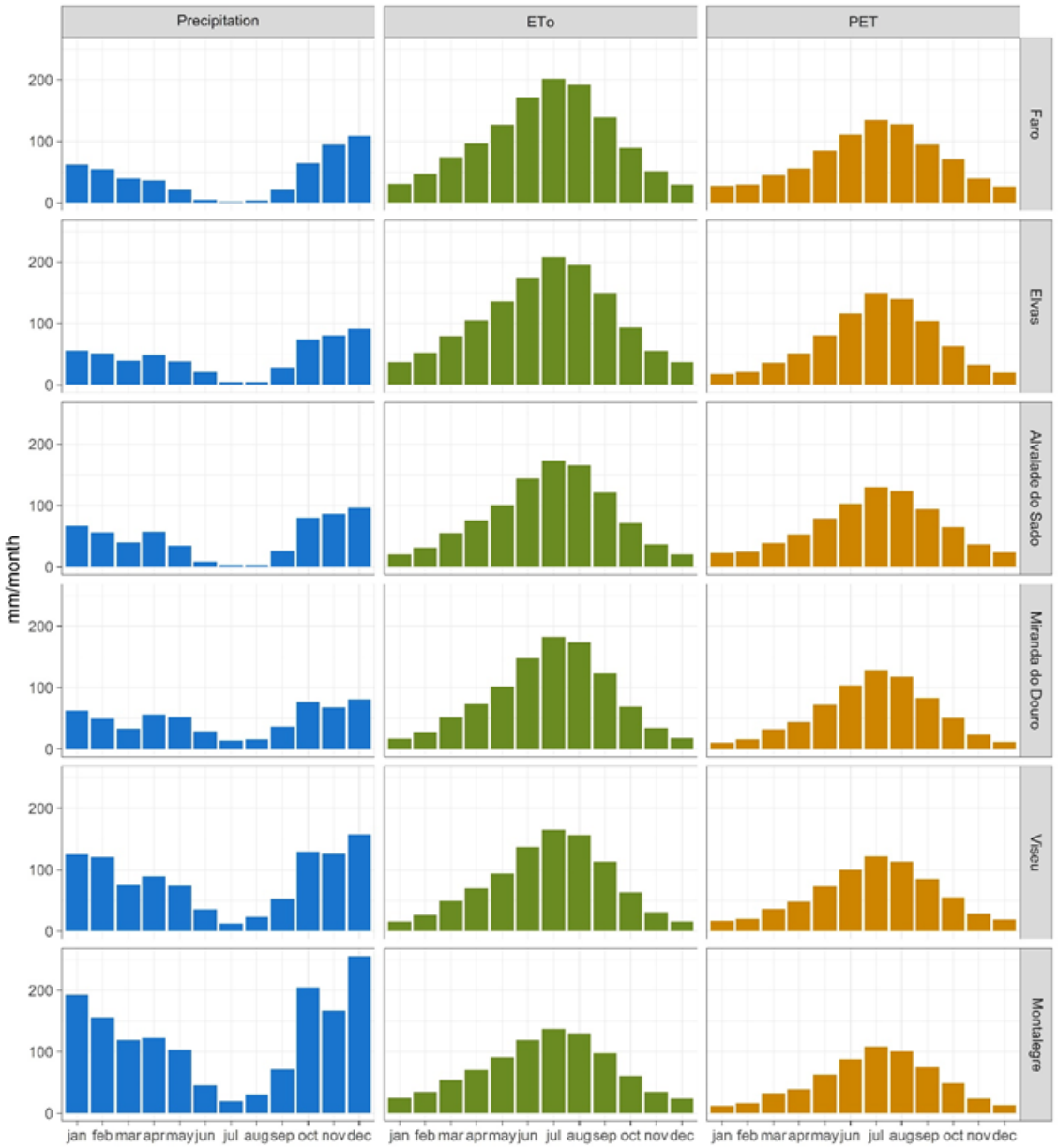

Figure 6-2 Intraannual variability of precipitation, Reference Evapotranspiration (PM-ET_o) and Potential Evapotranspiration (PET), considering monthly means relative to the period 1941-2006 for 6 selected stations and ordered by aridity, from dry-sub-humid to humid.

Differently, PM-ET_o and PET were higher in summer, with its maximum values in July or August for all stations and was lowest in the winter, when temperature is lower. There were noticeable differences between PM-ET_o and PET. The annual amounts of PM-ET_o were larger than the PET counterparts, reaching 1320 mm per year in Elvas with PM-ET_o but with PET, the annual average was only 829 mm per year. Moreover, the difference between PM-ET_o and PET was always larger than 200 mm $year^{-1}$. However, this difference was more pronounced in the summer months reaching 28 mm in July in Montalegre and 68 mm in July in Elvas and smaller in late autumn and winter with PET

being slightly larger than PM-ET_o in Alvalade and Viseu in December and January. These differences may impact the water balance results of PDSI and MedPDSI in the following section (6.5) and this issue will be discussed.

6.3 Computation of the PDSI

The PDSI was developed to be used as a meteorological drought index and is based upon a water supply and demand, computed with a monthly soil-water balance using monthly records of precipitation and temperature for a two layer soil (Palmer 1965). It was developed and calibrated to assess and quantify meteorological drought in the Great plains of USA considering the environmental and crop conditions of the area, mainly assuming the winter wheat as the drought reference crop (Palmer 1965). The PDSI measures the deviation between observed and the expected precipitation to maintain climatic normal moisture conditions. This deviation will then be used to compute the moisture anomaly index (Z_{index}), which is a standardized measure of the difference between the humidity conditions of a given month and the average humidity conditions for that month. Then, the final PDSI value is computed as a weighted combination of the Z_{index} value for that month and the PDSI value of the previous month.

Table 6-1 Classification of severity of drought/wetness events of the PDSI

Classification	Range of PDSI and MedPDSI Values
Extreme wet spell	≥ 4
Severe wet spell	3.00 to 3.99
Moderate wet spell	2.00 to 2.99
Mild wet spell	1.00 to 1.99
Incipient wet spell	0.50 to 0.99
Near Normal	0.49 to -0.49
Incipient drought	-0.50 to -0.99
Mild drought	-1.00 to -1.99
Moderate drought	-2.00 to -2.99
Severe drought	-3.00 to -3.99
Extreme drought	≤ -4.00

These weights determine if the PDSI is more sensitive to sudden changes in moisture anomaly or if the PDSI values are more influenced by the past moisture conditions. The PDSI was created to be a standardized measure of moisture anomaly and the PDSI computations procedures attempt to fit the index to the 11 categories defined in (Palmer 1965) to classify drought and wetness events (Table 6-1).

Soil Water Balance

In Palmer's formulation, the generic equation of the soil water balance computed on a monthly basis is described by:

$$\mathrm{PRE} = \mathrm{ET_{act}} + \mathrm{RO} + (\mathrm{R} - \mathrm{L}) \quad (6.1)$$

where PRE is the precipitation, ET_{act} the actual evapotranspiration, RO the runoff, R is the soil water recharge and L the soil water loss, all expressed in mm. The variation of the soil water reserve is the difference between R and L. R and L are mutually exclusive, meaning that in a given time interval (month) when there is recharge (R>0) L is null and, if there is water loss (L>0) the recharge is zero.

The Original PDSI was based on a two-soil layers water balance where the the water holding capacity (SWC) of the surface layer is 25 mm (and the underlying layer a SWC of 127 mm for the Western Kansas location and 228 mm for Central Iowa. These values depend upon soil characteristics and may be modified according the location specifications. For this application the PDSI was computed considering a surface layer with 25 mm of water holding capacity and underlying layer with 200 mm, so the PDSI results may be comparable with the MedPDSI which was computed considering a soil with a total available soil water, TAW = 150 mm/m and soil depth of 1.5 m.

The evapotranspiration occurs at its potential rate until water in the surface layer is depleted. The consumption of water of the underlying layer starts when the surface layer is empty.

If PET equals or exceeds precipitation, the water loss in the surface layer, L_s, is given by

$$\mathrm{L_s} = \min\left[\mathrm{S_s}, \mathrm{PET} - \mathrm{PRE}\right] \quad (6.2)$$

and the water loss in the underlying layer L_u is

$$\mathrm{L_u} = (\mathrm{PET} - \mathrm{PRE} - \mathrm{L_s})\frac{\mathrm{S_u}}{\mathrm{TAW}} \quad (6.3)$$

where S_s and S_u correspond to the stored water, by the end of the previous month, in the surface and underlying layers, respectively, and TAW is the total available soil water, i.e., the sum of the SWC of the two layers.

Recharge is assumed to occur every time precipitation exceeds PET and the stored water in one or both layers, by the end of the previous month, is below field capacity; the recharge of the underlying layer initiates when the surface layer reaches the field capacity. Water loss occurs after field capacity is attained in both layers and was designated as Runoff by (Palmer 1965), however it is the combination of surface runoff and deep percolation.

Besides PET, three additional potential terms were introduced by Palmer, the potential recharge (PR), potential loss (PL) and potential runoff (PRO) all expressing the hypothetical maximum conditions relative to their respective actual values in the soil water balance.

PR is defined as the amount of water needed to bring the soil water content to the field capacity:

$$\mathrm{PR} = \mathrm{TAW} - (\mathrm{S_S} + \mathrm{S_u}) \tag{6.4}$$

PL is the amount of water that the soil may be lost by evapotranspiration when PRE = 0 and is fractioned in the two layers:

$$\mathrm{PL} = \mathrm{PL_s} + \mathrm{PL_u} \tag{6.5}$$

where

$$\mathrm{PL_s} = \min[\mathrm{PET}, \mathrm{S_S}] \tag{6.6}$$

$$\mathrm{PL_u} = (\mathrm{PET} - \mathrm{PL_s})\frac{\mathrm{S_u}}{\mathrm{TAW}}, \mathrm{PL_u} \leq \mathrm{S_u} \tag{6.7}$$

PRO, as defined by Palmer, corresponds to the difference between potential precipitation and potential recharge and Palmer adopted for the potential precipitation the value of TAW. So PRO is given by:

$$\mathrm{PRO} = \mathrm{TAW} - \mathrm{PR} = \mathrm{S_s} + \mathrm{S_u} \tag{6.8}$$

The moisture anomaly index (Z_{index}) is a standardized measure of the difference between the humidity conditions of a given month and the average humidity conditions for that month.

The Z_{index} is obtained from the moisture departure (D), which is the deviation between the actual precipitation of the month i, PRE_i, and the precipitation that is expected to occur for that month to maintain climate conditions, $\widehat{PRE}_i$. D is then computed from the following equation:

$$D_i = PRE_i - \widehat{PRE}_i \quad (6.9)$$

where $\widehat{PRE}_i$ is

$$\widehat{PRE}_i = \alpha_j PET_i + \beta_j PR_i + \gamma_j PRO_i + \delta_j PL_i \quad (6.10)$$

where PET_i, PR_i, PRO_i and PL_i refer to time interval i. The coefficients α_j, β_j, γ_j, and δ_j are the ratios between the average of each of the actual values for ET, soil moisture recharge, runoff, and soil moisture depletion and the average of the corresponding potential values (PET, PR, PRO, and PL) over a calibration period. The j= 1 to 12 refers to the month of the year. Usually, these potential values are computed for the complete time series of each variable, however, a smaller period may be used as reference and this selection can have a significant impact on the frequency of extreme events detected in both drought indices (Karl 1986; Chapter 3). Results in Chapter 3 showed that when using non-stationary time series, with changes in mean through time, the selection of a reference period matters, i.e., if the reference period is dry (wet), then the PDSI will have more frequent wet (dry) events. Recent studies (Martins et al. 2012; Paulo et al. 2012) showed no significant trends for the PDSI and MedPDSI in Portugal for the period of time analyzed herein (1948-2006) and, for that reason, both potential coefficients of MedPDSI and PDSI were computed using the complete time series.

Moisture Anomaly Index

Z_{index} is then computed for month i as:

$$Z_{index\,i} = K_j D_i \quad (6.11)$$

where K_j is the climatic characteristic which is a dimensionless weighting factor, computed for each month j of the year, and is responsible for the standardization of the moisture anomaly to better suit local conditions. K was empirically calibrated by Palmer using 9 different location in the USA and can be defined as:

$$K_j = \widetilde{K}_j K'_j \quad (6.12)$$

where,

$$K'_j = 1.5\log_{10}\left[\frac{T_j+2.8}{\overline{D}_j}\right] + 0.5 \quad (6.13)$$

$$\text{and, } T_j = \frac{\overline{PE}_j + \overline{R}_j + \overline{\overline{RO}}_j}{\overline{P}_j + \overline{L}_j} \quad (6.14)$$

where T_j is a measure of the ratio between the average moisture demand and the average moisture supply for the studied region and for the month j:

finally, $\widetilde{K}_j$ is obtained with,

$$\widetilde{K}_j = \frac{17.67}{\sum_{i=1}^{12} \overline{D}_j K'_j}, \quad (6.15)$$

where $\overline{D}_j$ is the average of the absolute values of D for month j over the calibration period, the constant 17.67 is the annual sum of the weighted average departures. $\widetilde{K}$ can be interpreted as the ratio between the expected and the observed values of the annual means of D. Though K was introduced by Palmer to adjust D to better measure the magnitude of positive/negative moisture anomalies according to local conditions, it still produces spatially inconsistent PDSI values, mainly due to the 17.67 constant in (equation 6.15) obtained as the average Z_{index} of the 9 locations used by Palmer to empirically calibrate the PDSI. Wells et al. (2004) suggested a methodology that adjusts Z_{index} to local conditions by computing a local K_j which depends upon the characteristics of the individual time series, given by:

$$K_j = \begin{cases} K'_j \frac{-4}{PDSI_{2nd}}, \text{if } d_{i,j} < 0 \\ K'_j \frac{4}{PDSI_{98th}}, \text{if } d_{i,j} > 0 \end{cases} \quad (6.16)$$

By adjusting K_j as such, extreme drought and wet events will have a have distribution tails more acceptable for extreme events, i.e., 2% of all events should be extremely dry or extremely wet (Wells et al. 2004).

After computing the moisture anomaly index, the PDSI is computed with a backtracking procedure for each month i from:

$$X_i = 0.897X_{i-1} + \frac{1}{3}Z_{index\ i} \quad (6.17)$$

X_i and X_{i-1} are, respectively, the severity of the event relative to the month i and month i- 1, and $Z_{index\ i}$ is the moisture anomaly index in the period i. The values 0.897 and 0.33

are constant values derived by Palmer in 1965 and are called “duration factors” and were the same to for wet and dry spells.

Following Wells et al. (2004) the duration factors may be updated for every time series by replacing the empirical values in equation (6.17) by a generic equation as:

$$X_i = pX_{i-1} + qZ_{index\,i} \quad (6.18)$$

where p is computed as:

$$p = \left(1 - \frac{b}{b+a}\right) \quad (6.19)$$

and q is:

$$q = \frac{c}{b+a} \quad (6.20)$$

where b is the slope and a is the intercept relative to the linear regression of the cumulated values of $Z_{index\,i}$ during the driest periods of lengths l_d vs the lengths l_d of the dry periods (2, 4, 6,..., 20 months). The duration factors were proposed to be calibrated for the extremely dry and wet events with c = –4 and c = 4, respectively (Wells et al. 2004). The duration factors reflect the sensitivity of the index to the month’s precipitation amount, i.e., when p is high and q is lower, the precipitation anomaly in a month will have less impact in the index (Wells et al. 2004). For this study, in order to compute both the PDSI and the MedPDSI the first method proposed by (Dai 2011) was used, that consists on using all Z_{index} values to obtain the smallest/highest sum of Z_{index} for the driest/largest sums of Z_{index} for a given time length. In this case, 12 time lengths were considered, from 2 to 24 months.

6.4 MedPDSI soil water balance

The drought index tested in this study, the MedPDSI, is an adaptation of the PDSI for the Mediterranean conditions, by changing the PDSI water balance by a soil water balance applied to an olive orchard, in which the dual crop coefficient (K_c) approach was adopted, estimating separately soil evaporation and transpiration of the olive crop (Allen et al. 1998). The current MedPDSI model is a modification from that proposed by Pereira et al. (2007), with changes in the estimation of ET_{act} and available soil water, evaporation and runoff. Moreover, the self-calibrating procedures used for the computation of the PDSI, described in the previous section, were also included in the MedPDSI model.

The MedPDSI uses monthly precipitation and PM-ET_o, and can be computed for different soil types, according to soil texture, with different TAW or soil depths. The initial percentage of the soil water content can also be defined. In this application, a soil with a TAW = 150 mm/m and a rooting depth of a mature olive grove of 1.5 m (Allen et al. 1998) was adopted.

The generic equation for the soil water balance model proposed for the MedPDSI is:

$$\Delta ASW = PRE - ET_{act} - (RO + DP) \quad (6.21)$$

where ΔASW is the variation of the available soil water stored (ASW) in the root zone within the month, ET_{act} is the actual crop evapotranspiration, RO is the surface runoff due to non-infiltrated precipitation, and DP is the deep percolation through the bottom of the root zone.

ET_{act} is computed through the soil water balance. The counterpart potential term is the maximum crop evapotranspiration (ET_c), given by:

$$ET_c = K_c ET_o \quad (6.22)$$

where K_c is obtained using the FAO-56 dual K_c approach and ET_o is the reference evapotranspiration as

$$K_c = K_{cb} + K_e \quad (6.23)$$

where K_{cb} is the basal crop coefficient and K_e is the soil evaporation coefficient. Water use and evapotranspiration of olive orchards has been often studied, recently adopting the dual K_c approach (e.g.: Allen and Pereira 2009; Cammalleri et al. 2013; Paço et al. 2014). The basal crop coefficient K_{cb} refers to transpiration and is parameterized at the month scale for a typical rainfed olive grove with 30% ground cover based upon the referred studies. The resulting K_{cb} values are: 0.33 for the months of January to April and the autumn months of November and December, 0.28 for the summer months of June through September, and 0.30 for the transition months of May and October.

K_e is computed following the equation:

$$K_{e_i} = K_{cor}(0.2424 - 0.00131ET_{o_i} + 0.002875PRE_i + 0.00126PRE_{i-1}) \quad (6.24)$$

with K_e restricted to $0 \leq K_e \leq (1.2\text{-}K_{cb})$ and depending upon PM-ET_o, the precipitation of the current and of the previous month, respectively, PRE_i and PRE_{i-1}. K_e is further corrected for the evaporative characteristics of the surface soil layer with K_{cor}. For sandy soils, less capable of retaining water a $K_{cor} = 0.9$ was considered, for loam soils a $K_{cor} = 1.0$ was used, and for heavier, silt and clay soils, that retain more water a K_{cor} of 1.1 was used. Moreover, the K_e equation was obtained by applying a multi regression analysis to simulations of olive crop water balances performed for various types of climate in Portugal and considering different soils using the SIMDualKc model (Rosa et al. 2012). Figure 6-3 shows the K_e monthly mean for all the 26 locations used in this study. It reveals an appropriate variability of K_e, decreasing in summer when there is less available water in the soil and increasing in the rainy months.

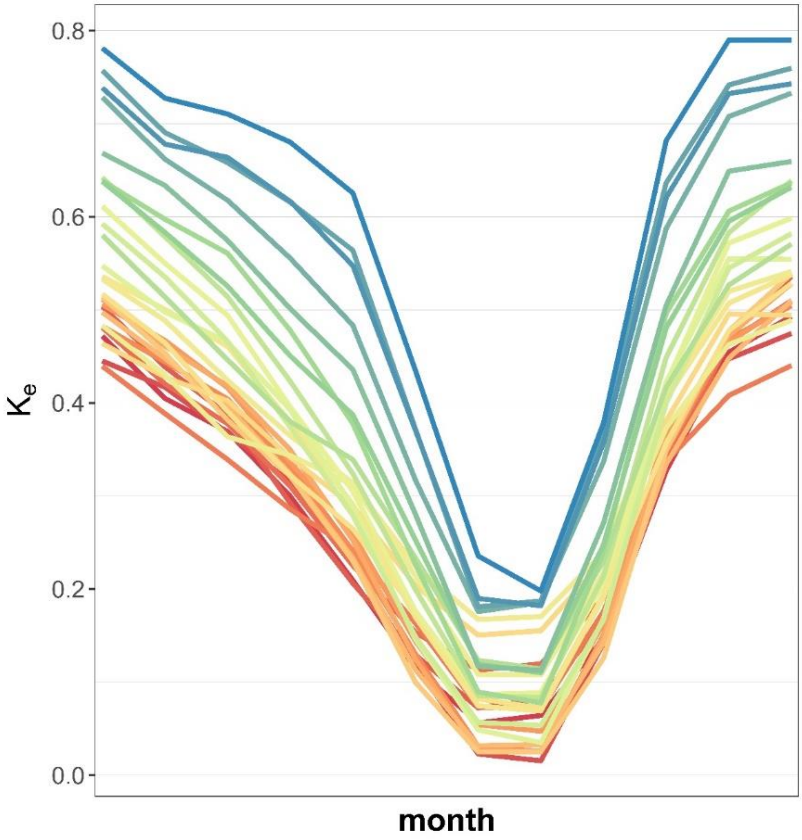

Figure 6-3 Evaporation coefficient (K_e) computed for all 26 locations, from the humid stations ( ) to the dry sub-humid stations ( ) considering a loam soil.

Following the methodology proposed by Doorenbos and Pruitt (1977) for the computation of the soil water balance, water is readily available for the crop between two boundaries that are dependent upon soil and crop characteristics. The upper boundary, R_{max}, refers to the available soil moisture at field capacity which is the amount of water that can be extracted by the vegetation from the soil, and is given by:

$$R_{max} = z_r TAW \quad (6.25)$$

where z_r (m) is the root depth (1.5 m for this application) and TAW is the total available water, i.e., the difference between field capacity and wilting point (mm m^{-1}) of a soil 1 m depth. The lower boundary of the optimal yield zone, also known as the optimal yield threshold (OYT) is obtained by:

$$OYT = (1 - p')R_{max} \quad (6.26)$$

in which p' is the soil water depletion fraction for no stress, i.e., the fraction of available soil water that allows for evaporation without stress for the crops. A p' = 0.65 was used in this application, following Allen et al. (1998).

Under stress conditions, i.e., when the available soil water in the beginning of the month is lower than the optimal yield threshold, OYT > $ASW_{ini,}$ then the available soil water content at the end of month (ASW_{fin}) is computed as:

$$ASW_{fin} = \frac{OYT*PRE}{ETc} + \left(ASW_{ini} - \frac{OYT*PRE}{ETc}\right) * \exp(-ETc * OYT) \quad (6.27)$$

and $ET_{act} < ET_c$ obtained as:

$$ET_{act} = ASW_{ini} - ASW_{fin} - PRE \quad (6.28)$$

since surface runoff and deep percolation are 0. Complementary, when OYT ≤ ASW_{ini}, there is no stress for the crop in that month which means that $ET_{act} = ET_c$, and the ASW_{fin} is given by:

$$ASW_{fin} = ASW_{ini} + PRE - ET_{act} \quad (6.29)$$

Moreover, if $ASW_{fin} > R_{max}$, the surface runoff plus deep percolation is obtained as the difference between ASW_{fin} and R_{max} and then ASW_{fin} is set equal to R_{max}.

After the soil water balance, the computational procedures for the MedPDSI are the same as those described for the PDSI, in section 6.3, although the determination of the potential loss (PL) for the MedPDSI is different from the PDSI, since equations 6.6 and 6.7 proposed by Palmer (1965) are not adequate for the MedPDSI. Palmer defined PL as the amount of soil moisture that could be lost if the precipitation of that month would be 0. Following this definition, PL, for the MedPDSI, was computed using equations 6.27 and

6.29 when in conditions of stress and no stress, respectively, but with the precipitation term as 0. Furthermore, PR is given by the difference between the TAW and the ASW_{ini} and PRO is given by TAW − PR.

6.5 Comparing PDSI and MedPDSI Soil Water Balance

Differences in PDSI and MedPDSI soil water balance models produce, necessarily, different results for the water balance terms. Moreover, these differences will be enhanced by the different evapotranspiration equations: the PDSI used PET, computed using the Thornthwaite equation whereas the MedPDSI used the reference evapotranspiration computed with FAO-PM Penman-Monteith equation. While PM-ET_o was generally higher than PET (Figure 6-2), ET_c, computed with equation 6.22, was often lower than PM-ET_o for most months, because $K_{cb} + K_e < 1.2$, resulting in mean ET_c values lower than PET. These differences were more noticeable in the summer, for all locations (Figure 6-4). Thus, this had an obvious impact in the resulting mean ET_{act} obtained from the both the PDSI and MedPDSI water balance. ET_{act} from the PDSI soil water balance ($ET_{act\ PDSI}$) was much lower than its potential counterparts in the summer months, when less water is available for evapotranspiration and it was closer, in mean, to PET in the rainy months. However, since ET_c was much smaller than PET in the summer, the differences between ET_c and ET_{act} from the MedPDSI soil water balance ($ET_{act\ MedPDSI}$) were lower than the PDSI counterparts.

The intra-annual variability of runoff plus deep percolation was also similar when comparing these outputs from the MedPDSI and PDSI (Figure 6-4). For both the PDSI and MedPDSI SWB, RO+DP increased with humidity, i.e., was smaller in Faro and higher in Montalegre, the most humid location of the selected stations. Moreover, RO+DP for both SWB, was higher in the rainy months, from December to March, reaching 0 in July and August in all locations. Furthermore, analysing the differences between the RO+DP that resulted from both SWB it was observed that with the PDSI, RO+DP was higher, for the locations of Faro and Elvas, in all months in which RO+DP occurred, being twice as larger in January and February in Faro.

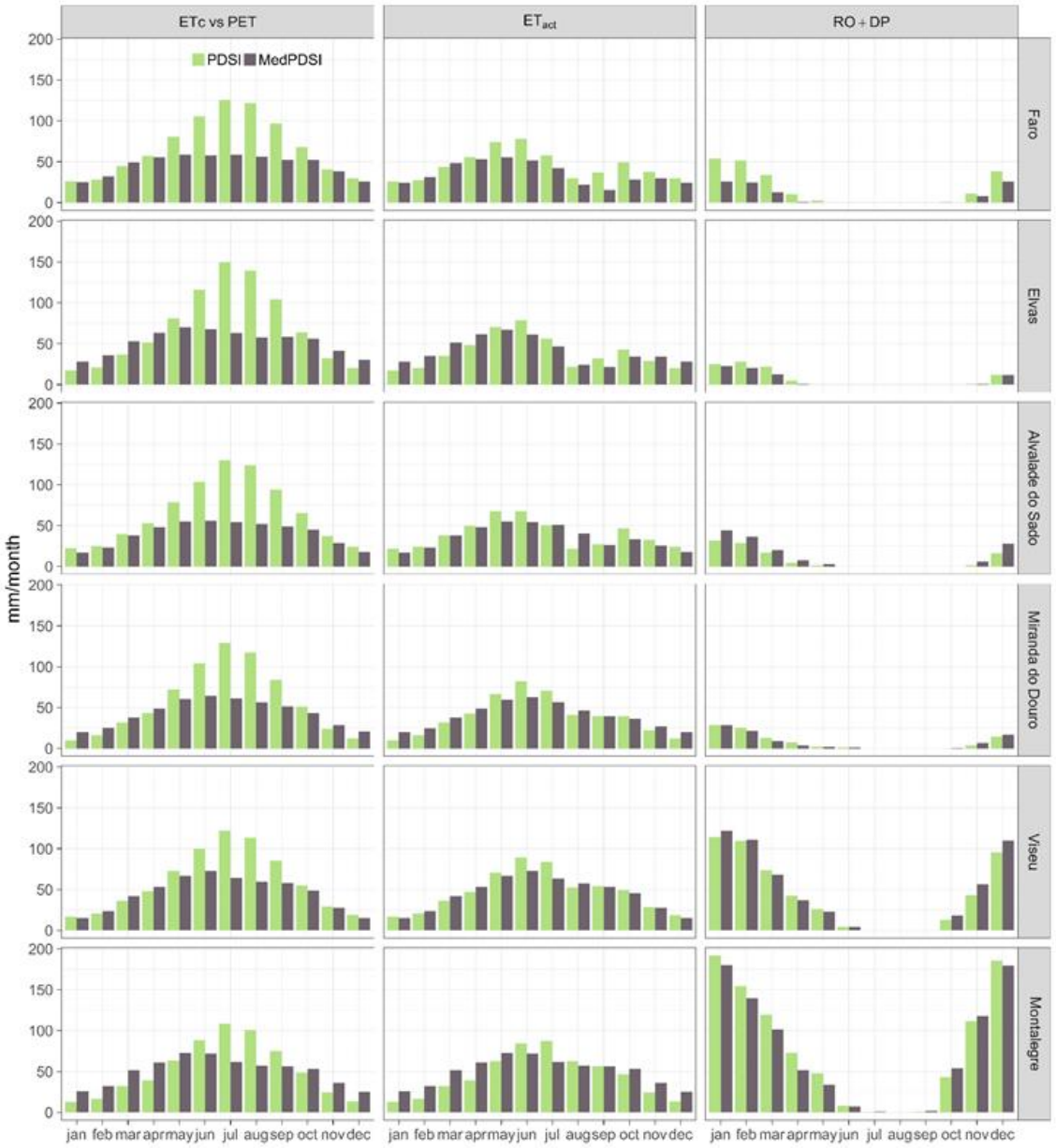

Figure 6-4 Intraannual variability of the water balance inputs (ET_c and PET) and outputs: actual evapotranspiration (ET_{act}) and runoff plus deep percolation (RO+DP), computed for the PDSI (■) and MedPDSI (■) for six selected locations.

The decision of using a soil with a depth of 1.5 m and a TAW of 150 mm for the MedPDSI SWB and a TAW of 225 mm for the PDSI contributed to a reduction of superficial runoff and deep percolation as more water was retained in the soil.

The time-series of ET_{act} from the MedPDSI and PDSI SWB relative to 3 locations, Elvas, Alvalade do Sado and Montalegre and regarding the period 1994-2006, which includes the drought of 2004-2006 were compared.

The comparison of the ET_{act} computed with the PDSI and MedPDSI SWB models for those three locations (Figure 6-5) showed that both models were able to capture, reasonably well, the variability of monthly actual evapotranspiration, for either normal condition or dry periods, such as the 2004-2006 drought that covered most of Portugal. Despite having some differences, the PDSI water balance was capable of explaining, ET_{act} variability.

With the PDSI model the ET_{act} extremes are frequently much larger than those of MedPDSI reaching $ET_{act} = 0$ in several occasions in Elvas and Alvalade do Sado. The difference between ET_c and PET may have impacted the $ET_{act\ PDSI}$, particularly in the end of spring, when there is still available water for evapotranspiration to occur at its potential rate but precipitation was low and available water for ET_{act} came mainly from the water stored in the soil in the previous month. This was observed in Figure 6-5a, in Elvas, in most all of June months, in particular in 1996 and 2004, but also in Alvalade do Sado and Montalegre (Figure 6-5b and 6-5c) in June of 1996 and the June of 2003, 2005, 2006, respectively.

Another difference between the models concerns to ET_{act} in the late summer months. This problem relative to the PDSI's soil water balance was identified by Alley (1984). As the author explained, the fact that the PDSI considers that $ET_{act} = PET$ if $PRE > PET$, might induce errors, since precipitation and evapotranspiration are not evenly distributed within the month, and, therefore stress can occur in a time window of the month, thus affecting the actual evapotranspiration amounts. This issue was particular evident in late summer in which, soil moisture at the beginning or end of the month may be very low. This pattern was quite clear in Figure 6-5b, in Alvalade do Sado in which it was frequent for the PDSI to overestimate ET_{act} in September and October, for example, in 1998 and 2004. Moreover, this was also present in Elvas and Montalegre, but to a lesser extend due to the climate of those locations. In Elvas where precipitation is lower, the recharge of the soil water is more gradual and this issue was less pronounced, but could still be observed in 1994, with large differences between the PDSI SWB and the MedPDSI. However, for Montalegre the high amount of monthly precipitation combined with a lower evaporative demand resulted that more water was conserved in the soil and thus, this issue was less likely to occur.

Despite the problems identified by Alley (1984) regarding the PDSI, most studies focus on the use of PET as the input for evaporative demand. PET as an evapotranspiration

estimation can overestimate the impact of the rising temperature due to climate change (Hobbins et al. 2004; Dai 2011; Chapter 4), thus using PET as input for drought indices may induce an unrealistic, biased, intensification of drought. Dai (2011) and Van der Schrier et al. (2011) found small differences in ET_{act} from the PDSI SWB using as ET estimators the PET and the FAO-PM equations. Thus, both studies concluded that ET_{act} was mostly limited by precipitation and not by the evapotranspiration, which means that the PDSI soil water balance is not sensitive to different evapotranspiration estimation procedures. Similar results were found by Vicente-Serrano et al. (2015). Moreover, it was also observed that the use of PET or the FAO-PM equation did not have relevant effects on the PDSI time series. While van der Schrier et al. (2011) found that the PDSI does not change much when either PET or PM-ET_o were used, Dai (2011) observed slight reduction of the overall global drying trend, using the PDSI computed with PM-ET_o. Sheffield et al. (2012), however, observed larger differences in PDSI computed with both PET and PM-ET_o, with the PDSI computed with PET showing much larger areas with a negative trend when compared to the PDSI computed with PM-ET_o. The authors attribute this difference to inconsistencies in the forcing data sets of the previous two studies.

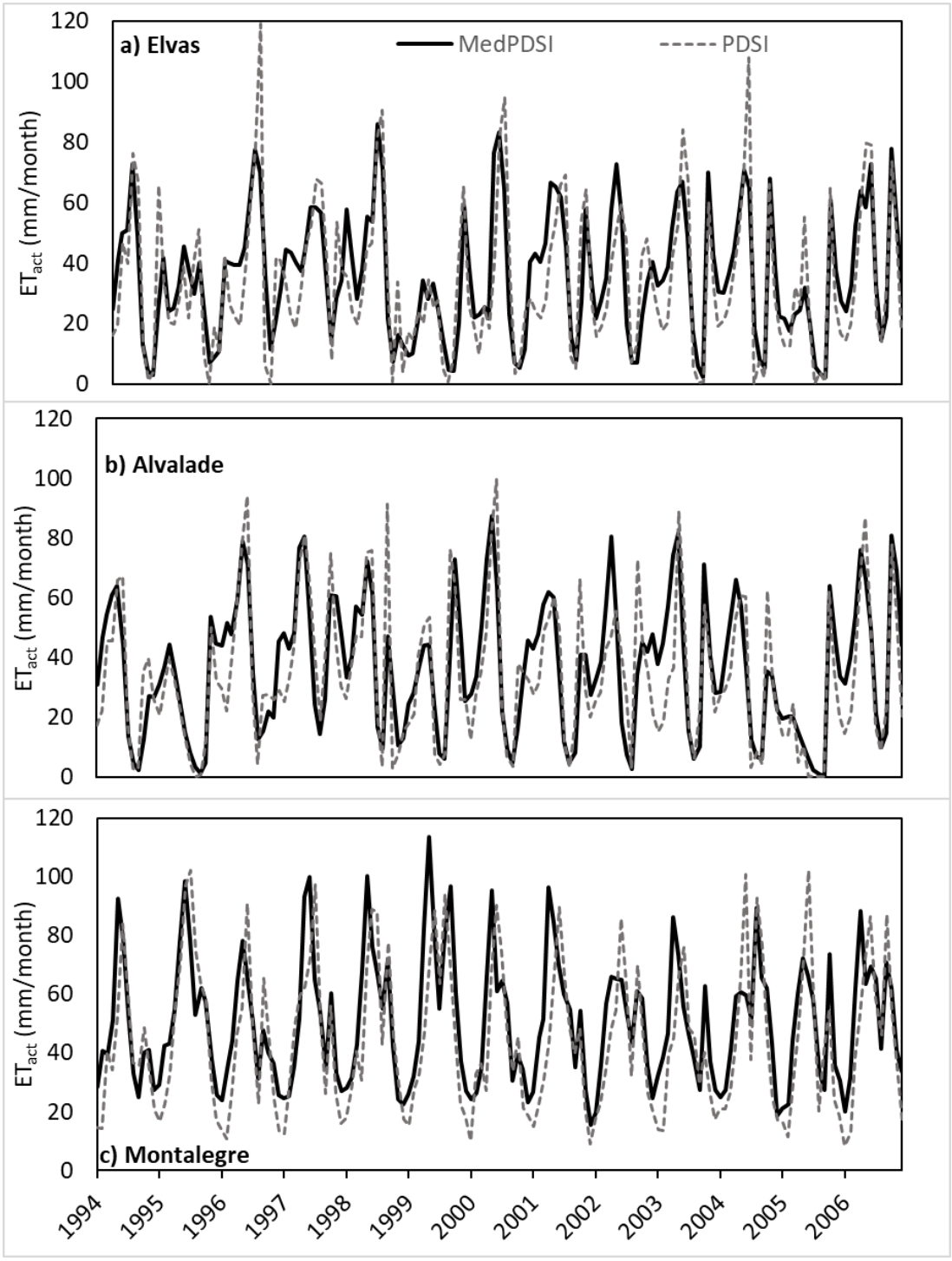

Figure 6-5 Comparison of actual evapotranspiration (ET_{act}) computed with PDSI, MedPDSI, for the period 1994-2006.

The RDI and the SPEI have opposite behaviors regarding ET estimators. The RDI is not very sensitive to different evapotranspiration estimations (Vangelis et al. 2013; Vicente-Serrano et al. 2015) while SPEI was much more sensible to changes in evapotranspiration (Vicente-Serrano et al. 2015) and to the use of different ET estimators, especially in semi-arid regions (Beguería et al. 2014). Nevertheless adopting a physical based equation such

as the FAO-PM equation improve the accuracy of the indices by removing the biases present with temperature-only ET estimators. Although it is important to use an accurate estimate of evapotranspiration, able to explain its true variability and magnitude, it is also essential that the relation between precipitation and PET or PM-ET_o is realistic. Thus, this is the main advantage of indices such as the PDSI and MedPDSI that use a soil water balance to describe the interactions of water supply and demand. Moreover, this was, in fact, the main drive to modify the PDSI. The new water balance in the MedPDSI is specific to a traditional olive orchard and, by using an adaptation of the dual K_c approach; the problems identified by Alley (1984) were partially addressed, making the MedPDSI SWB more capable of describing the Mediterranean conditions.

6.6 Comparing the PDSI and MedPDSI Climatic coefficients

Table 6-2 displays the monthly values of the climatic coefficients, α , β, δ and γ used in Equation 6.10 for computing $\widehat{PRE}$, for both the MedPDSI and PDSI procedures, for the 6 locations selected as representative of the different climates in continental Portugal. The climatic characteristic, K (Equation 6.15), computed following Palmer (1965) and Wells et al. (2004) is also shown in Table 6-2 following the procedures suggested by Wells et al. (2004), for the local calibration of K. α, which refers to the ratio between ET_{act} and PET (ET_c in the case of the MedPDSI) and for both the PDSI and the MedPDSI, was close to one in the rainy season in all locations, from November to April, when stress was less frequent and ET_{act} was close to its potential values. It decreased over the summer, with the exception of MedPDSI for Montalegre, as the water stress, imposed by the low soil water content, forces a reduction of evapotranspiration. This pattern and range of values was very similar to the ones obtained by Palmer (1965) for Western Kansas and Central Iowa. To analyse the differences of α in the summer, it is necessary to understand the differences between the ET_{act} and ET_c or PET, used respectively in the both the PDSI and MedPDSI SWB, which is depicted in Figure 6-4. PET in late spring and summer was much larger than ET_c, whereas ET_{act} was very similar for both SWB, this will make that α will tend to be lower in this period for the PDSI. Moreover, more humid locations and, in each location, more humid months, have a higher α. This coefficient reaches one for all months in Montalegre with the MedPDSI SWB, meaning that in average ET_{act} was very close to ET_c, which resulted from conditions of very low or no stress. This behaviour may be explained not only by the higher humidity of the climate in Montalegre but also

by the soil characteristics defined for this study, which determined a soil with a TAW of 150 mm and a soil depth of 1.5 m, which, combined with high monthly precipitation amounts, avoids the crop water stress.

Table 6-2 Water Balance potential coefficients (α, β, δ, γ) and climatic Characteristic (K) for Faro, Elvas and Alvalade do Sado

	MedPDSI					PDSI				
	Faro									
	α	β	γ	δ	K	α	β	γ	δ	K
January	0.98	0.35	0.16	0.09	1.02	0.98	0.27	0.16	0.10	0.87
February	0.99	0.23	0.14	0.18	0.97	0.98	0.21	0.15	0.20	0.90
March	0.98	0.11	0.07	0.24	1.14	0.93	0.13	0.08	0.28	1.01
April	0.96	0.08	0.01	0.45	1.46	0.87	0.08	0.01	0.51	1.20
May	0.94	0.01	0.00	0.61	1.45	0.73	0.00	0.00	0.72	1.28
June	0.89	0.00	0.00	0.85	2.02	0.51	0.00	0.00	0.93	1.41
July	0.72	0.00	0.00	0.98	1.74	0.27	0.00	0.00	0.99	1.79
August	0.39	0.00	0.00	0.91	2.14	0.12	0.00	0.00	0.98	2.46
September	0.29	0.03	0.00	0.48	1.70	0.21	0.00	0.00	0.84	1.73
October	0.54	0.17	0.02	0.16	1.11	0.60	0.09	0.09	0.56	0.90
November	0.79	0.29	0.14	0.11	0.85	0.85	0.24	0.20	0.18	0.70
December	0.94	0.45	0.25	0.09	0.65	0.96	0.38	0.28	0.10	0.60
	Elvas									
January	0.98	0.26	0.16	0.08	1.02	0.98	0.29	0.19	0.07	0.89
February	0.97	0.22	0.13	0.16	1.05	0.99	0.26	0.18	0.17	0.90
March	0.97	0.15	0.07	0.24	0.95	0.97	0.20	0.13	0.25	0.92
April	0.97	0.11	0.01	0.34	1.37	0.94	0.18	0.03	0.34	1.14
May	0.96	0.01	0.00	0.43	1.44	0.87	0.02	0.00	0.53	1.18
June	0.91	0.01	0.00	0.67	1.34	0.68	0.00	0.00	0.81	1.26
July	0.74	0.00	0.00	0.94	1.64	0.38	0.00	0.00	0.97	1.50
August	0.42	0.00	0.00	0.88	1.74	0.15	0.00	0.00	0.97	2.33
September	0.37	0.05	0.00	0.29	1.44	0.31	0.00	0.00	0.75	1.54
October	0.62	0.16	0.00	0.12	0.99	0.68	0.10	0.00	0.46	0.96
November	0.84	0.27	0.01	0.11	0.86	0.89	0.25	0.03	0.11	0.86
December	0.94	0.36	0.11	0.08	0.87	1.00	0.35	0.15	0.08	0.75
	Alvalade do Sado									
January	1.00	0.39	0.25	0.06	1.03	0.98	0.31	0.23	0.06	0.82
February	1.00	0.34	0.19	0.10	1.08	0.99	0.29	0.17	0.14	0.84
March	1.00	0.16	0.10	0.19	1.13	0.97	0.15	0.10	0.24	1.00
April	1.00	0.26	0.04	0.23	1.43	0.94	0.20	0.03	0.31	1.05
May	0.99	0.08	0.02	0.45	1.45	0.86	0.04	0.01	0.60	1.08
June	0.97	0.00	0.00	0.80	1.77	0.65	0.00	0.00	0.89	1.38
July	0.93	0.00	0.00	0.96	2.07	0.39	0.00	0.00	0.98	1.58
August	0.78	0.00	0.00	0.95	2.01	0.18	0.00	0.00	0.98	2.31
September	0.53	0.04	0.00	0.53	1.81	0.29	0.00	0.00	0.80	1.55
October	0.73	0.21	0.00	0.11	0.99	0.72	0.12	0.00	0.40	0.87
November	0.91	0.35	0.08	0.09	0.84	0.88	0.26	0.05	0.15	0.77
December	0.99	0.53	0.22	0.03	0.91	1.00	0.41	0.19	0.06	0.73

Table 6-2 (Continuation) Water Balance potential coefficients (α, β, δ, γ) and climatic Characteristic (K) for Miranda do Douro, Viseu and Montalegre

	MedPDSI					PDSI				
	Miranda do Douro									
	α	β	γ	δ	K	α	β	γ	δ	K
January	0.99	0.32	0.18	0.11	0.93	1.00	0.35	0.20	0.10	0.84
February	0.99	0.26	0.12	0.17	1.06	1.00	0.28	0.15	0.16	0.96
March	0.99	0.14	0.05	0.26	1.24	0.99	0.13	0.07	0.27	1.15
April	0.99	0.22	0.02	0.19	1.28	0.97	0.23	0.04	0.22	1.16
May	0.99	0.10	0.01	0.25	1.41	0.93	0.08	0.01	0.38	1.17
June	0.97	0.01	0.01	0.48	1.39	0.79	0.00	0.01	0.67	1.17
July	0.92	0.00	0.00	0.76	1.65	0.55	0.00	0.00	0.87	1.33
August	0.83	0.01	0.00	0.73	1.62	0.35	0.00	0.00	0.88	1.66
September	0.76	0.06	0.00	0.42	1.31	0.48	0.02	0.00	0.67	1.28
October	0.83	0.19	0.00	0.12	1.06	0.77	0.13	0.00	0.25	0.97
November	0.95	0.28	0.07	0.12	0.99	0.94	0.26	0.07	0.14	0.94
December	0.98	0.34	0.14	0.06	0.92	1.00	0.34	0.15	0.02	0.84
	Viseu									
January	1.00	0.75	0.57	0.04	0.60	1.00	0.60	0.58	0.07	0.53
February	1.00	0.65	0.50	0.05	0.50	1.00	0.66	0.51	0.07	0.45
March	1.00	0.39	0.30	0.14	0.68	0.99	0.35	0.33	0.19	0.60
April	1.00	0.46	0.17	0.16	0.89	0.98	0.43	0.20	0.19	0.76
May	1.00	0.42	0.11	0.18	1.06	0.97	0.36	0.12	0.28	0.83
June	1.00	0.07	0.02	0.45	1.26	0.90	0.03	0.02	0.59	1.06
July	0.99	0.00	0.00	0.79	1.97	0.69	0.00	0.00	0.89	1.47
August	0.97	0.01	0.00	0.68	1.64	0.47	0.00	0.00	0.84	1.55
September	0.93	0.10	0.00	0.30	1.26	0.63	0.05	0.00	0.51	1.11
October	0.95	0.37	0.21	0.05	0.68	0.90	0.30	0.28	0.14	0.58
November	1.00	0.65	0.42	0.06	0.61	0.98	0.56	0.44	0.10	0.56
December	1.00	0.65	0.57	0.05	0.47	1.00	0.57	0.57	0.08	0.44
	Montalegre									
January	1.00	1.00	0.81	0.01	0.32	1.00	0.96	0.87	0.02	0.29
February	1.00	0.85	0.62	0.04	0.36	1.00	1.00	0.69	0.01	0.31
March	1.00	0.76	0.45	0.11	0.46	1.00	0.66	0.53	0.12	0.43
April	1.00	0.72	0.23	0.08	0.81	1.00	0.67	0.33	0.06	0.68
May	1.00	0.66	0.16	0.12	0.97	0.99	0.72	0.21	0.18	0.77
June	1.00	0.16	0.03	0.34	1.14	0.95	0.12	0.04	0.48	1.00
July	1.00	0.00	0.00	0.70	1.74	0.81	0.00	0.00	0.83	1.46
August	1.00	0.03	0.00	0.57	1.50	0.62	0.01	0.00	0.76	1.47
September	1.00	0.23	0.02	0.23	0.96	0.75	0.16	0.01	0.43	0.87
October	1.00	0.59	0.42	0.03	0.48	0.96	0.53	0.50	0.04	0.42
November	1.00	0.79	0.64	0.04	0.40	1.00	0.75	0.70	0.05	0.37
December	1.00	0.85	0.84	0.00	0.28	1.00	0.82	0.90	0.00	0.26

β, γ and δ are, respectively, the coefficients referring to the ratio between the actual and their potential monthly values of recharge, runoff and loss, computed following Equations 6.4 to 6.9, with the adjustment of PL for the MedPDSI as described in the end of section 6.4. Similar patterns as for α were observed for β. It was larger in the rainy months, reaching, systemically values close to 0 in the dry season, from around April to September

in all locations. Moreover, values of β increased from Faro to Montalegre with the increase of precipitation amounts. Both β of the PDSI and MedPDSI had similar behaviours, with the same pattern of variability but with an important difference that is a reflection of how the two models consider how much water is available for recharge in the transition months of late summer. For all locations, β was larger with the MedPDSI in September and October, which is in agreement with the behavior of the soil water balance in late summer in both methods as discussed above. This may be explained by the fact that not all water available in the soil from the previous months combined with precipitation were used as ET_{act}, and thus recharge values were higher for the MedPDSI in this period. γ and δ, were both, overall, higher in every month for the PDSI when compared with the MedPDSI counterparts. This, again, resulted from a more realistic water balance of the MedPDSI, as it conserves more water in the soil from a month to another, resulting in higher γ and δ with the PDSI, values since PRO and PL were generally lower with this model.

The climatic characteristic, K, adjusts the moisture departure (D) to the characteristics of the local climate, thus allowing better comparisons of the PDSI over both space and time. However, K was originally obtained by Palmer (1965) using data referring to a few locations and may not be adaptable to other regions with different climates. For that reason, in order to reduce these inconsistencies, Wells et al. (2004) revised the computation of K, so it would be could be automatically adjusted to local conditions and allow for more accurate PDSI values that are comparable for different locations and periods. This methodology was followed in the computation of the MedPDSI and PDSI, and its monthly values are shown in Table 6-2, for the 6 selected locations. K was usually higher with the MedPDSI, except for the summer months in the driest locations of Faro, Elvas and Alvalade do Sado, in which the K values relative to August were higher with the PDSI. Furthermore, these values, for both indices, were within the ranges of those obtained by Palmer (1965), however using a difference methodology for computing K.

6.7 Comparing the PDSI and MedPDSI Moisture anomaly Index and duration factors

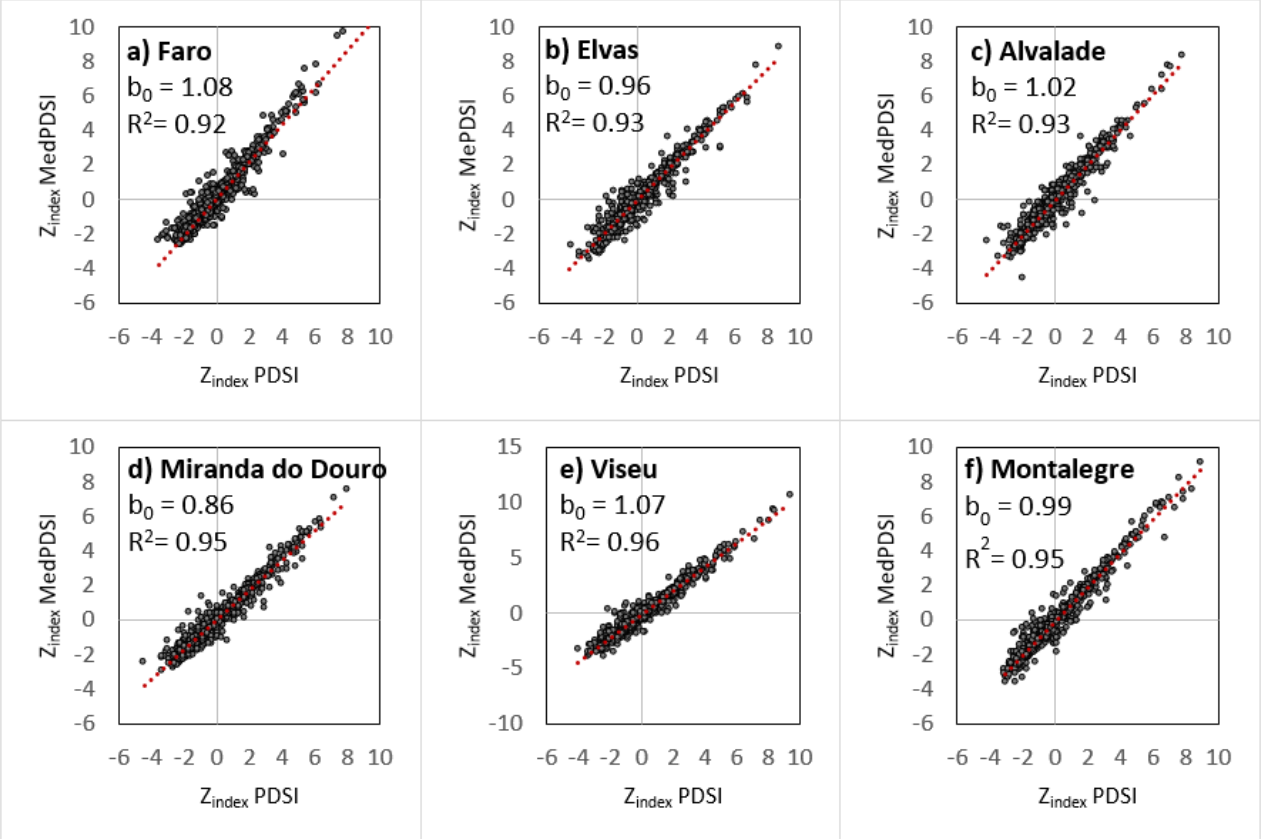

Figure 6-6 Comparison of the moisture anomaly (Z_{index}) index computed for the PDSI and the MedPDSI for selected stations.

Despite the differences observed between the water balance results, climatic coefficients and climatic characteristic discussed in the previous section, the moisture anomaly index (Z_{index}) presented a similar general behaviour in both PDSI and MedPDSI (Figure 6-6). The slope of the linear model when forced through the origin, b_0, is close to 1, varying from 0.90 in Elvas to 1.03 in Faro and the determination coefficient (R^2) is above 0.91 for all cases. Furthermore, in both indices the range of positive values was higher than the negatives, reaching Z_{index} values > 8 in all locations for both the PDSI and MedPDSI, whereas the negative values never passed the -5 values. Although such high positive values were rare, they appeared to be higher for the MedPDSI in the stations of Faro, Alvalade do Sado e Viseu, where the b_0 is positive. This suggested an overestimation of Z_{index} values by the MedPDSI, which is enhanced by the higher values of the index, since the near 0 and negative values appeared to be more evenly scattered around the 1:1 line (black in Figure 6-6), for all 6 locations. This behaviour of the Z_{index} time series is in

agreement with Loukas et al. (2002) in which the Z_{index} values are above -4, whith the most negative values ranging between -2 and -4, whereas the most positive values vary between 2 and 5, with some Z_{index} values reaching a magnitude higher than 6 and even 8.

The Z_{index} was then used to compute the PDSI and MedPDSI using the Equation 6.18, with the duration factors p and q following Wells et al. (2004) instead of p=0.897 q=1/3 derived by Palmer (1965). The duration factors are responsible to define the contribution of previous conditions, i.e., how much autocorrelation the index will have and how sensitive it is to the Z_{index} (Wells et al. 2004; Dai 2011), and were computed trough Equations 6.19 and 6.20 using cumulated driest and wettest series of Z_{index}. The determination of these cumulated values of $Z_{index\ i}$, was achieved using the method 1 proposed in Dai (2011), in which all values of Z_{index} were considered to obtain series of the lowest/highest sum of Z_{index}, for the driest/wettest periods and using the accumulation period intervals from 2 to 24 months. Moreover, in the original PDSI, Palmer used the same duration factors for dry and wet events, but for this application, different duration factors were computed for dry and events following Wells et al. (2004).

Figure 6-7 depicts the accumulated Z_{index} over the driest and wettest periods for the MedPDSI and PDSI for the 6 selected stations. Although with very similar accumulations of Z_{index}, the duration factors obtained for both indices have important differences. The PDSI dry duration factors in the most dry regions of Faro, Elvas and Alvalade do Sado were closer to the original p and q obtained with the original method (with p=0.897 and q=1/3), as p varied from 0.86 to 0.89 and q from 0.29 to 0.38. For the same locations, now, with the MedPDSI, similar p values were obtained, from 0.85 to 0.88, but q values were larger for the PDSI counterparts, varying from 0.39 to 0.52. The p and q values for the dry events in the remaining stations of Miranda do Douro, Viseu and Montalegre were further way from the ones of Palmer as the climate conditions have greater differences from the original conditions used to calibrate Palmer's PDSI. Now, p ranges from 0.79 to 0.89 with the PDSI and from 0.78 to 0.88 with the MedPDSI, but q increased for both indices. In these locations, however, q increased, especially with the MedPDSI, with values varying from 0.51 to 0.61, quite different from the original value of 1/3 but also for the PDSI as values ranged from 0.40 to 0.51. These results showed that, for most locations, the Z_{index} values had a higher contribution to the final value of the MedPDSI than for the PDSI, and though with smaller differences, the autocorrelation effect is less important in the MedPDSI, where p is lower, such as the cases of Miranda do Douro or

Viseu. Moreover, the p and q values for the dry periods relative to the MedPDSI were closer to each other, which showed that the MedPDSI tended to attribute more similar weights to X_{i-1} and Z_{index} than the PDSI.

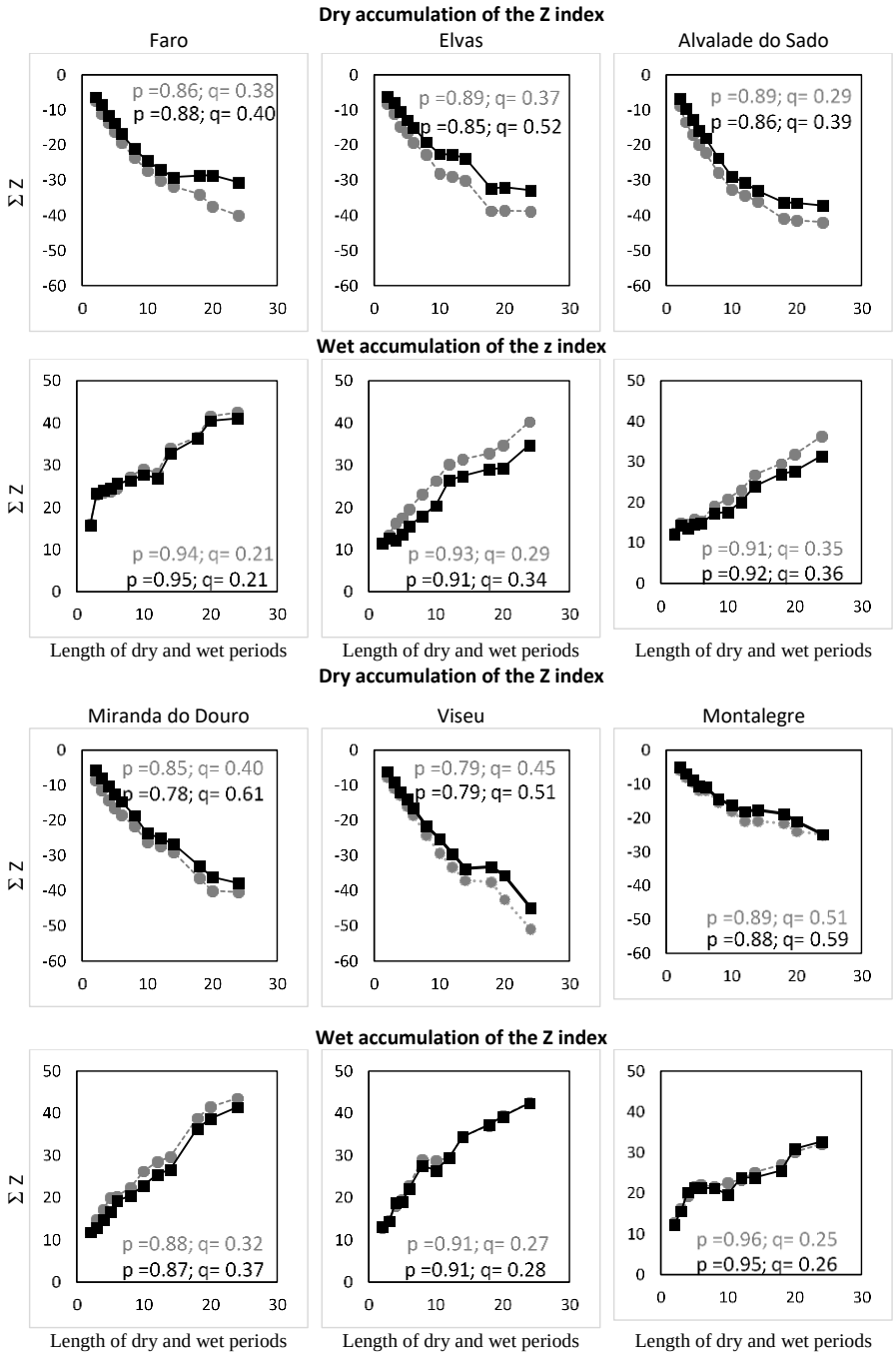

Figure 6-7 Accumulated Z_{index} over the driest and wettest periods for the MedPDSI (■) and PDSI (■) for selected stations

The analysis of the wet accumulation of the Z_{index} (Figure 6-7), showed higher concordance between the PDSI and MedPDSI than for the dry accumulation series. Results also showed higher values of p for all locations to both PDSI and MedPDSI with

values ranging 0.87 to 0.95 and q values from 0.21 to 0.39. Thus, it was apparent that for the wet events the memory of the index was important and the contribution of the Z_{index} was less significant. Moreover, comparable patterns were identified by Dai (2011) with p for wet events being larger, fluctuating from 0.85 to 0.95 in the Iberian Peninsula while p, for the dry events, being smaller within the range 0.8-0.9. Regarding q, the patterns were also similar, with lower values for both the wet and dry events (0.2 to 0.5).

6.8 Comparing the PDSI and MedPDSI Indices

In the previous sections, the components of the MedPDSI and PDSI were analyzed, comparing the water balance results, the climatic coefficients used to determine D and the climatic characteristic, which were both used to compute the Z_{index}. Then, differences in the moisture anomaly were explored between the PDSI and MedPDSI, followed by an analysis of the duration factors obtained with the two methods. In this section, however, the final values of the indices are compared, analyzing their time series (Figure 6-8) and their frequency of events (Table 6-3 and 6-4), in order to assess how the proposed modification of the PDSI model, from which resulted the MedPDSI, impact the behavior of both indices, in identifying dry and wet events. Furthermore, a comparison between the MedPDSI and the SPI was also performed (Figures 6-9 and 6-10), since the SPI is, nowadays the most common and accepted drought index, and it is important to understand how the MedPDSI compares against such index. Moreover, the 9-month time-scale was selected because it compares better with PDSI (Paulo et al. 2012).

The time variability of MedPDSI and PDSI was concordant for the same six locations used as examples throughout this study (Figure 6-8). Additionally in Figure 6-8, a narrower time-window, from 1990 to 2006, was added, showing consecutive dry events that resulted in moderate to extreme dry events, selected to better understand the differences between the two drought indices. By analyzing the complete time series of both indices it was clear that both were in agreement for all locations (Figure 6-8), since the MedPDSI and PDSI identified more of less the same dry and wet events, with similar time variability and also with comparable magnitude and duration of dry and wet events, in a 69 year period. Additionally, both indices had, for all locations, similar ranges, varying from -6 to 6, with the majority of the values comprised between -4 and 4. This is clearly an improvement due to the self-calibrating procedure that created a more stable variability of the index for various types of climate, thus allowing for better spatial and

temporal comparisons of the PDSI and MedPDSI. As Dai (2011) discussed, the original PDSI, computed for climatic conditions unlike the ones used to calibrate Palmer's PDSI, could originate time series with great variability, with ranges with no clear physical meaning, which hinder the capabilities of the index to be compared among different locations and periods.

Using the narrower time-window, important differences were highlighted. The MedPDSI reached negative values before the PDSI in almost occasions for the 6 locations (Figure 6-8), with the exception of Faro, in which the extreme dry events identified in 1996 and 2006 appear to be slightly anticipated by the PDSI. For the remaining locations, nevertheless, the severe and extreme dry events occurred sooner with the MedPDSI when compared with the PDSI. A clear example of this patterns are the droughts of 1992 in Elvas or the droughts of 1996 in Alvalade do Sado and 2005 in all locations except Faro. Furthermore, Figure 6-8 also revealed that, not only the MedPDSI often identifies dry events sooner than the PDSI, but those events are often more frequent and more severe with the former drought index, with the exception of Montalegre, in which severe, moderate and mild events were more frequent with the PDSI. For both time-windows in Figure 6-8 it is clear that the MedPDSI reaches extreme dry events more frequently than the PDSI and that those events are often more severe.

In Figure, 6-9 the frequency of events for each class of the MedPDSI and the PDSI were compared, and results helped to further explain the differences between both indices. Like with the Figure 6-8, it became clear that the MedPDSI identified extreme dry events more frequently than the PDSI in all 6 locations and that severe and moderate dry events were also more frequent in the MedPDSI in all locations except for Montalegre. In this location, the PDSI identified more often severe and moderate events than the MedPDSI. In contrast, the extreme wet events were more common with the PDSI for all locations and, as for the other wet classes, moderate to severe, there was no clear pattern, with similar frequency of events for both indices.

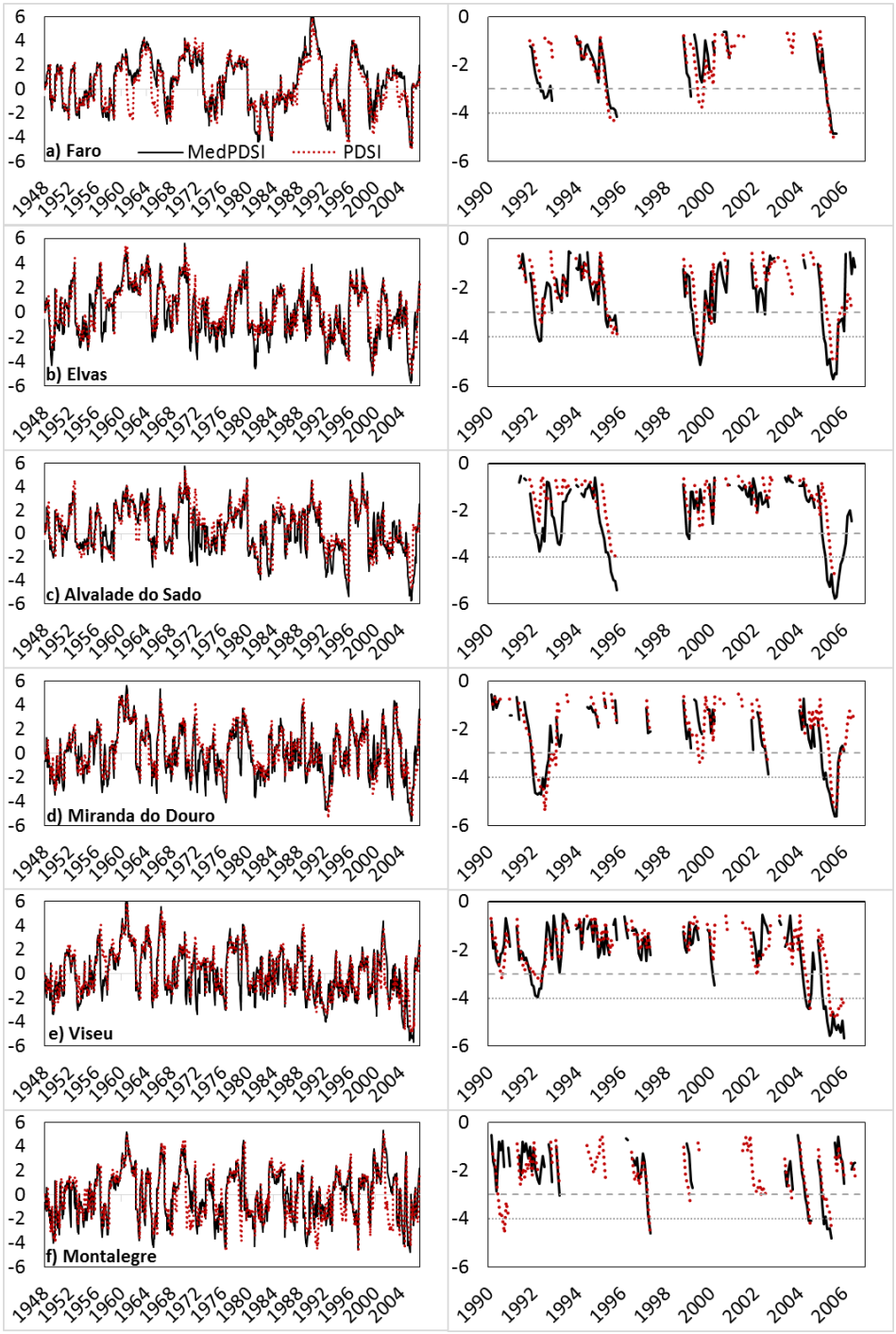

Figure 6-8 Time variability of the PDSI (red) and MedPDSI (black) for selected stations for the period 1948-2006 (on the left) and a time window with the droughts from 1990-2006 (on the right). The severe drought threshold is depicted by (- - - -) and extreme drought by (——).

Relevant results relative to Figure 6-9 were related with the self-calibration procedure. Wells et al. (2004) discussed that extreme events are, by definition rare, and should only account for 1 to 3% of the total occurrences and that extreme wet and dry events should have similar frequency. In fact, Figure 6-9 showed that the extreme events were always within that range, for both indices and with similar frequency when comparing extreme

dry and wet events. These results highlighted the importance of the self-calibrating procedures, as it adjusts the index to local condition and producing more symmetric time series from a statistical standpoint. The self-calibrating methodology produced similar results in Wells et al. (2004), Van der schrier et al. (2006), and in Dai (2011) whom compared the Sc-PDSI against the PDSI and its results showed a more evenly distribution of both wet and dry events. However, Dai (2011) also stated that when the original distribution of the PDSI differs substantially from Gaussian, the distribution of the Sc-PDSI would still not be close to normality. This is expected, since the self-calibration procedure does not standardize the index but helps adjusting the index to local conditions and creates more realistic distribution of events, in particular for the extreme events. The frequency distributions in Figure 6-9 are assymetric as there are some unbalances in the distribution of wet and dry mild and moderate. A good example is the distribution of mild events of the MedPDSI for Faro and for the PDSI in Viseu. Nevertheless, the frequency of dry and wet extremes was similar for both the PDSI and MedPDSI and negative and positive values of the index were evenly distribution in both indices.

Table 6-3 shows the average frequency (%) of drought and wet classes grouped by aridity for all 26 weather stations for the two indices. The results shown in this Table support those from Figures 6-8 and 6-9 that refer only to the 6 examples that were used throughout this study. Like it was observed in Figure 6-9, dry events, either extreme or severe, were more frequent with the MedPDSI, whereas, with the PDSI, extreme and severe wet events were more frequent. Moreover, analysing the distribution of events according to the aridity it was observed that there was no clear pattern differentiating the frequency of extremes wet or dry for each aridity zone in both drought indices. However, while grouping all dry or wet event, results showed that for the PDSI and the MedPDSI wet events increased from the most arid locations to the humid location, and conversely dry events decreased from the dry sub-humid to the humid locations.

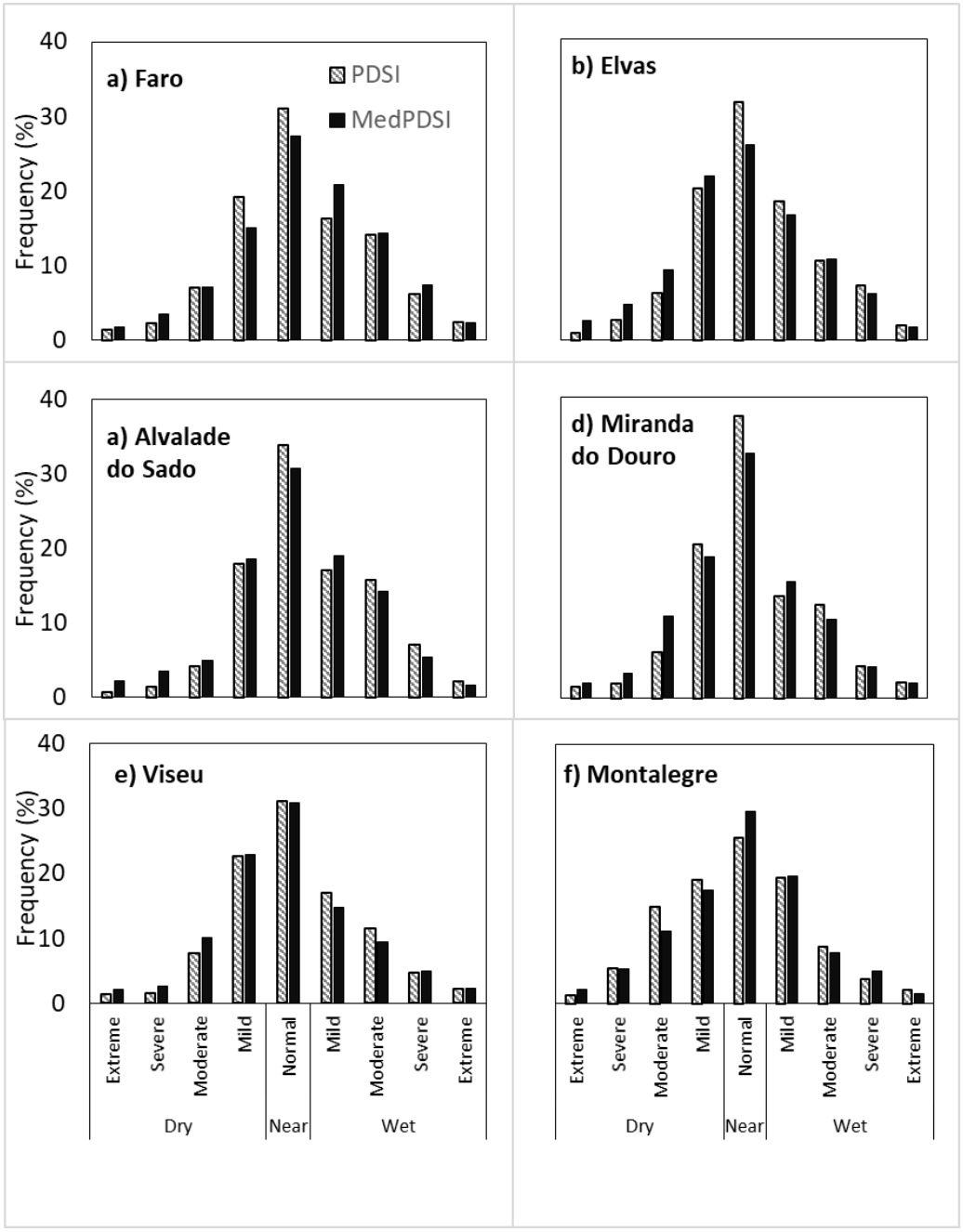

Figure 6-9 Frequency of events in each dry and wet class of the MedPDSI and PDSI for selected stations

The results above appear to improve upon those shown in Paulo et al. (2012) that, while analysing the distributions of the not self-calibrated PDSI and MedPDSI (although with a different scheme to compute the soil water balance), identified a negative bias in these indices and with a larger variability of extremes, often exceeding the threshold of 3%.

Table 6-3 Average Frequency (%) of drought/wet classed of the MedPDSI and PDSI grouped by aridity for all 26 weather stations

		Dry Sub-Humid		Moist Sub-Humid		Humid	
		MedPDSI	PDSI	MedPDSI	PDSI	MedPDSI	PDSI
Dry	Extreme	2.24	1.38	2.33	1.19	2.14	1.25
	Severe	4.17	2.61	3.43	2.42	4.96	3.19
	Moderate	8.58	6.72	9.00	6.61	10.51	10.01
	Mild	18.03	18.46	20.37	18.25	18.50	16.40
Near	Normal	30.13	32.36	31.43	32.08	30.83	27.72
Wet	Mild	17.83	17.31	15.47	16.71	17.03	18.83
	Moderate	11.63	12.24	11.27	12.82	9.64	13.62
	Severe	5.76	6.78	5.28	7.81	4.64	6.86
	Extreme	1.62	2.15	1.43	2.12	1.74	1.92

Besides comparing the MedPDSI against the PDSI, it was also relevant to compare the new index against the SPI, which follows a different approach to assess drought or wetness conditions. It is a multiscalar, statistical index, based only on precipitation and is a well accepted drought index, capable of characterizing the various forms of drought and capturing its main characteristics. Paulo et al. (2012) compared the SPI against the PDSI and a former version of the MedPDSI, computed with another approach for the water-balance, and SPEI, and found better correlations between the SPI-9 (computed for a time scale of 9 months) and the MedPDSI or PDSI, both computed with the original calibration coefficients derived by Palmer (1965). The authors also observed that the correlation coefficient was lower for the humid locations when comparing the PDSI or MedPDSI against the SPI-9, which was attributed to the fact that PDSI and MedPDSI indices result from a soil water balance and are more influenced by climate whereas SPI is a normalized index. Moreover Narasimhan and Srinivasan (2005) observed better correlations between PDSI and SPI-9 ($r = 0.87$) than with the SPI-12 ($r = 0.83$), which are in agreement with Lloyd-Hughes and Saunders (2002) having a correlation coefficient between the SPI-12 and the PDSI of 0.73.

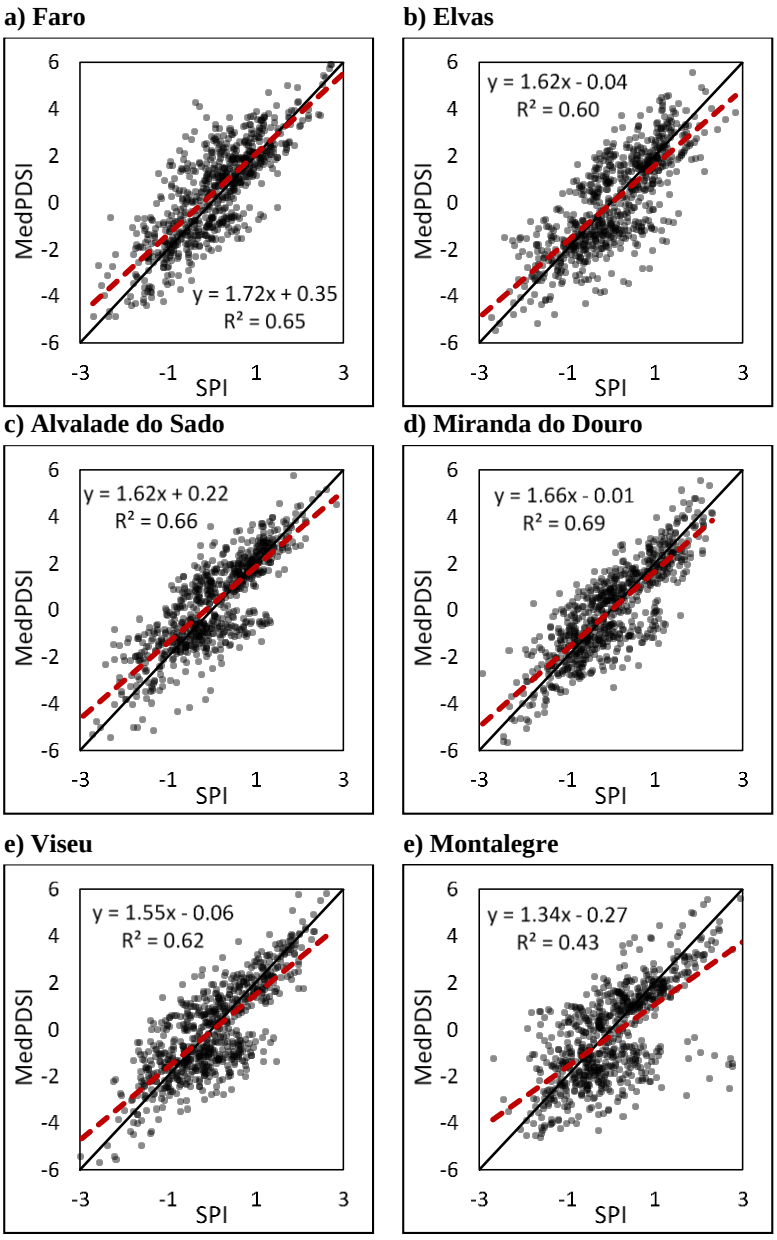

Figure 6-10 Comparing SPI-9 with MedPDSI with the respective linear regression and R^2

Figure 6-10, comparing the MedPDSI against SPI-9 showed similar patterns and are comparable with the studies mentioned previously. There is a good correlation between both indices, with R^2 between 0.43 in Montalegre and 0.69 in Miranda do Douro. The scattering observed in Figure 6-10, mainly between mild dry and mild wet events ($-2 <$ MedPDSI < 2) was also observed in Paulo et al. (2012) and is due to the backtracking procedure of the PDSI.

Figure 6-11 compares the time series of the MedPDSI and the SPI-9 for the complete period, 1948-2006, with a more restrict time-window (1990-2006) showing only the

relevant drought events. The reasonable agreement is also clear in Figure 6-11, with both indices showing similar time variability and identifying dry events with comparable severity and duration for the 6 locations. The major drought of 2004-2006 was well depicted in all cases. Severe and extreme droughts with the MedPDSI appeared to be more frequent and detected sooner than with SPI-9 for the most arid locations of Faro, Elvas, Alvalade do Sado and Miranda do Douro, although the results for the 2004-2006 drought were not so clear. Furthermore, for all cases, the SPI-9 seemed to transition more often between dry conditions to near normal conditions than the MedPDSI, with more frequent and smaller dry episodes than the MedPDSI. As expected results were worst for Montalagre, which had the poorest correlation between the MedPDSI and the SPI-9. Paulo et al. (2012) showed similar results, with comparable time-variability of the indices, but with the PDSI and MedPDSI identifying more frequently severe and extreme droughts.

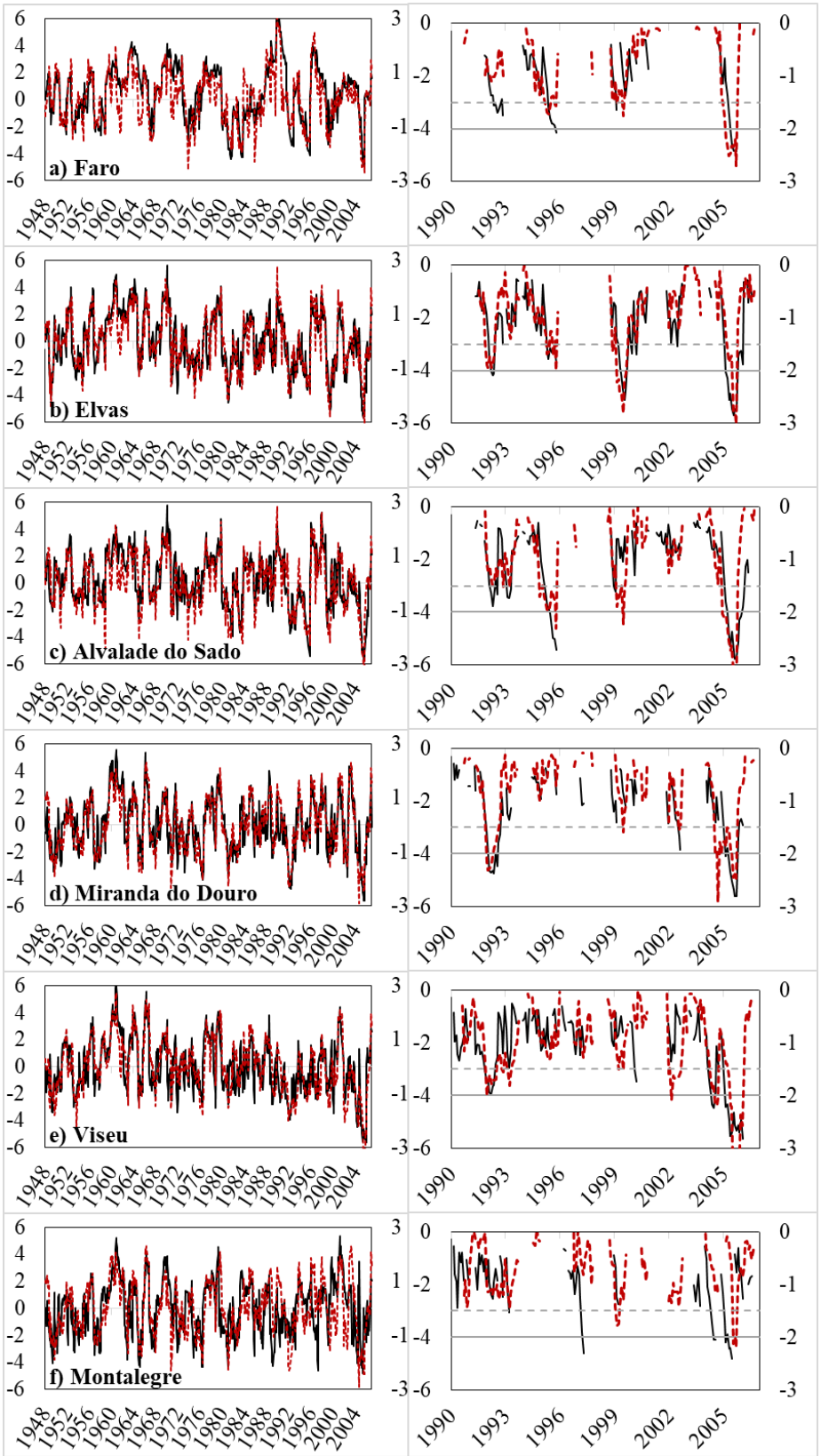

Figure 6-11 Time variability of the SPI-9 (red) and MedPDSI (black) for selected stations for the period 1948-2006 (on the left) and a time window with the droughts from 1990-2006 (on the right). The severe drought threshold is depicted by (----) and extreme drought by (___). The left yy axis correspond to the severity scale of the MedPDSI and the yy axis the right for the SPI-9 scale.

6.9 Conclusions

The proposed drought index MedPDSI has been developed considering the soil water balance of the olive crop and using an adaptation of the dual K_c approach. Monthly K_{cb} values were selected and K_e was determined for every month as a function of PM-ET_o and precipitation of the current and past month. The soil characteristics determine both TAW and soil evaporative conditions. The MedPDSI was computed with a loam soil depth of 1.5 m, which have a TAW of 150 mm m^{-1}, whereas the PDSI was computed considering a surface layer with 25 mm of water holding capacity and an underlying layer with 200 mm, so both soils would be comparable. The adoption of a new SWB approach showed comparable results between both methods, but with the MedPDSI producing a more realistic behavior of ET_{act} in late summer by considering a reduction of evapotranspiration even if PRE>ET since soil water storage is low. Moreover, the climatic coefficients of both drought indices were similar and reflected the local conditions of the climate as well as the initial conditions of both the PDSI and the MedPDSI.

The moisture anomaly index, Z_{index}, revealed a similar general behaviour for both MedPDSI and original PDSI methods, but the MedPDSI tended to produce higher values of Z_{index} during humid periods; as for dry periods, there were no clear trends for one method to produce lower values of Z_{index} than the other. Furthermore, for the dry accumulation of Z_{index}, the self calibrated PDSI showed duration factors closer to the original PDSI, whereas the MedPDSI presented larger q values. Differences in the duration factors were higher for the more humid climates. These differences between the duration factors for the MedPDSI and the PDSI revealed that the MedPDSI was more dependent of the moisture anomaly index for that month and less dependent on the value of the index of the previous month. p was higher for the wet accumulation of Z_{index} in both drought indices which may lead to the conclusion that for wet events the autocorrelation, i.e., its memory, had a larger role.

The analyses of the behavior of the drought indices, showed similar temporal patterns and magnitude of the MedPDSI and the PDSI, but there were important differences. Both were able to detect the same dry and wet events, with approximately the same duration periods and severity, however, the MedPDSI reached severe and extreme droughts more often and droughts were detected sooner when compared to the PDSI. Moreover, the

implementation of the self-calibrating procedure improved the frequency of extreme events in both indices, limiting their frequency to the interval of 1 to 3%, following a similar pattern of extremes of a Gaussian distribution. Furthermore, the comparison against the SPI computed for the time-scale of 9 months exhibited, also, comparable results. The correlation decreased for the most humid locations, which may indicate that a water balance, that consider soil water availability from a month to another, might have significant impacts on the variability of a drought index.

The results of this study revealed that the modifications implemented to the PDSI improved upon the original scheme proposed. The modification of the soil water balance of the PDSI were adequate for the climate conditions tested. The MedPDSI updated the PDSI soil water balance, developed considering the climate conditions and crop characteristics of the central United States of America, to a soil water balance adapted to the Mediterranean climate. The intermediate outputs of the MedPDSI water balance are well linked to the water supply and demand, and may be more realistic than the PDSI. However, further studies are required to understand how the MedPDSI behaves in other locations, with different climatic characteristics, and how other initial conditions, such as soil characteristics affect the water balance and drought detection. Moreover, for monitoring drought implementations, the backtracking of the MedPDSI should be removed and a software tool that allows the easy access to the MedPDSI computation should be created.

Chapter 7

Conclusions

The studies developed within the PhD program were published in peer-reviewed papers, which adapted versions were reproduced in Chapters 2 to 6. The main results obtained may be grouped in three themes:

(1) Understanding the way drought indices characteristics, namely, spatial patterns, long-term trends and cyclicity as well as frequency, duration and severity, are influenced by its parameterization or by different types of input data;

(2) Assessing the importance of an accurate reference evapotranspiration (ET) estimation aiming to drought monitoring, lead to compare different ET_o temperature based approaches against the physical based FAO-PM equation. Moreover, reanalysis products were tested as alternative to compute PM-ET_o when full data sets are not available. Thus, allowing to avoid the need to use temperature based methods that are not able to fully express PM-ET_o variability and may be biased due to climate change;

(3) Improving drought characterization and monitoring drought indices by modifying the PDSI water balance, considering results from previous studies (Chapter 3, 4 and 5), to update the MedPDSI drought index . To achieve that, the water balance of the PDSI was modified to a soil water balance applied to the olive orchard, in which soil evaporation and transpiration of the olive crop were estimated separately adopting a modified dual crop coefficient approach. In addition, MedPDSI was applied to 26 weather stations in Portugal using the monthly reanalysis products tested in Chapter 5 and adopting the self-calibrating procedure.

In Chapter 2 the stability of spatial and temporal patterns of droughts in Portugal were studied by applying the Principal Components Analysis to the SPI compute for several time scales using three precipitation data sets covering the period 1950–2003: (1) the observation data set composed of 193 rain-gauges distributed over Continental Portugal, (2) the PT02 high-resolution gridded data set provided by the Portuguese Meteorological Institute, and (3) the GPCC data set with 0.5° spatial resolution. The results suggested a high stability of the spatial patterns of drought, independent of the SPI time scale, the

database used and the reference period considered for the SPI calculation, identifying two sub-regions in northern and southern Portugal with independent climate variability. A third sub-region was identified in the Centre-East of Portugal but only when using SPI-24 calculated for PT02. In the scope of the analysis of the temporal variability of SPI in Portugal, the cyclicity of the droughts was also analysed using a Fourier analysis, applied to 74 time series of 66-year SPI-12. The most frequent significant cycles were identified and analysed for the month of December. The results showed that periodicities varied spatially in Portugal, but pointed to a 6 year cycle common to the whole country and a frequent cycle of 9.4 years in central and southern Portugal. Both cycles may be partially explained by the North Atlantic Oscillation (NAO) on the occurrence and severity of droughts in Portugal.

Chapter 3 focused on the effect of long-term variability of precipitation on the SPI and of precipitation and reference evapotranspiration on the PDSI. This effect was studied on the SPI by partitioning 10 long time series of precipitation, from 1863 to 2007, in different sub-periods and obtaining the SPI series for each sub-period. Precipitation thresholds were calculated corresponding to the categories of moderate, severe and extreme dry SPI. Results have shown that when SPI values derived from the full data record for a recent time period are lower/higher than the SPI values derived from data of the considered time period a recent downward/upward shift of precipitation has occurred. The effect of variability of the climate data on the PDSI was assessed using weather data from the NOAA-CIRES Twentieth Century Reanalysis Project version 2c, which spans from 1851 to 2014 with a spatial coverage of 2.0º latitude x 2.0º longitude. The weather data retrieved included precipitation and all the weather variables required to compute PM-ET_o, namely maximum and minimum temperature, relative humidity, downwards solar radiation and wind speed. To evaluate how the long-term climate variability influences the identification of dry events by drought indices, five different calibration periods were selected to estimate, respectively, the potential evapotranspiration, runoff, soil water recharge and loss by percolation of the soil water balance of the PDSI. The same analysis was performed in parallel with the SPI with a 9-month time scale using the same 5 calibration periods for the estimation of SPI distribution function parameters. The results showed very different indices, depending upon the calibration periods used. With the same temporal patterns for all locations studied, when drought indices were calibrated with the most recent period (1974-2014), the number of drought events (severe or

extreme) identified was lower in both PDSI and SPI-9, when compared to the indices calculated with the other calibration periods. However, the detection of extreme and severe wet events identified was greater when the drought indices were calculated using this period. In contrast, if the calibration period selected was the period 1892-1932, the opposite occurred with a greater amount of dry events detected and fewer wet events. These results showed the importance that the selection of the calibration period has for both the PDSI and the SPI.

The impact, in particular on drought indices such as PDSI, of the selection of the method used to calculate evapotranspiration is relevant and should not be overlooked. Traditionally the PDSI uses the potential evapotranspiration obtained using the Thornthwaite equation. However, there are other physical-based methods, such as the reference evapotranspiration computed by the FAO-56 method, which allows for more accurate estimates of evapotranspiration, although are more demanding in terms of weather data requirements. In Chapter 4 three evapotranspiration calculation methodologies were compared, namely the FAO-PM method using maximum and minimum temperature, relative humidity, solar radiation and wind speed, and two temperature-based equations using daily and monthly data for the period 1981-2012 in the Inner Mongolia region. Results of Chapter 4 showed that the temperature-based methods for the calculation of evapotranspiration are insufficient to correctly describe their variability and amplitude in all types of climate. Following these results in Chapter 5, the reanalysis products were tested as an alternative when *in situ* data are not available, leading to the conclusion that bias-corrected climatic data derived from reanalysis products are a good alternative to observations for both the calculation of monthly and daily reference evapotranspiration.

Following the results of the previous Chapters, an adaption of the PDSI, the MedPDSI (Chapter 6) was tested. The MedPDSI improves the PDSI mainly by modifying its soil water balance, adapting it to the climatic conditions of the Mediterranean. The reference evapotranspiration was calculated using a NCEP/NCAR data set that combines reanalysis with observed data in order to correct bias in the surface variables, whose performance was verified in Chapter 5 and following the methodology of bias correction tested, also, in Chapter 5. The soil water balance results obtained for the MedPDSI revealed important differences when compared to the PDSI. The actual evapotranspiration (ET_{act}) from the MedPDSI, showed a more realistic variability, mainly in the transition from dry to wet

months, when compared to the ET_{act} from PDSI. Moreover, droughts identified with MedPDSI were detected generally earlier, were longer and more severe, which is an advantage for drought management, since drought risk management systems may be implemented earlier for better manage of their impacts, mitigating the potential negative consequences of dry events.

Results obtained within the framework of this PhD program suggested that the MedPDSI may be a useful tool for agricultural drought monitoring and, together with understanding the main patterns of spatial and temporal variability of drought in Portugal, better drought risk management policies could be achieved. However, further studies are required for the MedPDSI to be used for drought monitoring, more specifically the backtracking procedure should be removed from the current MedPDSI computation and a software tool should be developed to allow easier access to the drought index. Moreover, the MedPDSI behavior under different regions and climates should be studied and compared against other drought indices such as the SPI or the SPEI and RDI. Furthermore, the MedPDSI should also be compared against indicators of hydrological and water resources variables, such as soil moisture or compared against crop yields.

Standardized, multiscalar versions of the MedPDSI could also be considered as further research topics. This could be achieved by either following similar methodologies as the ones suggested for the PDSI or by using the water balance outputs from the MedPDSI, for example, the actual evapotranspiration to develop a standardized measure of ET deficit, which may be a more versatile tool for monitoring different types of drought. Furthermore, the MedPDSI should also be tested in drought prediction studies with either statistical or physical based techniques. Taking advantage of the reanalysis products already tested in Chapter 5 and used in Chapter 6, climate reanalysis data could be combined with seasonal forecasts to assess the predictability capabilities of this type of applications and ultimately be used as an early warning system for agriculture management.

7.1 Research Outcome

ISI Journals

Martins DS, Paredes P, Raziei T, Pires C, Cadima J, Pereira LS (2017) Assessing reference evapotranspiration estimation from reanalysis weather products. An

application to the Iberian Peninsula. Int J Climatol 37:2378–2397. doi: 10.1002/joc.4852

Merabti A, Martins DS, Meddi M, Pereira LS (2018) Spatial and Time Variability of Drought Based on SPI and RDI with Various Time Scales. Water Resour Manag 32:1087–1100. doi: 10.1007/s11269-017-1856-6

Merabti A, Meddi M, Martins DS, Pereira LS (2018) Comparing SPI and RDI Applied at Local Scale as Influenced by Climate. Water Resour Manag 32:1071–1085. doi: 10.1007/s11269-017-1855-7

Moreira EE, Martins DS, Pereira LS (2015) Assessing drought cycles in SPI time series using a Fourier analysis. Nat Hazards Earth Syst Sci 15:571–585. doi: 10.5194/nhess-15-571-2015

Paredes P, Martins DS, Pereira LS, Cadima J, Pires C (2018) Accuracy of daily estimation of grass reference evapotranspiration using ERA-Interim reanalysis products with assessment of alternative bias correction schemes. Agric Water Manag 210:340–353. doi: 10.1016/J.AGWAT.2018.08.003

Paulo A, Martins D, Pereira LS (2016) Influence of Precipitation Changes on the SPI and Related Drought Severity. An Analysis Using Long-Term Data Series. Water Resour Manag 30:5737–5757. doi: 10.1007/s11269-016-1388-5

Raziei T, Martins DS, Bordi I, Santos JFJF, Portela MM, Pereira LS, Sutera A (2015) SPI Modes of Drought Spatial and Temporal Variability in Portugal: Comparing Observations, PT02 and GPCC Gridded Datasets. Water Resour Manag 29:487–504. doi: 10.1007/s11269-014-0690-3

Ren X, Martins DS, Qu Z, Paredes P, Pereira LS (2016a) Daily Reference Evapotranspiration for Hyper-Arid to Moist Sub-Humid Climates in Inner Mongolia, China: II. Trends of ETo and Weather Variables and Related Spatial Patterns. Water Resour Manag 30:3793–3814. doi: 10.1007/s11269-016-1385-8

Ren X, Qu Z, Martins DS, , Paredes P, Pereira LS (2016b) Daily Reference Evapotranspiration for Hyper-Arid to Moist Sub-Humid Climates in Inner Mongolia, China: I. Assessing Temperature Methods and Spatial Variability. Water Resour Manag 30:3769–3791. doi: 10.1007/s11269-016-1384-9

Pereira LS, Martins DS, Paulo A, Paredes P, Rosa R, Pires, C (2019) MEDPDSI, A modification of the Palmer Drought Severity Index focusing on olive groves with their comparison for various climates (in preparation).

Papers in Edited Proceedings

Paulo AA., Martins DS, Paredes P, Rosa RD, Pereira LS (2017) Modification of the Palmer Drought Severity Index for Mediterranean environments: Model and application. Proceedings of the 10th World Congress of EWRA 'Panta Rhei', 5-9 July 2017, Athens, Greece. 827-834.

Martins DS, Paulo AA, Pires C, Pereira LS (2017) Long-term variation of PDSI and SPI computed with reanalysis products. Proceedings of the 10th World Congress of EWRA 'Panta Rhei', 5-9 July 2017, Athens, Greece. 919-926.

Paredes P, Martins DS, Cadima J, Pires C, Pereira LS (2017) Accuracy of daily PM-ETo estimations with ERA-Interim reanalysis products. Proceedings of the 10th World Congress of EWRA 'Panta Rhei', 5-9 July 2017, Athens, Greece. 1577-1584.

Comunications

Martins DS, Barbosa S, Matias PG , Paulo AA, Pires C, Pereira LS (2014) Trend Analysis of Drought Extremes in Iberian Peninsula Using SPI. EcoHCC 2014. Instituto Politécnico de Tomar. Tomar.

References

Abtew W, Obeysekera J, Iricanin N (2011) Pan evaporation and potential evapotranspiration trends in South Florida. Hydrol Process 25:958–969. doi: 10.1002/hyp.7887

Aitken AC (1936) IV.—On Least Squares and Linear Combination of Observations. Proc R Soc Edinburgh 55:42–48. doi: 10.1017/S0370164600014346

Allen RG (1996) Assessing Integrity of Weather Data for Reference Evapotranspiration Estimation. J Irrig Drain Eng 122:97–106. doi: 10.1061/(ASCE)0733-9437(1996)122:2(97)

Allen RG (1997) Self-Calibrating Method for Estimating Solar Radiation From Air Temperature Advanced METRIC processing View project. Artic J Hydrol Eng. doi: 10.1061/(ASCE)1084-0699(1997)2:2(56)

Allen RG, Pereira LS (2009) Estimating crop coefficients from fraction of ground cover and height. Irrig Sci 28:17–34. doi: 10.1007/s00271-009-0182-z

Allen RG, Pereira LS, Howell TA, Jensen ME (2011) Evapotranspiration information reporting: I. Factors governing measurement accuracy. Agric Water Manag 98:899–920. doi: 10.1016/J.AGWAT.2010.12.015

Allen RG, Pereira LS, Raes D, Smith M (1998) Crop evapotranspiration : guidelines for computing crop water requirements. FAO Irrig. Drain. Pap. 56, FAO, Rome, 300p

Allen RG, Pereira LS, Smith M, Raes D, Wright JL (2005) *FAO-56* Dual Crop Coefficient Method for Estimating Evaporation from Soil and Application Extensions. J Irrig Drain Eng 131:2–13. doi: 10.1061/(ASCE)0733-9437(2005)131:1(2)

Allen RG, Pruitt WO, Wright JL, Howell TA, Ventura F, Snyder R, Itenfisu D, Steduto P, Berengena J, Yrisarry JB, Smith M, Pereira LS, Raes D, Perrier A, Alves I, Walter I, Elliott R (2006) A recommendation on standardized surface resistance for hourly calculation of reference ETo by the FAO56 Penman-Monteith method. Agric Water Manag 81:1–22. doi: 10.1016/J.AGWAT.2005.03.007

Allen RRG, Smith M, Pereira LSL, Perrier A, Pereira LSL (1994) An Update for the Calculation of Reference Evapotranspiration. ICID Bull 43:1–34

Alley WM (1985) The Palmer drought severity index as a measure of hydrologic drought. JAWRA J Am Water Resour Assoc 21:105–114. doi: 10.1111/j.1752-1688.1985.tb05357.x

Alley WM (1984) The Palmer Drought Severity Index: Limitations and Assumptions. J Clim Appl Meteorol 23:1100–1109. doi: 10.1175/1520-0450(1984)023<1100:TPDSIL>2.0.CO;2

Anayah FM, Kaluarachchi JJ (2014) Improving the complementary methods to estimate evapotranspiration under diverse climatic and physical conditions. Hydrol Earth Syst Sci 18:2049–2064. doi: 10.5194/hess-18-2049-2014

Angström A (1924) Solar and terrestrial radiation. Report to the international commission for solar research on actinometric investigations of solar and atmospheric radiation. Q J R Meteorol Soc 50:121–126. doi: 10.1002/qj.49705021008

Arlot S, Celisse A (2010) A survey of cross-validation procedures for model selection. Stat Surv 4:40–79. doi: 10.1214/09-SS054

Asadi Zarch MA, Sharma A (2015) Droughts in a warming climate: A global assessment of Standardized precipitation index (SPI) and Reconnaissance drought index (RDI). J Hydrol 526:183–195. doi: 10.1016/J.JHYDROL.2014.09.071

Azorin-Molina C, Vicente-Serrano SM, Sanchez-Lorenzo A, McVicar TR, Morán-Tejeda E, Revuelto J, El Kenawy A, Martín-Hernández N, Tomas-Burguera M (2015) Atmospheric evaporative demand observations, estimates and driving factors in

Spain (1961–2011). J Hydrol 523:262–277. doi: 10.1016/J.JHYDROL.2015.01.046
Baigorria G, Jones J, Shin D, Mishra A, O'Brien J (2007) Assessing uncertainties in crop model simulations using daily bias-corrected Regional Circulation Model outputs. Clim Res 34:211–222. doi: 10.3354/cr00703
Bandyopadhyay A, Bhadra A, Raghuwanshi NS, Singh R (2009) Temporal Trends in Estimates of Reference Evapotranspiration over India. J Hydrol Eng 14:508–515. doi: 10.1061/(ASCE)HE.1943-5584.0000006
Barbosa SM (2011) Testing for deterministic trends in global sea surface temperature. J Clim 24:2516–2522. doi: 10.1175/2010JCLI3877.1
Beguería S, Vicente-Serrano SM, Reig F, Latorre B (2014) Standardized precipitation evapotranspiration index (SPEI) revisited: parameter fitting, evapotranspiration models, tools, datasets and drought monitoring. Int J Climatol 34:3001–3023. doi: 10.1002/joc.3887
Belo-Pereira M, Dutra E, Viterbo P (2011) Evaluation of global precipitation data sets over the Iberian Peninsula. J Geophys Res 116:D20101. doi: 10.1029/2010JD015481
Bento V, Trigo I, Gouveia C, DaCamara C, Bento VA, Trigo IF, Gouveia CM, DaCamara CC (2018) Contribution of Land Surface Temperature (TCI) to Vegetation Health Index: A Comparative Study Using Clear Sky and All-Weather Climate Data Records. Remote Sens 10:1324. doi: 10.3390/rs10091324
Berengena J, Gavilán P (2005) Reference Evapotranspiration Estimation in a Highly Advective Semiarid Environment. J Irrig Drain Eng 131:147–163. doi: 10.1061/(ASCE)0733-9437(2005)131:2(147)
Berg AA, Famiglietti JS, Walker JP, Houser PR (2003) Impact of bias correction to reanalysis products on simulations of North American soil moisture and hydrological fluxes. J Geophys Res 108:ACL 2-1-ACL 2-15. doi: 10.1029/2002JD003334
Bierkens MFP, van Beek LPH (2009) Seasonal Predictability of European Discharge: NAO and Hydrological Response Time. J Hydrometeorol 10:953–968. doi: 10.1175/2009JHM1034.1
Bloomfield P (2000) Fourier Analysis of Time Series. An Introduction, J. Wiley & Sons, New York
Bonaccorso B, Bordi I, Cancelliere A, Rossi G, Sutera A (2003) Spatial Variability of Drought: An Analysis of the SPI in Sicily. Water Resour Manag 17:273–296. doi: 10.1023/A:1024716530289
Bonsal BR, Aider R, Gachon P, Lapp S (2013) An assessment of Canadian prairie drought: past, present, and future. Clim Dyn 41:501–516. doi: 10.1007/s00382-012-1422-0
Bordi I, Fraedrich K, Gerstengarbe F-W, Erner PC, Sutera A (2004a) Potential predictability of dry and wet periods: Sicily and Elbe-Basin (Germany). Theor Appl Climatol 77:125–138. doi: 10.1007/s00704-003-0029-0
Bordi I, Fraedrich K, Jiang J-M, Sutera A (2004b) Spatio-temporal variability of dry and wet periods in eastern China. Theor Appl Climatol 79:81–91. doi: 10.1007/s00704-004-0053-8
Bordi I, Fraedrich K, Petitta M, Sutera A (2006) Large-Scale Assessment of Drought Variability Based on NCEP/NCAR and ERA-40 Re-Analyses. Water Resour Manag 20:899–915. doi: 10.1007/s11269-005-9013-z
Bordi I, Sutera A (2002) An analysis of drought in Italy in the last fifty years. Il Nuovo Cimento 25C:185–206 de Lima MIP, Carvalho SCP, de Lima JLMP, Coelho MFES (2010) Trends in precipitation: analysis of long annual and monthly time series from

mainland Portugal. Adv Geosci 2
Bordi I, Sutera A (2001) Fifty Years of Precipitation: Some Spatially Remote Teleconnnections. Water Resour Manag 15:247–280. doi: 10.1023/A:1013353822381
Bouchet RJ (1963) Evapotranspiration réell e et potentielle, signification climatique. Int Assoc Sci Hydrol Publ 62:143–142
Brutsaert W (2006) Indications of increasing land surface evaporation during the second half of the 20th century. Geophys Res Lett 33:L20403. doi: 10.1029/2006GL027532
Burke EJ, Brown SJ (2008) Evaluating Uncertainties in the Projection of Future Drought. J Hydrometeorol 9:292–299. doi: 10.1175/2007JHM929.1
Burke EJ, Brown SJ, Christidis N, Burke EJ, Brown SJ, Christidis N (2006) Modeling the Recent Evolution of Global Drought and Projections for the Twenty-First Century with the Hadley Centre Climate Model. J Hydrometeorol 7:1113–1125. doi: 10.1175/JHM544.1
Cadol D, Kampf S, Wohl E (2012) Effects of evapotranspiration on baseflow in a tropical headwater catchment. J Hydrol 462–463:4–14. doi: 10.1016/J.JHYDROL.2012.04.060
Cai J, Liu Y, Lei T, Pereira LS (2007) Estimating reference evapotranspiration with the FAO Penman–Monteith equation using daily weather forecast messages. Agric For Meteorol 145:22–35. doi: 10.1016/J.AGRFORMET.2007.04.012
Cai JB, Liu Y, Xu D, Paredes P, Pereira LS (2009) Simulation of the soil water balance of wheat using daily weather forecast messages to estimate the reference evapotranspiration. Hydrol Earth Syst Sci 13:1045–1059. doi: 10.5194/hess-13-1045-2009
Calanca P, Roesch A, Jasper K, Wild M (2006) Global Warming and the Summertime Evapotranspiration Regime of the Alpine Region. Clim Change 79:65–78. doi: 10.1007/s10584-006-9103-9
Cammalleri C, Rallo G, Agnese C, Ciraolo G, Minacapilli M, Provenzano G (2013) Combined use of eddy covariance and sap flow techniques for partition of ET fluxes and water stress assessment in an irrigated olive orchard. Agric Water Manag 120:89–97
Chaouche K, Neppel L, Dieulin C, Pujol N, Ladouche B, Martin E, Salas D, Caballero Y (2010) Analyses of precipitation, temperature and evapotranspiration in a French Mediterranean region in the context of climate change. Comptes Rendus Geosci 342:234–243. doi: 10.1016/J.CRTE.2010.02.001
Chattopadhyay S, Chattopadhyay G (2011) The possible association between summer monsoon rainfall in India and sunspot numbers. Int J Remote Sens 32:891–907. doi: 10.1080/01431161.2010.517800
Che HZ, Shi GY, Zhang XY, Arimoto R, Zhao JQ, Xu L, Wang B, Chen ZH (2005) Analysis of 40 years of solar radiation data from China, 1961–2000. Geophys Res Lett 32:L06803. doi: 10.1029/2004GL022322
Cleveland R, WS, Cleveland W, McRae J, Terpenning I (1990) STL: a seasonal-trend decomposition procedure based on loess. J Off Sta 6:3–73
Cohen S, Ianetz A, Stanhill G (2002) Evaporative climate changes at Bet Dagan, Israel, 1964–1998. Agric For Meteorol 111:83–91. doi: 10.1016/S0168-1923(02)00016-3
Compo GP, Whitaker JS, Sardeshmukh PD, Matsui N, Allan RJ, Yin X, Gleason BE, Vose RS, Rutledge G, Bessemoulin P, Brönnimann S, Brunet M, Crouthamel RI, Grant AN, Groisman PY, Jones PD, Kruk MC, Kruger AC, Marshall GJ, Maugeri M, Mok HY, Nordli Ø, Ross TF, Trigo RM, Wang XL, Woodruff SD, Worley SJ (2011) The Twentieth Century Reanalysis Project. Q J R Meteorol Soc 137:1–28.

doi: 10.1002/qj.776
Cong ZT, Yang DW, Ni GH (2009) Hydrology and Earth System Sciences Does evaporation paradox exist in China?
Cristea NC, Kampf SK, Burges SJ (2013) Linear models for estimating annual and growing season reference evapotranspiration using averages of weather variables. Int J Climatol 33:376–387. doi: 10.1002/joc.3430
Croitoru A-E, Piticar A, Dragotă CS, Burada DC (2013) Recent changes in reference evapotranspiration in Romania. Glob Planet Change 111:127–136. doi: 10.1016/J.GLOPLACHA.2013.09.004
Cruz-Blanco M, Gavilán P, Santos C, Lorite IJ (2014) Assessment of reference evapotranspiration using remote sensing and forecasting tools under semi-arid conditions. Int J Appl Earth Obs Geoinf 33:280–289. doi: 10.1016/J.JAG.2014.06.008
Cruz-Blanco M, Santos C, Gavilán P, Lorite IJ (2015) Uncertainty in estimating reference evapotranspiration using remotely sensed and forecasted weather data under the climatic conditions of Southern Spain. Int J Climatol 35:3371–3384. doi: 10.1002/joc.4215
D'Agostino RB, Stephens MA (1986) Goodness-of-fit techniques. Series: Statistics, Text Books and Monographs; vol.68, 560 p.
Dai A (2011) Characteristics and trends in various forms of the Palmer Drought Severity Index during 1900–2008. J Geophys Res 116:D12115. doi: 10.1029/2010JD015541
Dai A (2006) Recent climatology, variability, and trends in global surface humidity. J Clim 19:3589–3606. doi: 10.1175/JCLI3816.1
Dai A, Trenberth KE, Qian T (2004) A Global Dataset of Palmer Drought Severity Index for 1870–2002: Relationship with Soil Moisture and Effects of Surface Warming. J Hydrometeorol 5:1117–1130. doi: 10.1175/JHM-386.1
Dai A, Zhao T (2017) Uncertainties in historical changes and future projections of drought. Part I: estimates of historical drought changes. Clim Change 144:519–533. doi: 10.1007/s10584-016-1705-2
De Bruin H, Trigo I, Gavilán P, Martínez-Cob A, González-Dugo M (2012) Reference crop evapotranspiration estimated from geostationary satellite imagery. Reference crop evapotranspiration estimated from geostationary satellite imagery. In Remote Sensing and Hydrology, Neale CM, Cosh MH (eds). IAHS: Wallingford, UK, 111–114
De Bruin HAR, Trigo IF, Bosveld FC, Meirink JF (2016) A Thermodynamically Based Model for Actual Evapotranspiration of an Extensive Grass Field Close to FAO Reference, Suitable for Remote Sensing Application. J Hydrometeorol 17:1373–1382. doi: 10.1175/JHM-D-15-0006.1
De Bruin HAR, Trigo IF, Gavilán Zafra P, Martínez-Cob A, González Dugo MP (2010) Reference crop evapotranspiration estimated from geostationary satellite imagery
de Lima MIP, Carvalho SCP, de Lima JLMP, Coelho MFES (2010) Trends in precipitation: analysis of long annual and monthly time series from mainland Portugal. Adv Geosci 25:155–160. doi: 10.5194/adgeo-25-155-2010
de Lima MIP, Santo FE, Ramos AM, Trigo RM (2015) Trends and correlations in annual extreme precipitation indices for mainland Portugal, 1941–2007. Theor Appl Climatol 119:55–75. doi: 10.1007/s00704-013-1079-6
Decker M, Brunke MA, Wang Z, Sakaguchi K, Zeng X, Bosilovich MG, Decker M, Brunke MA, Wang Z, Sakaguchi K, Zeng X, Bosilovich MG (2012) Evaluation of the Reanalysis Products from GSFC, NCEP, and ECMWF Using Flux Tower Observations. J Clim 25:1916–1944. doi: 10.1175/JCLI-D-11-00004.1

Dee DP, Uppala SM, Simmons AJ, Berrisford P, Poli P, Kobayashi S, Andrae U, Balmaseda MA, Balsamo G, Bauer P, Bechtold P, Beljaars ACM, van de Berg L, Bidlot J, Bormann N, Delsol C, Dragani R, Fuentes M, Geer AJ, Haimberger L, Healy SB, Hersbach H, Hólm E V., Isaksen L, Kållberg P, Köhler M, Matricardi M, McNally AP, Monge-Sanz BM, Morcrette J-J, Park B-K, Peubey C, de Rosnay P, Tavolato C, Thépaut J-N, Vitart F (2011) The ERA-Interim reanalysis: configuration and performance of the data assimilation system. Q J R Meteorol Soc 137:553–597. doi: 10.1002/qj.828

Doorenbos J, Pruitt WO (1977) Crop Water Requirements. Irrigation and Drainage Paper No. 24. FAO, Rome, Italy, 197p

Dracup JA, Lee KS, Paulson EG (1980) On the definition of droughts. Water Resour Res 16:297–302. doi: 10.1029/WR016i002p00297

Dubrovsky M, Svoboda MD, Trnka M, Hayes MJ, Wilhite DA, Zalud Z, Hlavinka P (2009) Application of relative drought indices in assessing climate-change impacts on drought conditions in Czechia. Theor Appl Climatol 96:155–171. doi: 10.1007/s00704-008-0020-x

Eisenhauer JG (2003) Regression through the Origin. Teach Stat 25:76–80. doi: 10.1111/1467-9639.00136

El-Shafie A, Alsulami HM, Jahanbani H, Najah A (2013) Multi-lead ahead prediction model of reference evapotranspiration utilizing ANN with ensemble procedure. Stoch Environ Res Risk Assess 27:1423–1440. doi: 10.1007/s00477-012-0678-6

Espadafor M, Lorite IJ, Gavilán P, Berengena J (2011) An analysis of the tendency of reference evapotranspiration estimates and other climate variables during the last 45 years in Southern Spain. Agric Water Manag 98:1045–1061. doi: 10.1016/J.AGWAT.2011.01.015

Estévez J, Gavilán P, Berengena J (2009) Sensitivity analysis of a Penman-Monteith type equation to estimate reference evapotranspiration in southern Spain. Hydrol Process 23:3342–3353. doi: 10.1002/hyp.7439

European Environment Agency (2018) Use of freshwater resources. https://www.eea.europa.eu/data-and-maps/indicators/use-of-freshwater-resources-2/assessment-3. Accessed 22 Feb 2019

Fang GH, Yang J, Chen YN, Zammit C (2015) Comparing bias correction methods in downscaling meteorological variables for a hydrologic impact study in an arid area in China. Hydrol Earth Syst Sci 19:2547–2559. doi: 10.5194/hess-19-2547-2015

Fatichi S, Barbosa SM, Caporali E, Silva ME (2009) Deterministic versus stochastic trends: Detection and challenges. J Geophys Res 114:D18121. doi: 10.1029/2009JD011960

Feng S, Hu Q, Qian W (2004) Quality control of daily meteorological data in China, 1951–2000: a new dataset. Int J Climatol 24:853–870. doi: 10.1002/joc.1047

Fisher RA (1929) Tests of Significance in Harmonic Analysis. Proc R Soc A Math Phys Eng Sci 125:54–59. doi: 10.1098/rspa.1929.0151

Fu G, Charles SP, Timbal B, Jovanovic B, Ouyang F (2016) Comparison of NCEP-NCAR and ERA-Interim over Australia. Int J Climatol 36:2345–2367. doi: 10.1002/joc.4499

Fujihara Y, Tanaka K, Watanabe T, Nagano T, Kojiri T (2008) Assessing the impacts of climate change on the water resources of the Seyhan River Basin in Turkey: Use of dynamically downscaled data for hydrologic simulations. J Hydrol 353:33–48. doi: 10.1016/J.JHYDROL.2008.01.024

Gámiz-Fortis SR, Hidalgo-Muñoz JM, Argüeso D, Esteban-Parra MJ, Castro-Díez Y (2011) Spatio-temporal variability in Ebro river basin (NE Spain): Global SST as

potential source of predictability on decadal time scales. J Hydrol 409:759–775. doi: 10.1016/J.JHYDROL.2011.09.014
Gao G, Chen D, Ren G, Chen Y, Liao Y (2006) Spatial and temporal variations and controlling factors of potential evapotranspiration in China: 1956–2000. J Geogr Sci 16:3–12. doi: 10.1007/s11442-006-0101-7
Gao G, Chen D, Xu C, Simelton E (2007) Trend of estimated actual evapotranspiration over China during 1960–2002. J Geophys Res 112:D11120. doi: 10.1029/2006JD008010
García JA, Serrano A, de la Cruz Gallego M (2002) A spectral analysis of Iberian Peninsula monthly rainfall. Theor Appl Climatol 71:77–95. doi: 10.1007/s704-002-8209-y
Garcia M, Raes D, Allen R, Herbas C (2004) Dynamics of reference evapotranspiration in the Bolivian highlands (Altiplano). Agric For Meteorol 125:67–82. doi: 10.1016/J.AGRFORMET.2004.03.005
Gavilán P, Lorite IJJ, Tornero S, Berengena J (2006) Regional calibration of Hargreaves equation for estimating reference ET in a semiarid environment. Agric Water Manag 81:257–281. doi: 10.1016/J.AGWAT.2005.05.001
Glenn EP, Neale CMU, Hunsaker DJ, Nagler PL (2011) Vegetation index-based crop coefficients to estimate evapotranspiration by remote sensing in agricultural and natural ecosystems. Hydrol Process 25:4050–4062. doi: 10.1002/hyp.8392
Gocic M, Trajkovic S (2010) Software for estimating reference evapotranspiration using limited weather data. Comput Electron Agric 71:158–162. doi: 10.1016/J.COMPAG.2010.01.003
Gong L, Xu C, Chen D, Halldin S, Chen YD (2006) Sensitivity of the Penman–Monteith reference evapotranspiration to key climatic variables in the Changjiang (Yangtze River) basin. J Hydrol 329:620–629. doi: 10.1016/J.JHYDROL.2006.03.027
Grouillet B, Ruelland D, Vaittinada Ayar P, Vrac M (2016) Sensitivity analysis of runoff modeling to statistical downscaling models in the western Mediterranean. Hydrol Earth Syst Sci 20:1031–1047. doi: 10.5194/hess-20-1031-2016
Guo H, Xu M, Hu Q (2011) Changes in near-surface wind speed in China: 1969-2005. Int J Climatol 31:349–358. doi: 10.1002/joc.2091
Gupta HV, Sorooshian S, Yapo PO (1999) Status of Automatic Calibration for Hydrologic Models: Comparison with Multilevel Expert Calibration. J Hydrol Eng 4:135–143. doi: 10.1061/(ASCE)1084-0699(1999)4:2(135)
Guttman NB (1999) Accepting the standardized precipitation index: A calculation algorithm. J Am Water Resour Assoc 35:311–322. doi: 10.1111/j.1752-1688.1999.tb03592.x
Guttman NB (1998) Comparing the Palmer Drought Index and the Standardized Precipitation Index. J Am Water Resour Assoc 34:113–121. doi: 10.1111/j.1752-1688.1998.tb05964.x
Guttman NB, Wallis JR, Hosking JRM (1992) Spatial comparability of the Palmer drought severity index. J Am Water Resour Assoc 28:1111–1119. doi: 10.1111/j.1752-1688.1992.tb04022.x
H. J. Farahani HJ, T. A. Howell TA, W. J. Shuttleworth WJ, W. C. Bausch WC (2007) Evapotranspiration: Progress in Measurement and Modeling in Agriculture. Trans ASABE 50:1627–1638. doi: 10.13031/2013.23965
Halenka T, Kalvová J, Chládová Z, Demeterová A, Zemánková K, Belda M (2006) On the capability of RegCM to capture extremes in long term regional climate simulation – comparison with the observations for Czech Republic. Theor Appl Climatol 86:125–145. doi: 10.1007/s00704-005-0205-5

Hamed KH, Rao RA (1998) A modified Mann-Kendall trend test for autocorrelated data. J Hydrol 204:182–196. doi: 10.1016/S0022-1694(97)00125-X
Han S, Xu D, Wang S (2012) Decreasing potential evaporation trends in China from 1956 to 2005: Accelerated in regions with significant agricultural influence? Agric For Meteorol 154–155:44–56. doi: 10.1016/j.agrformet.2011.10.009
Hargreaves GH, Allen RG (2003) History and Evaluation of Hargreaves Evapotranspiration Equation. J Irrig Drain Eng 129:53–63. doi: 10.1061/(ASCE)0733-9437(2003)129:1(53)
Hargreaves GH, Samani ZA (1985) Reference Crop Evapotranspiration from Temperature. Appl Eng Agric 1:96–99. doi: 10.13031/2013.26773
Harman H (1976) Modern Factor Analysis. 3rd ed. The University of Chicago Press, 487 pp
Harris I, Jones PD, Osborn TJ, Lister DH (2014) Updated high-resolution grids of monthly climatic observations - the CRU TS3.10 Dataset. Int J Climatol 34:623–642. doi: 10.1002/joc.3711
Hart QJ, Brugnach M, Temesgen B, Rueda C, Ustin SL, Frame K (2009) Daily reference evapotranspiration for California using satellite imagery and weather station measurement interpolation. Civ Eng Environ Syst 26:19–33. doi: 10.1080/10286600802003500
Hathaway DH (2010) The Solar Cycle. Living Rev Sol Phys 7:1. doi: 10.12942/lrsp-2010-1
Heddinghaus TR, Sabol P (1991) A Review of the Palmer Drought Severity Index and Where Do We Go from Here? Proc 7th Conf Appl Climatol Am Meteorol Soc 242–246
Heim R (2002) A Review of Twentieth-Century Drought Indices Used in the United States. Bull Am Meteorol Soc 83:1149–1165. doi: 10.1175/1520-0477(2002)083<1149:AROTDI>2.3.CO;2
Helsel D, Hirsch R (1992) Statistical Methods in Water Resources. Elsevier, Amsterdam, 522 pp
Hempel S, Frieler K, Warszawski L, Schewe J, Piontek F (2013) A trend-preserving bias correction – the ISI-MIP approach. Earth Syst Dyn 4:219–236. doi: 10.5194/esd-4-219-2013
Herrera S, Gutiérrez JM, Ancell R, Pons MR, Frías MD, Fernández J (2012) Development and analysis of a 50-year high-resolution daily gridded precipitation dataset over Spain (Spain02). Int J Climatol 32:74–85. doi: 10.1002/joc.2256
Hirsch RM (1982) A comparison of four streamflow record extension techniques. Water Resour Res 18:1081–1088. doi: 10.1029/WR018i004p01081
Hlavinka P, Trnka M, Semerádová D, Dubrovský M, Žalud Z, Možný M (2009) Effect of drought on yield variability of key crops in Czech Republic. Agric For Meteorol 149:431–442. doi: 10.1016/J.AGRFORMET.2008.09.004
Hobbins M, McEvoy DJ, Hain C (2017) Evapotranspiration, Evaporative Demand, and Drought. In: Wilhite DA, Pulwarty RS (eds) Drought and Water Crises, second Edi. CRC Press, Boca Raton, pp 259–288
Hobbins MT, Ramírez JA, Brown TC (2004) Trends in pan evaporation and actual evapotranspiration across the conterminous U.S.: Paradoxical or complementary? Geophys Res Lett 31:n/a-n/a. doi: 10.1029/2004GL019846
Hoekstra AY, Mekonnen MM, Chapagain AK, Mathews RE, Richter BD (2012) Global monthly water scarcity: Blue water footprints versus blue water availability. PLoS One 7:32688. doi: 10.1371/journal.pone.0032688
Hofer M, Marzeion B, Mölg T (2012) Comparing the skill of different reanalyses and

their ensembles as predictors for daily air temperature on a glaciated mountain (Peru). Clim Dyn 39:1969–1980. doi: 10.1007/s00382-012-1501-2

Hu Q, Willson GD (2000) Effects of temperature anomalies on the Palmer Drought Severity Index in the central United States. Int J Climatol 20:1899–1911. doi: 10.1002/1097-0088(200012)20:15<1899::AID-JOC588>3.0.CO;2-M

Huo Z, Dai X, Feng S, Kang S, Huang G (2013) Effect of climate change on reference evapotranspiration and aridity index in arid region of China. J Hydrol 492:24–34. doi: 10.1016/J.JHYDROL.2013.04.011

Hwang S, Graham WD, Geurink JS, Adams A (2014) Hydrologic implications of errors in bias-corrected regional reanalysis data for west central Florida. J Hydrol 510:513–529. doi: 10.1016/J.JHYDROL.2013.11.042

Im ES, Ahn JB, Kim DW (2012) An assessment of future dryness over Korea based on the ECHAM5-RegCM3 model chain under A1B emission scenario. Asia-Pacific J Atmos Sci 48:325–337. doi: 10.1007/s13143-012-0031-5

IPCC (2014) Climate Change 2014: Synthesis Report. Contribution of Working Groups I, II and III to the Fifth Assessment Report of the Intergovernmental Panel on Climate Change. [Core Writing Team, R.K. Pachauri (eds.)]., and L.A. Meyer. IPCC, Geneva, 151pp

Irmak S, Irmak A, Allen RG, Jones JW (2003) Solar and Net Radiation-Based Equations to Estimate Reference Evapotranspiration in Humid Climates. J Irrig Drain Eng 129:336–347. doi: 10.1061/(ASCE)0733-9437(2003)129:5(336)

Irmak S, Kabenge I, Skaggs KE, Mutiibwa D (2012) Trend and magnitude of changes in climate variables and reference evapotranspiration over 116-yr period in the Platte River Basin, central Nebraska–USA. J Hydrol 420–421:228–244. doi: 10.1016/J.JHYDROL.2011.12.006

Ishak AM, Bray M, Remesan R, Han D (2010) Estimating reference evapotranspiration using numerical weather modelling. Hydrol Process 24:3490–3509. doi: 10.1002/hyp.7770

J. A, N. J, N. B, R. A, Annandale J, Jovanovic N, Benadé N, Allen R (2002) Software for missing data error analysis of Penman-Monteith reference evapotranspiration. Irrig Sci 21:57–67. doi: 10.1007/s002710100047

Jabloun M, Sahli A (2008) Evaluation of FAO-56 methodology for estimating reference evapotranspiration using limited climatic data: Application to Tunisia. Agric Water Manag 95:707–715. doi: 10.1016/J.AGWAT.2008.01.009

Janssen PHM, Heuberger PSC (1995) Calibration of process-oriented models. Ecol Modell 83:55–66. doi: 10.1016/0304-3800(95)00084-9

Jensen M (1968) Water consumption by agricultural plants. In Water Deficits and Plant Growth: Development, Control, and Measurement, Kozlowski TT (ed). Academic Press: New York, NY, 1–22

Jensen M, Robb D, Franzoy C (1970) Scheduling irrigations using climate-crop-soil data. J. Irrig. Drain. Div 96: 25–38

Jeong D Il, Sushama L, Naveed Khaliq M (2014) The role of temperature in drought projections over North America. Clim Change 127:289–303. doi: 10.1007/s10584-014-1248-3

Jhajharia D, Dinpashoh Y, Kahya E, Singh VP, Fakheri-Fard A (2012) Trends in reference evapotranspiration in the humid region of northeast India. Hydrol Process 26:421–435. doi: 10.1002/hyp.8140

Jung M, Reichstein M, Ciais P, Seneviratne SI, Sheffield J, Goulden ML, Bonan G, Cescatti A, Chen J, de Jeu R, Dolman AJ, Eugster W, Gerten D, Gianelle D, Gobron N, Heinke J, Kimball J, Law BE, Montagnani L, Mu Q, Mueller B, Oleson K, Papale

D, Richardson AD, Roupsard O, Running S, Tomelleri E, Viovy N, Weber U, Williams C, Wood E, Zaehle S, Zhang K (2010) Recent decline in the global land evapotranspiration trend due to limited moisture supply. Nature 467:951–954. doi: 10.1038/nature09396

Kalnay E, Kanamitsu M, Kistler R, Collins W, Deaven D, Gandin L, Iredell M, Saha S, White G, Woollen J, Zhu Y, Leetmaa A, Reynolds R, Chelliah M, Ebisuzaki W, Higgins W, Janowiak J, Mo KC, Ropelewski C, Wang J, Jenne R, Joseph D, Kalnay E, Kanamitsu M, Kistler R, Collins W, Deaven D, Gandin L, Iredell M, Saha S, White G, Woollen J, Zhu Y, Chelliah M, Ebisuzaki W, Higgins W, Janowiak J, Mo KC, Ropelewski C, Wang J, Leetmaa A, Reynolds R, Jenne R, Joseph D (1996) The NCEP/NCAR 40-Year Reanalysis Project. Bull Am Meteorol Soc 77:437–471. doi: 10.1175/1520-0477(1996)077<0437:TNYRP>2.0.CO;2

Kanamitsu M, Ebisuzaki W, Woollen J, Yang S-K, Hnilo JJ, Fiorino M, Potter GL, Kanamitsu M, Ebisuzaki W, Woollen J, Yang S-K, Hnilo JJ, Fiorino M, Potter GL (2002) NCEP–DOE AMIP-II Reanalysis (R-2). Bull Am Meteorol Soc 83:1631–1644. doi: 10.1175/BAMS-83-11-1631

Karl TR (1986) The Sensitivity of the Palmer Drought Severity Index and Palmer's Z-Index to their Calibration Coefficients Including Potential Evapotranspiration. J Clim Appl Meteorol 25:77–86. doi: 10.1175/1520-0450(1986)025<0077:TSOTPD>2.0.CO;2

Karl TR (1983) Some Spatial Characteristics of Drought Duration in the United States. J Clim Appl Meteorol 22:1356–1366. doi: 10.1175/1520-0450(1983)022<1356:SSCODD>2.0.CO;2

Kendall M (1975) Rank correlation methods, 4th edn. London, Charles Griffin. Griffin, London

Keyantash J, Dracup JA, Keyantash J, Dracup JA (2002) The Quantification of Drought: An Evaluation of Drought Indices. Bull Am Meteorol Soc 83:1167–1180

Kim D, Rhee J (2016) A drought index based on actual evapotranspiration from the Bouchet hypothesis. Geophys Res Lett 43:10,277-10,285. doi: 10.1002/2016GL070302

Kim T-W, Valdés JB (2003) Nonlinear Model for Drought Forecasting Based on a Conjunction of Wavelet Transforms and Neural Networks. J Hydrol Eng 8:319–328. doi: 10.1061/(ASCE)1084-0699(2003)8:6(319)

Kisi O, Cengiz TM (2013) Fuzzy Genetic Approach for Estimating Reference Evapotranspiration of Turkey: Mediterranean Region. Water Resour Manag 27:3541–3553. doi: 10.1007/s11269-013-0363-7

Kogan FN (1990) Remote sensing of weather impacts on vegetation in non-homogeneous areas. Int J Remote Sens 11:1405–1419. doi: 10.1080/01431169008955102

Kottek M, Grieser J, Beck C, Rudolf B, Rubel F (2006) World Map of the Köppen-Geiger climate classification updated. Meteorol Zeitschrift 15:259–263. doi: 10.1127/0941-2948/2006/0130

Kousari MR, Asadi Zarch MA, Ahani H, Hakimelahi H (2013) A survey of temporal and spatial reference crop evapotranspiration trends in Iran from 1960 to 2005. Clim Change 120:277–298. doi: 10.1007/s10584-013-0821-5

Küçük M, Kahya E, Cengiz TM, Karaca M (2009) North Atlantic Oscillation influences on Turkish lake levels. Hydrol Process 23:893–906. doi: 10.1002/hyp.7225

Kwiatkowski D, Phillips PCB, Schmidt P, Shin Y (1992) Testing the null hypothesis of stationarity against the alternative of a unit root: How sure are we that economic time series have a unit root? J Econom 54:159–178. doi: 10.1016/0304-4076(92)90104-Y

Labat D (2006) Oscillations in land surface hydrological cycle. Earth Planet Sci Lett 242:143–154. doi: 10.1016/J.EPSL.2005.11.057

Landeras G, Ortiz-Barredo A, López JJ (2008) Comparison of artificial neural network models and empirical and semi-empirical equations for daily reference evapotranspiration estimation in the Basque Country (Northern Spain). Agric Water Manag 95:553–565. doi: 10.1016/J.AGWAT.2007.12.011

Lecina S, Martínez-Cob A, Pérez PJ, Villalobos FJ, Baselga JJ (2003) Fixed versus variable bulk canopy resistance for reference evapotranspiration estimation using the Penman–Monteith equation under semiarid conditions. Agric Water Manag 60:181–198. doi: 10.1016/S0378-3774(02)00174-9

Legates DR, McCabe GJ (1999) Evaluating the use of "goodness-of-fit" Measures in hydrologic and hydroclimatic model validation. Water Resour Res 35:233–241. doi: 10.1029/1998WR900018

Li B, Su H, Chen F, Li S, Tian J, Qin Y, Zhang R, Chen S, Yang Y, Rong Y (2013) The changing pattern of droughts in the Lancang River Basin during 1960–2005. Theor Appl Climatol 111:401–415. doi: 10.1007/s00704-012-0658-2

Li Z, Zheng F-L, Liu W-Z (2012) Spatiotemporal characteristics of reference evapotranspiration during 1961–2009 and its projected changes during 2011–2099 on the Loess Plateau of China. Agric For Meteorol 154–155:147–155. doi: 10.1016/J.AGRFORMET.2011.10.019

Liang F, Xia XA (2005) Long-term trends in solar radiation and the associated climatic factors over China for 1961-2000. Ann Geophys 23:2425–2432

Liang L, Li L, Liu Q (2011) Precipitation variability in Northeast China from 1961 to 2008. J Hydrol 404:67–76. doi: 10.1016/J.JHYDROL.2011.04.020

Liang L, Li L, Liu Q (2010) Temporal variation of reference evapotranspiration during 1961–2005 in the Taoer River basin of Northeast China. Agric For Meteorol 150:298–306. doi: 10.1016/J.AGRFORMET.2009.11.014

Liou Y-A, Kar S (2014) Evapotranspiration Estimation with Remote Sensing and Various Surface Energy Balance Algorithms—A Review. Energies 7:2821–2849. doi: 10.3390/en7052821

Liu L, Hong Y, Looper J, Riley R, Yong B, Zhang Z, Hocker J, Shafer M (2013a) Climatological Drought Analyses and Projection Using SPI and PDSI: Case Study of the Arkansas Red River Basin. J Hydrol Eng 18:809–816. doi: 10.1061/(ASCE)HE.1943-5584.0000619

Liu Q, McVicar TR (2012) Assessing climate change induced modification of Penman potential evaporation and runoff sensitivity in a large water-limited basin. J Hydrol 464–465:352–362. doi: 10.1016/J.JHYDROL.2012.07.032

Liu Q, Yang Z, Cui B, Sun T (2010) The temporal trends of reference evapotranspiration and its sensitivity to key meteorological variables in the Yellow River Basin, China. Hydrol Process 24:n/a-n/a. doi: 10.1002/hyp.7649

Liu X, Zhang D (2013) Trend analysis of reference evapotranspiration in Northwest China: The roles of changing wind speed and surface air temperature. Hydrol Process 27:3941–3948. doi: 10.1002/hyp.9527

Liu Y, Hwang Y (2015) Improving drought predictability in Arkansas using the ensemble PDSI forecast technique. Stoch Environ Res Risk Assess 29:79–91. doi: 10.1007/s00477-014-0930-3

Liu Y, Pereira L (1997) Calculation methods for reference evapotranspiration with limited weather data. J Hydraul Eng 6:7–31 (in Chinese)

Liu Y, Pereira L (2001) Calculation methods for reference evapotranspiration with limited weather data. J Hydraulic Eng (3):11-17 (in Chinese)

Liu Y, Zhuang Q, Chen M, Pan Z, Tchebakova N, Sokolov A, Kicklighter D, Melillo J, Sirin A, Zhou G, He Y, Chen J, Bowling L, Miralles D, Parfenova E (2013b) Response of evapotranspiration and water availability to changing climate and land cover on the Mongolian Plateau during the 21st century. Glob Planet Change 108:85–99. doi: 10.1016/J.GLOPLACHA.2013.06.008

Liu Y, Zhuang Q, Pan Z, Miralles D, Tchebakova N, Kicklighter D, Chen J, Sirin A, He Y, Zhou G, Melillo J (2014) Response of evapotranspiration and water availability to the changing climate in Northern Eurasia. Clim Change 126:413–427. doi: 10.1007/s10584-014-1234-9

Liu Z, Zhou P, Zhang F, Liu X, Chen G (2013c) Spatiotemporal characteristics of dryness/wetness conditions across Qinghai Province, Northwest China. Agric For Meteorol 182–183:101–108. doi: 10.1016/J.AGRFORMET.2013.05.013

Lloyd-Hughes B, Saunders MA (2002) A drought climatology for Europe. Int J Climatol Int J Clim 22:1571–1592. doi: 10.1002/joc.846

Lohmann S, Schillings C, Mayer B, Meyer R (2006) Long-term variability of solar direct and global radiation derived from ISCCP data and comparison with reanalysis data. Sol Energy 80:1390–1401. doi: 10.1016/J.SOLENER.2006.03.004

López-Moreno JI, Hess TM, White SM (2009) Estimation of reference evapotranspiration in a mountainous mediterranean site using the Penman-Monteith equation with limited meteorological data. JACA 164:

López-Urrea R, Martín de Santa Olalla F, Fabeiro C, Moratalla A (2006) Testing evapotranspiration equations using lysimeter observations in a semiarid climate. Agric Water Manag 85:15–26. doi: 10.1016/J.AGWAT.2006.03.014

Lorente-Plazas R, Montávez JP, Jerez S, Gómez-Navarro JJ, Jiménez-Guerrero P, Jiménez PA (2015) A 49 year hindcast of surface winds over the Iberian Peninsula. Int J Climatol 35:3007–3023. doi: 10.1002/joc.4189

Loukas A, Vasiliades L, Research ND-H, 2002 undefined Hydroclimatic variability of regional droughts in Greece using the Palmer Moisture Anomaly Index. iwaponline.com

Loukas A, Vasiliades L, Tzabiras J (2008) Climate change effects on drought severity. Adv Geosci 17:23–29. doi: 10.5194/adgeo-17-23-2008

Lucero OA, Rodríguez NC (2002) Spatial organization in Europe of decadal and interdecadal fluctuations in annual rainfall. Int J Climatol 22:805–820. doi: 10.1002/joc.756

Ma M, Ren L, Yuan F, Jiang S, Liu Y, Kong H, Gong L (2014) A new standardized Palmer drought index for hydro-meteorological use. Hydrol Process 28:5645–5661. doi: 10.1002/hyp.10063

Majidi M, Alizadeh A, Vazifedoust M, Farid A, Ahmadi T (2015) Analysis of the Effect of Missing Weather Data on Estimating Daily Reference Evapotranspiration Under Different Climatic Conditions. Water Resour Manag 29:2107–2124. doi: 10.1007/s11269-014-0782-0

Mallikarjuna P, Jyothy SA, Murthy DS, Reddy KC (2014) Performance of Recalibrated Equations for the Estimation of Daily Reference Evapotranspiration. Water Resour Manag 28:4513–4535. doi: 10.1007/s11269-014-0733-9

Mann H (1945) Non-parametric test against trend. Econometrica 13:245–259

Maraun D (2013) Bias correction, quantile mapping, and downscaling: Revisiting the inflation issue. J Clim 26:2137–2143. doi: 10.1175/JCLI-D-12-00821.1

Martí P, González-Altozano P, Gasque M (2011) Reference evapotranspiration estimation without local climatic data. Irrig Sci 29:479–495. doi: 10.1007/s00271-010-0243-3

Martí P, González-Altozano P, López-Urrea R, Mancha LA, Shiri J (2015) Modeling reference evapotranspiration with calculated targets. Assessment and implications. Agric Water Manag 149:81–90. doi: 10.1016/J.AGWAT.2014.10.028

Martí P, Zarzo M (2012) Multivariate statistical monitoring of ETo: A new approach for estimation in nearby locations using geographical inputs. Agric For Meteorol 152:125–134. doi: 10.1016/J.AGRFORMET.2011.08.008

Martinez CJ, Thepadia M (2010) Estimating Reference Evapotranspiration with Minimum Data in Florida. J Irrig Drain Eng 136:494–501. doi: 10.1061/(ASCE)IR.1943-4774.0000214

Martins DS, Paulo AA, Pires C, Pereira LS (2017) Long-term variation of PDSI and SPI computed with reanalysis products. Eur Water 60:271–278

Martins DS, Raziei T, Paulo AA, Pereira LS (2012) Spatial and temporal variability of precipitation and drought in Portugal. Nat Hazards Earth Syst Sci 12:1493–1501. doi: 10.5194/nhess-12-1493-2012

Maurer EP, Das T, Cayan DR (2013) Errors in climate model daily precipitation and temperature output: time invariance and implications for bias correction. Hydrol Earth Syst Sci 17:2147–2159. doi: 10.5194/hess-17-2147-2013

Mavromatis T (2007) Drought index evaluation for assessing future wheat production in Greece. Int J Climatol 27:911–924. doi: 10.1002/joc.1444

Mazzarella A, Palumbo F (1992) Rainfall fluctuations over Italy and their association with solar activity. Theor Appl Climatol 45:201–207. doi: 10.1007/BF00866193

McCarl BA, Villavicencio X, Wu X (2008) Climate Change and Future Analysis: Is Stationarity Dying? Am J Agric Econ 90:1241–1247. doi: 10.1111/j.1467-8276.2008.01211.x

McEvoy DJ, Huntington JL, Abatzoglou JT, Edwards LM, McEvoy DJ, Huntington JL, Abatzoglou JT, Edwards LM (2012) An Evaluation of Multiscalar Drought Indices in Nevada and Eastern California. Earth Interact 16:1–18. doi: 10.1175/2012EI000447.1

Mckee TB, Doesken NJ, Kleist J (1993) The relationship of drought frequency and duration to time scales. Eighth Conf Appl Climatol 17–22

McKee TB, Doesken NJ, Kleist J (1995) Drought monitoring with multiple time scales, in: 9th Conference on Applied Climatology, Am. Meteor. Soc., Boston, 233–236

McVicar TR, Roderick ML, Donohue RJ, Li LT, Van Niel TG, Thomas A, Grieser J, Jhajharia D, Himri Y, Mahowald NM, Mescherskaya A V., Kruger AC, Rehman S, Dinpashoh Y (2012) Global review and synthesis of trends in observed terrestrial near-surface wind speeds: Implications for evaporation. J Hydrol 416–417:182–205. doi: 10.1016/J.JHYDROL.2011.10.024

McVicar TR, Van Niel TG, Li L, Hutchinson MF, Mu X, Liu Z (2007) Spatially distributing monthly reference evapotranspiration and pan evaporation considering topographic influences. J Hydrol 338:196–220. doi: 10.1016/J.JHYDROL.2007.02.018

McVicar TR, Van Niel TG, Li LT, Roderick ML, Rayner DP, Ricciardulli L, Donohue RJ (2008) Wind speed climatology and trends for Australia, 1975–2006: Capturing the stilling phenomenon and comparison with near-surface reanalysis output. Geophys Res Lett 35:L20403. doi: 10.1029/2008GL035627

Mekonnen MM, Hoekstra AY (2016) Sustainability: Four billion people facing severe water scarcity. Sci Adv 2:e1500323. doi: 10.1126/sciadv.1500323

Mestas-Nuñez AM (2000) Orthogonality properties of rotated empirical modes. Int J Climatol 20:1509–1516. doi: 10.1002/1097-0088(200010)20:12<1509::AID-JOC553>3.0.CO;2-Q

Mishra AK, Desai VR (2005) Drought forecasting using stochastic models. Stoch Environ Res Risk Assess 19:326–339. doi: 10.1007/s00477-005-0238-4
Mishra AK, Singh VP (2010) A review of drought concepts. J. Hydrol. 391:202–216
Mitra K, Mukherji S, Dutta SN (1991) Some indications of 18·6 year LUNI-Solar and 10–11 year solar cycles in rainfall in North-West India, the plains of Uttar Pradesh and North-Central India. Int J Climatol 11:645–652. doi: 10.1002/joc.3370110606
Mo KC, Chelliah M (2006) The modified Palmer drought severity index based on the NCEP North American Regional Reanalysis. J Appl Meteorol Climatol 45:1362–1375. doi: 10.1175/JAM2402.1
Monacelli G, Galluccio MC, Abbafati M (2005) Drought assessment and forecasting - Drought Within The Context Of The Region VI. World Meteorol Organ Work Gr Hydrol Reg Assoc VI 8:
Monteith J (1965) Evaporation and environment. 19th Symposia of the Society for Experimental Biology, 19. University Press, Cambridge, 205–234
Moratiel R, Snyder RL, Durán JM, Tarquis AM (2011) Trends in climatic variables and future reference evapotranspiration in Duero Valley (Spain). Nat Hazards Earth Syst Sci 11:1795–1805. doi: 10.5194/nhess-11-1795-2011
Moreira E, Pires C, Pereira L (2016) SPI Drought Class Predictions Driven by the North Atlantic Oscillation Index Using Log-Linear Modeling. Water 8:43. doi: 10.3390/w8020043
Moreira E, Russo A, Trigo R, Moreira E, Russo A, Trigo RM (2018) Monthly Prediction of Drought Classes Using Log-Linear Models under the Influence of NAO for Early-Warning of Drought and Water Management. Water 10:65. doi: 10.3390/w10010065
Moreira EE, Mexia JT, Pereira LS (2012) Are drought occurrence and severity aggravating? A study on SPI drought class transitions using log-linear models and ANOVA-like inference. Hydrol Earth Syst Sci 16:3011–3028. doi: 10.5194/hess-16-3011-2012
Moreira EE, Paulo AA, Pereira LS, Mexia JT (2006) Analysis of SPI drought class transitions using loglinear models. J Hydrol 331:349–359. doi: 10.1016/J.JHYDROL.2006.05.022
Moriasi DN, Arnold JG, Van Liew MW, Bingner RL, Harmel RD, Veith TL (2007) Model Evaluation Guidelines for Systematic Quantification of Accuracy in Watershed Simulations. Trans ASABE 50:885–900. doi: 10.13031/2013.23153
Nandagiri L, Kovoor GM (2006) Performance Evaluation of Reference Evapotranspiration Equations across a Range of Indian Climates. J Irrig Drain Eng 132:238–249. doi: 10.1061/(ASCE)0733-9437(2006)132:3(238)
Narasimhan B, Srinivasan R (2005) Development and evaluation of Soil Moisture Deficit Index (SMDI) and Evapotranspiration Deficit Index (ETDI) for agricultural drought monitoring. In: Agricultural and Forest Meteorology. Elsevier, pp 69–88
Nash JE, Sutcliffe JV (1970) River flow forecasting through conceptual models part I — A discussion of principles. J Hydrol 10:282–290. doi: 10.1016/0022-1694(70)90255-6
Nastos PT, Philandras CM, Kapsomenakis J, Eleftheratos K (2011) Variability and trends of mean maximum and mean minimum air temperature in Greece from ground-based observations and NCEP–NCAR reanalysis gridded data. Int J Remote Sens 32:6177–6192. doi: 10.1080/01431161.2010.507798
Niemeyer S (2008) New drought indices. In : López-Francos A. (ed.). Drought management: scientific and technological innovations. Zaragoza : CIHEAM, 2008. p. 267-274 (Options Méditerranéennes : Série A. Séminaires Méditerranéens; n. 80

Norris JR, Wild M (2009) Trends in aerosol radiative effects over China and Japan inferred from observed cloud cover, solar "dimming," and solar "brightening." J Geophys Res 114:D00D15. doi: 10.1029/2008JD011378

North GR, Bell TL, Cahalan RF, Moeng FJ, North GR, Bell TL, Cahalan RF, Moeng FJ (1982) Sampling Errors in the Estimation of Empirical Orthogonal Functions. Mon Weather Rev 110:699–706. doi: 10.1175/1520-0493(1982)110<0699:SEITEO>2.0.CO;2

Nowroozi AA (1967) Table for Fisher's Test of Significance in Harmonic Analysis. Geophys J Int 12:517–520. doi: 10.1111/j.1365-246X.1967.tb03132.x

Paço TA, Pôças I, Cunha M, Silvestre JC, Santos FL, Paredes P, Pereira LS (2014) Evapotranspiration and crop coefficients for a super intensive olive orchard. An application of SIMDualKc and METRIC models using ground and satellite observations. J Hydrol 519:2067–2080

Palmer WC (1965) Meteorological drought. Off Climatol Res Pap Weather Bur Washington, DC 45:58

Paredes P, Fontes JC, Azevedo EB, Pereira LS (2018a) Daily reference crop evapotranspiration in the humid environments of Azores islands using reduced data sets: accuracy of FAO-PM temperature and Hargreaves-Samani methods. Theor Appl Climatol 134:595–611. doi: 10.1007/s00704-017-2295-2

Paredes P, Fontes JC, Azevedo EB, Pereira LS Daily reference crop evapotranspiration with reduced data sets in the humid environments of Azores islands using estimates of actual vapor pressure, solar radiation, and wind speed. Theor Appl Climatol 134:. doi: 10.1007/s00704-017-2329-9

Paredes P, Martins DS, Pereira LS, Cadima J, Pires C (2018b) Accuracy of daily estimation of grass reference evapotranspiration using ERA-Interim reanalysis products with assessment of alternative bias correction schemes. Agric Water Manag 210:340–353. doi: 10.1016/J.AGWAT.2018.08.003

Paredes P, Ribeiro A, Pires C, Pereira L (2015) Usabilidade de previsões sazonais de ensemble da temperatura e precipitação na modelação da rega e da produção. Aplicação a cevada e milho. In Predictabilidade Sazonal de Secas. Avaliação ao Nível Regional e Agrícola, Pires CAL, Pereira LS (eds). ISA Pres

Paredes P, Rodrigues G (2010) Necessidades de água para a rega de milho em Portugal Continental considerando condições de seca. In Gestão do Risco em Secas. Métodos, tecnologias e desafios, Pereira LS, Mexia JT, Pires CAL (eds). Edições Colibri e CEER: Lisboa, Portugal, 301–319

Partal T (2009) Modelling evapotranspiration using discrete wavelet transform and neural networks. Hydrol Process 23:3545–3555. doi: 10.1002/hyp.7448

Paulo AA, Ferreira E, Coelho C, Pereira LS (2005) Drought class transition analysis through Markov and Loglinear models, an approach to early warning. Agric Water Manag 77:59–81. doi: 10.1016/J.AGWAT.2004.09.039

Paulo AA, Pereira LS (2006) Drought Concepts and Characterization. Water Int 31:37–49. doi: 10.1080/02508060608691913

Paulo AA, Pereira LS (2008) Stochastic Prediction of Drought Class Transitions. Water Resour Manag 22:1277–1296. doi: 10.1007/s11269-007-9225-5

Paulo AA, Pereira LS, Matias PG (2003) Analysis of local and regional droughts in southern Portugal using the theory of runs and the standardized precipitation index. In: Tools for drought mitigation in Mediterranean regions, edited by: G Rossi, a Cancelliere, L S Pereira, T Oweis, M Shatanawi. In: Tools for Drought Mitigation in Mediterranean Regions. pp 55–78

Paulo AA, Rosa RD, Pereira LS (2012) Climate trends and behaviour of drought indices

based on precipitation and evapotranspiration in Portugal. Nat Hazards Earth Syst Sci 12:1481–1491. doi: 10.5194/nhess-12-1481-2012
Pebesma EJ (2004) Multivariable geostatistics in S: The gstat package. Comput Geosci 30:683–691. doi: 10.1016/j.cageo.2004.03.012
Pereira LS (2017) Water, Agriculture and Food: Challenges and Issues. Water Resour Manag 31:2985–2999. doi: 10.1007/s11269-017-1664-z
Pereira LS, Allen RG, Smith M, Raes D (2015) Crop evapotranspiration estimation with FAO56: Past and future. Agric Water Manag 147:4–20. doi: 10.1016/J.AGWAT.2014.07.031
Pereira LS, Cai LG, Hann MJ (2003) Farm water and soil management for improved water use in the North China Plain. Irrig Drain 52:299–317. doi: 10.1002/ird.98
Pereira LS, Cordery I, Iacovides I (2009) Coping with water scarcity: Addressing the challenges. Springer Netherlands, Dordrecht
Pereira LS, Perrier A, Allen RG, Alves I (1999) Evapotranspiration: Concepts and Future Trends. J Irrig Drain Eng 125:45–51. doi: 10.1061/(ASCE)0733-9437(1999)125:2(45)
Pereira LS, Rosa RD, Paulo AA (2007) Testing a Modification of the Palmer Drought Severity Index for Mediterranean Environments. In: Methods and Tools for Drought Analysis and Management. Springer Netherlands, Dordrecht, pp 149–167
Peterson TC, Golubev VS, Groisman PY (1995) Evaporation losing its strength. Nature 377:687–688. doi: 10.1038/377687b0
Phillips PCB, Perron P (1988) Testing for a unit root in time series regression. Biometrika 75:335–346. doi: 10.1093/biomet/75.2.335
Pierce D (2014) ncdf: interface to unidata netCDF data files. R package version 1.6.8. http://CRAN.R-project.org/package=ncdf (accessed 30 October 2015)
Pires CA, Perdigão RAP, Pires CA, Perdigão RAP (2007) Non-Gaussianity and Asymmetry of the Winter Monthly Precipitation Estimation from the NAO. Mon Weather Rev 135:430–448. doi: 10.1175/MWR3407.1
Pires CAL (2015) Introdução. In: Pires CAL, Pereira LS (eds) Predictabilidade Sazonal das secas. Avaliação ao nível regional e agrícola. Lisboa, pp 3–18
Pollock D (1999) A Handbook of Time-Series Analysis. Signal Processing and Dynamics, Academic Press, London
Polonskii AB, Basharin D V., Voskresenskaya EN, Worley S (2004) North Atlantic Oscillation: Description, Mechanisms, and Influence on the Eurasian Climate. Phys Oceanogr 14:96–113. doi: 10.1023/B:POCE.0000037873.85289.6e
Popova Z, Ivanova M, Martins D, Pereira LS, Doneva K, Alexandrov V, Kercheva M (2014) Vulnerability of Bulgarian agriculture to drought and climate variability with focus on rainfed maize systems. Nat Hazards 74:865–886. doi: 10.1007/s11069-014-1215-3
Popova Z, Kercheva M, Pereira LS (2006) Validation of the FAO methodology for computing ETo with limited data. Application to south Bulgaria. Irrig Drain 55:201–215. doi: 10.1002/ird.228
Portela M, Santos J, Naghettini N, Matos J, Silva A (2012) Superfícies de limiares de precipitação Para identificação de secas em Portugal continental: uma aplicação complementar do índice de precipitação padronizada, SPI. Recursos Hídricos 33(02):5–23
Prokoph A, Adamowski J, Adamowski K (2012) Influence of the 11 year solar cycle on annual streamflow maxima in Southern Canada. J Hydrol 442–443:55–62. doi: 10.1016/J.JHYDROL.2012.03.038
Qian Y, Kaiser DP, Leung LR, Xu M (2006) More frequent cloud-free sky and less

surface solar radiation in China from 1955 to 2000. Geophys Res Lett 33:n/a-n/a. doi: 10.1029/2005GL024586
Quiring SM (2009) Developing objective operational definitions for monitoring drought. J Appl Meteorol Climatol 48:1217–1229. doi: 10.1175/2009JAMC2088.1
Quiring SM, Papakryiakou TN (2003) An evaluation of agricultural drought indices for the Canadian prairies. Agric For Meteorol 118:49–62. doi: 10.1016/S0168-1923(03)00072-8
R Core Team (2014) R: a language and environment for statistical computing. R Foundation for Statistical Computing, Vienna, Austria. http://www.R-project.org/ (accessed 30 October 2015)
Rahimikhoob A (2014) Comparison between M5 Model Tree and Neural Networks for Estimating Reference Evapotranspiration in an Arid Environment. Water Resour Manag 28:657–669. doi: 10.1007/s11269-013-0506-x
Raziei T, Bordi I, Pereira LS (2008) A precipitation-based regionalization for Western Iran and regional drought variability. Hydrol Earth Syst Sci 12:1309–1321. doi: 10.5194/hess-12-1309-2008
Raziei T, Bordi I, Pereira LS (2013) Regional Drought Modes in Iran Using the SPI: The Effect of Time Scale and Spatial Resolution. Water Resour Manag 27:1661–1674. doi: 10.1007/s11269-012-0120-3
Raziei T, Bordi I, Pereira LS (2011) An Application of GPCC and NCEP/NCAR Datasets for Drought Variability Analysis in Iran. Water Resour Manag 25:1075–1086. doi: 10.1007/s11269-010-9657-1
Raziei T, Martins DS, Bordi I, Santos JFJF, Portela MM, Pereira LS, Sutera A (2015) SPI Modes of Drought Spatial and Temporal Variability in Portugal: Comparing Observations, PT02 and GPCC Gridded Datasets. Water Resour Manag 29:487–504. doi: 10.1007/s11269-014-0690-3
Raziei T, Pereira LS (2013a) Spatial variability analysis of reference evapotranspiration in Iran utilizing fine resolution gridded datasets. Agric Water Manag 126:104–118. doi: 10.1016/J.AGWAT.2013.05.003
Raziei T, Pereira LS (2013b) Estimation of ETo with Hargreaves–Samani and FAO-PM temperature methods for a wide range of climates in Iran. Agric Water Manag 121:1–18. doi: 10.1016/J.AGWAT.2012.12.019
Raziei T, Saghafian B, Paulo AA, Pereira LS, Bordi I (2009) Spatial Patterns and Temporal Variability of Drought in Western Iran. Water Resour Manag 23:439–455. doi: 10.1007/s11269-008-9282-4
Ren X, Martins DS, Qu Z, Paredes P, Pereira LS (2016a) Daily Reference Evapotranspiration for Hyper-Arid to Moist Sub-Humid Climates in Inner Mongolia, China: II. Trends of ETo and Weather Variables and Related Spatial Patterns. Water Resour Manag 30:3793–3814. doi: 10.1007/s11269-016-1385-8
Ren X, Qu Z, Diogo &, Martins S, Paredes P, Pereira LS, Martins DS, Paredes P, Pereira LS (2016b) Daily Reference Evapotranspiration for Hyper-Arid to Moist Sub-Humid Climates in Inner Mongolia, China: I. Assessing Temperature Methods and Spatial Variability. Water Resour Manag 30:3769–3791. doi: 10.1007/s11269-016-1384-9
Rencher A (1998) Multivariate statistical inference and applications. John Wiley & Sons, Inc.
Rhoades DA, Salinger MJ (1993) Adjustment of temperature and rainfall records for site changes. Int J Climatol 13:899–913. doi: 10.1002/joc.3370130807
Ribeiro AFS, Pires CAL (2016) Seasonal drought predictability in Portugal using statistical–dynamical techniques. Phys Chem Earth, Parts A/B/C 94:155–166. doi:

10.1016/J.PCE.2015.04.003
Richman MB (1986) Rotation of principal components. J Climatol 6:293–335. doi: 10.1002/joc.3370060305
Rijsberman FR (2006) Water scarcity: Fact or fiction? Agric Water Manag 80:5–22. doi: 10.1016/J.AGWAT.2005.07.001
Rodrigo FS, Esteban-Parra MJ, Pozo-Vázquez D, Castro-Díez Y (2000) Rainfall variability in southern Spain on decadal to centennial time scales. Int J Climatol 20:721–732. doi: 10.1002/1097-0088(20000615)20:7<721::AID-JOC520>3.0.CO;2-Q
Rodríguez-Puebla C, Encinas AH, Sáenz J (2000) Winter precipitation over the Iberian peninsula and its relationship to circulation indices. Hydrol Earth Syst Sci Discuss 5:233–244
Rodríguez-Puebla C, Nieto S (2009) Trends of precipitation over the Iberian Peninsula and the North Atlantic Oscillation under climate change conditions. Int J Climatol 30:n/a-n/a. doi: 10.1002/joc.2035
Rodríguez Díaz JA, Weatherhead EK, Knox JW, Camacho E (2007) Climate change impacts on irrigation water requirements in the Guadalquivir river basin in Spain. Reg Environ Chang 7:149–159. doi: 10.1007/s10113-007-0035-3
Rosa R, Paulo A, Matias P, Espírito Santo M, Pires C (2010) Tratamento da qualidade das séries de dados climáticos quanto a homogeneidade, aleatoriedade e tendência e completagem de séries de dados, in: Gestão do Risco em Secas, edited by: Pereira, L. S., Mexia, J. T., and Pires, C. A. L., Métodos, Tecnologias e D
Rosa RD, Paredes P, Rodrigues GC, Alves I, Fernando RM, Pereira LS, Allen RG (2012) Implementing the dual crop coefficient approach in interactive software. 1. Background and computational strategy. Agric Water Manag 103:8–24. doi: 10.1016/J.AGWAT.2011.10.013
Rossi G (2000) Drought mitigation measures: a comprehensive framework. In: Vogt JV, Somma F (eds) Drought and drought mitigation in Europe. Kluver Academic Publishers, Dordrecht, pp 233–246
Rushton KR, Ward C (1979) The estimation of groundwater recharge. J Hydrol 41:345–361. doi: 10.1016/0022-1694(79)90070-2
Russo S, Dosio A, Sterl A, Barbosa P, Vogt J (2013) Projection of occurrence of extreme dry-wet years and seasons in Europe with stationary and nonstationary Standardized Precipitation Indices. J Geophys Res Atmos 118:7628–7639. doi: 10.1002/jgrd.50571
Rusticucci MM, Kousky VE, Rusticucci MM, Kousky VE (2002) A Comparative Study of Maximum and Minimum Temperatures over Argentina: NCEP–NCAR Reanalysis versus Station Data. J Clim 15:2089–2101. doi: 10.1175/1520-0442(2002)015<2089:ACSOMA>2.0.CO;2
Saadi S, Todorovic M, Tanasijevic L, Pereira LS, Pizzigalli C, Lionello P (2015) Climate change and Mediterranean agriculture: Impacts on winter wheat and tomato crop evapotranspiration, irrigation requirements and yield. Agric Water Manag 147:103–115. doi: 10.1016/J.AGWAT.2014.05.008
Samani Z (2000) Estimating Solar Radiation and Evapotranspiration Using Minimum Climatological Data. J Irrig Drain Eng 126:265–267. doi: 10.1061/(ASCE)0733-9437(2000)126:4(265)
Samani Z (2004) Discussion of "History and Evaluation of Hargreaves Evapotranspiration Equation"by George H. Hargreaves and Richard G. Allen. J Irrig Drain Eng 130:447–448. doi: 10.1061/(ASCE)0733-9437(2004)130:5(447.2)
Santander Meteorology Group (2012) fume: FUME package. R package version 1.0.

http://CRAN.R-project. org/package=fume
Santos J, Corte-real J, Leite S (2007) Atmospheric large-scale dynamics during the 2004/2005 winter drought in portugal. Int J Climatol 27:571–586. doi: 10.1002/joc.1425
Santos JA, Corte-Real J, Leite SM (2005) Weather regimes and their connection to the winter rainfall in Portugal. Int J Climatol 25:33–50. doi: 10.1002/joc.1101
Santos JF, Portela MM (2007) Tendências em séries de precipitação mensal em Portugal continental: aplicação do teste de Mann-Kendall
Santos JF, Pulido-Calvo I, Portela MM (2010) Spatial and temporal variability of droughts in Portugal. Water Resour Res 46:. doi: 10.1029/2009WR008071
Scargle JD (1982) Studies in astronomical time series analysis. II - Statistical aspects of spectral analysis of unevenly spaced data. Astrophys J 263:835. doi: 10.1086/160554
Schneider U, Becker A, Meyer-Christoffer A, Ziese M, Rudolf B (2010) Global Precipitation Analysis Products of the GPCC. Global Precipitation Climatology Centre (GPCC), DWD, Internet Publication (http://www. dwd.de)
Sen PK (1968) Estimates of the Regression Coefficient Based on Kendall's Tau. J Am Stat Assoc 63:1379. doi: 10.2307/2285891
Sepulcre-Canto G, Horion S, Singleton A, Carrao H, Vogt J (2012) Development of a Combined Drought Indicator to detect agricultural drought in Europe. Nat. Hazards Earth Syst. Sci. 12:3519–3531
Shadmani M, Marofi S, Roknian M (2012) Trend Analysis in Reference Evapotranspiration Using Mann-Kendall and Spearman's Rho Tests in Arid Regions of Iran. Water Resour Manag 26:211–224. doi: 10.1007/s11269-011-9913-z
Sharma S (1996) Applied Multivariate Techniques. John Wiley & Sons, New York, 512pp
Sheffield J, Goteti G, Wood EF, Sheffield J, Goteti G, Wood EF (2006) Development of a 50-Year High-Resolution Global Dataset of Meteorological Forcings for Land Surface Modeling. J Clim 19:3088–3111. doi: 10.1175/JCLI3790.1
Sheffield J, Wood EF (2008) Projected changes in drought occurrence under future global warming from multi-model, multi-scenario, IPCC AR4 simulations. Clim Dyn 31:79–105. doi: 10.1007/s00382-007-0340-z
Sheffield J, Wood EF, Roderick ML (2012) Little change in global drought over the past 60 years. Nature 491:435–438. doi: 10.1038/nature11575
Sheffield J, Ziegler AD, Wood EF, Chen Y, Sheffield J, Ziegler AD, Wood EF, Chen Y (2004) Correction of the High-Latitude Rain Day Anomaly in the NCEP–NCAR Reanalysis for Land Surface Hydrological Modeling. J Clim 17:3814–3828. doi: 10.1175/1520-0442(2004)017<3814:COTHRD>2.0.CO;2
Shi G-Y, Hayasaka T, Ohmura A, Chen Z-H, Wang B, Zhao J-Q, Che H-Z, Xu L, Shi G-Y, Hayasaka T, Ohmura A, Chen Z-H, Wang B, Zhao J-Q, Che H-Z, Xu L (2008) Data Quality Assessment and the Long-Term Trend of Ground Solar Radiation in China. J Appl Meteorol Climatol 47:1006–1016. doi: 10.1175/2007JAMC1493.1
Shiri J, Kişi Ö, Landeras G, López JJ, Nazemi AH, Stuyt LCPM (2012) Daily reference evapotranspiration modeling by using genetic programming approach in the Basque Country (Northern Spain). J Hydrol 414–415:302–316. doi: 10.1016/J.JHYDROL.2011.11.004
Shiri J, Nazemi AH, Sadraddini AA, Landeras G, Kisi O, Fard AF, Marti P (2013) Global cross-station assessment of neuro-fuzzy models for estimating daily reference evapotranspiration. J Hydrol 480:46–57. doi: 10.1016/J.JHYDROL.2012.12.006
Sienz F, Bothe O, Fraedrich K (2011) Monitoring and quantifying future climate

projections of dryness and wetness extremes: SPI bias. Hydrol Earth Syst Sci Discuss 8:10635–10677. doi: 10.5194/hessd-8-10635-2011

Sienz F, Bothe O, Fraedrich K (2012) Monitoring and quantifying future climate projections of dryness and wetness extremes: SPI bias. Hydrol Earth Syst Sci 16:2143–2157. doi: 10.5194/hess-16-2143-2012

Sillmann J, Kharin V V., Zwiers FW, Zhang X, Bronaugh D, Donat MG (2014) Evaluating model-simulated variability in temperature extremes using modified percentile indices. Int J Climatol 34:3304–3311. doi: 10.1002/joc.3899

Simmons AJ, Willett KM, Jones PD, Thorne PW, Dee DP (2010) Low-frequency variations in surface atmospheric humidity, temperature, and precipitation: Inferences from reanalyses and monthly gridded observational data sets. J Geophys Res 115:D01110. doi: 10.1029/2009JD012442

Smith M, Allen R, Monteith J, Perrier A, Pereira L, Segeren A (1991) Report of the expert consultation on procedures for revision of FAO guidelines for prediction of crop water requirements. UN-FAO, Rome, Italy, 54pp

Soares PMM, Cardoso RM, Miranda PMA, de Medeiros J, Belo-Pereira M, Espirito-Santo F (2012a) WRF high resolution dynamical downscaling of ERA-Interim for Portugal. Clim Dyn 39:2497–2522. doi: 10.1007/s00382-012-1315-2

Soares PMM, Cardoso RM, Miranda PMA, de Medeiros J, Belo-Pereira M, Espirito-Santo F (2012b) WRF high resolution dynamical downscaling of ERA-Interim for Portugal. Clim Dyn 39:2497–2522. doi: 10.1007/s00382-012-1315-2

Song ZW, Zhang HL, Snyder RL, Anderson FE, Chen F (2010) Distribution and Trends in Reference Evapotranspiration in the North China Plain. J Irrig Drain Eng 136:240–247. doi: 10.1061/(ASCE)IR.1943-4774.0000175

Sousa PM, Trigo RM, Aizpurua P, Nieto R, Gimeno L, Garcia-Herrera R (2011) Trends and extremes of drought indices throughout the 20th century in the Mediterranean. 11:33–51. doi: 10.5194/nhess-11-33-2011

Srivastava PK, Han D, Islam T, Petropoulos GP, Gupta M, Dai Q (2016) Seasonal evaluation of evapotranspiration fluxes from MODIS satellite and mesoscale model downscaled global reanalysis datasets. Theor Appl Climatol 124:461–473. doi: 10.1007/s00704-015-1430-1

Srivastava PK, Han D, Rico-Ramirez MA, Islam T (2014) Sensitivity and uncertainty analysis of mesoscale model downscaled hydro-meteorological variables for discharge prediction. Hydrol Process 28:4419–4432. doi: 10.1002/hyp.9946

Srivastava PK, Han D, Rico Ramirez MA, Islam T (2013) Comparative assessment of evapotranspiration derived from NCEP and ECMWF global datasets through Weather Research and Forecasting model. Atmos Sci Lett 14:118–125. doi: 10.1002/asl2.427

Srivastava PK, Islam T, Gupta M, Petropoulos G, Dai Q (2015) WRF Dynamical Downscaling and Bias Correction Schemes for NCEP Estimated Hydro-Meteorological Variables. Water Resour Manag 29:2267–2284. doi: 10.1007/s11269-015-0940-z

Stahl K, Kohn I, Blauhut V, Urquijo J, De Stefano L, Acácio V, Dias S, Stagge JH, Tallaksen LM, Kampragou E, Van Loon AF, Barker LJ, Melsen LA, Bifulco C, Musolino D, De Carli A, Massarutto A, Assimacopoulos D, Van Lanen HAJ (2016) Impacts of European drought events: Insights from an international database of text-based reports. Nat Hazards Earth Syst Sci 16:801–819. doi: 10.5194/nhess-16-801-2016

Streets DG, Wu Y, Chin M (2006) Two-decadal aerosol trends as a likely explanation of the global dimming/brightening transition. Geophys Res Lett 33:L15806. doi:

10.1029/2006GL026471
Svoboda M, LeComte D, Hayes M, Heim R, Gleason K, Angel J, Rippey B, Tinker R, Palecki M, Stooksbury D, Miskus D, Stephens S, Svoboda M, LeComte D, Hayes M, Heim R, Gleason K, Angel J, Rippey B, Tinker R, Palecki M, Stooksbury D, Miskus D, Stephens S (2002) The Drought Monitor. Bull Am Meteorol Soc 83:1181–1190. doi: 10.1175/1520-0477-83.8.1181
Tabari H, Grismer ME, Trajkovic S (2013) Comparative analysis of 31 reference evapotranspiration methods under humid conditions. Irrig Sci 31:107–117. doi: 10.1007/s00271-011-0295-z
Tang B, Tong L, Kang S, Zhang L (2011a) Impacts of climate variability on reference evapotranspiration over 58 years in the Haihe river basin of north China. Agric Water Manag 98:1660–1670. doi: 10.1016/J.AGWAT.2011.06.006
Tang W-J, Yang K, Qin J, Cheng CCK, He J (2011b) Solar radiation trend across China in recent decades: a revisit with quality-controlled data. Atmos Chem Phys 11:393–406. doi: 10.5194/acp-11-393-2011
Tate EL, Gustard A (2000) Drought Definition: A Hydrological Perspective. Springer, Dordrecht, pp 23–48
Telesca L, Vicente-Serrano SM, López-Moreno JI (2013) Power spectral characteristics of drought indices in the Ebro river basin at different temporal scales. Stoch Environ Res Risk Assess 27:1155–1170. doi: 10.1007/s00477-012-0651-4
Temesgen B, Allen RG, Jensen DT (1999) Adjusting Temperature Parameters to Reflect Well-Watered Conditions. J Irrig Drain Eng 125:26–33. doi: 10.1061/(ASCE)0733-9437(1999)125:1(26)
Temesgen B, Eching S, Davidoff B, Frame K (2005) Comparison of Some Reference Evapotranspiration Equations for California. J Irrig Drain Eng 131:73–84. doi: 10.1061/(ASCE)0733-9437(2005)131:1(73)
Terink W, Hurkmans RTWL, Torfs PJJF, Uijlenhoet R (2010) Evaluation of a bias correction method applied to downscaled precipitation and temperature reanalysis data for the Rhine basin. Hydrol Earth Syst Sci 14:687–703. doi: 10.5194/hess-14-687-2010
Terink W, Immerzeel WW, Droogers P (2013) Climate change projections of precipitation and reference evapotranspiration for the Middle East and Northern Africa until 2050. Int J Climatol 33:3055–3072. doi: 10.1002/joc.3650
Thomas A (2008) Development and properties of 0.25-degree gridded evapotranspiration data fields of China for hydrological studies. J Hydrol 358:145–158. doi: 10.1016/J.JHYDROL.2008.05.034
Thomas A (2000) Spatial and temporal characteristics of potential evapotranspiration trends over China. Int J Climatol 20:381–396. doi: 10.1002/(SICI)1097-0088(20000330)20:4<381::AID-JOC477>3.0.CO;2-K
Thornthwaite CW (1948) An Approach toward a Rational Classification of Climate. Geogr Rev 38:55. doi: 10.2307/210739
Tian-Jun Z, Tao H (2013) Projected Changes of Palmer Drought Severity Index under an RCP8.5 Scenario. Atmos Ocean Sci Lett 6:273–278. doi: 10.3878/j.issn.1674-2834.13.0032
Todorovic M (1999) Single-Layer Evapotranspiration Model with Variable Canopy Resistance. J Irrig Drain Eng 125:235–245. doi: 10.1061/(ASCE)0733-9437(1999)125:5(235)
Todorovic M, Karic B, Pereira LS (2013) Reference evapotranspiration estimate with limited weather data across a range of Mediterranean climates. J Hydrol 481:166–176. doi: 10.1016/J.JHYDROL.2012.12.034

Trajkovic S (2007) Hargreaves versus Penman-Monteith under Humid Conditions. J Irrig Drain Eng 133:38–42. doi: 10.1061/(ASCE)0733-9437(2007)133:1(38)
Trajkovic S (2005) Temperature-Based Approaches for Estimating Reference Evapotranspiration. J Irrig Drain Eng 131:316–323. doi: 10.1061/(ASCE)0733-9437(2005)131:4(316)
Trajkovic S, Kolakovic S (2009) Estimating Reference Evapotranspiration Using Limited Weather Data. J Irrig Drain Eng 135:443–449. doi: 10.1061/(ASCE)IR.1943-4774.0000094
Trapletti A, Hornik K (2018) Tseries: time series analysis and computational finance. R package version 0.10–45
Trenberth KE, Dai A, van der Schrier G, Jones PD, Barichivich J, Briffa KR, Sheffield J (2014) Global warming and changes in drought. Nat Clim Chang 4:17–22. doi: 10.1038/nclimate2067
Trigo RM, Osborn TJ, Corte-Real JM (2002) The North Atlantic Oscillation influence on Europe: Climate impacts and associated physical mechanisms. Clim Res 20:9–17. doi: 10.3354/cr020009
Trigo RM, Pozo-Vázquez D, Osborn TJ, Castro-Díez Y, Gámiz-Fortis S, Esteban-Parra MJ (2004) North Atlantic oscillation influence on precipitation, river flow and water resources in the Iberian Peninsula. Int J Climatol 24:925–944. doi: 10.1002/joc.1048
Tsakiris G, Pangalou D, Vangelis H (2007) Regional Drought Assessment Based on the Reconnaissance Drought Index (RDI). Water Resour Manag 21:821–833. doi: 10.1007/s11269-006-9105-4
Tsiropoula G (2003) Signatures of solar activity variability in meteorological parameters. J Atmos Solar-Terrestrial Phys 65:469–482. doi: 10.1016/S1364-6826(02)00295-X
Tunalıoğlu R, Durdu ÖF (2012) Assessment of future olive crop yield by a comparative evaluation of drought indices: a case study in western Turkey. Theor Appl Climatol 108:397–410. doi: 10.1007/s00704-011-0535-4
UNEP (2006) Global environment outlook year book: an overview of changing environmrnt, Hertfordshire, England, 82p. United Nations Environment Programme
UNEP (1997) World atlas of desertification, 2nd edn. United Nations Environment Programme, Arnold, London, 182p
Uppala SM, KÅllberg PW, Simmons AJ, Andrae U, Bechtold VDC, Fiorino M, Gibson JK, Haseler J, Hernandez A, Kelly GA, Li X, Onogi K, Saarinen S, Sokka N, Allan RP, Andersson E, Arpe K, Balmaseda MA, Beljaars ACM, Berg L Van De, Bidlot J, Bormann N, Caires S, Chevallier F, Dethof A, Dragosavac M, Fisher M, Fuentes M, Hagemann S, Hólm E, Hoskins BJ, Isaksen L, Janssen PAEM, Jenne R, Mcnally AP, Mahfouf J-F, Morcrette J-J, Rayner NA, Saunders RW, Simon P, Sterl A, Trenberth KE, Untch A, Vasiljevic D, Viterbo P, Woollen J (2005) The ERA-40 re-analysis. Q J R Meteorol Soc 131:2961–3012. doi: 10.1256/qj.04.176
Valiantzas JD (2013) Simplified forms for the standardized FAO-56 Penman–Monteith reference evapotranspiration using limited weather data. J Hydrol 505:13–23. doi: 10.1016/J.JHYDROL.2013.09.005
Van Der Schrier G, Barichivich J, Briffa KR, Jones PD (2013) A scPDSI-based global data set of dry and wet spells for 1901-2009. J Geophys Res Atmos 118:4025–4048. doi: 10.1002/jgrd.50355
van der Schrier G, Briffa KR, Jones PD, Osborn TJ, Schrier G van der, Briffa KR, Jones PD, Osborn TJ (2006) Summer Moisture Variability across Europe. J Clim 19:2818–2834. doi: 10.1175/JCLI3734.1
van der Schrier G, Jones PD, Briffa KR (2011) The sensitivity of the PDSI to the Thornthwaite and Penman-Monteith parameterizations for potential

evapotranspiration. J Geophys Res 116:D03106. doi: 10.1029/2010JD015001
Vangelis H, Tigkas D, Tsakiris G (2013) The effect of PET method on Reconnaissance Drought Index (RDI) calculation. J Arid Environ 88:130–140. doi: 10.1016/J.JARIDENV.2012.07.020
Vasiliades L, Loukas A (2009) Hydrological response to meteorological drought using the Palmer drought indices in Thessaly, Greece. Desalination 237:3–21. doi: 10.1016/j.desal.2007.12.019
Ventura F, Spano D, Duce P, Snyder RL (1999) An evaluation of common evapotranspiration equations. Irrig Sci 18:163–170. doi: 10.1007/s002710050058
Vicente-Serrano SM (2006) Differences in Spatial Patterns of Drought on Different Time Scales: An Analysis of the Iberian Peninsula. Water Resour Manag 20:37–60. doi: 10.1007/s11269-006-2974-8
Vicente-Serrano SM, Azorin-Molina C, Sanchez-Lorenzo A, Revuelto J, López-Moreno JI, González-Hidalgo JC, Moran-Tejeda E, Espejo F (2014) Reference evapotranspiration variability and trends in Spain, 1961–2011. Glob Planet Change 121:26–40. doi: 10.1016/J.GLOPLACHA.2014.06.005
Vicente-Serrano SM, Beguería S, López-Moreno JI, Vicente-Serrano SM, Beguería S, López-Moreno JI (2010) A Multiscalar Drought Index Sensitive to Global Warming: The Standardized Precipitation Evapotranspiration Index. J Clim 23:1696–1718. doi: 10.1175/2009JCLI2909.1
Vicente-Serrano SM, Beguería S, Lorenzo-Lacruz J, Camarero JJ, López-Moreno JI, Azorin-Molina C, Revuelto J, Morán-Tejeda E, Sanchez-Lorenzo A, Vicente-Serrano SM, Beguería S, Lorenzo-Lacruz J, Camarero JJ, López-Moreno JI, Azorin-Molina C, Revuelto J, Morán-Tejeda E, Sanchez-Lorenzo A (2012) Performance of Drought Indices for Ecological, Agricultural, and Hydrological Applications. Earth Interact 16:1–27. doi: 10.1175/2012EI000434.1
Vicente-Serrano SM, Van der Schrier G, Beguería S, Azorin-Molina C, Lopez-Moreno J-I (2015) Contribution of precipitation and reference evapotranspiration to drought indices under different climates. J Hydrol 526:42–54. doi: 10.1016/J.JHYDROL.2014.11.025
Vogel RM, Stedinger JR (1985) Minimum variance streamflow record augmentation procedures. Water Resour Res 21:715–723. doi: 10.1029/WR021i005p00715
Vörösmarty CJ, Green P, Salisbury J, Lammers RB (2000) Global water resources: Vulnerability from climate change and population growth. Science (80-) 289:284–288. doi: 10.1126/science.289.5477.284
Wang H, Rogers JC, Munroe DK, Wang H, Rogers JC, Munroe DK (2015a) Commonly Used Drought Indices as Indicators of Soil Moisture in China. J Hydrometeorol 16:1397–1408. doi: 10.1175/JHM-D-14-0076.1
Wang JXL, Gaffen DJ (2001) Late-twentieth-century climatology and trends of surface humidity and temperature in China. J Clim 14:2833–2845. doi: 10.1175/1520-0442(2001)014<2833:LTCCAT>2.0.CO;2
Wang K, Dickinson RE (2012) A review of global terrestrial evapotranspiration: Observation, modeling, climatology, and climatic variability. Rev Geophys 50:. doi: 10.1029/2011RG000373
Wang S, SS, Wang S, AW, Duan A, Liu Z, Luo C (2010) Evaluation on several methods for estimating ETo and modified Hargreaves formulas. J Irrig Drain 29:29-33 (in Chinese)
Wang W, Shao Q, Peng S, Xing W, Yang T, Luo Y, Yong B, Xu J (2012) Reference evapotranspiration change and the causes across the Yellow River Basin during 1957-2008 and their spatial and seasonal differences. Water Resour Res 48:. doi:

10.1029/2011WR010724
Wang Y, Jiang T, Bothe O, Fraedrich K (2007) Changes of pan evaporation and reference evapotranspiration in the Yangtze River basin. Theor Appl Climatol 90:13–23. doi: 10.1007/s00704-006-0276-y
Wang Y, Li J, Feng P, Hu R (2015b) A Time-Dependent Drought Index for Non-Stationary Precipitation Series. Water Resour Manag 29:5631–5647. doi: 10.1007/s11269-015-1138-0
Wehner M, Easterling DR, Lawrimore JH, Heim RR, Vose RS, Santer BD (2011) Projections of Future Drought in the Continental United States and Mexico. J Hydrometeorol 12:1359–1377. doi: 10.1175/2011JHM1351.1
Wells N, Goddard S, Hayes MJ, Wells N, Goddard S, Hayes MJ (2004) A Self-Calibrating Palmer Drought Severity Index. J Clim 17:2335–2351. doi: 10.1175/1520-0442(2004)017<2335:ASPDSI>2.0.CO;2
White D, Richman M, Yarnal B (1991) Climate regionalization and rotation of principal components. Int J Climatol 11:1–25. doi: 10.1002/joc.3370110102
Wilhite DA (2000) Chapter 1 Drought as a Natural Hazard: Concepts and Definitions
Wilhite DA, Glantz MH (1985) Understanding the Drought Phenomenon: The Role of Definitions
Wilhite DA, Svoboda MD, Hayes MJ (2007) Understanding the complex impacts of drought: A key to enhancing drought mitigation and preparedness. Water Resour Manag 21:763–774. doi: 10.1007/s11269-006-9076-5
WMO, GWP (2016) Handbook of Drought Indicators and Indices (M. Svoboda and B.A. Fuchs). Integrated Drought Management Programme (IDMP), Integrated Drought Management Tools and Guidelines Series 2. Geneva.
World Meteorological Organization (2012) Standardized Precipitation Index User Guide (M. Svoboda, M. Hayes and D. Wood). (WMO-No. 1090), Geneva
Wu H, Svoboda MD, Hayes MJ, Wilhite DA, Wen F (2007) Appropriate application of the standardized precipitation index in arid locations and dry seasons. Int J Climatol 27:65–79. doi: 10.1002/joc.1371
Xia XA, Wang PC, Chen HB, Liang F (2006) Analysis of downwelling surface solar radiation in China from National Centers for Environmental Prediction reanalysis, satellite estimates, and surface observations. J Geophys Res 111:D09103. doi: 10.1029/2005JD006405
Xing W, Wang W, Shao Q, Peng S, Yu Z, Yong B, Taylor J (2014) Changes of reference evapotranspiration in the Haihe River Basin: Present observations and future projection from climatic variables through multi-model ensemble. Glob Planet Change 115:1–15. doi: 10.1016/J.GLOPLACHA.2014.01.004
Xu C, Gong L, Jiang T, Chen D, Singh VP (2006) Analysis of spatial distribution and temporal trend of reference evapotranspiration and pan evaporation in Changjiang (Yangtze River) catchment. J Hydrol 327:81–93. doi: 10.1016/J.JHYDROL.2005.11.029
Xu Y-P, Pan S, Fu G, Tian Y, Zhang X (2014) Future potential evapotranspiration changes and contribution analysis in Zhejiang Province, East China. J Geophys Res Atmos 119:2174–2192. doi: 10.1002/2013JD021245
Yadava MG, Ramesh R (2007) Significant longer-term periodicities in the proxy record of the Indian monsoon rainfall. New Astron 12:544–555. doi: 10.1016/J.NEWAST.2007.04.001
Yan H, Shi H, Xue Z, Zhang Y, Liu H (2008) Comparison of estimating ET0 with different methods in Hetao Irrigation District in Inner Mongolia. Trans Chinese Soc Agric Eng 2008:. doi: 10.3969/J.ISSN.1002-6819.2008.4.019

Yang F, Zhou G (2011) Characteristics and modeling of evapotranspiration over a temperate desert steppe in Inner Mongolia, China. J Hydrol 396:139–147. doi: 10.1016/J.JHYDROL.2010.11.001

Yang Z, Liu Q, Cui B (2011) Spatial distribution and temporal variation of reference evapotranspiration during 1961–2006 in the Yellow River Basin, China. Hydrol Sci J 56:1015–1026. doi: 10.1080/02626667.2011.590810

Ye J, Guo A, Sun G (2009) Statistical Analysis of Reference Evapotranspiration on the Tibetan Plateau. J Irrig Drain Eng 135:134–140. doi: 10.1061/(ASCE)0733-9437(2009)135:2(134)

Yin Y, Wu S, Chen G, Dai E (2010) Attribution analyses of potential evapotranspiration changes in China since the 1960s. Theor Appl Climatol 101:19–28. doi: 10.1007/s00704-009-0197-7

Yoder RE, Odhiambo LO, Wright WC (2005) Evaluation of methods for estimating daily reference crop evapotranspiration at a site in the humid southeast United States. Appl Eng Agric 21:197–202. doi: 10.13031/2013.18153

You Q, Kang S, Flügel W, Pepin N, Yan Y, Huang J (2010) Decreasing wind speed and weakening latitudinal surface pressure gradients in the Tibetan Plateau. Clim Res 42:57–64. doi: 10.3354/cr00864

You Q, Sanchez-Lorenzo A, Wild M, Folini D, Fraedrich K, Ren G, Kang S (2013) Decadal variation of surface solar radiation in the Tibetan Plateau from observations, reanalysis and model simulations. Clim Dyn 40:2073–2086. doi: 10.1007/s00382-012-1383-3

Yue S, Wang C (2004) The Mann-Kendall Test Modified by Effective Sample Size to Detect Trend in Serially Correlated Hydrological Series. Water Resour Manag 18:201–218. doi: 10.1023/B:WARM.0000043140.61082.60

Zargar A, Sadiq R, Khan FI (2014) Uncertainty-Driven Characterization of Climate Change Effects on Drought Frequency Using Enhanced SPI. Water Resour Manag 28:15–40. doi: 10.1007/s11269-013-0467-0

Zargar A, Sadiq R, Naser B, Khan FI (2011) A review of drought indices. Environ Rev 19:333–349. doi: 10.1139/a11-013

Zhang B, He C (2016) A modified water demand estimation method for drought identification over arid and semiarid regions. Agric For Meteorol 230–231:58–66. doi: 10.1016/J.AGRFORMET.2015.11.015

Zhang Q, Xu C-Y, Chen X (2011a) Reference evapotranspiration changes in China: natural processes or human influences? Theor Appl Climatol 103:479–488. doi: 10.1007/s00704-010-0315-6

Zhang Q, Xu C-Y, Chen YD, Ren L (2011b) Comparison of evapotranspiration variations between the Yellow River and Pearl River basin, China. Stoch Environ Res Risk Assess 25:139–150. doi: 10.1007/s00477-010-0428-6

Zhao M, Running SW, Nemani RR (2006) Sensitivity of Moderate Resolution Imaging Spectroradiometer (MODIS) terrestrial primary production to the accuracy of meteorological reanalyses. J Geophys Res 111:G01002. doi: 10.1029/2004JG000004

Zhao T, Guo W, Fu C, Zhao T, Guo W, Fu C (2008) Calibrating and Evaluating Reanalysis Surface Temperature Error by Topographic Correction. J Clim 21:1440–1446. doi: 10.1175/2007JCLI1463.1

Zheng X, Zhu J (2015) Temperature-based approaches for estimating monthly reference evapotranspiration based on MODIS data over North China. Theor Appl Climatol 121:695–711. doi: 10.1007/s00704-014-1269-x

Zuo D, Xu Z, Yang H, Liu X (2012) Spatiotemporal variations and abrupt changes of

potential evapotranspiration and its sensitivity to key meteorological variables in the Wei River basin, China. Hydrol Process 26:1149–1160. doi: 10.1002/hyp.8206